THE UNIVERSITY *of* EDINBURGH

Establishing *Drosophila* as a model to study the functional relevance of conserved heart genes

James H. Catterson

Thesis submitted to the University of Edinburgh for the Degree of Doctor of Philosophy

2013

Declaration

I hereby declare that this thesis has been composed by myself and describes my own work with the following exception:

- Dr. Paul Hartley performed the bioinformatics that led to the generation and annotation of the fly heart ‘enrichment’ lists (in Chapter 4, methods are described in Chapter 2).

I confirm that this thesis has not been previously submitted for any other degree.

James H. Catterson

2013

Abstract

Background/Aims

Understanding the fundamental mechanisms underlying the development of congenital heart disease and cardiomyopathies is a goal of researchers worldwide, with the ultimate goal being the establishment of effective therapeutics for the amelioration of cardiac dysfunction. Unfortunately these disorders are often polygenic in aetiology, making it difficult for researchers to probe complex interactions that may contribute to the severity of the disease. Over the last decade, the adult fruit fly (*Drosophila melanogaster*) has emerged as an invaluable tool with which to study the genetic and molecular mechanisms underlying heart function. The aim of my thesis research was to establish the adult fruit fly as a model of human heart function, and to exploit this powerful genetic system to screen for conserved genes affecting the development and function of its cardiac syncytium.

Methodology/Results

Baseline measures of heart function and other factors contributing to variability in heart function (i.e. age, temperature, and the time of day) were assessed to establish the adult *Drosophila* heart model. I then performed an *a priori* RNAi screen, knocking down expression of individual conserved genes via cardiomyocyte-specific overexpression utilising the yeast GAL4/UAS system. Heart-specific ablation of *Fermitin 1* and *Fermitin 2 (Fit1, Fit2),* the two *Drosophila* orthologs of *Kindlin 2* (*Kind2*, a gene thought to be important for cardiomyocyte-cardiomyocyte junction integrity in human myocardium), caused severe cardiomyopathy

characterised by the failure of cardiomyocytes to develop as a functional syncytium and loss of synchrony between cardiomyocytes. I generated a null allele of *Fit1* via P-element mobilisation, but this had no impact on heart development or function. Similarly, the silencing of *Fit2* failed to affect heart development or function. In contrast, the silencing of *Fit2* in the cardiomyocytes of *Fit1*-null flies disrupted syncytium development, leading to severe cardiomyopathy. Temperature-sensitive cardiac-specific GAL4/GAL80^{ts} lines were also generated, and knockdown of *Fit* (*Fit1* and *Fit2*) function at different developmental stages was assessed. I observed the strongest effects of *Fit* knockdown on adult cardiac morphology during stages of heart development and remodelling, with significant cardiomyocyte decoupling. After 3-weeks of *Fit* knockdown during adulthood, cardiomyocytes were significantly decoupled, and these hearts were significantly arrhythmic compared to control animals.

Conclusions/Discussion

My data provide clarity about the role of *Kind2* by demonstrating a cell autonomous role for this family in the development of a functional cardiac syncytium in *Drosophila*. My findings also show that the *Fermitins* can functionally compensate for each other in order to control syncytium development. Therefore, my thesis demonstrates the power of the fruit fly as a model of human cardiac physiology, and supports the concept that abnormalities in cardiomyocyte KIND2 expression or function may contribute to cardiomyopathies in humans.

Acknowledgements

Firstly, I would like to thank Dr. Paul Hartley for supervising me throughout my PhD. Paul is genuinely one of the brightest people I have ever had the pleasure of meeting, and if I end up half as bright as Paul I'll count myself lucky. You're the Dr. Cox to my J.D. Thank you for putting up with me for the past 4 years, and for being so generous with your time. You have made me a better scientist.

I would also like to thank Prof. Margarete Heck for kindly agreeing to become one of my supervisors. I could always rely on Margarete for guidance, experimental suggestions, and a good discussion (whatever the topic!). Thanks for including me in your group. Thanks also to Prof. Tony Harmar who inspired me to pursue my new-found interest in Circadian Biology and apply for a PhD (...in Cardiovascular Biology!). I would like to express gratitude to the British Heart Foundation for deciding to pay me to do things I love doing – the joke's on them!

Thanks to the rest of Heck lab (past and present) with special thanks to Dr. Sharron Vass for helpful discussions, technical assistance, and pure deed braw Scottish banter. Thanks also to Michal Janiszewski and Ekin Bolukbasi who have also become my great friends. It's amazing what information is revealed at the Fly Station!

Thanks to my PhD partners-in-crime Emma and Ewa. You guys made doing a PhD worthwhile, and I count you both as my very close friends. Thanks also to the "auld yins" in the years above including Yvonne, Xia, Lucy, and Rachel, and the "young yins" in the year below including Rachel, Rob, Kat, Chris, Ania, Kirsten, and

Evatong. There were many belly laughs, late nights, and sore heads that I will cherish.

My parents Alison and James Catterson, sister Holly, brother Jojo, and my grandparents June and Harold Wright, and Helen and James Catterson, for their unconditional love, support (financial and otherwise!), and praise throughout my studies. If I could have changed anything from the past 8 years, it would have been to visit you all more often. I love you.

And finally, I want to thank my gorgeous soul mate, and best friend, Lizzie. If there was a best thing about doing this PhD, it was that it meant I could meet you. Not once did you complain about the late nights and weekends I spent working in the lab. You have filled a hole in my life I didn't even know needed filling. You mean the world to me.

I dedicate this thesis to my family, my friends,

and the love of my life,

Lizzie.

Without you, I wouldn't be me.

Publications

List of publications by James H. Catterson.

1. **Fermitins, the orthologs of mammalian Kindlins, regulate the development of a functional cardiac syncytium in *Drosophila melanogaster*.** **Catterson JH**, Heck MMS, Hartley PS. ***PLoS One.*** 2013 May 15;8(5):e62958.

2. **Diurnal expression of the thrombopoietin gene is regulated by CLOCK.** Tracey CJ, Pan X, **Catterson JH**, Harmar AJ, Hussain MM, Hartley PS. ***J Thromb Haemost.*** 2012 Apr;10(4):662-9.

3. **Cyclophilin A is a damage-associated molecular pattern molecule that mediates acetaminophen-induced liver injury.** Dear JW, Simpson KJ, Nicolai MP, **Catterson JH**, Street J, Huizinga T, Craig DG, Dhaliwal K, Webb S, Bateman DN, Webb DJ. ***J Immunol.*** 2011 Sep 15;187(6):3347-52.

4. **Dietary modulation of *Drosophila* sleep-wake behaviour.** **Catterson JH**, Knowles-Barley S, James K, Heck MM, Harmar AJ, Hartley PS. ***PLoS One.*** 2010 Aug 10;5(8):e12062.

Contents

List of figures

List of tables

List of abbreviations

ºC	Degree Celsius
%FS	Percentage of Fractional Shortening
α-Cat	Alpha-catenin
αMHC	Alpha myosin heavy chain
αPS	Alpha subunit of position-specific integrin
βPS	Beta subunit of position-specific integrin
Δ2-3	P-element transposase without the 2-3 intron
AJ	Adherens junctions
Alas	Aminolevulinate synthase
ANKR	Ankyrin repeat
ANOVA	Analysis Of Variance
APF	After puparium formation
Arm	Armadillo
AVI	Audio Video Interleave
BDSC	Bloomington *Drosophila* Stock Center
bHLH	Basic helix-loop-helix protein
BMP	Bone morphogenetic protein
bp	Base pair
Bpm	Beats per minute
Bteb2	Basic transcription element-binding protein 2
CaS	Canton-S
CCD camera	Charge-coupled device camera
cDNA	Complementary DNA
CG number	Celera Gene number
Ches1	Checkpoint suppressor homologue
Clk	Clock

CO_2	Carbon dioxide
Col6a2	Collagen, type VI, alpha 2
Cre	Cre recombinase
CSV	Comma Separated Value
C-terminus	Carboxyl terminus
Cyc	Cycle
DAPI	4', 6-diamidino-2-phenylindole
DAVID	Database for annotation, visualization and integrated discovery
DE-cadherin	*Drosophila* E-cadherin
DEPC	Diethyl pyrocarbonate
DN	Dominant negative
DNA	Deoxyribonucleic acid
dNTP	2'-deoxyribonucleoside 5'-triphosphate
Dot	Dorothy
Dpp	Decapentaplegic
DroID	*Drosophila* Interactions Database
Dscam	Down Syndrome Cell Adhesion Molecule
dsRNA	Double stranded RNA
DTT	Dithiothreitol
ECM	Extracellular matrix
EDD	End diastolic diameter
EDTA	Ethylenediamine-N,N,N',N'-tetraacetic acid
EMS	Ethyl methane sulphonate
ESD	End systolic diameter
EtBr	Ethidium bromide
Eve	Even-skipped
F3	F3 subdomain
F-actin	Filamentous actin

FAK	Focal adhesion kinase
Fak56D	Focal adhesion kinase-56D
Fas	Faint sausage
FERM domain	4.1 protein, Ezrin, Radixin and Moesin
Fit1	Fermitin 1
$Fit1^{\Delta 161}$	Δ161 allele of Fermitin 1
Fit2	Fermitin 2
Fuca	α-L-fucosidase
GAL4	Yeast GAL4 protein
$GAL80^{ts}$	Temperature-sensitive yeast GAL80 protein
GEO	Gene Expression Omnibus
GFP	Green Fluorescent Protein
GSK-3β	Glycogen synthase kinase-3β
H_2O	Water
Hand	Heart and neural crest derivatives
HCl	Hydrochloric acid
HCN	Hyperpolarisation-activated cyclic nucleotide gated ion channel
HEPES	N-(2-hydroxyethyl)piperazine-N'-(2-ethanesulfonic acid)
Ho	Heme oxygenase
Hox	Homeobox
Hr	Hour
hpRNA	Hairpin RNA
Hz	Hertz
If	Inflated
IgG	Immunoglobulin G
ILK	Integrin-linked kinase
IPP	ILK/PINCH/Parvin complex
J domain	Junctional domain

KAc	Potassium acetate
Kb	Kilobase-pair(s)
KCNQ	KCNQ potassium channel
Kind1	Kindlin 1
Kind2	Kindlin 2
Kind3	Kindlin 3
Kir2.1	Inward-rectifier potassium channel
KLF15	Krüppel-like factor 15
KO	Knockout
L domain	Luminal domain
LD	Light-dark cycle
LiCl	Lithium chloride
LIM domain	Lin11, Isl-1 & Mec-3
M-line	Sarcomere midline
Mef2	Myocyte enhancer factor 2
Mew	Multiple edematous wings
Mlp84B	Muscle LIM protein at 84B
M-MLV	Moloney Murine Leukemia Virus
M-mode	Motion mode
Mys	Myospheroid
NaCl	Sodium chloride
NijA	Ninjurin A
NijB	Ninjurin B
Nkx2-5	Nk2 transcription factor related, locus 5
NoRT	No Reverse Transcriptase
Not3	CCR4-NOT transcription complex, subunit 3
N-terminus	Amino terminus
OCT	Optical Coherence Tomography

Odd	Odd-skipped
OTE	Off-target effect
Pan	Pangolin
PAT3	Paralysed Arrest at two-fold protein 3
PAT4	Paralysed Arrest at two-fold protein 4
PAT6	Paralysed Arrest at two-fold protein 6
PBS	Phosphate Buffered Saline
PBST	PBS-Triton-X
PCR	Polymerase Chain Reaction
Per	Period
PH domain	Pleckstrin homology domain
PINCH	Particularly Interesting New Cysteine-Histidine rich protein
PN	Pericardial nephrocyte
Raf	Rapidly Accelerated Fibrosarcoma
RNA	Ribonucleic acid
RNAi	RNA-mediated interference
RNase	Ribonuclease
Robo	Roundabout
RP49	Ribosomal protein 49
Rpm	Revolutions per minute
Rpr	Reaper
RT	Reverse Transcriptase
RT-PCR	Reverse Transcriptase - Polymerase Chain Reaction
Sb	Stubble
Scb	Scab
SDS	Sodium Dodecyl Sulfate
SEM	Standard Error of the Mean
Ser	Serrate

Shg	Shotgun
Shi^{ts}	Temperature-sensitive shibire toxin
SIP	Siah-interacting protein
siRNA	Small interfering RNA
Slo	Slowpoke
SNP	Single nucleotide polymorphism
SSNC	Second-site non-complementation
Stck	Steamer duck
Svp	Seven-up
Syn1	Syntrophin-like 1
TAE	Tris acetate buffer with EDTA
TCF	T cell factor
TCF4	T cell factor 4
TE	Tris buffer with EDTA
TIFF	Tagged Image File Format
Timp	Tissue inhibitor of metalloproteases
Tin	Tinman (Nkx2-5)
Tld	Tolloid
TM3	Third Multiple 3
TNT	Tetanus toxin light chain
TRiP	Transgenic RNAi Project
Tris	Tris[hydroxymethyl]aminomethane
Triton X-100	Octylphenol ethoxylate
Tub	Tubulin
TUNEL	Terminal deoxynucleotidyl transferase dUTP nick end labeling
UAS	Upstream Activating Sequence
Unc-112	Uncoordinated protein 112
Unc-45	Uncoordinated protein 45

UV	Ultraviolet light
V	Volts
VASP	Vasodilator-Stimulated Phosphoprotein
VDRC	Vienna *Drosophila* RNAi Center
w^{1118}	White-eyed fly
Wg	Wingless
Wnt	Wingless-related integration site
WT	Wild type
yw	Yellow-bodied white-eyed fly
ZT	Zeitgeber time

Chapter 1

Introduction

1.1 Use of *Drosophila melanogaster* as a model organism

During the early 20th century, the American geneticist Thomas Hunt Morgan and his colleagues at Columbia University established the chromosomal theory of inheritance after his identification of sex-linked traits in fruit flies with eye colour mutations (MORGAN 1910). From then on, Morgan and his talented team pioneered the use of this tiny invertebrate to elucidate the universal role played by the genes and the chromosome in heredity, a feat for which Morgan was awarded a Nobel Prize in 1933. Since then, the number of research groups using the fruit fly (*Drosophila melanogaster*) as a model organism to study various cellular and biological processes has greatly increased. Thomas Hunt Morgan and his early "drosophilists" also established an open network for the cooperative sharing of fly stocks, and importantly, ideas between different fly labs – a philosophy which still runs through *Drosophila* research labs to this day (KOHLER 1994), despite many of today's scientific pressures (ASHBURNER *et al.* 2005). This philosophy of maintaining open communication/collaboration of mutant stocks/ideas helped advance the use of *Drosophila* to model a diverse array of fundamental aspects of biology including developmental biology, neurobiology, cancer, cardiovascular disease, metabolism, and behavioural genetics (BELLEN *et al.* 2010; BIER 2005; BRUMBY and RICHARDSON 2005; WOLF and ROCKMAN 2011).

1.1.1 Advantages of using *Drosophila melanogaster* as a model organism

The fruit fly possesses many unique advantages which will ensure its continued use as a model organism of choice for years to come. These advantages include the ease of which these animals can be handled, and their comparatively low

cost of maintenance. Fruit flies also have a short generation time – around 10 days at 25°C - with high fecundity in females, allowing for the study of subsequent generations within a comparatively short period of time (i.e. weeks/months for fruit flies compared to months/years for mice). The lack of meiotic recombination in males and a genome that consists of two allosomes - X, Y; and three autosomes - 2, 3, 4, makes genetic analysis facile. Furthermore, the existence of "balancer chromosomes", characterised by chromosomal inversions and dominant "marker" mutations (e.g. *Serrate* – Ser^{1}, flies carrying this allele have serrated wings) that prevent recombination, means that it is possible to maintain homozygous lethal alleles as heterozygous stocks without constantly selecting against wild-type alleles (GREENSPAN 1997).

Outwardly, the fruit fly has many readily distinguishable features, which can be altered by specific mutations in a reproducible manner – certain mutations resulting in highly characteristic phenotypes (e.g. white eyes, curly wings, stubbly bristles etc.). Similarly, fruit flies are sexually dimorphic meaning that males and females are readily distinguished from each other. These genetic markers, visible under the stereomicroscope, allow for quick identification and, importantly, tracking of specific genotypes – therefore simplifying genetic screening. Collectively, these factors, along with significant research programs to mutate, disrupt, or modify every gene in *Drosophila* has led to numerous genetic screens that have resulted in the identification and characterisation of conserved essential signalling and developmental pathways (BELLEN *et al.* 2004; RYDER *et al.* 2004; SPRADLING *et al.* 1999; ST JOHNSTON 2002).

Around 700 million years ago, the protostome-deuterostome split separated vertebrates from invertebrates, yet many developmental processes are conserved between *Drosophila* and humans (HOLLEY *et al.* 1995; ST JOHNSTON 2002). Indeed, it was revealed that around 75% of known human disease-associated genes have clear *Drosophila* orthologs (REITER *et al.* 2001), with many models of human disease - including diabetes, obesity, mitochondrial, and neurodegenerative disorders - subsequently developed in *Drosophila* (BIER 2005; CAUCHI and VAN DEN HEUVEL 2006; MARSH and THOMPSON 2006; SUH *et al.* 2007). Interestingly, a number of genes important for human development were first identified in *Drosophila*, including the *Tinman* (*tin*) gene. Flies carrying a homozygous *tin* mutation did not develop a heart – hence the gene name, taken from the Wizard of Oz character (BODMER 1993; EPSTEIN 2000). Similarly, humans carrying mutations in the *tin* ortholog, *Nkx2-5*, exhibit congenital heart defects (IKEDA *et al.* 2002; SCHOTT *et al.* 1998). Therefore the conservation of genes and genetic pathways between flies and higher eukaryotes validates *Drosophila* research and illustrates its practicality for the study of human cardiac pathophysiology.

1.1.2 The life cycle of *Drosophila melanogaster*

Drosophila melanogaster is a holometabolous insect – i.e. undergoing complete metamorphosis by progressing through four distinct developmental stages: embryo, larvae, pupae and adult (summarised in Figure 1.1). Like all ectothermic species, the developmental period of the fruit fly is temperature-dependent. At 25°C, the complete life cycle of *Drosophila* takes approximately 10 days from fertilised embryo to adult. At around 8-12 hours after eclosion, the adult female fly becomes sexually receptive, and after subsequent courtship behaviour – followed by

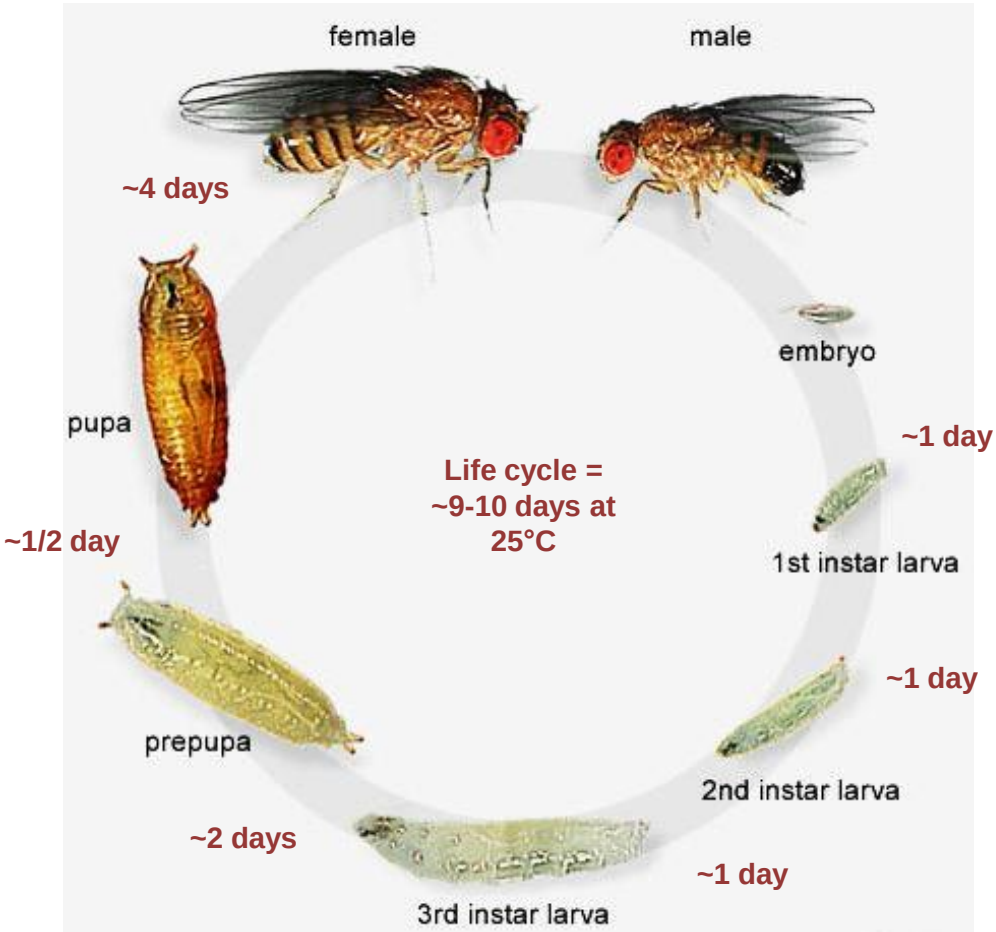

Figure 1.1. Life cycle of *Drosophila melanogaster*.
Around 8-12 hours after eclosion, the female *Drosophila* becomes sexually receptive. Successful copulation by the male *Drosophila* fertilises the oocytes. The female can lay up to 100 embryos/day, post-fertilisation. Once laid, *Drosophila* embryos take approximately 22-24 hours to develop and hatch into 1st instar larvae. First instar larvae undergo a series of molts into the 2nd and 3rd instar larvae, with constant growth. Twenty-four hours before puparation, third instar larvae enter the wandering stage and form an immobile white puparium (prepupa), which quickly darkens and hardens. *Drosophila* then undergo metamorphosis over approximately 4-5 days, then eclose from the pupae as adult flies. Figure adapted from FlyMove (http://flymove.uni-muenster.de/).

copulation – the oocytes of the female are fertilised by the male. Females lay eggs shortly after fertilisation takes place. After fertilisation occurs, the early syncytial embryo undergoes 13 rounds of cell division, after which cell membranes invaginate, dividing the syncytium into individual somatic cells and allowing gastrulation to occur – i.e. the formation of endoderm, mesoderm, and ectoderm (LAWRENCE 1992). The developing embryo undergoes well-characterised morphogenetic movements during embryogenesis, including the development of a beating heart, until finally hatching from the surrounding cuticle into a 1st-instar larva. At 25°C, the embryonic stage lasts approximately 24 hours. At this temperature, the first and second instar stages also last approximately 24 hours each, while the third instar stage lasts approximately 48 hours, and ends with the formation of the puparium and the start of metamorphosis. During larval development, the differentiation of imaginal discs takes place – i.e. discrete populations of cells that eventually develop into structures in the adult fly, such as eyes, wings, and legs. During metamorphosis, the larval tissues are absorbed or remodelled, with imaginal tissues undergoing extensive morphogenetic movements to form structures in the adult. Approximately 4-5 days after puparium formation, the fully developed imago ecloses from its pupal case. The length of the *Drosophila* life cycle is subject to changing temperature – with periods becoming longer at lower temperatures (e.g. 19 days at 18°C) and shorter at higher temperatures (ASHBURNER *et al.* 2005).

1.2 The *Drosophila* heart

The *Drosophila* heart has been an excellent model of cardiovascular development since the discovery of the homeobox transcription factor *tinman* (AZPIAZU and FRASCH 1993; BODMER 1993; BODMER *et al.* 1990), and the recognition that it was conserved in humans (BIER and BODMER 2004; SCHOTT *et al.* 1998). Indeed, *Drosophila* is the pre-eminent invertebrate model organism that contains a rhythmically beating heart with developmental and functional similarities to the mammalian heart, and has been used to model cardiac development and pathology (PIAZZA and WESSELLS 2011). Although the fly heart is simple in comparison with higher organisms, research on the *Drosophila* heart has yielded new insights into the development of the mammalian heart. Within the last 10 years, however, researchers have also turned their attention to the genetic mechanisms and pathways involved in heart function. There is significant conservation of the molecular mechanisms underlying cardiogenesis in animals, and therefore it is likely the genetic control of cardiac function may also be conserved (OCORR *et al.* 2007b). Significantly, similar to the human heart, the *Drosophila* heart does not solely consist of cardiomyocytes. There are pericardial nephrocytes (PN) and a layer of syncytial ventral longitudinal muscles closely associated with the cardiac tube – making it difficult to tease out cardiomyocyte-specific information from screens in which adult *Drosophila* 'heart tissue' is analysed.

Drosophila cardiomyocytes share many ultrastructural features with human cardiomyocytes. Ultrastructural studies have demonstrated readily identifiable sarcomeres (i.e. the basic muscle units) in both human and *Drosophila* cardiomyocytes with common features including tight bundles of myofibrils made up

of thick myosin and thin actin protein filaments that attach at Z-discs (LEHMACHER *et al.* 2012). Sarcomere lengths are similar between species (i.e. approximately 2µm) (HANFT *et al.* 2008), while T tubules and gap junctions (formed from invertebrate innexin proteins – orthologous to vertebrate connexins) have also been identified in *Drosophila* and human cardiomyocytes (CHINTAPALLI *et al.* 2007; CROMPTON *et al.* 1995; MEDIONI *et al.* 2009; STEBBINGS *et al.* 2002).

Many of the proteins contributing to excitation-contraction coupling in mammalian heart are conserved both genetically and functionally in *Drosophila* cardiomyocytes, including ion channels predicted to be involved in cardiac pace-making (e.g. I_h-channel/HCN (hyperpolarisation-activated cyclic nucleotide gated) channel in vertebrates) (MONIER *et al.* 2005), and sarcomeric proteins including myosin and troponin (CAMMARATO *et al.* 2008; CHOMA *et al.* 2011; WOLF *et al.* 2006). The *Drosophila* heart can therefore be thought of as a 'functional syncytium', with the cardiomyocyte junctions likely propagating the action potentials in a similar fashion as to that seen in mammalian cardiomyocytes. Indeed, efforts to effectively measure real-time myocardial calcium handling have recently been developed, and recapitulate aspects of diseased mammalian myocardium (LIN *et al.* 2011). Thus, the similarity between the above-mentioned proteins and their effect on the heart function indicate these processes evolved from a common evolutionary ancestor that preceded the invertebrate-vertebrate split (OCORR *et al.* 2007b).

The following will describe the heart development process in *Drosophila*, from the embryo to the adult fly, and the recent advances in the utilisation of the fruit fly as a model of human cardiac function and functional abnormalities leading to heart disease pathogenesis.

1.2.1. Heart development in the *Drosophila* embryo

The *Drosophila* heart is formed from a precisely coordinated set of signals originating in the embryonic mesoderm (MEDIONI *et al.* 2009; PIAZZA and WESSELLS 2011; WOLF and ROCKMAN 2011). An essential step is the secretion of Decapentaplegic (Dpp) and Wingless (Wg) ligands – the *Drosophila* orthologs of the bone morphogenetic protein (BMP) and Wnt protein respectively – which trigger cell fate specification in the developing mesoderm (JUNION *et al.* 2012). The *wg* gene is expressed in a series of stripes which help define the embryonic mesoderm along the anterior-posterior axis, while *dpp* acts along the dorsal-ventral axis – therefore the perpendicular intersection of both signalling ligands acts to instruct the specification of each cell in the developing cardiac mesoderm (FRASCH 1995; LAWRENCE *et al.* 1995). The *Nkx2-5* transcription factor ortholog, *tinman*, provides mesoderm-specific context for these signals and is subsequently required for differentiation of myocardial cells, whereby expression defines contractile cardiomyocytes from *seven-up*-(*svp*)-expressing (and *tin*-repressing) ostial precursors (ZAFFRAN *et al.* 2006). Cardiomyocyte differentiation proceeds under the control of differentiation genes – with some genes direct targets of *tin* – including *Hand* and *svp* (HAN and OLSON 2005; LO and FRASCH 2001).

Before migration proceeds, the two rows of cardiac cells undergo mesenchymal to epithelial transition, and establish contacts between each other to form a continuous monolayer (RUGENDORFF *et al.* 1994). As the process occurs, these cells start to express a variety of membrane markers and polarity determinants – including many cell adhesion proteins such as *faint sausage* (*fas*) and *Toll*, a transmembrane receptor (HAAG *et al.* 1999; WANG *et al.* 2005). Additionally,

conserved extracellular matrix-cell adhesion proteins such as laminins (YARNITZKY and VOLK 1995), integrins (STARK *et al.* 1997), and cadherins (HAAG *et al.* 1999), maintain the developing tissue architecture. When the cardiac cell rows are aligned, they migrate together towards the dorsal midline – remaining in contact with the "leading edge" of the overlying ectodermal layer as it proceeds towards dorsal closure – where they adhere to the opposing row of cardiac cells, form a lumen, and therefore, the dorsal vessel (i.e. the heart) (HARTENSTEIN 1993). Slit/Robo signalling is essential for maintaining cell polarity during this process and for adhesion at the midline (MEDIONI *et al.* 2008; MEDIONI *et al.* 2009). *Drosophila* cardiogenesis is illustrated in Figure 1.2A.

The dorsal vessel is divided into the anterior and posterior aorta, and the pumping heart chamber – a result of positional information from homeobox transcription factors including the *Bithorax* complex (PONZIELLI *et al.* 2002). The dorsal vessel is arranged in sets of *tin*-positive cardioblasts (that form contractile cells of the heart) separated by pairs of *svp*-positive ostioblasts (that form the valve-like ostial cells of the heart) – illustrated in Figure 1.2B. Additionally, non-contractile pericardial cells adhere closely to the heart and form septate junctions (YI *et al.* 2008), while the dorsal vessel is surrounded by an extracellular matrix formed from pericardin – a type IV collagen-like protein (CHARTIER *et al.* 2002).

1.2.2. The larval heart

During the larval stage, the heart grows progressively larger from the small embryo-sized dorsal vessel to the robust beating organ it will come to resemble in the adult. The heart increases in size proportionately, but in the absence of cell

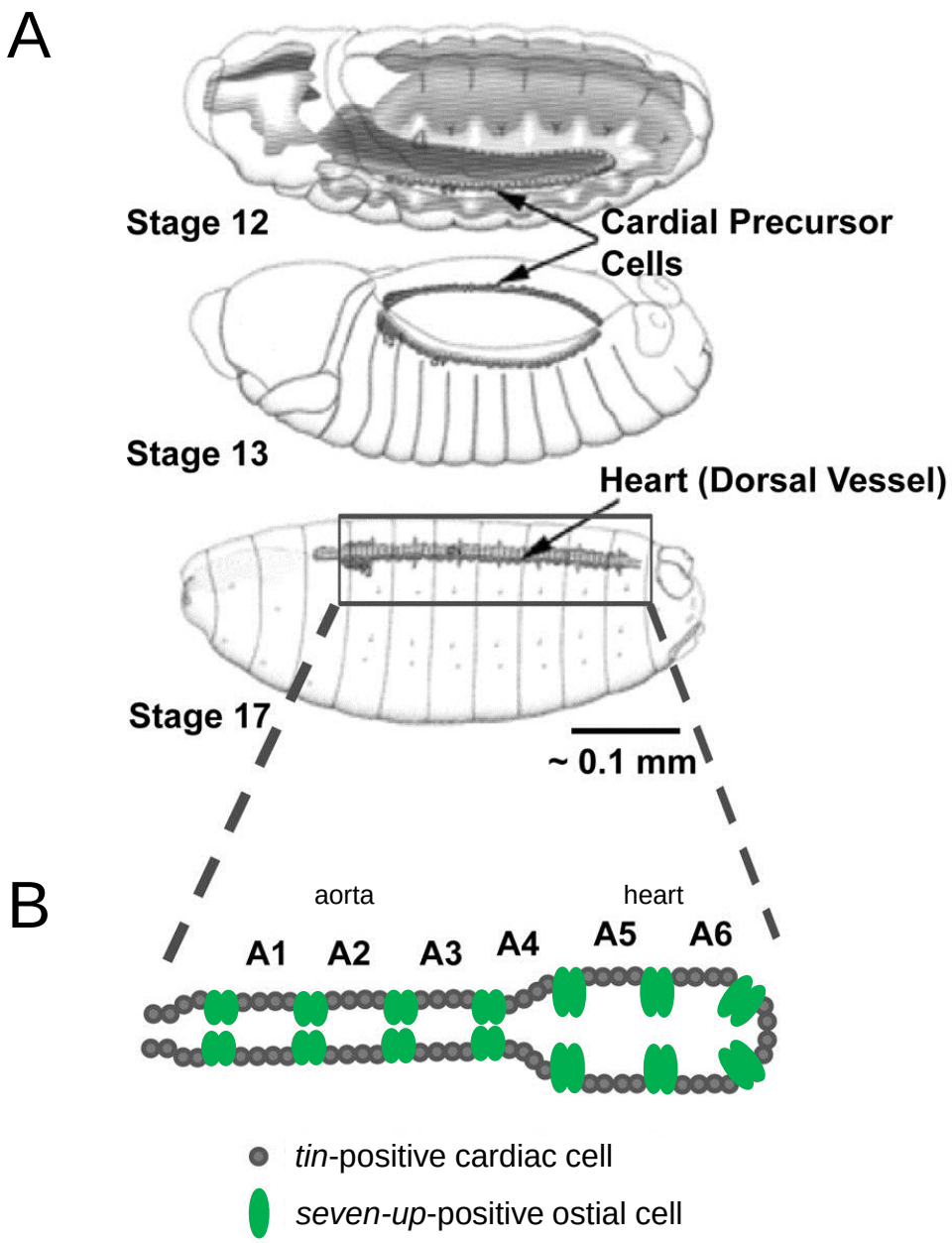

Figure 1.2. The embryonic *Drosophila* heart.
A, at around embryonic stage 12, following differentiation of the cardiac mesoderm from the visceral mesoderm, the cardiac field forms two rows of cardial precursor cells. These cells then migrate to the dorsal midline during dorsal closure (approximately embryonic stage 13-14), where they adhere to each other to form a tube with a hollow lumen (this process is completed by stage 17). Cardiomyocytes become specified – a process controlled by a cell-autonomous expression of conserved transcription factors. **B**, schematic of the embryonic heart illustrating the anterior aorta and the heart proper, with cells labelled either *tin*-positive cardioblasts or *seven-up*-positive ostioblasts – indicating the characteristics (and subsequent fate) of these of these cells. The figure is adapted from Hartenstein (HARTENSTEIN 1993), and Wolf and Rockman (WOLF and ROCKMAN 2011).

division/proliferation. Instead, the cells that make up the larval heart become hypertrophic – growing 200-500-fold (MEDIONI *et al.* 2009).

1.2.3. The adult heart forms by cardiac remodelling during metamorphosis

Unlike most of the structures and tissues of the adult fly, which are rebuilt entirely from undifferentiated larval precursor cells (THUMMEL 1996), the adult abdominal heart is formed through remodelling/reprogramming of already differentiated and functional larval cardiomyocytes (MOLINA and CRIPPS 2001; MONIER *et al.* 2005) – a process controlled by the steroid hormone ecdysone approximately 30-hr after puparium formation (APF) (ZEITOUNI *et al.* 2007). Therefore, since the effect of abnormal development can be seen in adult tissues, congenital defects can be modelled.

Most of the myogenic larval heart is destroyed by programmed cell death, with the adult heart remodelled from the posterior larval aorta – the larval anterior aorta forms the adult aorta in the thorax. The most anterior portion of the larval heart chamber differentiates into the terminal chamber (MONIER *et al.* 2005). During the cardiac remodelling process, larval aorta myocytes increase in size and myofibril number, and differentiate into functional cardiomyocytes that gain myogenic cardiac activity – i.e. the ability to rhythmically contract (ZEITOUNI *et al.* 2007). Adult cardiomyocytes exhibit characteristic transverse, spiralling myofibrils. A robust conical chamber is formed adjacent to the thorax/abdomen boundary that expels haemolymph through the aorta, proceeding through the thorax, sending nutrients towards the head. Four pairs of inflow tracts, known as ostia, differentiate from *svp*-expressing cells, while three pairs of intracardiac valve cells divide the adult heart up

into four chambers (LEHMACHER *et al.* 2012). Finally, a layer of syncytial longitudinal muscles develop from a population of cells originating from the lymph glands, and ensheathe the cardiac tube from the ventral side (SHAH *et al.* 2011). This cardiac remodelling process is illustrated in Figure 1.3.

1.2.4. The adult *Drosophila* heart

The adult *Drosophila* heart, therefore, consists of a single layer of 52 paired cardiomyocytes forming intercalated disc-like junctions between neighbouring cardiomyocytes (LEHMACHER *et al.* 2012), with myofibrils grouped in a highly regular and circular manner, which is ventrally covered in a syncytial sheet of ventral longitudinal muscle, and tethered along the midline of the dorsal cuticle by pairs of alary muscles (MILLER 1950; WOLF and ROCKMAN 2011) – illustrated in Figure 1.4. Additionally, PNs closely adhere to, and run in parallel along the length of the cardiac tube. Embryonic and larval hearts lack neural innervation, generating a completely myogenic cardiac impulse. The adult heart, however, is innervated by pairs of transverse glutaminergic nerves (DULCIS and LEVINE 2003). There are also anterior and posterior pacemakers that generate retrograde and anterograde calcium transients (LIN *et al.* 2011). This means that the heart can pump haemolymph anteriorly (i.e. towards the head), and posteriorly.

1.2.5. Pericardial nephrocytes

As mentioned previously, large pericardial nephrocytes (PNs) flank the adult *Drosophila* heart tube. At the end of cardiogenesis, there are 3 types of pericardial cells that associate with the heart: dorsal *Even-skipped* (*Eve*)/*Tinman* (*Tin*) -expressing cells, ventral *Tin*-expressing cells, and lateral *Odd-skipped* (*Odd*) -

Cardiac remodelling during metamorphosis

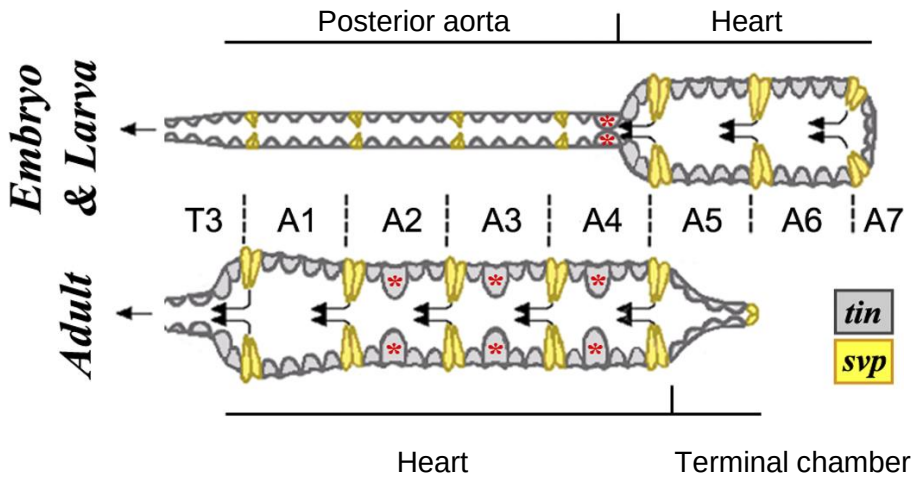

Figure 1.3. Cardiac remodelling during metamorphosis.
Schematic showing larval and adult cardiac tube. The larval heart is divided into an anterior ‘‘aorta,’’ and a posterior ‘‘heart.’’ During metamorphosis, the larval posterior aorta is remodelled, forming adult heart, while most of the larval heart is eliminated by programmed cell death. Adult ostial cells differentiate from larval *svp*-positive cells (yellow), while contractile cardiomyocytes differentiate from *tin*-positive cells (grey) in segments A1 to A4. Three pairs of intracardiac valves are formed in abdominal segments A2 to A4 (red asterisks), while segment A5 cardiomyocytes differentiate to form the terminal chamber. Heart segments A6 and A7 are eliminated by apoptosis. The figure is adapted from Zeitouni (ZEITOUNI *et al.* 2007).

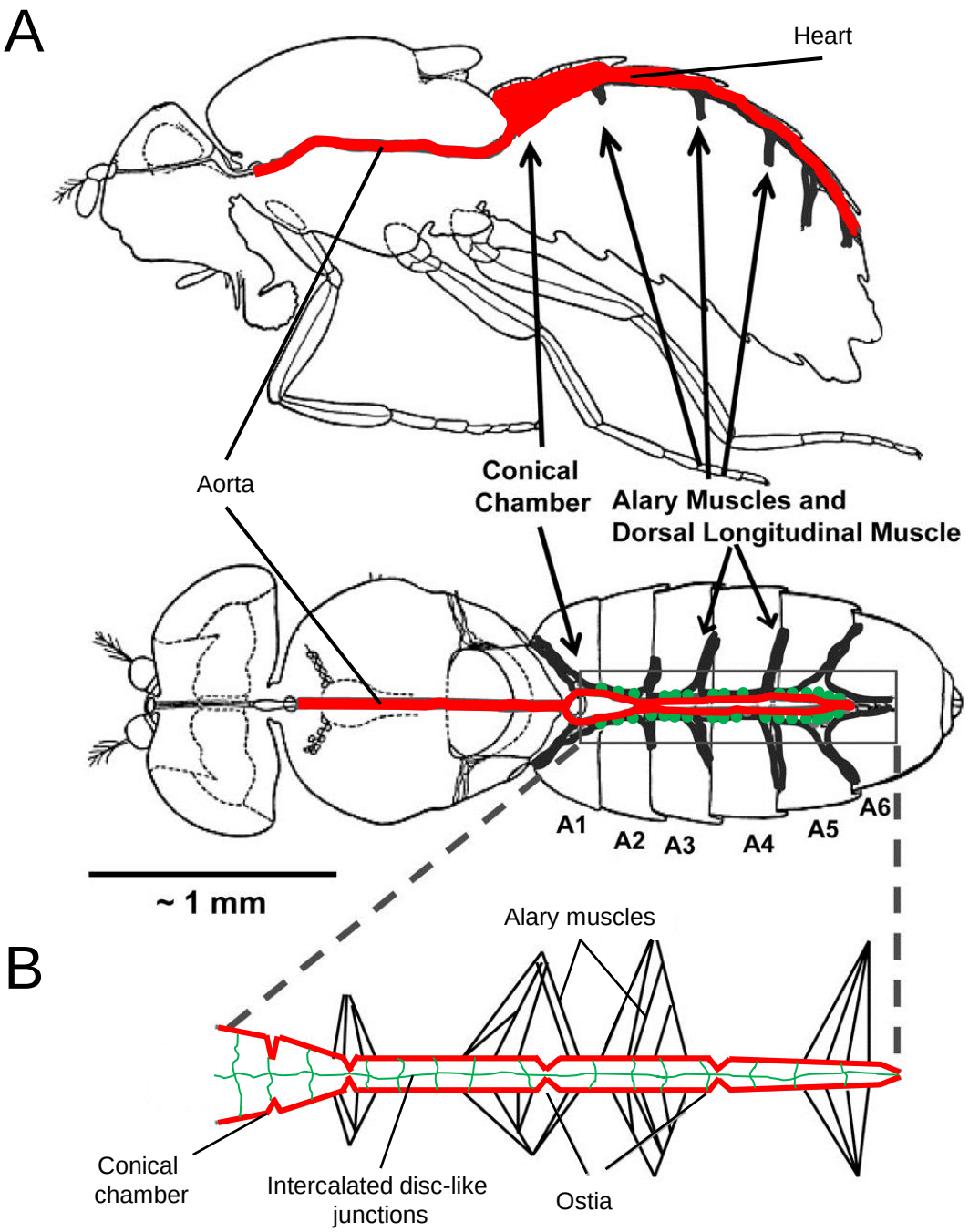

Figure 1.4. The adult *Drosophila* circulatory system.
A, parasagittal and longitudinal sections of the adult *Drosophila.* The fly heart runs along the middle of the dorsal abdominal wall, with the large conical chamber located in the A1 abdominal segment on the thorax-abdomen boundary. The abdominal heart pumps haemolymph up through the aorta (thorax) to the head. Alary muscles tether the heart tube to the dorsal abdominal wall. Pericardial nephrocytes (green) are closely juxtaposed along the length of the abdominal heart. **B**, close-up view of the cardiac tube with alary muscles, conical chamber, intercalated disc-like junctions between adjacent cardiomyocytes (green), and inflow tracts (ostia) labelled. The figure is adapted from Miller (MILLER 1950), and Wolf and Rockman (WOLF and ROCKMAN 2011).

expressing cells (WARD and SKEATH 2000). Approximately 30-36 *Odd*-expressing pericardial cells are maintained into larval and adult stages and were recently characterized as nephrocytes with similar filtration functions as mammalian glomerular podocytes (WEAVERS *et al.* 2009). In the adult *Drosophila*, PNs have been shown to function as classical nephrocytes, sequestering macromolecules from the haemolymph (DAS *et al.* 2008a). Indeed, it was recently discovered that the *Drosophila* orthologs of Cubilin and Amnionless functioned as co-receptors for protein uptake in the PNs (ZHANG *et al.* 2013). It is thought that the close proximity between the PNs and the heart allow for effective haemolymph filtration and detoxification – i.e. since these cells are attached to the beating heart they will come into contact with a higher volume of haemolymph for filtration/detoxification, as opposed to if these cells were stationary. Therefore, the PNs are incidentally involved in work in this thesis due to their position, and close adherence to the cardiac tube.

1.2.6. Heart function in *Drosophila*

Functionally, the adult *Drosophila* heart is remarkably similar to the human heart – with an average basal heart rate of around 2-2.5 Hz (120-150 bpm). There are a number of ways to measure cardiac function in *Drosophila,* and functional measurements in flies tend to focus on the more robust anterior section – this is especially true for the conical chamber region using Optical Coherence Tomography (OCT) – as it has a more robust beating movement. The following will compare the advantages and disadvantages of the 2 main methods used by *Drosophila* heart researchers to assess cardiac function in the adult fly - OCT and videomicroscopy.

1.2.6.1. Optical Coherence Tomography

Non-invasive *in vivo* measurements of heart function can be performed using OCT – an infrared-based method (a technique which has also been called 'optical ultrasound') which measures light that has scattered from the tissue being penetrated. This technique has been demonstrated, by Matthew Wolf and colleagues, as appropriate for measuring cardiac function in the adult fruit fly – with the identification of genes (including *weary*, *rhomboid-3*, and *CG3226*) important in the development of dilated cardiomyopathy (CASAD *et al.* 2012; KIM *et al.* 2010; WOLF *et al.* 2006; YU *et al.* 2010) and hypertrophic cardiomyopathy (due to aberrant *Raf* signalling) (YU *et al.* 2013). The advantages of using this system include the ability to measure heart function in live flies, non-invasively. This means that heart function could potentially be tracked over the lifespan of an individual fly. Additionally, this technique obviates the need for the fly to be cut open to visualise the beating heart – thereby preventing any loss of internal haemolymph pressure potentially important for maintaining homeostasis, or unintended damage to the heart due to adjacent organ removal. OCT may be somewhat limited in its spatial resolution, but this non-invasive technique makes it useful for high throughput screening (OCORR *et al.* 2007b; WOLF and ROCKMAN 2011).

1.2.6.2. Videomicroscopy

The other main technique used to measure heart function in adult *Drosophila*, and the technique that will be utilised in this thesis, is videomicroscopy – a method established by Rolf Bodmer and colleagues. This method, illustrated in Figure 1.5, involves visualising the adult fly heart then video-recording of heart function down a

Measuring adult *Drosophila* heart function

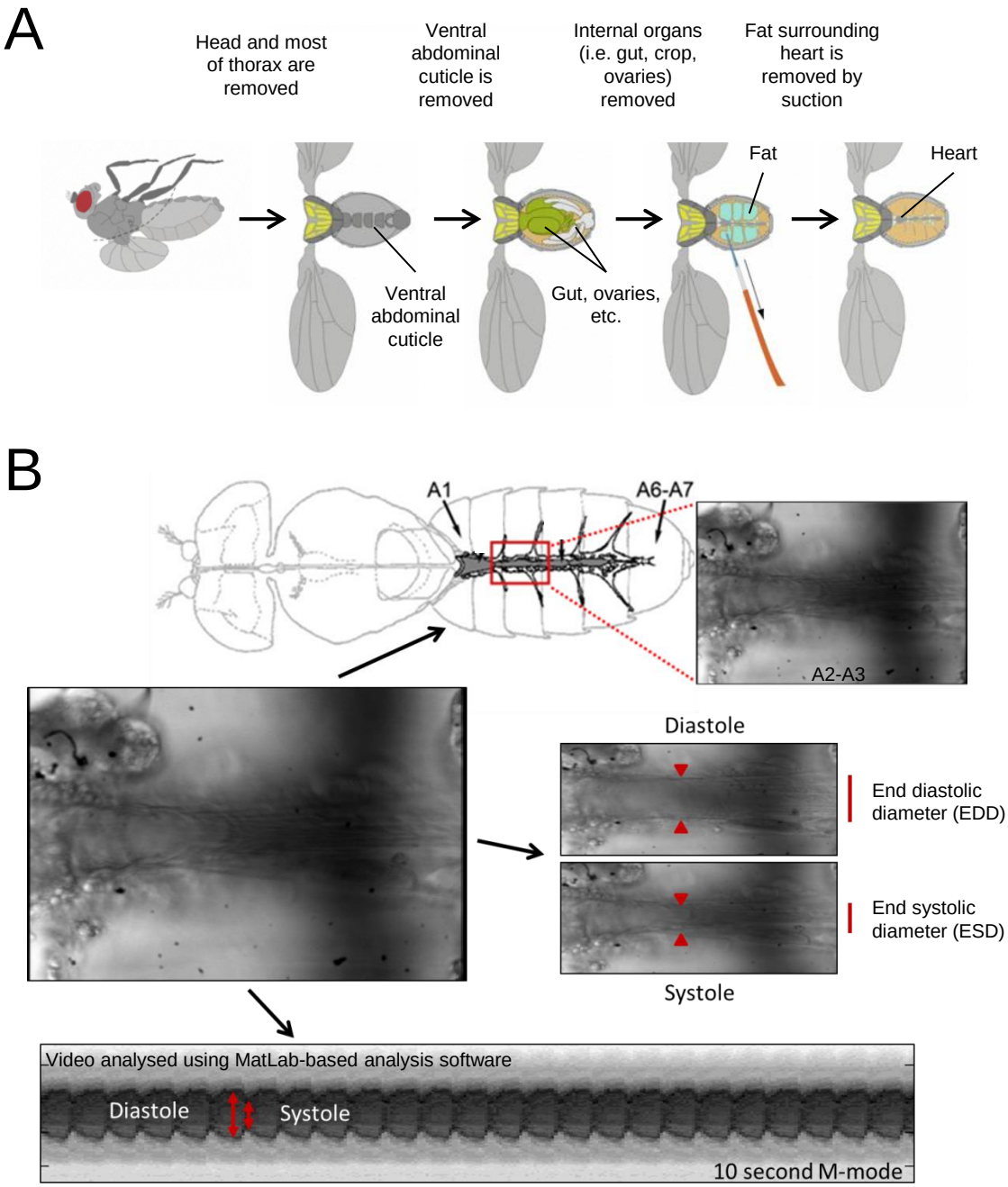

Figure 1.5. Measuring heart function in the adult *Drosophila*.
A, the head, thorax, and ventral abdominal cuticle are removed. Then the internal organs (including gut, crop, ovaries etc) are removed to visualise the beating heart. Finally, fat surrounding the heart (which can affect heart analysis) is sucked off using a microcapillary tube – the heart is now ready to be recorded **B**, video recordings are made around the A2-A3 abdominal section. Videos are then analysed using MatLab-based analysis software developed specifically for fly heart analysis. Output parameters include heart rate, heart period, systolic/diastolic interval, fractional shortening, and arrhythmicity index. The figure is adapted from Miller (MILLER 1950), and Vogler and Ocorr (VOGLER and OCORR 2009).

microscope (VOGLER and OCORR 2009). This invasive method is terminal for the fly, and involves cutting the fly open, removing internal organs and fat for visualisation of the beating heart attached to the dorsal cuticle – a procedure which can take as little as 2 minutes to perform. The fly heart can beat myogenically in artificial haemolymph for many hours – allowing subsequent microscopic analysis. Video analysis is performed by a MatLab based software designed specifically to analyse fly heart function (OCORR *et al.* 2009). Output parameters using this software include heart rate, heart period, systolic/diastolic interval, fractional shortening, and arrhythmicity index – making this method of heart analysis highly informative. Similarly, end diastolic/systolic diameters (EDD/ESD) can be measured – similar to OCT. This technique is a proven method of fly heart analysis and has been crucial in the identification of evolutionarily conserved genes important for human heart function – including *not3* (NEELY *et al.* 2010b), *Dscam* and *Col6a2* (GROSSMAN *et al.* 2011), *Unc-45* (MELKANI *et al.* 2011), *pannier* (QIAN and BODMER 2009), *neuromancer* (QIAN *et al.* 2008), *Mlp84B* (MERY *et al.* 2008), and *Kcnq* (OCORR *et al.* 2007c). Similarly, this technique has been used to elucidate conserved mechanisms of heart function in *Drosophila* models of ageing (TAGHLI-LAMALLEM *et al.* 2008; WESSELLS *et al.* 2009; WESSELLS *et al.* 2004), obesity (BIRSE *et al.* 2010), and diabetes (LIM *et al.* 2011; LUONG *et al.* 2006; NA *et al.* 2013). The advantages of using this system include the large volume of data that can be obtained from the analysis software, with each parameter providing subtly different information about the health of the heart – i.e. some values such as heart rate may be normal in mutants, while others such as degree of arrhythmicity may not. From a technical perspective, this method also allows functionally-analysed hearts to be used

directly for immunostaining – meaning staining/morphological measurements can be directly correlated with function – whereas with OCT, both analysis and immunostaining would be performed separately. A potential caveat of this method is the potential difference in heart function between live flies - i.e. *in vivo* using OCT – and flies that have been splayed apart to view the heart in an *in situ* semi-intact heart preparation. Indeed, heart rate appears to be faster in *in vivo* (OCT) measurements compared to semi-intact preparations – e.g. 4-5 Hz vs. 2-3 Hz (VOGLER and OCORR 2009; WOLF and ROCKMAN 2011).

1.3 Genetic tools available in *Drosophila*

The success of *Drosophila* as a model organism can be attributed to the availability of a variety of genetic tools which make it possible to perform large unbiased forward genetic screens thereby identifying genetic interactions involved in biological processes (ST JOHNSTON 2002). The genetic screen - which aims to identify genes involved in a given biological process - is one of the tools that sets *Drosophila* apart from higher eukaryotic model organisms, and has a successful history. One of the most famous examples is the Nobel Prize-winning 'Heidelberg screen' that described mutations affecting body patterning in the *Drosophila* embryo (NUSSLEIN-VOLHARD and WIESCHAUS 1980; NUSSLEIN-VOLHARD *et al.* 1984). This screen was revolutionary because it was the first mutagenesis in any multicellular organism that aimed to identify most or all of the mutations that affected a given process – as opposed to discovering new alleles of existing genes, or identifying how many genes were in a particular genome region (ST JOHNSTON 2002). By its design, this screen would not have identified genes essential for internal patterning, such as

the nervous system, since this was not the structure being screened; or maternal-effect genes – i.e. genes which are pre-loaded into the egg during oogenesis (NUSSLEIN-VOLHARD *et al.* 1987; SCHUPBACH and WIESCHAUS 1986).

During the early years of *Drosophila* research, scientists were mainly focussed on isolating naturally occurring mutations that exhibited scorable phenotypes. Starting with the Nobel prize-winning discovery by Hermann Muller that genetic mutations in *Drosophila* could be induced by X-rays (MULLER 1927), other techniques were also developed to induce mutations into the *Drosophila* genome – these included ethyl methane sulphonate- (EMS), and P-element transposon-mutagenesis (BELLEN *et al.* 2010).

EMS causes very high mutational frequencies, and feeding it to flies makes EMS-mutagenesis more efficient than other methods of mutagenesis – e.g. P-element transposition. The nature of EMS as a mutagen means it mostly leads to single base pair changes (i.e. point mutations) that cause missense or nonsense mutations (ST JOHNSTON 2002). The problem with this mutagenesis is the difficulty in mapping these single base pair changes to specific genes – however, the establishment of single nucleotide polymorphism (SNP) maps will help (BERGER *et al.* 2001).

1.3.1 P-element mutagenesis

P-element transposons are mobile genetic elements found naturally in the *Drosophila* genome. When induced to transpose, their insertion into a gene can result in mutation of this gene, with loss-of-function possible. One of the advantages of this mutagenesis technique is that mutated genes can be ‘tagged’ by the marker-containing P-element (RUBIN and SPRADLING 1982). A caveat of this technique is

that some parts of the genome are hot/cold spots for P-element insertion. However, the number of genes having P-element (or equivalent) insertions is constantly growing and at present covers two-thirds of all annotated *Drosophila* protein-coding genes (BELLEN *et al.* 2011). P-element insertions often result in hypomorphic mutations due to insertion site frequently occurring near or within promoter regions (SPRADLING *et al.* 1995). These alleles can be useful for the study of a particular gene's function, but it is usually advantageous to have a complete loss-of-function allele. Thankfully, existing P-element insertions can be used to generate new mutations close to the original insertion after subsequent mobilisation by a transposase source – most often Δ2-3 transposase. Imprecise excision mutagenesis snips the P-element from the genome, while also potentially removing genome sequences that flanked its original position. This method allows for targeted gene disruption and is useful for the generation of null mutants (ADAMS and SEKELSKY 2002; VOELKER *et al.* 1984). P-element excision mutagenesis is illustrated in Figure 1.6.

1.3.2 The GAL4/UAS system

A more sophisticated method of targeted gene expression came in the form of the GAL4/UAS system (BRAND and PERRIMON 1993). In principle, the yeast transcription factor, GAL4 protein, binds to the Upstream Activation Sequence (UAS) and promotes transcription of the gene of interest located downstream of the UAS – illustrated in Figure 1.7. The yeast *Gal4* gene has been inserted nearby a number of genomic enhancers – known as "enhancer trapping" – which allows the expression of the GAL4 protein, and hence transcription of the gene of interest, in a tissue-specific manner. Ectopic overexpression of the gene of interest in specific

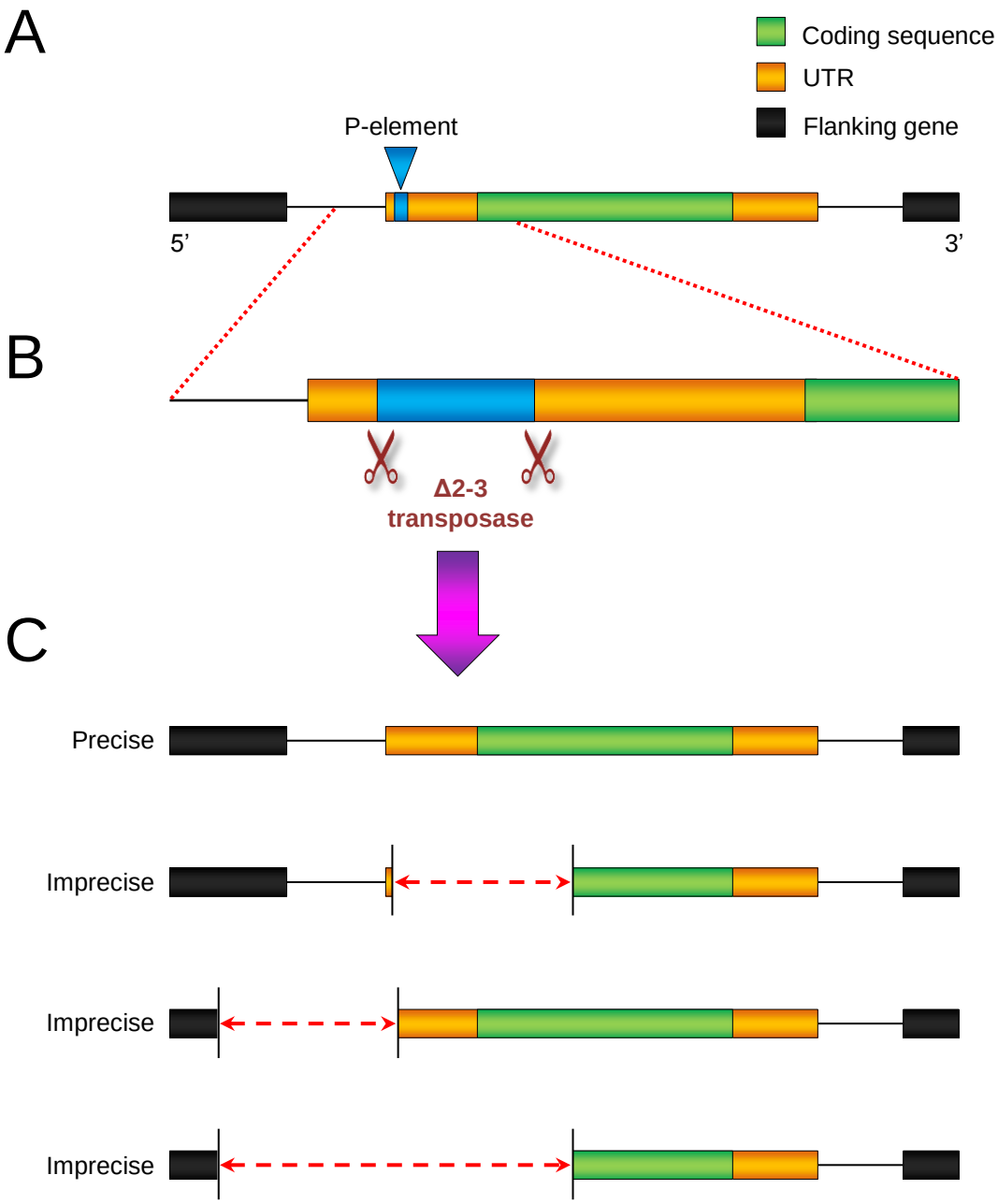

Figure 1.6. P-element excision mutagenesis.
A, a P-element construct (blue) is inserted into a genomic location in/near a target gene. In this case, the P-element is inserted into the 5' untranslated region (UTR). **B**, Δ2-3 P-transposase catalyses excision of the element. **C**, several possible repair products are represented. Homology-directed repair from the homologous chromosome can generate a 'precise excision'. Three different 'imprecise excision' events – i.e. small deletions that extend in one or both directions - are illustrated.

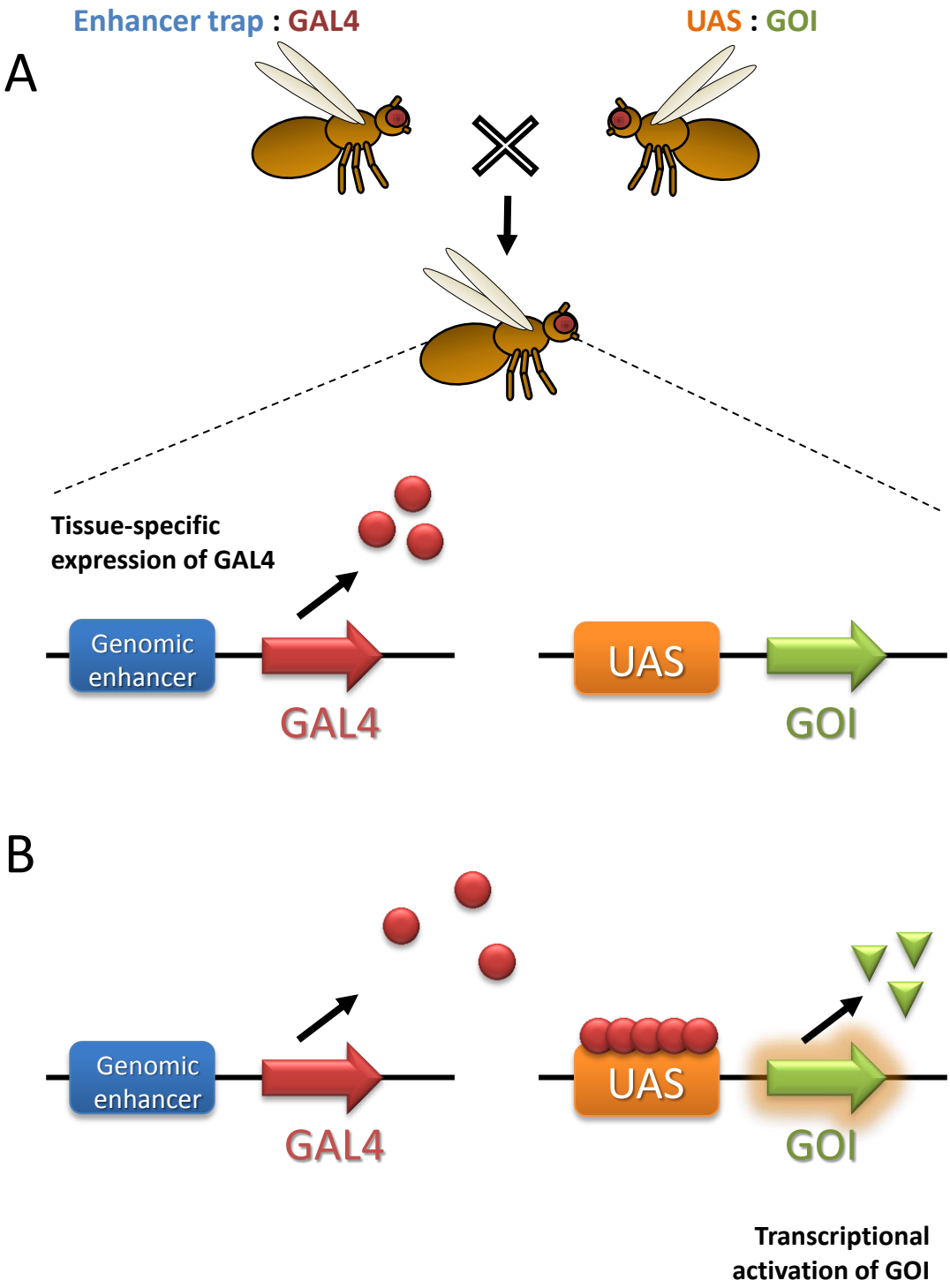

Figure 1.7. Directed gene expression using the GAL4/UAS binary system.
A, directed gene expression is achieved by crossing flies containing the GAL4 transcription factor under the control of a tissue-specific promoter, with flies that have an **U**pstream **A**ctivation **S**equence (UAS) inserted upstream of the gene of interest (GOI). **B**, the resulting progeny express GAL4 which now binds to the UAS and therefore expresses the GOI in a tissue-specific manner.

tissues is achieved by crossing the relevant enhancer trap GAL4 line, with transgenic flies which harbour a yeast-specific UAS sequence in front of the gene of interest.

The GAL4/UAS system has become a powerful tool for performing genetic screens where the ectopic expression of the gene of interest in a particular tissue results in a scorable phenotype (RORTH 1996; RORTH *et al.* 1998). The rigidly structured compound adult *Drosophila* eye has been widely utilised as a tissue for scoring phenotypes, and has well characterised signalling events controlling eye formation. Disruption of this process by ectopic gene expression, can lead to aberrant eye phenotypes without affecting overall viability. This type of genetic screen can offer clues about the function of the gene in question and its involvement in the formation of the eye. Additionally, it is possible to perform screens whereby modifiers of a particular aberrant eye phenotype can be identified. In other words, mutations in other genes may act as "suppressors" or "enhancers" of the phenotype caused by the ectopic gene expression in the eye. This allows for the identification of novel genetic interactions (MUKHERJEE *et al.* 2005).

1.3.3 Transgenic RNA interference (RNAi) in *Drosophila*

The discovery of gene silencing using double stranded RNA in the *C. elegans* (FIRE *et al.* 1998), led researchers to develop this gene targeting system in *Drosophila*. A major advantage of RNAi knockdown in *C. elegans* is that genetic knockdown in occurs by feeding on dsRNA-expressing bacteria. However, gene inactivation is ubiquitous using this method, and knockdown cannot be restricted to certain cell types. In the fruit fly, transgenic RNAi is cell-autonomous, and so targeted expression via the GAL4/UAS system can be useful for cell- or tissue-

specific assessment of gene function (PERRIMON *et al.* 2010). In *Drosophila*, transgenic constructs containing gene fragments 'inverted repeats' which form hairpin RNAs (hpRNA) after transcription and are driven by the GAL4/UAS system. These double-stranded RNAs (dsRNA) are then processed by the Dicer protein into small interfering RNAs (siRNA) which direct sequence-specific degradation of endogenous target mRNA. This process is illustrated in Figure 1.8. The generation of RNAi libraries under the control of the GAL4/UAS system was a major development and allowed researchers to perform precise genome-wide RNAi screens in their tissue of choice – unlike in *C. elegans* where gene inactivation is ubiquitous (DIETZL *et al.* 2007; NI *et al.* 2008). Since then, a number of genome-wide transgenic RNAi screens have been performed in *Drosophila* investigating medically-relevant topics including obesity (POSPISILIK *et al.* 2010), conserved regulators of heart function (NEELY *et al.* 2010b), susceptibility to bacterial infection (CRONIN *et al.* 2009), notch signalling (MUMMERY-WIDMER *et al.* 2009), pain perception (NEELY *et al.* 2010a), neural stem cell self-renewal (NEUMULLER *et al.* 2011), and Parkinson's disease (FERNANDES and RAO 2011).

A limitation of some of the currently available transgenic RNAi lines is the inherent problem of false discovery (MOHR and PERRIMON 2012) – i.e. false positives and false negatives – highlighted by meta-analyses which reveal poor reproducibility among related screens (BUSHMAN *et al.* 2009; MULLER *et al.* 2008). False-positives are mostly due to off-target effects (OTEs), which occur when transcripts other than the intended target are recognised by the RNAi, and are degraded. However, this problem has been largely addressed by the careful design of RNAi constructs using algorithms designed to avoid sequences that have "19 or more

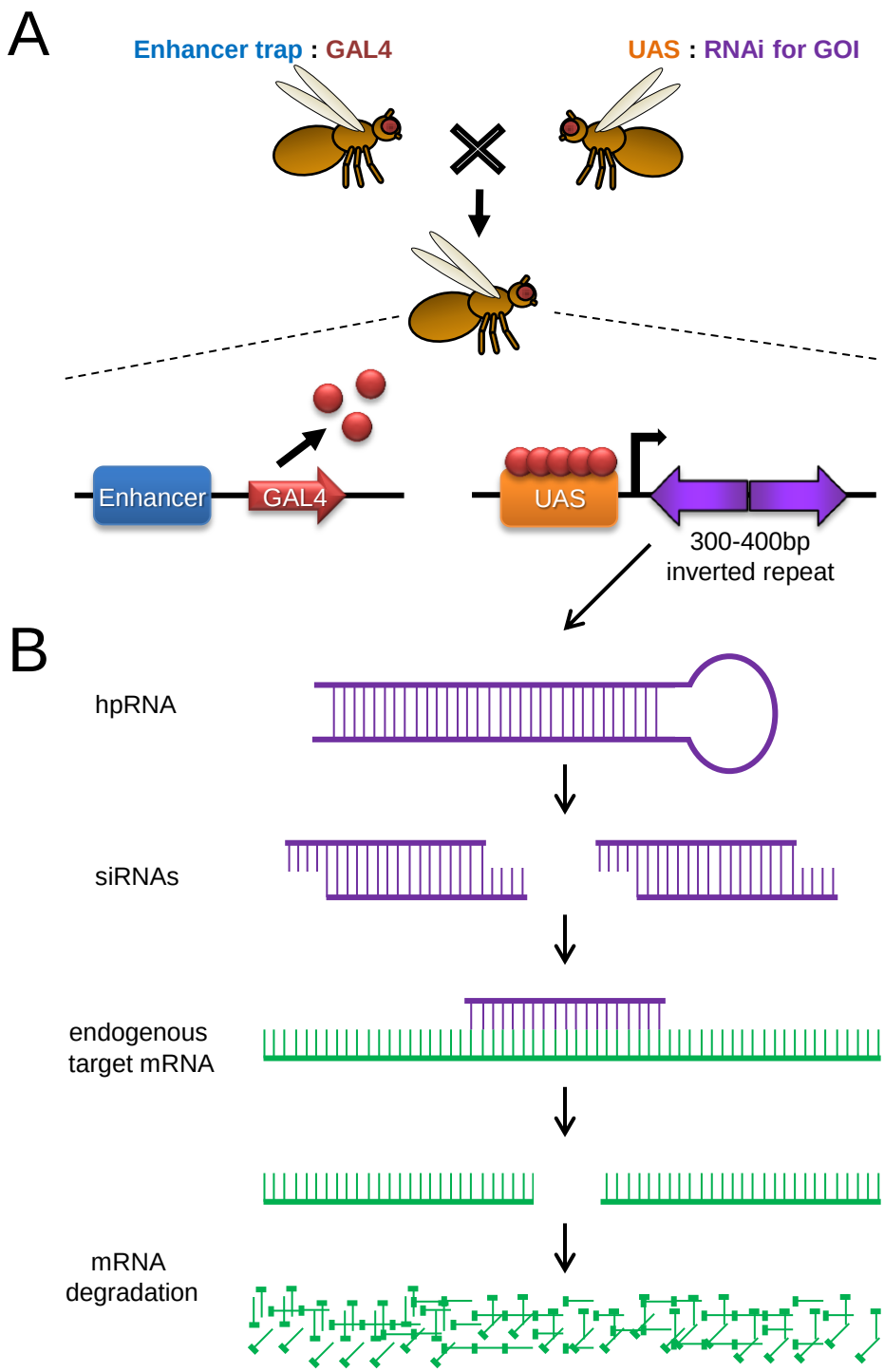

Figure 1.8. Transgenic RNAi expression in *Drosophila*.
A, tissue-specific RNAi expression for the gene of interest (GOI) is achieved by GAL4/UAS system. Each RNAi line contains a GOI fragment cloned as an inverted repeat which forms a double-stranded hairpin RNA (hpRNA) when transcribed. **B**, hpRNAs are processed by Dicer into siRNAs which direct sequence-specific cleavage of endogenous target mRNA. This is then followed by degradation of the endogenous target mRNA – thus preventing mRNA translation and inhibition of gene expression.

base pairs of contiguous nucleotide identity to another mature transcript" as 19-mers can induce target RNAi knockdown (MOHR and PERRIMON 2012). Additionally, OTEs can also be caused by shorter perfect/imperfect matches to other mRNA sequences, akin to microRNA having multiple targets. Further work in this area is continuing and will ultimately lead to more effective reagent design and accurate RNAi knockdown.

1.4 The Kindlin family

The Kindlin family of cell adhesion proteins (known as Fermitins in *Drosophila*) are evolutionarily conserved from worms to humans (ROGALSKI *et al.* 2000; WHITE and MCLEAN 2005), and are involved in integrin activation and cell-matrix adhesion (LARJAVA *et al.* 2008). In humans, the Kindlin family comprises 3 members – Kindlin 1, an epithelial-specific Kindlin associated with the skin-blistering genetic disorder Kindler syndrome (SIN *et al.* 2011); Kindlin 2, the ubiquitous Kindlin that is highly enriched in smooth/striated muscle (including cardiac tissue) (DOWLING *et al.* 2008a; MONTANEZ *et al.* 2008); and Kindlin-3, found to be present in haematopoietic and endothelial cells (BIALKOWSKA *et al.* 2010; USSAR *et al.* 2006). Pull-down assays with cytoplasmic β-integrin tails have shown that the core binding sites for kindlins is the membrane-distal NxxY motif (KARAKOSE *et al.* 2010). A large number of proteins have been shown to interact with the cytoplasmic tails of β-integrins, but before the discovery of kindlins, talin was the only protein demonstrated to trigger integrin activation (TADOKORO *et al.* 2003) – illustrated in Figure 1.9A.

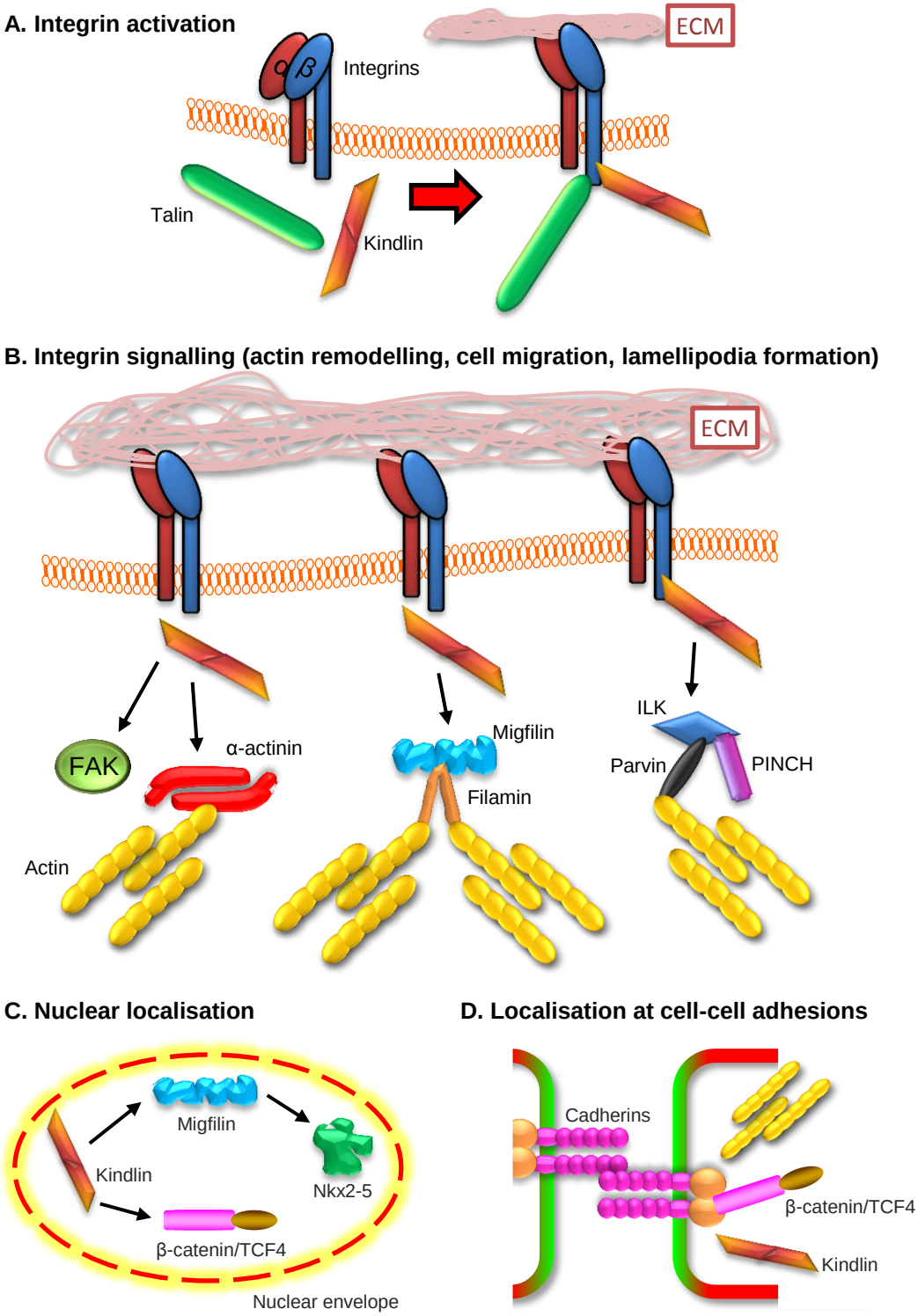

Figure 1.9. Kindlin-2-interaction partners and subcellular localisation.
A+**B**, upon integrin activation, Kindlin-2 (in conjunction with Talin) connect integrins to the cytoskeleton (via a variety of Kindlin-2 binding partners including ILK/PINCH/Parvin complex, Migfilin/Filamin, and FAK/α-actinin), triggering biochemical signalling. **C**, both Kindlin-2 and Migfilin can also function in the nucleus. Kindlin-2 can form a tripartite transcriptional complex with β-catenin and TCF4, while Migfilin can initiate cardiac differentiation by forming a transcriptional complex with the heart transcription factor, Nkx2-5. **D**, Kindlin-2 can also localise to cell-cell junctions, where it is thought to associate with the cadherin-binding protein, β-catenin. The figure is adapted from Karaköse *et al*. (KARAKÖSE *et al*. 2010).

1.4.1. Kindlin-2 and its role in integrin signalling

Kindlin-2 was the first kindlin family member to be associated with integrin-based adhesion. Studies in *C. elegans* identified UNC-112 (UNCoordinated), the nematode ortholog of kindlin-2, that co-localised with integrins at cell-matrix adhesion sites, while mutations in UNC-112 led to abnormal dense body and M-line formation – i.e. the worm equivalents of costameres and intercalated discs (ROGALSKI *et al.* 2000). Upon integrin activation, kindlins localise at adhesion sites and connect integrins to the actin cytoskeleton via different pathways (BOTTCHER *et al.* 2009). Talin and Kindlin cooperate to activate integrins, but the exact sequence of events that lead to integrin activation (i.e. sequential binding? Simultaneous binding? Binding to separate β-integrin tails then clustering?) is still to be determined (MOSER *et al.* 2009). Although the underlying mechanisms behind integrin signalling are still not fully understood, it has been shown that Kindlin-2 may mediate linkage between integrins and the actin cytoskeleton by binding to other adapter/signalling proteins including ILK (MACKINNON *et al.* 2002), Migfilin (TU *et al.* 2003), Focal Adhesion Kinase (FAK), α-actinin (HAS *et al.* 2009), and β-catenin (YU *et al.* 2012) – illustrated in Figure 1.9B. It is possible Integrin-linked kinase (ILK) and Migfilin act as a relay via interactions with their binding proteins including PINCH and Parvin (CHISWELL *et al.* 2008), and Filamin and Vasodilator-Stimulated Phosphoprotein (VASP) (ZHANG *et al.* 2006), respectively. Indeed, Kindlin-2 co-localises with ILK and Migfilin at focal adhesion sites, while *Kind-2* depletion disrupts ILK recruitment to these cell adhesions (MONTANEZ *et al.* 2008).

1.4.2. Additional putative roles for Kindlin-2 in the cell

1.4.2.1. Cell-cell adhesion

Interestingly, Kindlins are not exclusively found at integrin-based cell-extracellular matrix (ECM) adhesion sites. Indeed, Kindlin-2 also co-localises with cadherin-based cell-cell adhesion sites along the lateral and apical plasma membrane of keratinocytes (LAI-CHEONG *et al.* 2008; USSAR *et al.* 2006). This localisation may indicate a role for Kindlin-2 in the establishment or maintenance of cell-cell adherens junctions. In agreement with this, Kindlin-2 was also found localised at adherens junctions in the colon and heart (DOWLING *et al.* 2008a; USSAR *et al.* 2008). The cadherin intracellular tail is associated with several proteins such as catenins (α and β), α-actinin and Vinculin – these proteins are important for signalling and establish a link to the actin cytoskeleton (NAGAFUCHI 2001). It is currently not known how Kindlin-2 is recruited to cell-cell adherens junctions, but a recent study has linked Kindlin-2 with the multifunctional cadherin-binding protein β-catenin (NELSON 2008; YU *et al.* 2012). In this study, Yu and colleagues demonstrated that Kindlin-2 formed a complex with activated β-catenin *in vivo* and stabilised the active form of β-catenin, preventing it from GSK-3β-mediated degradation. Therefore, this study indicates Kindlin-2 may act as an important mediator linking integrin-based cell-ECM adhesion and cadherin-based cell-cell adhesion – illustrated in Figure 1.9D.

1.4.2.2. Transcriptional activator

Wnt signalling requires the translocation of β-catenin to the nucleus for the activation of target genes by the formation of a transcriptional complex with TCF4. Yu and colleagues also identified a new role for Kindlin-2 as an activator of

transcription (YU *et al.* 2012) – illustrated in Figure 1.9C. Kindlin-2 was found to form a tripartite complex with β-catenin and TCF4, which could subsequently activate transcription. This paper demonstrates that Kindlin-2 can shuttle to and from the nucleus, and highlights the different roles Kindlin-2 performs within the cell. Kindlin-2 was previously shown to be present in the nuclei of cancerous smooth muscle cells (KATO *et al.* 2004), gastric cancer (SHEN *et al.* 2012), and the invasion front of malignant mesothelioma – where it was also noted to have significant nuclear localisation (AN *et al.* 2010). Additionally, it was previously shown that Migfilin, a Kindlin-2 binding partner, localises to the nucleus in a Ca^{2+}-dependent manner and regulates transcription (WU 2005). Interestingly, Migfilin can translocate to the nucleus where it forms a complex with the cardiac transcription factor Nkx2-5, and promotes cardiac differentiation via transcriptional activation of cardiac-specific genes (AKAZAWA *et al.* 2004).

1.4.3. The role of Kindlin-2 in the heart

Findings from several animal models suggest that the formation of intercalated discs may require integrins and integrin binding proteins (EHLER *et al.* 2001; KNOLL *et al.* 2007; PERRIARD *et al.* 2003; SHAI *et al.* 2002; WHITE *et al.* 2006). A clearer understanding of the role of these proteins is important because mutations and polymorphisms that affect intercalated disc formation may be associated with the development of cardiomyopathies in humans (BASSO *et al.* 2006; PERRIARD *et al.* 2003; VASILE *et al.* 2006).

Mouse KIND2 protein is enriched at intercalated discs, however genetic ablation of *Kind2* in mice causes early embryonic lethality at the peri-implantation

stage, before cardiogenesis (DOWLING *et al.* 2008a; MONTANEZ *et al.* 2008). In zebrafish, the global knock-down of *Kind2* causes cardiac hyperplasia, disrupts intercalated disc formation and significantly reduces cardiac contractility (DOWLING *et al.* 2008a). Since mechanical coupling between integrins and the contractile apparatus appears to be essential for normal muscle function, the muscle defects observed in the absence of kindlin-2 highlight the requirement for kindlin-2 in connecting integrins to the actin cytoskeleton. These findings link *Kind2* with the development of a functional cardiac syncytium; however a cardiomyocyte-specific test of this hypothesis is yet to be conducted.

Drosophila expresses two orthologs of human KIND2, *Fermitin1* (*Fit1*) and *Fermitin2* (*Fit2*) that contain a highly conserved FERM domain which is required for binding to the cytoplasmic tail of β-integrins (SHI *et al.* 2007). Both *Fit1* and *Fit2* message and protein are detected in adult heart tissue, consistent with a role in cardiac function (CAMMARATO *et al.* 2011; CHINTAPALLI *et al.* 2007). Additionally, the Fermitins have been identified in RNAi screens as important for muscle assembly (BAI *et al.* 2008) and heart development in the *Drosophila* embryo (KIM *et al.* 2004). However, the function of these proteins has not been elucidated. It would be hypothesised that disruption of cardiomyocyte *KIND2* may lead to abnormal intercalated discs and cardiomyopathies in humans.

1.5 Cell adhesion in *Drosophila*

Cell adhesion plays an essential role during the development and adult life of multicellular organisms. There are two main forms of adhesion that can be distinguished: cell-cell adhesion – i.e. adhesion between cells; and cell-ECM

adhesion – i.e. adhesion between cells and the extracellular matrix. Cell-ECM-cell adhesion has also been identified, however (BROWN 2011). These different modes of cell adhesion are illustrated in Figure 1.10. In cell-cell adhesion, the canonical receptors linking neighbouring cells are cadherins, which can bind to cadherins on adjacent cells via homodimerisation of their extracellular domains (HARRIS and TEPASS 2010). In cell-ECM adhesion (and cell-ECM-cell adhesion), heterodimeric integrin receptors bind specific ECM proteins (BARCZYK *et al.* 2010). Interestingly, integrins have also been implicated in cell-cell adhesion (ESTRADA *et al.* 2007).

The utilisation of *Drosophila* to model aspects of cell adhesion has the advantage of the smaller number of adhesion genes relative to vertebrates – making the complete removal of the function of a particular type of protein more straightforward. There are 3 classical cadherins (E-cadherin and two N-cadherins), and 7 integrins (5 α-integrin subunits (αPS1-5) and 2 β-integrin subunits (βPS and βν)) in *Drosophila* (HILL et al. 2001; LEGATE et al. 2006), compared to 4 classical cadherins and 26 integrins (18 α-integrin subunits and 8 β-integrin subunits) in humans (GOODMAN and PICARD 2012; HYNES 2002). Cadherins and integrins recruit cytoplasmic proteins and assemble into adhesion complexes linking their large extracellular domains with the intracellular actin cytoskeleton – in *Drosophila*, the number of genes encoding each cadherin/integrin-binding protein is also fewer compared to vertebrates (e.g. 1 fly talin compared to 2 human talin proteins) (BROWN *et al.* 2002).

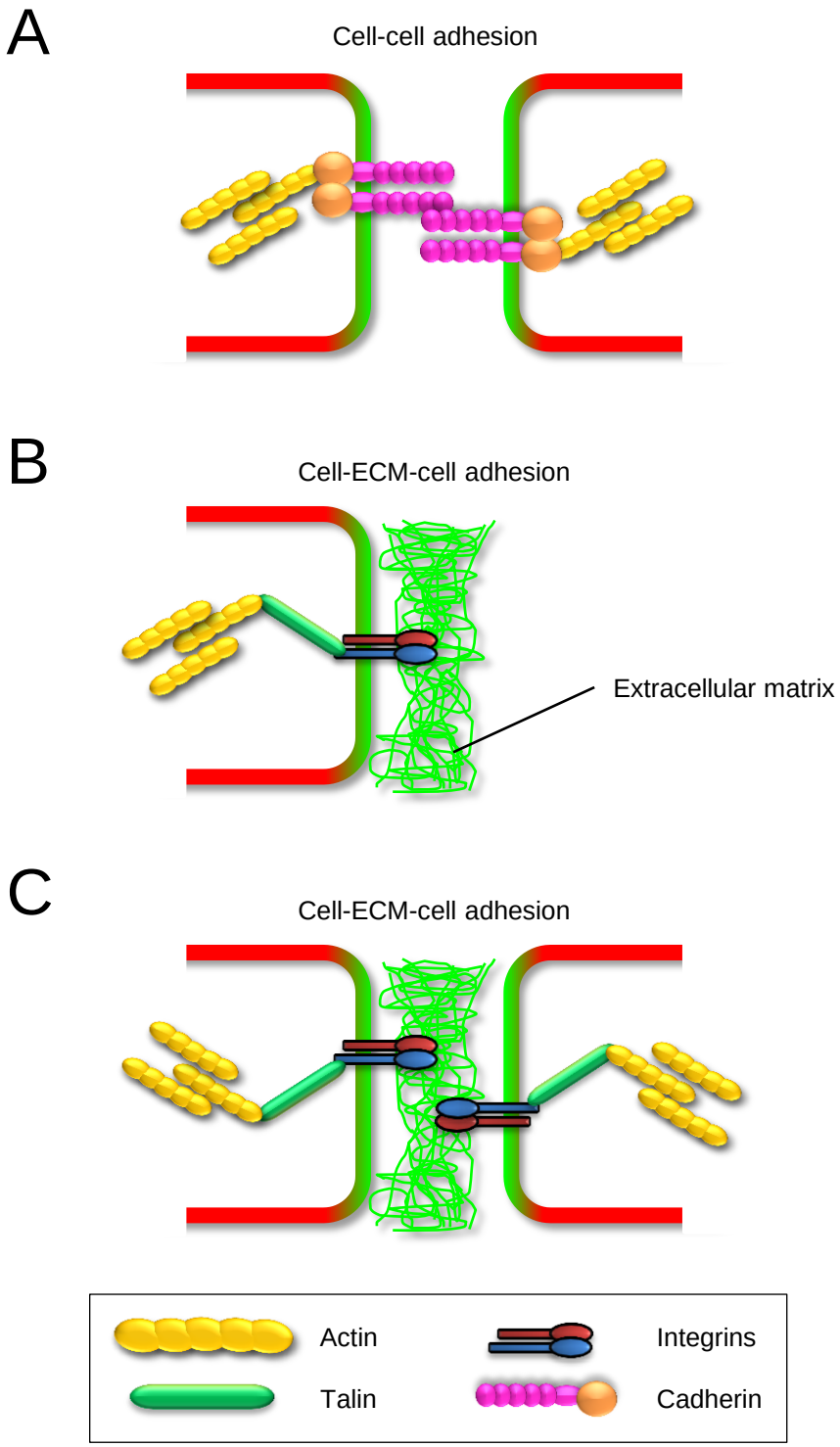

Figure 1.10. Types of cell adhesion in *Drosophila*.
There are three mechanisms of cell adhesion that form between adjacent cells in *Drosophila*. **A**, cadherin-based cell-cell adhesion. **B**+**C**, integrin-based cell-ECM and cell-ECM-cell adhesion.

1.5.1. Cadherin-based cell-cell adhesion

Cadherins have been identified in studies on vertebrates and *Drosophila* as essential molecules responsible for the formation of adherens junctions (AJ) – i.e. a cell junction which is anchored to the actin cytoskeleton (ODA and TAKEICHI 2011). Cadherins are transmembrane molecules that contain large distinctive extracellular repeat domains, and a cytoplasmic region that binds p120-catenin and β-catenin/Armadillo (arm) at distinct regions. p120-catenin helps stabilise cadherins at the cell membrane, and β-catenin links cadherins with the actin cytoskeleton via α-catenin – both essential for AJ function (BULGAKOVA *et al.* 2012). In *Drosophila*, cadherins are not only required for static cell-cell adhesion, but also for regulating dynamic morphogenetic processes including embryogenesis (HARRIS and TEPASS 2010; NISHIMURA and TAKEICHI 2009). AJ cadherins were the first members of the cadherin family to be identified and have been called classical cadherins. Most classical cadherins function as receptors that form homodimers and mediate cell-cell recognition and adhesion. However, there also exist atypical cadherins including Flamingo, Daschous, and Fat - all involved in planar cell polarity and growth regulation (HALBLEIB and NELSON 2006). The common thread linking all cadherins is their ability to form homophilic or heterophilic interactions with other cadherin proteins – resulting in a variety of cellular events including adhesion, and signalling (ODA and TAKEICHI 2011).

1.5.2. Integrin-based cell-ECM(-cell) adhesion

Members of the integrin family of transmembrane receptors mediate adhesion between neighbouring cells and the ECM (BOKEL and BROWN 2002; BROWER 2003;

DE ARCANGELIS and GEORGES-LABOUESSE 2000). Unlike homodimeric cadherin proteins, each integrin consists of a heterodimer of one α and one β subunit. The integrin heterodimer complex is a transmembrane glycoprotein with large extracellular domains – that bind to ECM proteins - and short cytoplasmic tails – that form complexes with intracellular adhesion proteins (BROWN 2011; HYNES 2002). Integrins mediate fundamental cellular process including cell adhesion, outside-in/inside-out signalling, and cell migration. For stable cell adhesion to their substrate, integrins provide a physical link between the ECM and the actin cytoskeleton. Integrins can act as signalling receptors relaying information from the exterior to the interior (and *vice versa*), thereby influencing transcription – resulting in growth, differentiation, or survival signals (GIANCOTTI and RUOSLAHTI 1999; MIRANTI and BRUGGE 2002). The subunits of *Drosophila* integrins are highly similar to those of vertebrates, with strong structural conservation likely derived from the specific "intrasubunit and intersubunit interactions that underlie the exquisite bidirectional signalling properties of intact heterodimers" (BROWER 2003; HYNES 2002).

1.5.3. Using *Drosophila* to elucidate cell-adhesion mechanisms

Mutation of the genes encoding the three primary *Drosophila* integrin subunits (αPS1, αPS2 and βPS) has allowed scientists to decipher the properties of these proteins (and their binding partners) in an effort to answer fundamental questions relating to cell adhesion. Indeed, there are two developing *Drosophila* tissues which have been highly tractable in experiments assessing integrin function – the formation of stable muscle attachments during embryogenesis, and the formation of the adult wing during larval/pupal development (BAI *et al.* 2008; BOKEL and BROWN 2002; BROWER 2003) – illustrated in Figure 1.11.

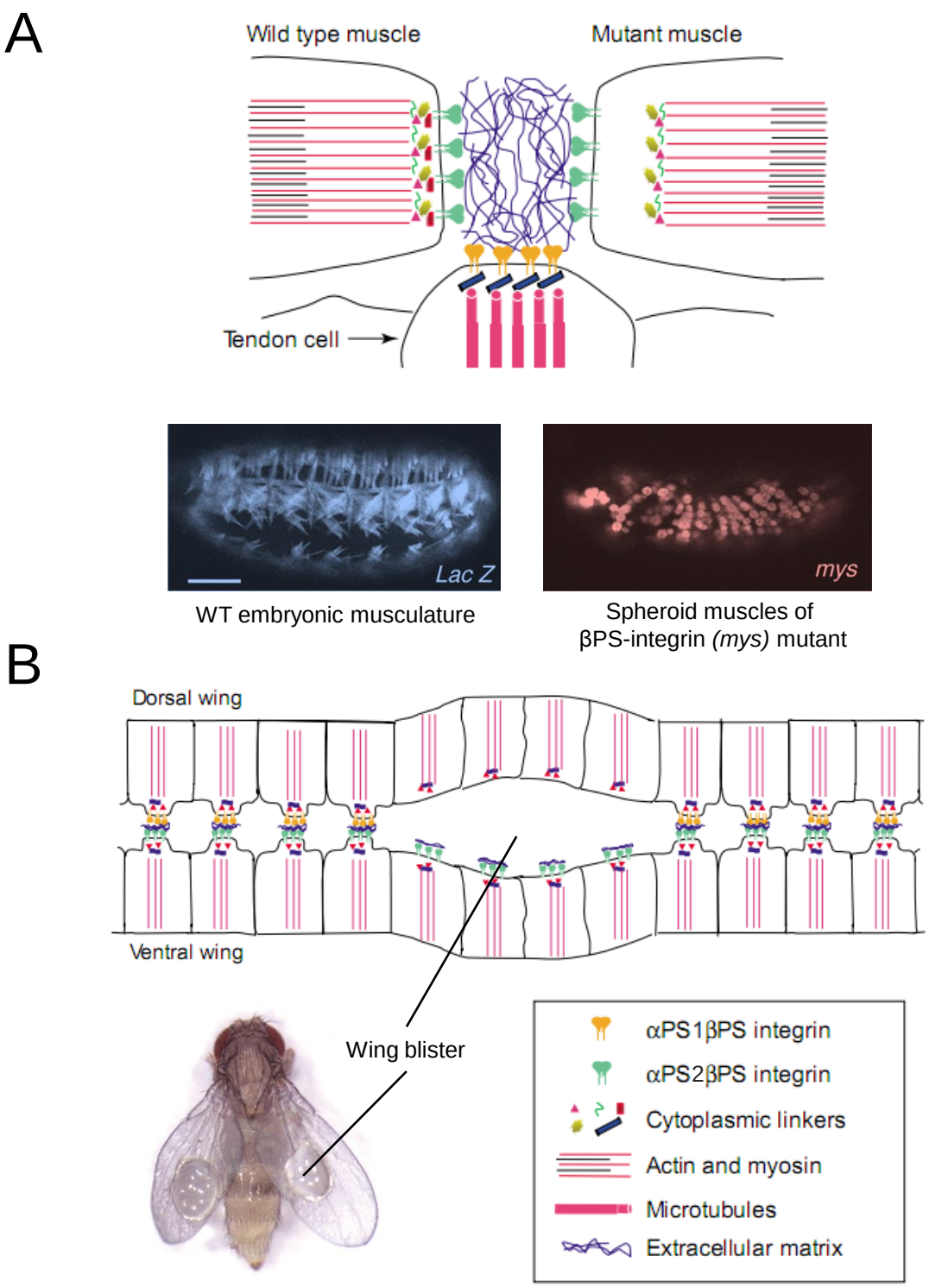

Figure 1.11. Using *Drosophila* to elucidate integrin-ECM functions.
A, during embryogenesis, somatic muscles attach to each other and epithelial tendon cells via integrin-ECM adhesion. The mutant example in the cartoon might be seen in *Ilk* (i.e. cytoplasmic linker) mutants. Micrographs show WT (*Lac Z*) and βPS-integrin (*mys*) knockdown embryos, with resulting 'rounded-up' phenotype. Scale bar = 50µm. **B**, the developing wing consists of dorsal and ventral epithelia that face each other with their basal sides. Loss of integrin function from clonal patches results in liquid-filled wing blisters. This easily scorable phenotype provides an efficient screen for mutations in proteins involved in adhesion. The figure is adapted from Brower (BROWER 2003), Bai *et al.* (BAI *et al*. 2008), and Bökel and Brown (BÖKEL and BROWN 2002).

For the formation of stable muscle attachments in the developing embryo (Figure 1.11A), somatic muscles attach to ECM, making connections between αPS2βPS-expressing muscles and αPS1βPS-expressing tendon cells (i.e. myotendinous junctions), as well as direct αPS2βPS-mediated muscle-ECM-muscle junctions (BROWER 2003). In contrast, in the adult *Drosophila* wing (Figure 1.11B), which forms primarily during metamorphosis, αPS1βPS-expressing dorsal cells are juxtaposed with αPS2βPS-expressing ventral cells – essentially forming cell-ECM-cell junctions. In the absence of integrin function, the wing layers separate resulting in a fluid-filled blister – an easily scorable phenotype, which has little effect on overall viability, and has been utilised extensively to screen for the identification of mutations involved in integrin-ECM adhesion including integrin-binding partners (BAKER *et al.* 2002; BROWER *et al.* 1995; PROUT *et al.* 1997; WALSH and BROWN 1998).

1.5.4. Linking integrins and their intracellular binding partners to the cytoskeleton

Identification of all the mammalian cytoplasmic proteins required for integrin function is continuing, but thus far the integrin 'adhesome' consists of a complex network of 156 components linked together and modified by 690 interactions (ZAIDEL-BAR *et al.* 2007) – but this number is likely an underestimate in light of advancing proteomics methods (GEIGER and ZAIDEL-BAR 2012). Similarly, in *Drosophila*, the identification of conserved integrin-associated proteins has demonstrated the importance of this type of adhesion, not only for the mechanical connection of the external to the internal environments, but also for downstream signalling processes that promote cell polarity, survival, migration, differentiation

(HARBURGER and CALDERWOOD 2009) – illustrated in Figure 1.12. Among the numerous integrin-associated proteins identified, only a few, including Talin, Integrin-linked-kinase (ILK), PINCH, and Parvin, have been demonstrated to be essential and evolutionarily conserved.

1.5.4.1. Talin

Talin (*rhea*) was first isolated due to its wing blister phenotype (PROUT *et al.* 1997), and *talin*-null mutants have highly similar phenotypes to βPS-integrin (*mys*) null mutants, including germ band retraction failure, and muscle detachment with subsequent embryonic lethality (BROWN *et al.* 2002). Talin is necessary to cluster integrins at focal adhesions on the basal imaginal disc epithelium, and for the formation of myotendinous junctions. In *Drosophila*, talin has been demonstrated to be a core component of the integrin-adhesion complex and is so far the only integrin-associated protein absolutely required for integrin adhesion, and is also crucial for the recruitment of other integrin-associated proteins (DELON and BROWN 2007; ZERVAS *et al.* 2011). The talin protein contains multiple integrin binding sites, and binding of the talin FERM (F for 4.1 protein, E for ezrin, R for radixin and M for moesin) domain to the β-integrin tail increased integrin affinity for extracellular ligands (i.e. inside-out signalling) (DELON and BROWN 2007) – supporting the idea that talin-integrin binding is an early event in integrin-ECM adhesion. Additionally, it also possible that talin can stabilise weakly-interacting integrin-ECM connections, potentially via conformational change (NAYAL *et al.* 2004). Similar to other FERM proteins, talin forms an intramolecular interaction that results in autoinhibition, and targeted disruption this autoinhibition prevents morphogenetic movements during embryogenesis. Indeed, loss of talin autoinhibition results in higher stability at

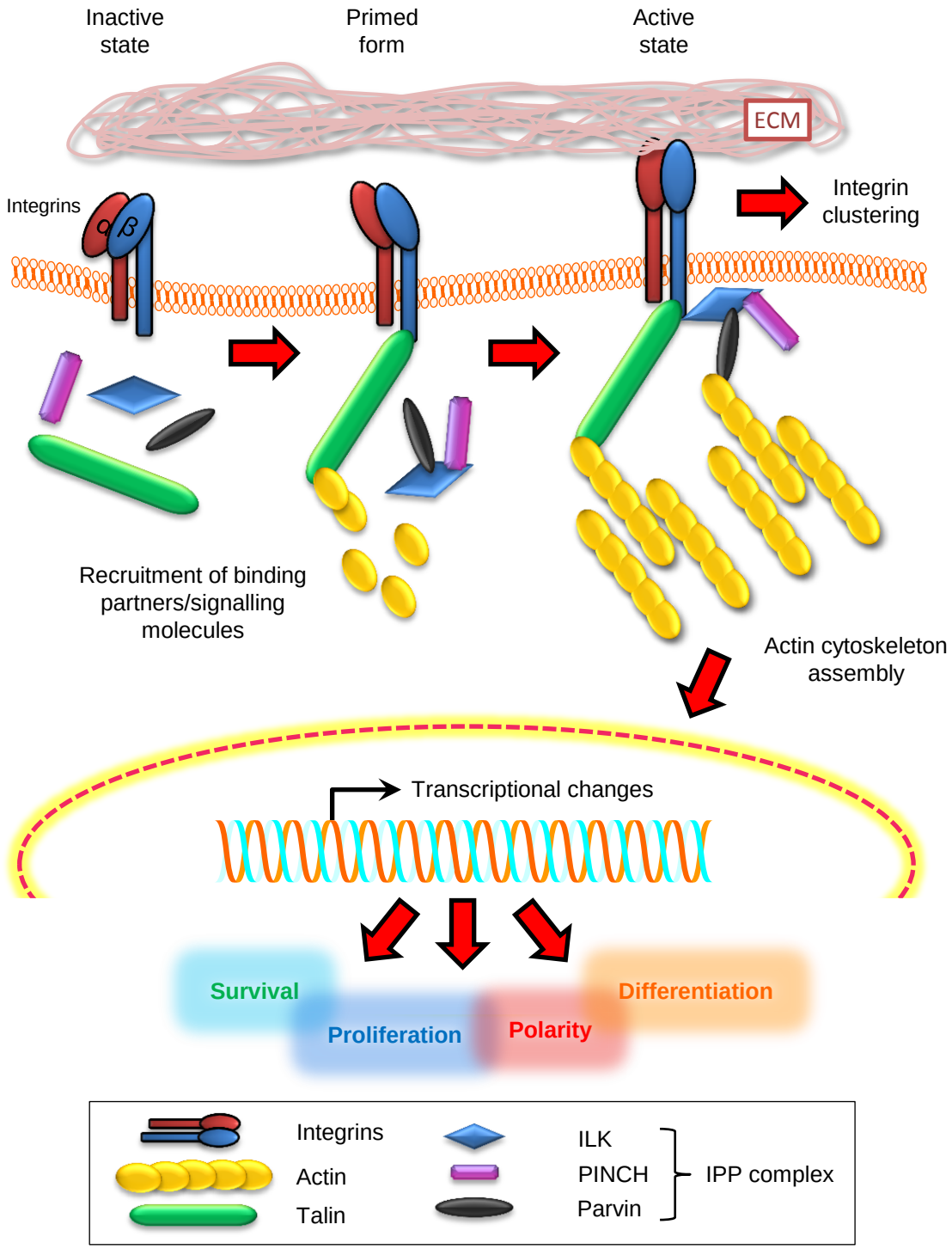

Figure 1.12. Assembly of integrin-ECM adhesions.
Integrins are present at the cell surface in an unbound 'inactive' configuration, with a low affinity for ligands, and are not attached to the ECM. Intracellular events, such as Talin-binding at the β-integrin cytoplasmic tail, trigger integrin activation and lead to the 'primed' integrin configuration. The integrin extracellular domains extend bind specific ECM molecules. Following activation, signalling cascades lead to the assembly of a multi-protein complex (including ILK, PINCH, and Parvin) at the site of cell adhesion to the ECM, and forge a connection with the actin cytoskeleton - Talin and Parvin can both connect directly to the actin cytoskeleton. The mature integrin-ECM adhesion forms clusters of active, ligand- and cytoskeleton-bound integrins that can activate signalling/transcriptional pathways.

integrin-ECM adhesions, suggesting the autoinhibitory function of talin alternates between modulating adhesion turnover and adhesion stability during morphogenesis (ELLIS *et al.* 2013).

1.5.4.2. Integrin-linked kinase (ILK)

ILK was initially identified by its ability to bind directly to the cytoplasmic tail of the β1 integrin subunit (HANNIGAN *et al.* 1996), and contains five tandem ankyrin repeats (ANKRs), a putative phosphoinositide-binding site and a pseudokinase domain (CHISWELL *et al.* 2008; WICKSTROM *et al.* 2010). ILK is required to link integrins and the actin cytoskeleton in somatic *Drosophila* embryonic muscles (ZERVAS *et al.* 2001), and as a link between the integrin adhesion complex and contractile apparatus in developing *C. elegans* muscle (MACKINNON *et al.* 2002). ILK binds to a large number of proteins (including PINCH, and Parvin), identified by yeast two-hybrid screening (BOULTER and VAN OBBERGHEN-SCHILLING 2006), indicating it is a core scaffolding component. However, it was found that complete elimination of integrins resulted in loss of ILK recruitment to integrin-ECM adhesion sites, with talin-loss also leading to a similar phenotype – indicating talin functions upstream of ILK, and that talin is required for ILK recruitment (ZERVAS *et al.* 2011). This agrees with mutant embryonic musculature phenotypes indicating ILK loss results in less severe phenotypes than βPS-integrin/talin loss (DELON and BROWN 2007). At present, the data does not support ILK directly binding with integrins/talin, but the essential cytoskeletal protein Wech has been shown to bind both talin and ILK, indicating a key link between these proteins (LOER *et al.* 2008). Conversely, in *C. elegans* there is a proposed mechanism through which ILK binds to the Kindlin ortholog, UNC-112, which in turn binds the β-integrin tail

(QADOTA *et al.* 2012) – although this has not been directly tested in *Drosophila*, similar mechanisms exist in mammalian cells, indicating this mechanism could be conserved (DOWLING *et al.* 2008b; USSAR *et al.* 2006).

1.5.4.3. PINCH (Particularly Interesting New Cysteine-Histidine rich protein)

Similar to talin, *Drosophila* PINCH (*steamer duck*, *stck*) was identified in a screen for potential integrin effectors (PROUT *et al.* 1997), with loss resulting in embryonic lethality, while clonal *stck* mutations in the developing wing led to wing blisters (CLARK *et al.* 2003). PINCH contains five tandem LIM domains – i.e. zinc-finger motifs that function to encourage protein binding, indicating PINCH is also a core scaffolding component at integrin-ECM attachment sites (PRONOVOST *et al.* 2013). In agreement with a role for PINCH in integrin adhesion, PINCH protein is co-localised with βPS-integrin at areas where integrin-ECM adhesion connects to the actin cytoskeleton in both muscle and wing epithelia, while loss of βPS-integrin results in PINCH mislocalisation at myotendinous junctions (CLARK *et al.* 2003). As mentioned previously, PINCH couples with ILK *in vivo* (binding to ILK ANKRs via its LIM1 domain) and have similar loss of function phenotypes, yet ILK (in addition to βPS-integrin and talin) appeared to accumulate normally at integrin-ECM attachment sites in embryonic lethal *stck* mutants (ZERVAS *et al.* 2011). Therefore, PINCH is a critical component of the integrin-ECM molecular machinery, and is essential for integrin-dependent cell adhesion.

1.5.4.4. Parvin

Despite characterisation of the tripartite ILK/PINCH/Parvin (IPP) complex, and its importance for integrin adhesion in mammals (LEGATE *et al.* 2006), parvin

and the IPP complex has only recently been characterised in *Drosophila* (VAKALOGLOU *et al.* 2012). Each member is encoded by a single gene in *Drosophila*, in contrast to two PINCH genes and three parvin genes in mammals. Parvin contains two calponin homology domains and binds to the ILK kinase domain (TU *et al.* 2001). In *parvin*-null mutants, the embryonic-lethal muscle phenotype was identical to both ILK and PINCH loss of function mutants – with a loss of connection between the actin cytoskeleton and the integrin-ECM attachment site (VAKALOGLOU *et al.* 2012). Parvin is, therefore, essential for embryogenesis and is crucial for the assembly of the integrin-adhesion complex *in vivo*.

1.5.5. Integrins in the *Drosophila* heart

The developing *Drosophila* heart has been a useful model with which to dissect various signalling molecules and cell adhesion proteins important for heart morphogenesis (VANDERPLOEG *et al.* 2012). Cell adhesion proteins demonstrated to be important for cardiomyocyte adhesion and lumen formation in the developing *Drosophila* heart include Laminin A, Cadherin, Slit, Robo, and Integrins (HAAG *et al.* 1999; KNOX *et al.* 2011; MEDIONI *et al.* 2008; VANDERPLOEG *et al.* 2012). During the dorsal closure stage of embryogenesis, the two cardioblast rows meet at the midline, then form a hollow tube by "apposing their dorsal and ventral edges with the corresponding cardioblasts of the opposing row, thus encapsulating a lumen" (HELENIUS and BEITEL 2008) – the opposing cardiomyocytes each connecting at dorsal and ventral junctional (J) domains with corresponding luminal (L) domains (MEDIONI *et al.* 2008). Previous studies have shown that cadherin-based adherens junctions assemble at the J domain (HAAG *et al.* 1999), while more recent work has also established that integrins are also required for cardioblast polarisation during

cardioblast migration (i.e. during dorsal closure), and are essential for lumen formation and are proposed to function by stabilising the repellent Slit/Robo signalling in the lumen (VANDERPLOEG *et al.* 2012). Talin and ILK have also been demonstrated to be essential for cardioblast alignment and lumen formation (VANDERPLOEG *et al.* 2012). Thus far, however, there have been no studies investigating the role of integrins and their binding partners after cardiogenesis in *Drosophila*.

1.5 Aims of this PhD project

The fundamental mechanisms underlying the development of congenital heart disease and cardiomyopathies are often polygenic in aetiology, making it difficult for researchers to probe complex interactions that may contribute to the severity of the disease. Over the last decade, the adult fruit fly (*Drosophila melanogaster*) has emerged as an invaluable tool with which to study the genetic and molecular mechanisms underlying heart function. Therefore, the overall objective of this PhD was to develop the adult fruit fly as a model of human heart function in our lab, and to utilise this powerful genetic system to screen for conserved genes affecting the development and function of its cardiac syncytium.

The specific aims of the work described in this PhD thesis were to:

1. Develop the adult *Drosophila* heart model by performing baseline measurements of heart function and other factors contributing to variability in heart function (i.e. age, and the time of day).

2. Perform an *a priori* RNAi screen, knocking down expression of individual conserved genes via cardiomyocyte GAL4/UAS-overexpression.
    a. Genes identified from this screen included *Fermitin 1* and *Fermitin 2 (Fit1, Fit2)*, the two *Drosophila* orthologs of *Kindlin 2* which caused severe cardiomyopathy.

3. Generate and characterise null alleles of *Fit1* and *Fit2* via P-element mobilisation and assess for any impact on heart development or function.

4. Generate and characterise temperature-sensitive cardiac-expressing GAL4/GAL80^{ts} lines and assess the effect of knockdown of *Fit* function at different developmental stages.

Chapter 2

Materials & Methods

2.1 Commonly used reagents and buffers

Artificial haemolymph

Artificial haemolymph contains 108 mM Na^+, 5 mM K^+, 2 mM Ca^{2+}, 8 mM $MgCl_2$, 1 mM NaH_2PO_4, 4 mM $NaHCO_3$, 10 mM sucrose, 5 mM trehalose, and 5 mM HEPES (pH 7.1)(all from Sigma, Poole, Dorset). Stock haemolymph (minus sucrose and trehalose) was made and refrigerated. Sucrose and trehalose were added to haemolymph prior to use in order to prevent bacterial contamination. Artificial haemolymph concentrations are from Vogler and Ocorr (VOGLER and OCORR 2009) who based their recipe on those found in (SINGLETON and WOODRUFF 1994; WANG *et al.* 2003).

DAPI

4', 6-diamidino-2-phenylindole (Sigma, Poole, Dorset) to stain nuclei, stock solution at 1 mg/mL in dH_2O, stored at –20˚C. Used at 0.1 µg/mL (1:10,000 dilution).

DNA lysis buffer

With final concentrations – 100 mM Tris-HCl pH 7.5, 100 mM EDTA pH 8.0, 100 mM NaCl, 0.5% SDS (all from Sigma, Poole, Dorset). For example, 100 µL DNA prep volume = 10 µL 1 M Tris-HCl pH 7.5 + 20 µL 0.5 M EDTA pH 8.0 + 2.5 µL 4 M NaCl + 5 µL 10% SDS + 62.5 µL dH_2O.

DTT

Stock solution at 1 M dithiothreitol (Fisher Scientific, Loughborough, UK) in dH_2O stored at –20˚C.

EDTA

Ethylenediamine-N,N,N',N'-tetraacetic acid, Stock solution 0.5 M solution in dH_2O, pH 8.0 (EDTA from Sigma, Poole, Dorset, UK).

Ethidium Bromide (EtBr)

Stock solution at 10 mg/mL in dH_2O, used at 300 ng/mL (Sigma, Poole, Dorset, UK).

Formaldehyde

16% Formaldehyde ampules (methanol free) (#28908, Fisher Scientific, Loughborough, UK).

LiCl

6 M lithium chloride (#L9650, Sigma, Poole, Dorset, UK)

KAc

5 M potassium acetate (#P1190, Sigma, Poole, Dorset, UK)

Molecular weight markers

100 kb DNA ladder (#G210A, Promega, Southampton, UK).

1 kb DNA ladder (#G571A, Promega, Southampton, UK).

Phalloidin

AlexaFluor 546-conjugated phalloidin (13.2 nM) to stain F-actin (Invitrogen, Paisley, UK)

Phosphate Buffered Saline (PBS) (10x)

Ten tablets dissolved in 200 mL of dH_2O yields 0.1 M phosphate buffer, 0.027 M potassium chloride and 1.37 M sodium chloride, pH 7.4, at 25°C (#P4417, Sigma, Poole, Dorset, UK).

PBS-T

1x PBS with 0.1% TritonX-100 (diluted from 10% w/v stock solution of TritonX-100 in dH_2O) (#X100, Sigma, Poole, Dorset, UK).

TAE (50x)

2 M Tris-acetate, 50 mM EDTA, pH 8.0 – e.g. For 1 L 50x TAE, 242 g Tris base, 100 mL 0.5 M EDTA, and 57.1 mL glacial acetic acid (all Sigma, Poole, Dorset, UK) made up to 1 L with dH_2O.

TE (1x)

10 mM Tris-HCl, 1 mM EDTA, pH 8 (Sigma, Poole, Dorset, UK).

2.2 *Drosophila* husbandry

Flies were propagated in polypropylene bottles and vials (VWR, 734-1249 and 734-2254 respectively) containing standard 'Bloomington' medium (see recipe below) in a 25°C incubator on a 12:12 hr photoperiod. Flies were kept in a 25°C incubator for experiments or in an 18°C incubator for stocks with tipping onto a new vial with fresh food once every month. Fly stocks used in this PhD thesis are listed in Table 2.1. Unless otherwise stated, flies were in the w^{1118} background. *Canton-S* (*CaS*) flies were also used as controls. Female flies were used for all heart analysis due to their larger size and ease of dissection compared to male flies.

2.2.1 *Drosophila* strains received from other labs/institutions

Prof. John Tower (Department of Biological Sciences, University Of Southern California, US) kindly provided *UAS-ultraGFP* flies. Prof. Manfred Frasch (Department of Biologie, Friedrich-Alexander-University Erlangen-Nuremberg, Germany) kindly provided *tinCΔ4-GAL4* flies. Prof. Achim Paululat (Department of Zoology & Developmental Biology, University of Osnabrück, Germany) kindly provided *handC-GAL4* flies. Per^{01} flies on the *yw* background were kindly provided by Prof. Ralph Stanewsky (Organismal Biology, Queen Mary University, UK). *UAS-ΔClk* and *UAS-ΔCyc* flies were kindly provided by Prof. Paul Hardin (Department of Biology, Texas A&M University, US). *yw* flies were kindly provided by Dr. Guiseppa Pennetta (Centre for Integrative Physiology, University Of Edinburgh, UK). All other lines were ordered from the Bloomington *Drosophila* Stock Center (BDSC, Indiana University, Bloomington, IN, US) and the Vienna *Drosophila* RNAi Center (VDRC, Campus Vienna Biocenter, Vienna, Austria).

Table 2.1 – Fly stocks used in this PhD thesis

Phenotype	Genotype	Chromosome affected	Source	Stock No.	Nature of allele
Canton-S	WT	-	Heck Lab	-	-
w^{1118}	w^{1118}; ;	X	Bloomington	3605	White eyes. Spontaneous mutation - loss of function allele. Partial deletion of *w*.
yw	y^{1} w^{*}; ;	X	Guiseppa Pennetta, University Of Edinburgh	-	White eyes, yellow body. Spontaneous mutations - loss of function alleles. Partial deletion of *w*. Deletion of the *y* promoter, not enhancer. A to C tranversion in the ATG translation initiation codon.
$yper^{01}w$	y^{1}, w^{*}, per^{01}; ;	X	Ralf Stanewsky, Queen Mary University Of London	-	Yellow body/white eyes (due to *yw*). Amorphic *per* allele. Point mutation. Nucleotide substitution: C?T. Amino acid replacement: Q464?. Amber nonsense mutation in exon 4.
Fit1	y^{1} w^{67c23};; $P\{y^{+mDint2}$ $w^{BR.E.BR}$=SUPor-P}$Fit1^{KG05576}$ ry^{506}	X; ; 3	Bloomington	13902	11,467 Kb inserted P-element. Insertion site - 64A6, 3L:4103622..4103622 (R5). May be segregating *TM3*, Sb^{1}
Fit2	y^{1} w^{67c23};; $P\{w^{+mC}$ $y^{+mDint2}$=EPgy2}$Fit2^{EY08530}$	X; ; 3	Bloomington	16899	10,908 Kb inserted P-element. Insertion site - 73E4, 3L:17017464..17017464 (R5)
Δ2-3 transposase	y^{1} w^{*}; *CyO*, $H\{w^{+mC}$=PDelta2-3}$HoP2.1/Bc^{1}$	X: 2	Bloomington	2078	Source of P-element transposase. Transposase also marked by *CyO* allele.
mys	mys^{1}/*FM4*	X	Bloomington	59	Amorphic allele - genetic evidence. Deletion of at least 1kb beginning in central portion of coding region and extending towards 3' of gene, probably beyond the 3' end of the gene.

arm	$y^1\ arm^4\ w^*/FM7c,$ $P\{ry^{+t7.2}=ftz/lacC\}YH1$	X	Bloomington	616	Amorphic allele - genetic evidence. Nucleotide substitution: C2968T.
mew	$y^1\ mew^{M6}\ f^{36a}$ $P\{ry^{+t7.2}=neoFRT\}18A/FM7c$	X	Bloomington	1483	Amorphic allele - genetic evidence. Inversion breakpoint is within the coding region between nucleotides 1405 and 1848.
if	$g^2\ if^{B2}\ f^{36a}/FM7c$	X	Bloomington	2176	Amorphic allele - genetic evidence. EMS-induced, strong allele, small amount of detectable protein.
rhea	$y^1\ w^1;;\ P\{w^{+t*}\ ry^{+t*}=white\text{-}un1\}70C$ $rhea^1\ P\{neoFRT\}80B/TM6B,$ $P\{w^{+mC}=iab\text{-}2(1.7)lacZ\}6B,\ Tb^1$	X; ; 3	Bloomington	2296	A frameshift occurs after codon 1139, and the new reading frame terminates after two codons.
stck	$y^1\ w^1;;\ P\{neoFRT\}82B\ stck^{3R\text{-}17}$ $P\{w^{+t*}\ ry^{+t*}=white\text{-}un1\}90E/TM6B,$ $P\{w^{+mC}=iab\text{-}2(1.7)lacZ\}6B,\ Tb^1$	X; ; 3	Bloomington	2302	Loss of function allele. 571bp deletion in *stck* encompassing nucleotides 2095-2664.
pan	$;;;\ pan^2/P\{w^{+mC}=ActGFP\}unc\text{-}13^{GJ}$	4	Bloomington	4759	Amorphic allele - genetic evidence. Single base deletion (ATT to AT at I106) causing a frameshift.
ilk	$;;\ mwh^1\ Ilk^1\ red^1\ e^4/TM3,\ Sb^1$	3	Bloomington	4861	Amorphic allele - genetic evidence. Nucleotide substitution: G?A. Amino acid replacement: W211?.
UAS-rpr	$w^{1118}\ P\{w^{+mC}=UAS\text{-}rpr.C\}27$	X	Bloomington	5823	Expresses the cell death gene, *reaper*, under GAL4 control.
UAS-ultra-GFP	$w;\ P\{w^{+mC}\ UAS\text{-}2xEGFP^{m5B29}\};\ P\{UAS\text{-}2xEGFP^{m6B1}\}$	X; 2; 3	John Tower University Of Southern California	-	Highly expresses GFP when under the control of a GAL4 driver.
UAS-Clk^{DN}	$w;\ P\{w^{+mC}\ UAS\text{-}clk\Delta\}$	X; 2	Paul Hardin Texas A&M University	-	Expresses dominant-negative version of CLOCK when under control of a GAL4 driver.

UAS-Cyc^{DN}	*w; P{w^{+mC} UAS-cycΔ}*	X; 2	Paul Hardin Texas A&M University	-	Expresses dominant-negative version of CYCLE when under control of a GAL4 driver.
UAS-clk^{VDRC}	*w;; P{w^{+mC} UAS-dsClock}/TM3, Sb (Sterile)*	X; ; 3	VDRC	42834	Expresses RNAi when under GAL4 control. For your RNAi experiments please use flies over the balancers and screen the progeny against the balancer.
UAS-cyc^{VDRC}	*w;; P{w^{+mC} UAS-dsCycle)/TM3, Sb (Sterile)*	X; ; 3	VDRC	11765	Expresses RNAi when under GAL4 control. For your RNAi experiments please use flies over the balancers and screen the progeny against the balancer.
UAS-per^{VDRC}	*w, P{w^{+mC} UAS-dsPeriod}*	X	VDRC	5709	Insertions on the 1st chromosome are not balanced, and we keep these strains by crossing the RNAi males to X-compound virgins. In this case only the males have red eyes, never the females.
UAS-Fit1^{VDRC}	*w; P{w^{+mC} UAS-dsFit1}*	X; 2	VDRC	46494	Expresses RNAi when under GAL4 control.
UAS-Fit1^{TRiP}	*y^{1} v^{1};; P{y$^{+t7.7}$ v$^{+t1.8}$=TRiP.JF01986}attP2*	X; ; 3	Bloomington	25966	Expresses RNAi when under GAL4 control.
UAS-Fit2^{VDRC}	*w;; P{w^{+mC} UAS-dsFit2}*	X; ; 3	VDRC	37010	Expresses RNAi when under GAL4 control.
UAS-Mys^{VDRC}	*w; P{w^{+mC} UAS-dsMys}*	X; 2	VDRC	29619	Expresses RNAi when under GAL4 control.
UAS-Mew^{VDRC}	*w; P{w^{+mC} UAS-dsMew}*	X; 2	VDRC	44890	Expresses RNAi when under GAL4 control.
UAS-If^{VDRC}	*w;; P{w^{+mC} UAS-dsIf}*	X; ; 3	VDRC	44885	Expresses RNAi when under GAL4 control.
UAS-Arm^{VDRC}	*w;; P{w^{+mC} UAS-dsArm}*	X; ; 3	VDRC	7767	Expresses RNAi when under GAL4 control.
UAS-Fak56D^{VDRC}	*w;; P{w^{+mC} UAS-dsFak56D}*	X; ; 3	VDRC	17957	Expresses RNAi when under GAL4 control.
UAS-Bteb2^{VDRC}	*w; P{w^{+mC} UAS-dsBteb2}*	X; 2	VDRC	110761	Expresses RNAi when under GAL4 control.

UAS-Syn1^{VDRC}	*w; P{w^{+mC} UAS-dsSyn1}*	X; 2	VDRC	27893	Expresses RNAi when under GAL4 control.
UAS-Stck^{VDRC}	*w; P{w^{+mC} UAS-dsStck}*	X; 2	VDRC	52537	Expresses RNAi when under GAL4 control.
UAS-Ches1^{VDRC}	*w;; P{w^{+mC} UAS-dsChes1}*	X; ; 3	VDRC	15742	Expresses RNAi when under GAL4 control.
UAS-NijA^{VDRC}	*w;; P{w^{+mC} UAS-dsNijA}*	X; ; 3	VDRC	5208	Expresses RNAi when under GAL4 control.
UAS-Tld^{VDRC}	*w; P{w^{+mC} UAS-dsTld}*	X; 2	VDRC	1215	Expresses RNAi when under GAL4 control.
UAS-NijB^{VDRC}	*w, P{w^{+mC} UAS-dsNijB}*	X	VDRC	48786	Expresses RNAi when under GAL4 control.
UAS-Alas^{VDRC}	*w, P{w^{+mC} UAS-dsAlas}*	X	VDRC	48774	Expresses RNAi when under GAL4 control.
UAS-Timp^{VDRC}	*w;; P{w^{+mC} UAS-dsTimp}*	X; ; 3	VDRC	15372	Expresses RNAi when under GAL4 control.
Actin5C-GAL4	*y^{1} w*; P{w^{+mC}=Act5C-GAL4}25FO1/CyO, y^{+}*	X; 2	Bloomington	4414	Unpublished, P{AyGAL4} with the >y^{+}> cassette flipped out, essentially an Act5C-GAL4 fusion gene.
tinCΔ4-GAL4	*w*;; P{w^{+mC} tinCΔ4-GAL4}*	X; ; 3	Manfred Frasch University Of Erlangen Nuremberg	-	A deletion derivative of the 303bp *tin* cardiac enhancer element, in which nucleotides 154 to 192 of the element have been deleted
handC-GAL4	*w*; P{w^{+mC} handC-GAL4}*	X; 2	Achim Paululat University Of Osnabrück	-	The insertion line on the 2nd chromosome shows a much stronger expression due to unknown reason than the one on the 3rd chromosome.
da-GAL4	*w^{1118}; P{da-GAL4.w^{-}}3*	X; ; 3	Bloomington	8641	Expresses GAL4 in the pattern of the da gene. A P transposase-induced w[-] derivative of P{w[+mW.hs]=GAL4-da.G32}
tub-GAL80^{ts} 2nd	*w*; P{w^{+mC}=tubP-GAL80^{ts}}10; TM2/TM6B, Tb^{1}*	X; 2; 3	Bloomington	7108	Temperature-sensitive GAL80 expressed under the control of the *alphaTub84B* promoter, restrictive temp is 30°C.
tub-GAL80^{ts} 3rd	*w*;; P{w^{+mC}=tubP-GAL80^{ts}}2/TM2*	X; ; 3	Bloomington	7017	Temperature-sensitive GAL80 expressed under the control of the

					alphaTub84B promoter, restrictive temp is 30°C; homozygotes present in stock.
2;3 Balanced	*w^{*}; Kr^{If-1}/CyO; D^{1}/TM3, Ser^{1}*	X; 2; 3	Bloomington	7198	Multiply balanced stock. *Kr^{If-1}* causes eye phenotype. *CyO* causes wing phenotype. *D^{1}* causes wing 45° angle phenotype. *TM3, Ser^{1}* serrated wing phenotype.
GFP Balancer	*w^{*};; Sb^{1}/TM3, P{w^{+mC}=ActGFP}JMR2, Ser^{1}*	X; ; 3	Bloomington	4534	GFP; green balancer; see http://www-ibmc.u-strasbg.fr/ridi/GreenBalancers/DiapoFrame.html for ref and pics of expression pattern.

2.2.2 Fly food

2.2.2.1 'Bloomington' medium ingredients

Ingredients for Bloomington medium: 1.4 L dH_2O, 12 g agar (Sigma, Poole, Dorset, A1296-500G), 100 g sucrose (Sigma, S9378), 60 g yeast (Sigma, 51475), 15 g soybean flour (Sigma, S9633), 100 g corn meal (Sigma, C6304), 8 g dried yeast (Fermipan Red, 5604475114016). 10 mL propionic acid (Sigma, P5561) and 3.8 g methyl 4-hydroxybenzoate (Sigma, H3647) dissolved in 38 mL ethanol (VWR) are added to prevent bacterial/fungal infections.

2.2.2.2 'Bloomington' medium recipe

In a 5 L beaker, 700 mL dH_2O, 12 g agar, and 100 g sucrose were added then stirred and heated in a microwave for 6 min. After this, another 700 mL dH_2O (to make 1.4 L total), was added and while stirred, 60 g yeast, 15 g soybean flour, and 100 g corn meal was added. The mixture was stirred until it appeared homogenous, then heated in microwave for 2 min. After this time, most of the ingredients sank to the bottom, and slightly congealed. The mixture was stirred again until homogenous, and then heated again for another 2 min. The heating/stirring was repeated a further 3-4 times until the mixture appeared homogenous when removed from the microwave –i.e. there were no layers at the bottom of the beaker. While stirred, 10 mL propionic acid, 38 mL methyl 4-hydroxybenzoate/ethanol, and 8 g dried yeast was added. The mixture was then stirred vigorously until it was homogenous, had a smooth consistency and was without lumps. The medium was then poured into vials (~10 mL per vial) and bottles (~75 mL per bottle). If less food was required, the

ingredients were simply fractioned so they represented the same percentage of the mix, and heated in the microwave for a shorter amount of time.

2.2.3 Setting up fly crosses

Virgin females from one stock were collected by CO_2 anaesthesia within 8 hours of eclosion, and crossed with males from the other desired stock in roughly a 2:1 ratio (e.g. 8 virgin females to 4 males). Flies were left to mate and lay eggs for more than 3 days. The parents were then tipped after about 1 week and the progeny eclosed from the same vial. Crosses were carried out at 18, 25 or 29°C depending on the requirements of the experimental set-up.

2.3 Baseline measurements of factors which may affect cardiac function in adult *Drosophila*

2.3.1 Assessing effect of ageing on cardiac function

Five sets of ~30-40 newly-eclosed (i.e. <12-hour old) *CaS* flies (~20 males and ~20 females) were collected and put into individual vials containing Bloomington medium. These vials were then kept in the 25°C incubator for 7 days, then flies were subsequently tipped into fresh vials – the old vials were discarded. Five new sets of newly eclosed *CaS* flies were also collected and put into vials at the same time as the week-old flies. This process was repeated each week until there were vials containing flies from 1-week old to 6-weeks old. Cardiac function of these flies was then assessed.

2.3.2 Assessing time-of-day effects on cardiac function

For diurnal rhythm experiments, 2 incubators were set up with lighting on electronic timers for different 12:12-hour light/dark lighting schedules – this is summarised in Figure 2.1. Five sets of ~30-40 newly-eclosed (i.e. <12-hour old) *CaS* flies (~20 males and ~20 females) were collected and put into individual vials containing Bloomington medium. These vials were then kept in different incubators for 7 days (without disturbance) so that flies could become entrained to the different light/dark cycles. The first incubator was set up for lights to come on at 5.30am and go off at 5.30pm. The second incubator was set up for lights to come on at 8.30pm and go off at 8.30am. This was done so that flies at different periods of their circadian/diurnal cycle could be analysed, at the same time of day. Cardiac function of these flies was then assessed.

2.4 Preparing and assessment of adult *Drosophila* cardiac function

2.4.1 Semi-intact heart preparation of the adult fly

This is a modified technique from Vogler and Ocorr (VOGLER and OCORR 2009). Adult female flies were anaesthetised with CO_2 and placed dorsal side down into a petri dish (35mm Culture Dish (Product #430165), Corning Life Sciences, Tewksbury, MA, USA) coated with a thin layer of petroleum jelly (Vaseline, Unilever, Leatherhead, Surrey); this lets the hydrophobic cuticle in the wings and body stick to the dish so that manipulation is easier. Eventually, as the technique became facile, as many as 16 fly hearts could be surgically exposed/recorded at a time.

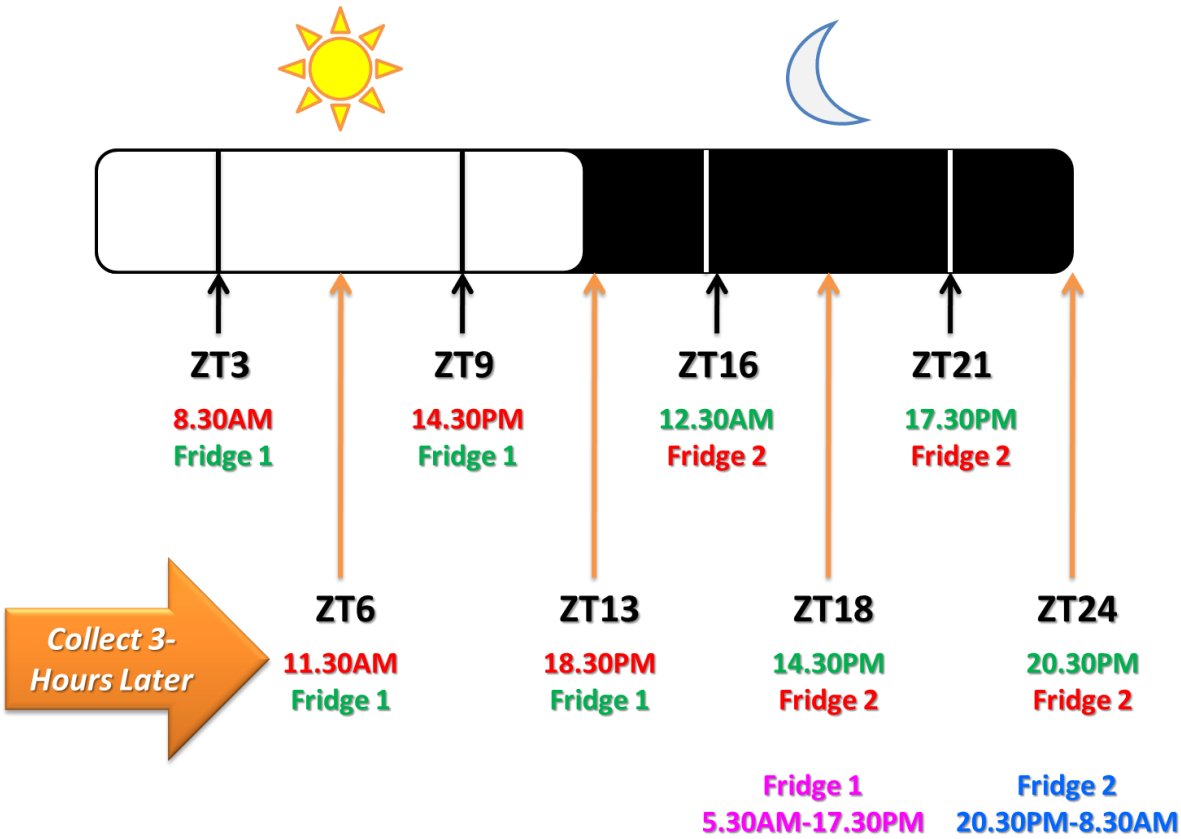

Figure 2.1. Incubator lighting schedule.
Two incubators were set up with 12:12 light/dark schedule. One incubator had lights scheduled for 5.30am 'lights on' to 5.30pm 'lights off', while the other was phase-shifted by 9 hours – i.e. 8.30pm 'lights on' to 8.30am 'lights off' – essentially for ease of heart analysis during daylight hours.

An initial cut was made using a curved pair of spring scissors (Roboz Surgical Instrument Co., Gaithersburg, MD USA) with the blades placed under the legs and angled down toward the dorsal surface of the thorax – illustrated in Figure 2.2A. The legs and most of the ventral abdomen were removed with a single cut. The posterior tip of the abdomen was also removed with a single cut. The ventral abdominal cuticle was then pinched with forceps and the pinched tissue was removed with a single cut of the spring scissors; severing the connection between the gut and the abdominal cuticle, and revealing the innervated internal organs of the abdomen – illustrated in Figure 2.2B. The preparation was then quickly submerged in artificial haemolymph solution – to avoid dehydration of the tissue. The gut and other abdominal organs (e.g. ovaries) and their neuronal inputs were removed (usually as a single mass) using fine forceps. Removal of the internal organs revealed the beating heart tube still attached to the dorsal cuticle, surrounded by opaque fat bodies – illustrated in Figure 2.2C.

Excess fat was aspirated using finely drawn glass microcapillaries (100µL, CAMAG, Hungerford, Berkshire, UK) – illustrated in Figure 2.2D. It should be noted that extreme care was taken to avoid touching the heart and associated tissues with scissors/forceps/microcapillaries as this can be detrimental to heart function. Removal of the fat surrounding the heart made it easier to analyse each wall of the heart when it came to analysing each video. Finally, artificial haemolymph was replaced with fresh solution and the heart was ready to be analysed by video microscopy.

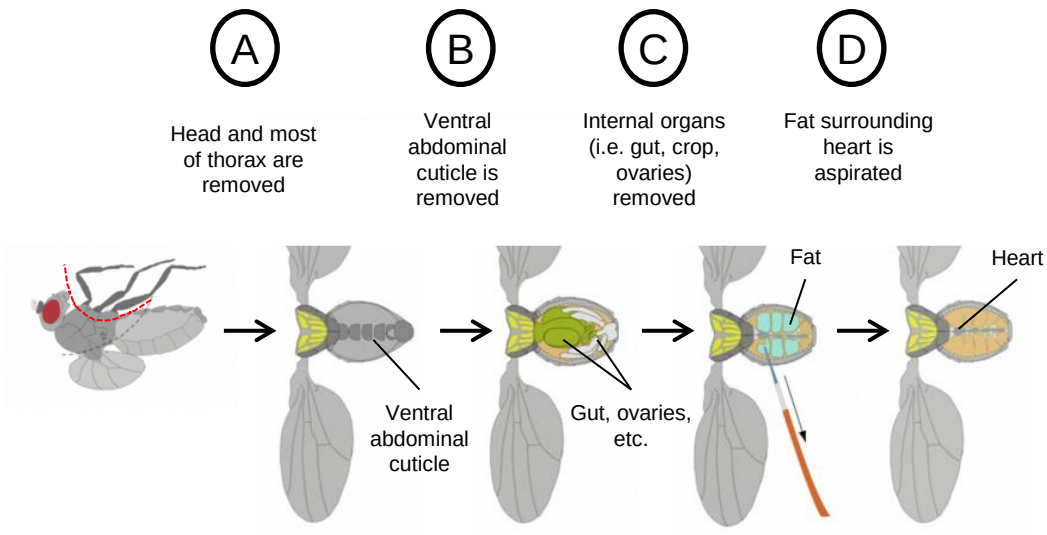

Figure 2.2. Preparing the adult *Drosophila* heart for assessment of heart function.

A, the legs and most of the ventral thorax are removed (red dashed line). **B**, the ventral abdominal cuticle is then removed by pinching the ventral abdominal cuticle with forceps, and the pinched tissue is then removed with a single scissor cut, exposing the internal organs of the adult fly. **C**, the internal organs (including gut, crop, ovaries etc) are removed to visualise the beating heart. **D**, fat lying along the dorsal cuticle wall, and surrounding the heart (which can affect heart analysis) is aspirated using a microcapillary tube. Assessment of cardiac function can now proceed. The figure is adapted from the video accompanying Vogler and Ocorr (VOGLER and OCORR 2009).

2.4.2 Recording the beating adult fly heart using videomicroscopy

The submerged adult *Drosophila* heart preparation was viewed under normal brightfield conditions using a 40x dipping lens attached to a Zeiss Axioskop 2 mot plus epifluorescence microscope (Carl Zeiss Ltd., Cambridge, UK). High speed digital movies of the fly heart in the A2-A3 abdominal segment were recorded using a MyoCam CCD camera (IonOptix, Milton, MA, US), with video acquisition by Pinnacle Software (Pinnacle Systems, Iver Heath, UK) – illustrated in Figure 2.3A. For most fly heart recordings in this thesis, three 10-second recordings of each heart were taken, and the results of the 3 videos was averaged. For others, only one 10-second video was recorded for each fly – but higher *n* numbers were used.

2.4.3 Analysis of fly heart function movies

A MatLab-based 'Fly Heart Analysis' video analysis program was used to analyse heart video recordings (OCORR *et al.* 2009) – illustrated in Figure 2.3B. Since the Fly Heart Analysis program could not perform movement analysis on compressed AVI files, videos had to be decompressed from their Pinnacle software-recorded compressed-AVI files, and saved as large uncompressed AVI files using the freeware program VirtualDub (http://www.virtualdub.org/). Videos can now be analysed using the Fly Heart Analysis program. The MatLab-based analysis software is explained fully in Ocorr *et al*. (OCORR *et al.* 2009), and much of the information explained below can be found there.

2.4.3.1 Pre-processing and fractional shortening (%FS) calculations

Firstly, for each video being analysed by the analysis program it first needed to be pre-processed. Points of the heart wall were marked to indicate maximal

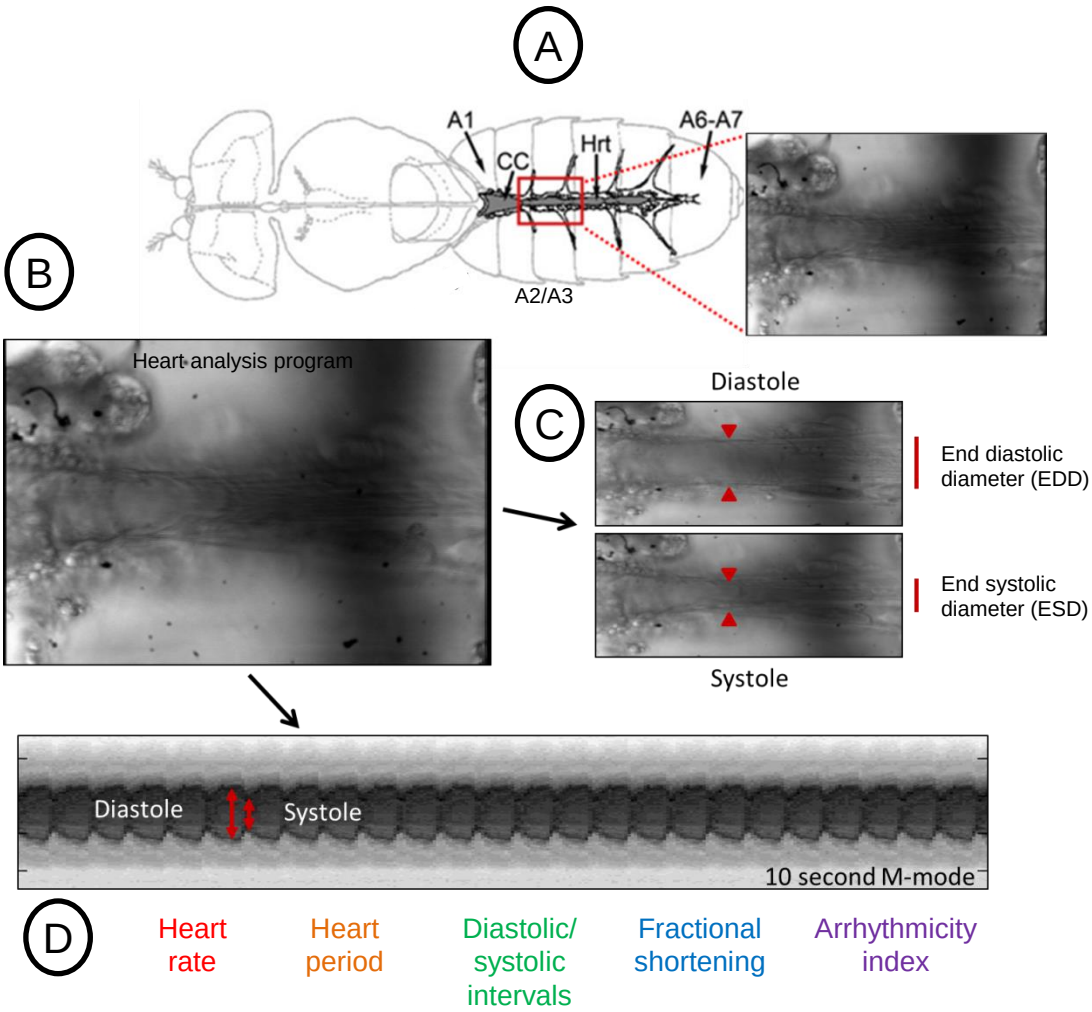

Figure 2.3. Heart function recording and video analysis.
A, video recordings were made around the A2-A3 abdominal section. **B**, heart video recordings were then analysed using MatLab-based 'Fly Heart Analysis' software developed specifically for fly hearts. **C**, for each video, points of the heart wall are marked to indicate maximal diastole and systole. **D**, the analysis software then analyses each video, assessing movement via two algorithms – explained further in text. Output parameters include heart rate, heart period, systolic/diastolic interval, fractional shortening, and arrhythmicity index. A 10-second M-mode, indicating a rhythmic fly heart, is shown as one of the outputs of the analysis program. The figure is adapted from Miller (MILLER 1950).

diastole and systole – illustrated in Figure 2.3C. Recordings were advanced one frame at a time allowing precise identification of the frames where maximal contraction and relaxation of the heart occurred. The heart diameters obtained in this step were also used to calculate the percentage fractional shortening (%FS) and it provided an estimate of the contractility of the heart. Fractional shortening represented the extent to which the heart edges moved toward each other during a contraction. The formula used to calculate %FS was: ((Diastolic diameter - Systolic diameter)/Diastolic diameter) x 100. The points identified in this set were used only for diameter and fractional shortening measurements and are not used for movement detection.

2.4.3.2 Detection of movement

After pre-processing, the analysis software automatically analysed each video, assessing movement via two algorithms – 'average frame darkness' and 'pixel by pixel' (OCORR *et al.* 2009). The first algorithm, average frame darkness, averaged the darkness intensity for an entire frame, then normalised the value to an interval between 0 and 1, then plotted this normalised average, for each frame in the movie, with time. The second algorithm, pixel by pixel, analysed the change in darkness of each individual pixel in each frame compared to the next frame. Pixels that changed intensity above a set threshold were summed for each frame, and plotted for every frame in the movie, with time.

2.4.3.3 Output analysis check

Although movement detection was performed automatically by the analysis program the output was also checked for accuracy. To make sure the detection

intervals agreed with movement in the actual movie, an M-mode image made from 1-pixel slices of the movie, stacked horizontally over time for each frame was displayed, and was compared to the output analysis for errors. Systolic intervals were identified as the interval between two successive diastoles. The beginning of systole was indicated in the M-mode by a vertical blue line and the end of systole was indicated by a vertical red line. This display made it relatively straightforward to compare algorithm output to the actual heart movements.

2.4.3.4 Output analysis for each fly/genotype/condition

Once the output for a given movie was accepted the program used that information to automatically calculate a number of parameters. These included heart rate, heart period, systolic/diastolic interval, fractional shortening, and arrhythmicity index – illustrated in Figure 2.3D. Statistical output was provided for each movie individually and for the entire data set in the form of a comma separated value (.csv) file which was opened in spreadsheet programs such as Microsoft Excel (OCORR *et al.* 2009). In this PhD thesis, data obtained from hearts were averaged for each fly (depending if three 10-second videos were taken), and then grouped for each genotype/condition, with mean +/- standard error of the mean (SEM) calculated. Statistical tests were either performed in Microsoft Excel or GraphPad Prism, depending on the test required. One-way analysis of variance (ANOVA) followed by Tukey's post-hoc test was used to identify differences between three or more means derived from uneven sample sizes. The student's unpaired t-test was used to identify significant differences between two means of uneven sample size. A statistical difference of $p<0.05$ was regarded as significant.

2.5 Fluorescent labelling and imageing of adult heart structures

2.5.1 Staining adult *Drosophila* hearts

Fluorescent labelling of *Drosophila* heart structures was performed similar to the protocol described in Alayari *et al.* (ALAYARI *et al.* 2009). Staining of hearts could be performed after functional analysis. The initial fixing step was performed in the 35 mm petri dish so that the splayed abdomen will keep a 'flatter' shape, which made these hearts easier to stain and especially mount. Fixing in this way also meant all the heart preparations had the same treatment. The artificial haemolymph was removed and the semi-intact heart preparations were fixed in 4% formaldehyde (Fisher Scientific, Loughborough, UK) in PBS for 20 mins with gentle agitation. Hearts were then removed from the 35 mm petri dish and placed into a well of a 96-well plate containing 50-200 µL PBS-Triton-X (PBST)(Sigma, Poole, Dorset, UK). Using fine forceps, the edge of the dorsal cuticle was gripped, with care not to touch the heart, and semi-intact heart prep was placed carefully in the well of the 96-well plate. Up to 4 hearts could be stained in each well, and each well could contain different antibodies/stains at different concentrations. Hearts were washed 3X for 10 min in PBST with constant agitation. Hearts were then incubated with primary antibodies/other stains in PBST overnight at 4°C with constant agitation. Hearts were washed 3X 10 mins in PBST and incubated with secondary antibodies for 1-hour at room temp with constant agitation. Finally, hearts were then washed 3X 10 mins in PBST with a final 10 min wash in PBS alone. Hearts can be stored in the 96-well plate in PBS for up to a week at 4°C before mounting. The washing steps are very

important to attain high quality images that have minimal non-specific labelling, and additional washing steps can be performed depending on preference.

2.5.2 Mounting and imageing adult *Drosophila* hearts

To mount, 10 µL of 50% glycerol (Sigma, Poole, Dorset, UK) was placed in the centre of a 22x22 mm coverslip. Hearts were then removed from the 96-well plate using fine forceps and placed heart-side down (i.e. dorsal cuticle facing up) on the mounting medium. Care must be taken when moving these semi-intact heart preps not to touch the heart. Four hearts can be mounted per coverslip, and hearts were orientated in the same direction on each slide, for subsequent ease of imageing. A microscope slide was then placed on top of the coverslip, trapping the hearts in between, with the mounting medium creating a thin layer between the coverslip and the microscope slide, thereby slightly flattening the heart preparations and making them easier to image using an epifluorescence microscope.

Hearts visualised using a Zeiss Axioskop 2 mot plus epifluorescence microscope (Carl Zeiss Ltd., Cambridge, UK) and TIFF images were taken using Openlab imageing software (PerkinElmer, Cambridgeshire, UK). Images were taken using the 10x and 40x objective lenses.

2.5.3 Antibodies and stains used to label adult *Drosophila* heart structures

Mouse anti-βPS-integrin monoclonal antibody (used at 1:10 concentrations of hybridoma supernatant (100 µg/mL), Developmental Studies Hybridoma Bank, #CF.6G11) was used to stain cell junctions and was also useful as a PN stain. This hybridoma developed by Brower *et al.* (BROWER *et al.* 1984) was obtained from the Developmental Studies Hybridoma Bank developed under the auspices of the

NICHD and maintained by The University of Iowa, Department of Biology, Iowa City, IA 52242. AlexaFluor 488 (green) donkey anti-mouse IgG (4 µg/mL – i.e. 1:500 of a 2 mg/mL stock) was used as a secondary antibody to detect the mouse monoclonal primary antibody (#A-21202, Invitrogen, Paisley, UK). AlexaFluor 546-conjugated (red/orange) phalloidin (13.2 nM – i.e. 1:500 of a 6.6 µM stock) was used to stain filamentous (F)-actin and visualise the cytoarchitecture of the fly cardiomyocytes (#A22283, Invitrogen, Paisley, UK). DAPI (100 ng/mL – i.e. 1:10,000 of a 1 mg/mL stock) was used to stain nuclei (#D9542-1MG, Sigma, Poole, Dorset, UK). PBST was used to dilute the stock solutions before application to the fly heart.

2.6 Sorting enriched heart genes from the FlyAtlas dataset

The published tab-delimited FlyAtlas dataset (CHINTAPALLI *et al.* 2007) was downloaded from the FlyAtlas website (http://www.flyatlas.org/) and opened in Microsoft Excel. There was a total of 18,769 genes listed in the dataset. To attain a list of the most highly enriched genes in the *Drosophila* heart, the 'heart ratio' value (i.e. the mean expression of the gene in the adult fly heart divided by the mean expression of the gene in the whole fly) was then sorted from largest to smallest value. Heart enriched genes were defined as having an enrichment greater than 3-fold compared to whole fly.

To attain a list of heart enriched genes which were also highly homologous to human genes, ENSEMBL Gene ID numbers were obtained for the list of highly enriched *Drosophila* heart genes from the GEO Accession viewer website (in this case GPL1322 - http://www.ncbi.nlm.nih.gov/geo/query/acc.cgi?acc=GPL1322).

These *Drosophila* ENSEMBL Gene ID numbers were then aligned with human ENSEMBL Gene ID numbers, obtained from the ENSEMBL BioMart (http://www.ensembl.org/index.html). This list was generated and then annotated by **Dr. Paul Hartley** with relevant information obtained from these websites/databases:

- FlyBase (http://flybase.org/)
- OMIM (http://www.ncbi.nlm.nih.gov/omim)
- BioMart (http://www.ensembl.org/biomart/martview/)
- DAVID (http://david.abcc.ncifcrf.gov/)
- DroID (http://droidb.org/)
- UniProt (http://www.uniprot.org/)
- SWISS-MODEL (http://swissmodel.expasy.org/).

Many genes in the fly did not have human orthologs so these genes were expunged from the list. Similarly, some *Drosophila* genes appeared to have many orthologs in the human – most likely due to gene duplication events – e.g. the *Drosophila* βPS-integrin (*myospheroid*) has 3 orthologous human β-integrin orthologs - β1, β2, and β7. Therefore, the large list of 18,769 FlyAtlas genes was sorted for heart enriched genes, then sorted for similarity to human orthologs. These heart-enriched, human-related genes are listed in the Appendix.

2.7 Measurement of PN size

ImageJ (http://rsbweb.nih.gov/ij/) was used to measure PN diameter. In ImageJ, the 'straight line' drawing tool was selected and a line was drawn between neighbouring PNs. The diameter of 15 PNs per fly was measured, with 4 flies per genotype (i.e. 60 measurements/genotype). Data was then grouped for each genotype and mean +/- SEM was calculated. One-way analysis of variance (ANOVA) followed by Tukey's post-hoc test was used to identify differences between three or

more means derived from uneven sample sizes. The student's unpaired t-test was used to identify significant differences between two means of uneven sample size. A statistical difference of $p<0.05$ was regarded as significant.

2.8 Measurement of distance between neighbouring contralateral cardiomyocytes

ImageJ (http://rsbweb.nih.gov/ij/) was used to measure the distance between neighbouring cardiomyocytes. In ImageJ, the 'straight line' drawing tool was selected and a line was drawn between neighbouring contralateral cardiomyocytes. Lines were drawn from the nearest edges between adjacent cardiomyocytes. The scale was calibrated (Analyse>Set Scale) to measure in microns, and distances were measured using the 'Measure' function (Analyse>Measure, or CTRL+M) in ImageJ. Four measurements were taken for each fly heart, and up to 7 flies were used for each genotype – resulting in 16-28 measurements from 4-7 independent flies for each genotype. Data was then grouped for each genotype and mean +/- SEM was calculated. One-way analysis of variance (ANOVA) followed by Tukey's post-hoc test was used to identify differences between three or more means derived from uneven sample sizes. The student's unpaired t-test was used to identify significant differences between two means of uneven sample size. A statistical difference of $p<0.05$ was regarded as significant.

2.9 Extraction of genomic DNA

Around 10 larvae/pupae/adults were homogenised in 100 µL DNA lysis buffer (100 mM Tris-HCl pH 7.5, 100 mM EDTA pH 8.0, 100 mM NaCl, 0.5%

SDS) using a hand held pestle (Kimble Chase Kontes, Fisher Scientific, Loughborough, UK) in 1.5 mL microcentrifuge tubes. Lysates were incubated for 30 min at 65°C in a hot block. 200 µL LiCl/KAc solution (e.g. 142.5 µL 6 M LiCl + 57.5 µL 5 M KAc) was added, the tubes inverted several times and incubated for 10 min on ice. Samples were spun at room temp for 15 min at 12,000 rpm in a microcentrifuge. 250 µL of supernatant was then transferred to a new autoclaved microcentrifuge tube, excluding floating crud. 150 µL isopropanol was added and the tubes were inverted several times to mix. Samples were spun at room temp for 20 min at 12,000 rpm. The supernatant was discarded, then another quick spin, then aspirated again to remove all of the supernatant. The pellet was washed in cold 70% ethanol then spun at room temp for 10 min at 12,000 rpm. The supernatant was discarded, then another quick spin, then aspirated again to remove all of the supernatant. The pellets were air-dried for 1 hour then resuspended in 75 µL TE overnight at 4°C. Samples were quantified using a NanoDrop ND-1000 Spectrophotometer (NanoDrop, Wilmington, DE, US), then stored at -20°C.

2.10 Genomic PCR

2.10.1 Amplification of long DNA fragments (i.e. >1.5 kb)

PCR reactions were performed in thin-walled PCR tubes (0.2 mL flat cap, Fisher Scientific, Loughborough, UK). On ice, two separate mixes were set up – template/dNTP/primer mix (25 µL), and polymerase/buffer mix (25 µL) – which were added together (50 µL reaction volume). Primers (Eurofins MWG Operon, Acton, London, UK) were kept in stocks of 1 µM. The full list of primers used in this thesis is listed in Table 2.2. For each sample in the template/dNTP/primer mix, 500

nM (0.5 µL) of each forward and reverse primer, 200 µM of each dNTP (or 1 µL of 10 mM dNTP mix (#U1511, Promega, Southampton, UK)), and 250 ng of genomic DNA was made up to 25 µL using dH_2O (if necessary). For each sample in the polymerase/buffer mix, 0.75 µL Expand High Fidelity enzyme (3.5 U/µL, #11732650001, Roche, West Sussex, UK) and 5 µL of 10x Expand High Fidelity buffer with 15 mM $MgCl_2$ (1.5 mM final concentration) was added to 19.25 µL dH_2O (i.e. 25 µL total).

Both of these 25 µL mixes were then added together and mixed well by pipetting up and down. PCR reactions were performed in an Eppendorf Mastercycler gradient thermal cycler (Eppendorf UK Limited, Stevenage, UK) according to the following protocol: a) 95°C for 5 min, b) 95°C for 30 s, c) 53-65°C (temperature was dependent on the melting temperature of the primers designed) for 30 s, d) 72°C for 1-5 min (time was dependent on the size of the product designed), (steps b-d were repeated for 35-40 cycles), 72°C for 10mins and then held at 4°C. For PCR products longer than 3 kb, the elongation temperature was reduced to 68°C.

2.10.2 Amplification of short DNA (and cDNA) fragments (i.e. <1.5 kb)

PCR reactions were performed in thin-walled PCR tubes (0.2 mL flat cap, Fisher Scientific, Loughborough, UK). On ice, two separate mixes were set up – template/dNTP/primer mix (12.5 µL), and polymerase/buffer mix (12.5 µL) – which were added together (25 µL reaction volume). Primers (Eurofins MWG Operon, Acton, London, UK) were kept in stocks of 1 µM. For each sample in the template/dNTP/primer mix, 500 nM (0.25 µL) of each forward and reverse primer, 200 µM of each dNTP (or 0.5 µL of 10 mM dNTP mix (#U1511, Promega,

Southampton, UK)), and 250 ng of genomic DNA (or cDNA) was made up to 12.5 µL using dH_2O (if necessary). For each sample in the polymerase/buffer mix, 0.125 µL GoTaq DNA Polymerase (5 U/µL, #M3171, Promega, Southampton, UK) and 5 µL of 5x Green GoTaq Reaction Buffer was added to 7.375 µL dH_2O (i.e. 12.5 µL total).

Both of these 12.5 µL mixes were then added together and mixed well by pipetting up and down. PCR reactions were performed in an Eppendorf Mastercycler gradient thermal cycler (Eppendorf UK Limited, Stevenage, UK) according to the following protocol: a) 95°C for 5 min, b) 95°C for 30 s, c) 53-65°C (temperature was dependent on the melting temperature of the primers designed) for 30 s, d) 72°C for 30 s-1 min (time was dependent on the size of the product designed), (steps b-d were repeated for 35-40 cycles), and then held at 4°C.

Table 2.2 – List of primers used in this PhD thesis		
Primer	**Primer sequence (5'-3')**	**Product size**
Full length Fit1 F	CATCCGTTCCGATAAGTTCG	3,616 bp
Full length Fit1 R	ACAAGCCAGCCACCATTTAC	
Wider Fit1 F	TGTGGTACGGGAGTTTGTCA	4,844 bp
Wider Fit1 R	ACAAGCCAGCCACCATTTAC	
$Fit1^{\Delta 161}$ F	CATCCGTTCCGATAAGTTCG	2,589 bp WT, 916 bp in *Fit1*$^{\Delta 161}$ flies
$Fit1^{\Delta 161}$ R	CCAACAGCTCCTCCTTCTTG	
Check for $Fit1^{\Delta 161}$ F	CTGCTCTGCTGCTGGTTTAT	1,945 bp WT, 250 bp in *Fit1*$^{\Delta 161}$ flies
Check for $Fit1^{\Delta 161}$ R	GAACCTTTGAGGCTTGAGGA	
Full length Fit2 F	GCAATCCGGGCTTTTATATG	3,754 bp
Full length Fit2 R	TCGATTAAGCTTCACGATATAAGTTT	
Fit1 RT-PCR F	AACAGTGAGGTCTGGGTGAGAT	398 bp for RT-PCR
Fit1 RT-PCR R	AACAGCTCCTCCTTCTTGTGTC	
Fit2 RT-PCR F	ACGGTATCAACAGTGAGGTGTG	390 bp for RT-PCR
Fit2 RT-PCR R	GATGCCCGTCGAACTTAATG	
RP49-330 F	GACAATCTCCTTGCGCTTCT	330 bp for PCR, 268 bp for RT-PCR
RP49-330 R	CCAGTCGGATCGATATGCTAA	
RP49-128 F	CGGATCGATATGCTAAGCTGT	128 bp
RP49-128 R	CGACGCACTCTGTTGTCG	
CG14995 RT-PCR F	GCGGCGGAGAGAATATTTGA	286 bp for RT-PCR
CG14995 RT-PCR F	AGGTGCACCACAATCCCTAT	
Ack RT-PCR F	AATGGCAGTGGAGCTGTTCT	396 bp for RT-PCR
Ack RT-PCR R	TAAGCTCCAGTTGGTCTGCT	
a10 RT-PCR F	TTGGCCTTGGACTTCATCTC	331 bp for RT-PCR
a10 RT-PCR R	TGGAAAGAATGGTGGAGCAG	

CG7730 RT-PCR F	CAGGAGCTGGCTACAAAGTT	358 bp for RT-PCR
CG7730 RT-PCR R	GGGATTTCGTTGAGGGTTCT	
CG14989 RT-PCR F	TGGTCACAATCCTCATCCTG	229 bp for RT-PCR
CG14989 RT-PCR F	ACCCATCTGACCACAAAAGC	
CG14990 RT-PCR F	GTAGTGCGACTGGGCAAAAT	240 bp for RT-PCR
CG14990 RT-PCR F	GACTACTTCTGGGGCAATCA	
GAL4 F	TTCTTCTGTCGACGATGTGC	242 bp
GAL4 R	AATTGGTTAGAGCGGTGGTG	
$GAL80^{ts}$ F	ATCGAGATTGCTGGAAATGG	224 bp
$GAL80^{ts}$ R	AATCGGTTACCACGCTCATC	

2.11 Agarose gel electrophoresis

Agarose gels were prepared at concentration of 1% agarose (Sigma, Poole, Dorset, UK) dissolved in 1x TAE buffer. If the amplicon size was small, a higher agarose concentration was used (e.g. 1.2% agarose). Similarly, if the amplicon was large then a lower agarose concentration was used (e.g. 0.8% agarose). Samples were loaded with the appropriate DNA step ladder – either 100 kb DNA ladder (Promega, #G210A) or 1 kb DNA ladder (Promega, #G571A) – depending on the size of the PCR product. Gels were electrophoresed at 100-120 V (until the yellow marker reached ¾ of the way down the gel) in electrophoresis tanks in 1x TAE buffer containing 300 ng/mL EtBr (i.e. 3 µL of 10 mg/mL stock in 1 L 1x TAE buffer). Different sizes/concentrations of gels were used depending on the number of samples and/or the degree of separation required. Images of electrophoresed gels were taken with Uvitec Gel Doc system (Uvitec, Cambridge, UK).

2.12 RNA extraction

2.12.1 Extracting RNA from whole animals

RNA from embryos/larvae/pupae/adults was extracted using a combination of phenol/chloroform and RNAid matrix (Anachem, Bedfordshire, UK) extraction methods. Samples were homogenised in 300 µL Trizol (Invitrogen, Paisley, UK) - homogenised in 100 µL then made up to 300 µL to avoid spillages - using a hand-held homogeniser on dry ice, then left to stand at room temp for 5 min. To this homogenate, 200 µL of chloroform per 1 mL Trizol (i.e. 60 µL if 300 µL Trizol) was added and the tubes were shaken then vortexed for 15 s and left to stand at room temp for 3 min. Samples were centrifuged at 12,000 rpm for 15 min at 4°C then the aqueous phase was transferred to a fresh tube. To this, 8 µL of well-suspended RNAid matrix was added (RNAid matrix was vortexed after every 3 samples to keep suspended), vortexed then agitated for 3-5mins. Samples were spun at 12,000 rpm for 1 min to pellet and the supernatant discarded. 300 µL RNAid wash solution (Anachem, Bedfordshire, UK) was used to resuspend the pellets using large pipette tips then vortexed. The samples were centrifuged at 12,000 rpm for 1 min to pellet. The wash step was repeated twice more. The supernatant was discarded then the pellet resuspended in 20-25 µL RNAse-free H_2O (#P1193, Promega, Southampton, UK). Samples were then incubated in a hot-block at 60°C for 12 min (vortexing after 6 min). Samples were spun at 12,000 rpm for 1 min then put on ice. The supernatant was then removed and aliquoted (e.g. 3 x 6 µL), snap-frozen on dry ice, and the remainder (after a final spin at 12,000 rpm) was used for quantification on the NanoDrop (NanoDrop, Wilmington, DE, US).

2.12.2 Extracting RNA from adult *Drosophila* hearts

For fly heart RT-PCR, total RNA was extracted from 20 dissected hearts of 1-week old adult females using TRIzol (Invitrogen, Paisley, UK) phenol-chloroform extraction method with isopropanol precipitation. Extracted hearts were placed in a petri dish containing a pool of 500 µL TRIzol. The heart-containing TRIzol solution was then transferred into a 1.5 mL microcentrifuge tube, vortexed for 15 s then kept on ice for 3 min. To this homogenate, 200 µL of chloroform per 1 mL TRIzol (i.e. 100 µL if 500 µL TRIzol) was added and the tubes were shaken then vortexed for 15 s and left to stand at room temp for 3 min. Samples were centrifuged at 12,000 rpm for 15 min at 4°C then the aqueous phase was transferred to a fresh tube. To this, 700 µL of isopropanol (VWR, Leicestershire, UK) per 1 mL TRIzol (i.e. 350 µL if 500 µL TRIzol) was added to precipitate the RNA, vortexed then left to stand for 5 min. Samples were spun at 12,000 rpm for 15 min at 4°C, and the supernatant discarded. 1 mL 70% ethanol/dH_2O was used to wash the pellets, then samples were spun at 12,000 rpm for 10 min at 4°C. This wash step was repeated twice more. After the final wash, the supernatant was discarded, and the pellet left to air dry on ice for 15 min. The pellet was then resuspended in 15-20 µL nuclease-free DEPC-treated H_2O – RNA dissolved more readily when the DEPC-treated H_2O was preheated to 55°C. The supernatant was then removed and aliquoted (e.g. 3 x 6 µL), snap-frozen on dry ice, and the remainder (after a final spin at 12,000 rpm) was used for quantification on the NanoDrop (NanoDrop, Wilmington, DE, US).

2.13 DNAse treatment to remove potential DNA contamination of RNA samples

Depending on the RNA concentration (which can be very low from adult *Drosophila* hearts), each sample was diluted in nuclease-free DEPC-H_2O to make all samples have the same RNA concentration (e.g. 60 ng/µL). On ice, each RNA sample was then treated with RQ1 RNase-free DNase (#M6101, Promega, Southampton, UK). 1 µL of RQ1 RNase-free DNase and 1 µL RQ1 DNase 10x Reaction Buffer was added to 8 µL RNA (= 10 µL total), which was then incubated at 37°C for 30 min. Then 1 µL RQ1 DNase Stop Solution was added to each sample (= 11 µL) and incubated at 65°C for 10 min.

2.14 Reverse transcription and cDNA synthesis

In a new PCR tube, 6.5 µL of DNAse-treated RNA was then added to 4 µL oligo-dT primer (=10.5 µL total) (Eurofins MWG Operon, Acton, London, UK) and incubated at 65°C for 10 min. Then 9.5 µL of Reverse Transcriptase (RT) mix – containing 4 µL M-MLV RT 5x Buffer (#M1701, Promega, Southampton, UK), 2 µL DTT, 2 µL dNTP mix, 0.5 µL RNasin Plus RNase Inhibitor (#N2611, Promega, Southampton, UK), and 1 µL M-MLV Reverse Transcriptase (#M1701, Promega, Southampton, UK) – was added to the oligo-dT-primed RNA (= 20 µL total). For NoRT (no reverse transcriptase) controls, 1 µL H_2O was added instead of M-MLV Reverse Transcriptase. Samples were then incubated at 43°C for 1 hour. The cDNA was then ready to serve as a template for PCR reactions – 2.5 µL of the 20 µL cDNA template was usually used per PCR reaction, thus 8 PCRs were performed per sample.

2.15 Quantitative PCR

Quantitative PCR was performed on a Roche LightCycler® using 2X 480 Probes Master mix (Roche, Hertfordshire, UK) and primer/probe sets from both Roche and Eurofins MWG Operon (Ebersberg, Germany). The relevant probes were obtained from the Universal ProbeLibrary (Roche, Hertfordshire, UK). Briefly, cDNA sample was added to 2X master mix, 100 µM forward primer, 100 µM reverse primer, 10 µM UPL probe and nuclease-free H2O and added to each LightCycler plate well. This was pre-incubated at 95°C for 10 min for activation of DNA Polymerase and denaturation of the DNA. Amplification of the cDNA then occurs via cycles of denaturation (95°C for 10 s), annealing (60°C for 30 s) and extension (72°C for 1 s) for 50 cycles.

2.16 Assessing developmental lethality

Flies were allowed to lay eggs in egg cages containing fructose-agar plates with some yeast paste for 4-h. Eggs were then counted. Egg plates were left in the 25°C incubator for 30-h – until all the fertilised embryos had hatched. Unhatched eggs were then counted. Larvae were then left to develop to the pupal stage. Pupae were then counted. After all pupae eclosed, the number of adults was then counted. The experiment was repeated 3 times. The percentage of eggs that hatched was calculated by subtracting the number of unhatched eggs from the total number of eggs laid (i.e. the number of larvae that hatched), then dividing this number by the total number of eggs laid, then x 100. The percentage of larvae that pupated was calculated by the number of pupae divided by the number of hatched larvae, then x

100. The percentage of pupae that eclosed was calculated by the number of adults divided by the number of pupae, then x 100.

2.17 Measurement of lifespan

Five cohorts of 30 newly-eclosed (i.e. <12-hour old) flies of the relevant genotype (10 males and 20 females, n = 150 per cohort) were collected and put into vials containing Bloomington medium. These vials were then kept in the 29°C incubator for the duration of the experiment. Survival was measured every time the flies were transferred to fresh food (twice a week) - dead flies discarded after transfer. Values from the 5 vials per genotype were then averaged and survivorship curves (±SEM) were then plotted.

2.18 Targeted second-site non-complementation mini-screen

To set up crosses for the mini-screen, ~15 flies of the relevant genotypes (e.g. 5 w^{1118} males and 10 mys^{1} virgin females) were collected and put into individual vials containing Bloomington medium and kept in the 29°C incubator. After laying eggs for 4 days, these flies were then tipped into a new vial to lay for a further 4 days. This was repeated a final time for 3 experimental replicates – after the final 4 days, the parents were discarded. In all, 168 crosses were set up. Progeny from each cross were sorted and counted based on their phenotype. Absolute numbers for each screen were entered into individual Microsoft Excel spreadsheets for each set of crosses, and observed/expected progeny ratio calculations were performed. In all, 21,380 flies were counted in this mini-screen. Full results of the screen with absolute numbers are listed in the Appendix.

Lines used in this screen included: w^{1118} = wildtype, *Fit1*^{KG05576} = P-element inserted into *Fit1* 5' UTR, *Fit2*^{EY08530} = P-element inserted into *Fit2* 5' UTR, *Fit1*$^{\Delta 81}$ = apparent precise excision, *Fit1*$^{\Delta 161}$ = predicted *Fit1*-null, *Fit1*$^{\Delta 193}$ = *Fit1*-null, *Fit1*$^{\Delta 161}$ *Fit2*^{EY08530} = predicted double *Fit1/Fit2*-null/hypomorph, *mys*^{1} = βPS-integrin, *mew*^{M6} = αPS2-integrin, *if*^{B2} = αPS1-integrin, *rhea*^{1} = talin, *Ilk*^{1} = integrin-linked kinase, *stck*$^{3R-17}$ = PINCH, *arm*^{4} = β-catenin, *pan*^{2} = TCF.

Chapter 3

Investigating the effect of ageing, and diurnal rhythms on adult heart function in *Drosophila*

3.1 Introduction

3.1.1 *Drosophila* as a model of human cardiac physiology

Although the fly heart differs from the human heart in many respects (e.g. size and structure), the function is conserved between species. It is a muscular pump that contracts rhythmically to distribute haemolymph (blood) and nutrients throughout the organism. Indeed, the recognition that much of the regulatory genetic network controlling heart differentiation is conserved from flies to mammals means that models of congenital heart disease can be formulated (OCORR *et al.* 2007b). *Drosophila* has been advocated as a model of the changes in heart function that occur with ageing. In ageing flies, as in humans, heart function and performance become increasingly irregular with arrhythmia becoming more frequent; reminiscent of increases in arrhythmias and heart failure in elderly humans (NEELY *et al.* 2010b). Indeed, genetic screens have been performed in *Drosophila* and have identified candidate genes that directly translate into conserved mammalian orthologs involved in heart function (NEELY *et al.* 2010b). Conversely, a recent study identified heart rate-associated loci in the human genome, and confirmed their effects in *Drosophila* (DEN HOED et al. 2013). However, care must be taken when extrapolating hypotheses to the human heart as these two systems also exhibit many differences (MEDIONI *et al.* 2009).

3.1.2 The structure of the *Drosophila* heart

The *Drosophila melanogaster* heart is a tubular structure consisting of a single layer of contractile cardiomyocytes, pericardial cells that are aligned parallel to each side of the heart wall, ancillary alary muscles and a sheath of ventral

longitudinal myocytes (ALAYARI *et al.* 2009) – summarised in Figure 3.1. The cellular mechanisms involved in heart function are similar for both insects and vertebrates. For example, the fruit fly heart is capable of spontaneous rhythmic activity for the circulation of haemolymph. Insects have an open circulatory system, but their relatively high metabolism requires that this system be efficient in circulating haemolymph (DULCIS and LEVINE 2003). Heart function in flies and humans is also regulated by genes with conserved structures and functions (OCORR *et al.* 2007b).

3.1.3 Factors which may affect *Drosophila* heart function

3.1.3.1 Age is known to affect *Drosophila* heart function

In humans, age is a major risk factor for developing cardiovascular abnormalities, and cardiac arrhythmias have been shown to increase with age – with higher incidences of atrial fibrillation and ventricular arrhythmias in the elderly (LAKATTA 2003). Previous studies have demonstrated that heart function declines with increasing age of the fruit fly (WESSELLS *et al.* 2004), and has been used as a measure of functional senescence (OCORR *et al.* 2007a; OCORR *et al.* 2007b; WESSELLS *et al.* 2004). Indeed, the *Drosophila* heart was shown to become more arrhythmic with increasing age (OCORR *et al.* 2007a; OCORR *et al.* 2007c), while younger hearts displayed a lower degree of arrhythmicity.

3.1.3.2 Circadian time

Circadian rhythms are biological processes that display an endogenous, entrainable cycle of approximately 24 hours. Examples include, sleep/wake behaviour, body temperature, hormone production, and cell regeneration

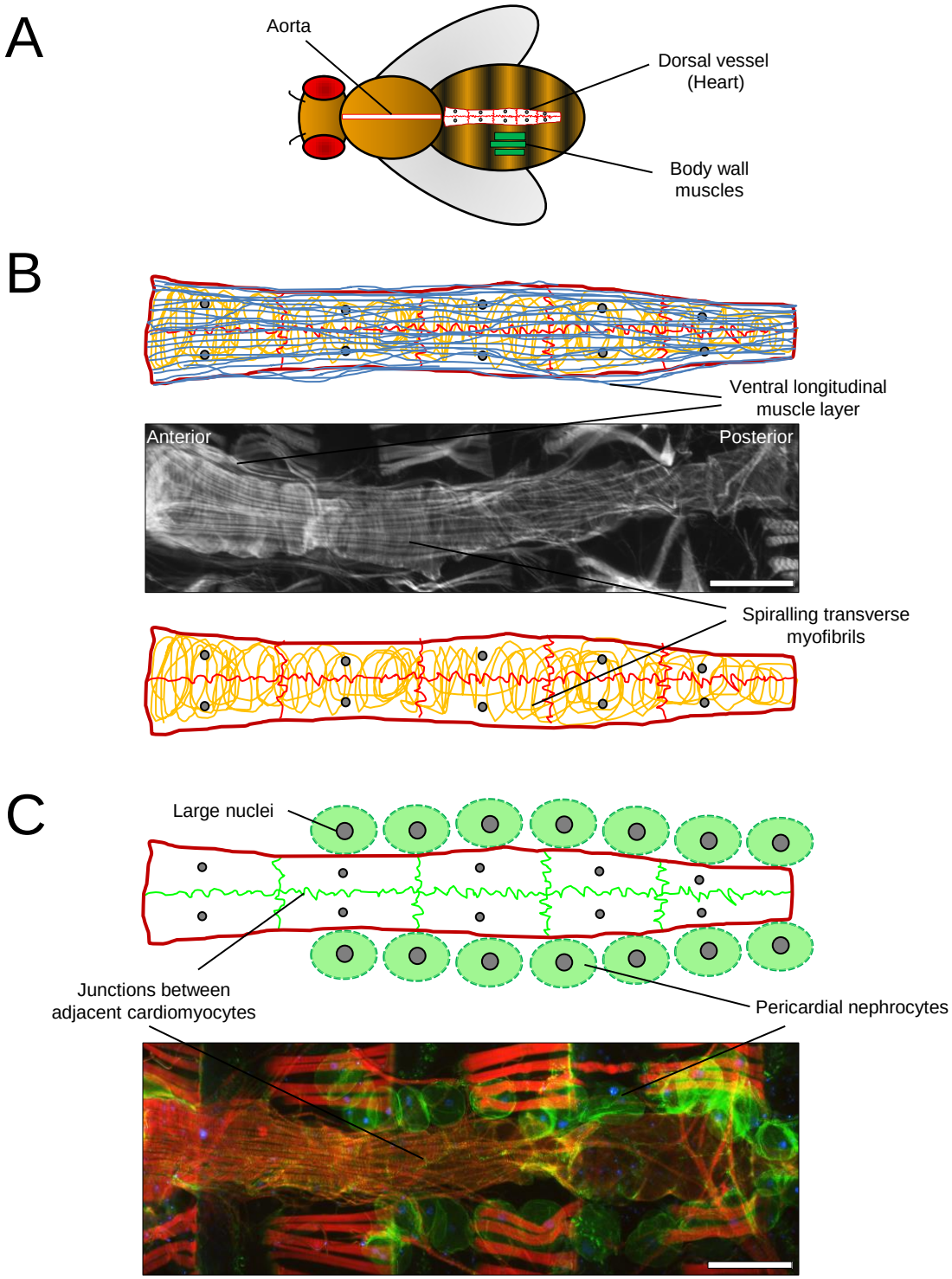

Figure 3.1. The adult heart of *Drosophila melanogaster*.
A, the adult *Drosophila* heart runs along the back of the dorsal abdomen. **B**, schematic of the cardiac tube highlighting the ventral longitudinal muscle layer, and the spiralling transverse myofibrils. These structures are indicated on a fluorescent grayscale image of the *Drosophila* heart labelled with phalloidin. **C**, schematic of the cardiac tube and the attached pericardial nephrocytes (large cells that flank the heart), with the junctions between cardiomyocytes also labelled green. These structures are also highlighted on a fluorescent image of the heart and pericardial nephrocytes. Hearts are stained with Alexa-conjugated phalloidin (red), anti-βPS integrin antibody (green), and DAPI (blue). Scale bar = 100µm.

(FOSTER and KREITZMAN 2004). These rhythms are important to prepare the organism for events and stresses that occur throughout the day. Indeed, the mammalian heart has been shown to anticipate changes within its environment over the course of the day (YOUNG *et al.* 2001), and is said to exhibit a diurnal rhythm in function.

Although the canonical clock genes (i.e. *Clock*, *Period*, *Cycle*, *Timeless*) are expressed in the fly heart (CHINTAPALLI *et al.* 2007), changes in *Drosophila* heart function over the course of the day have not previously been studied. Therefore, it was reasoned that since functional recordings of the fly heart may be performed at different points during the day, that it was necessary to assess whether there was a significant degree of variability in heart function over the diurnal cycle.

Accordingly, genetic techniques and morphological analysis was used to develop the adult *Drosophila* as a model of human heart function, and the involvement of ageing, and time of day (i.e. diurnal rhythms) on cardiovascular function/morphology was assessed.

3.2 Verification of the model and hypothesis

In order to verify the adult *Drosophila* model of heart function developed by Rolf Bodmer's lab, the effects of ageing on heart function were assessed. Findings from the previous studies have demonstrated that heart function declines with age.

It was also hypothesised that circadian rhythms may contribute to heart function variability in the adult *Drosophila*.

3.2.1 Aims

1) Recapitulate the findings of the Bodmer lab by assessing heart function

   a. In flies at different ages (i.e. 1 wk to 6 wk old)

2) Investigate the role of the circadian clock on adult *Drosophila* heart function

3.3 Results

As the human heart ages, there is a decline in a variety of functional cardiac parameters (e.g. increased arrhythmias, impaired response to heart stress) that correlate with increased morbidity and early mortality (OCORR *et al.* 2007a; OCORR *et al.* 2007b). To verify the adult *Drosophila melanogaster* as a model of human heart function, adult female fly hearts were functionally assessed via videomicroscopy and quantitative analysis of these videos using a MatLab-based software analysis program (OCORR *et al.* 2009). Briefly, flies were anaesthetised (using CO_2), dissected in artificial haemolymph to expose the abdominal heart, then assessed by video analysis of each 10-second heart clip – output parameters include heart rate, heart period, systolic interval, diastolic interval, arrhythmicity index, and fractional shortening.

3.3.1 *Drosophila* heart function decreased with age

To verify the adult *Drosophila melanogaster* as a model of human heart ageing, wildtype adult female *Canton-S* (*CaS*) flies were aged and had their heart function assessed over a period of 6-weeks – the results are shown in Figure 3.2. As expected, heart rate declined as the flies aged (2.15Hz (±0.13) 1-wk old vs. 1.58Hz (±0.15) 6-wk old, $p<0.05$), while the heart period (i.e. the length of time the heart takes to go through one systolic/diastolic cycle) increased (0.51s (±0.04) 1-wk old vs. 0.67s (±0.06) 6-wk old, $p<0.05$), thus the model was verified as providing data comparable to that from the Bodmer group. The arrhythmicity index was significantly higher in younger flies (0.2 (±0.03) 2-wk old vs. 0.06 (±0.01) 6-wk old, $p<0.01$) compared to older counterparts (OCORR *et al.* 2007a). Cardiac contractility

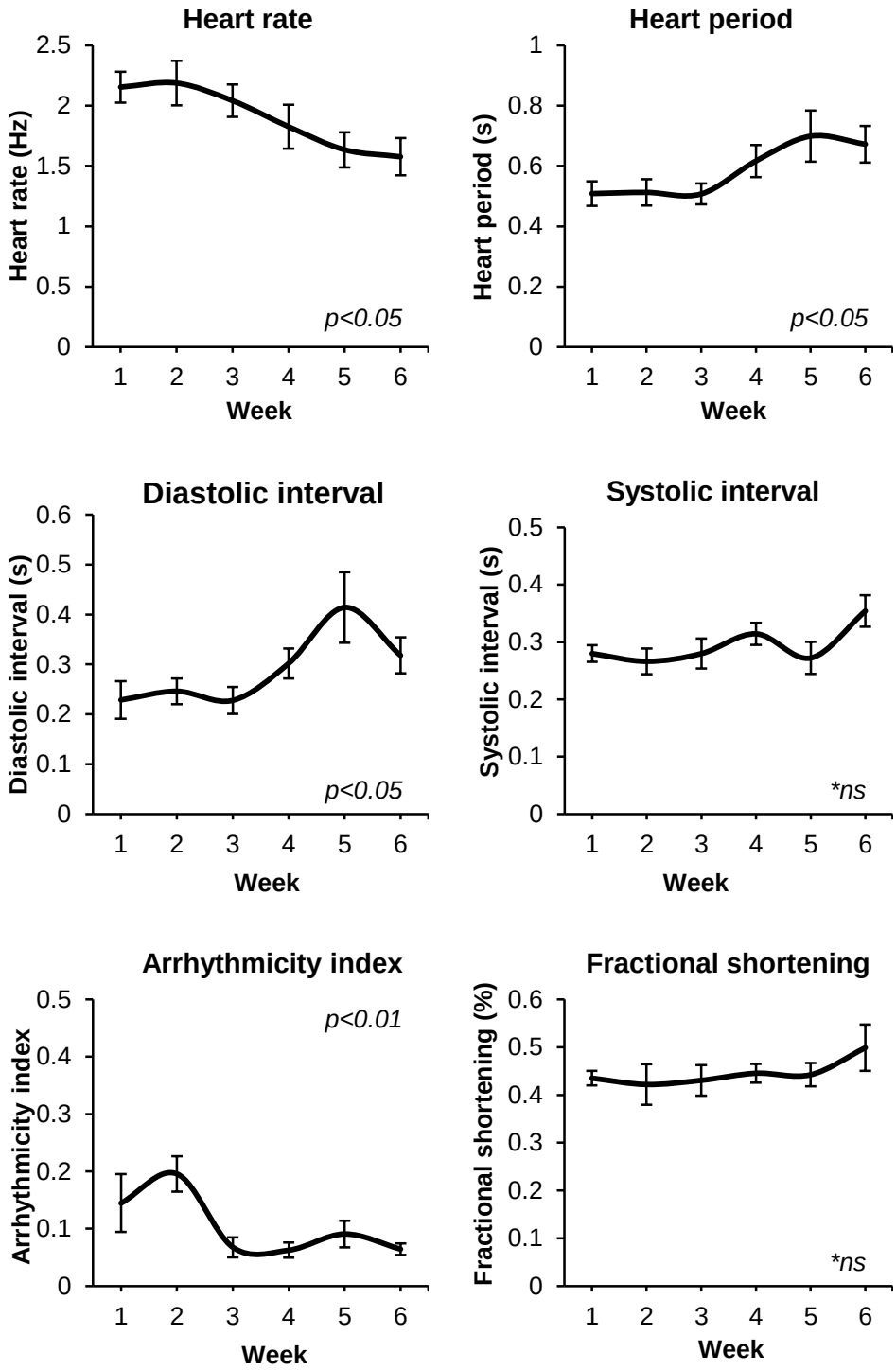

Figure 3.2. Heart function exhibits an age-related decline in *Drosophila.*

Heart function of wildtype (*CaS* female) flies from 1 to 6-wk old. There was a gradual (and significant) decrease in heart rate, with an accompanying significant increase in heart period, and diastolic interval as the flies aged. Surprisingly, there was a significant decrease in arrhythmicity in older flies compared to younger. There was no significant difference in any of the other functional parameters measured over the day. Results are mean ± SEM, n = 7-8 flies per time point (3 videos per fly). One-way ANOVA was performed.

(i.e. fractional shortening – the degree to which the heart walls contract) remained unchanged over the 6-week analysis period in these flies.

3.3.2 Assessing diurnal variation in *Drosophila* heart function

3.3.2.1 Wildtype *Canton-S* flies did not exhibit a significant diurnal rhythm in heart function

The mammalian heart has been shown to anticipate and adapt to changes within its environment over the course of the day, and there are intrinsic diurnal rhythms in heart rate, blood pressure, metabolism, and contractile function (MORRIS *et al.* 2012; YOUNG *et al.* 2001). Therefore, the adult fly heart was assessed for changes in heart function over the 24-hr light/dark cycle. Wildtype *CaS* flies were entrained to a 12:12-hr light:dark schedule for 1-week. Heart function was then assessed at 6 different time-points over the course of the day (i.e. 1, 4, 9, 13, 16, and 21 hours after 'lights on' – 3 time-points during the subjective day, 3 time-points during the subjective night). The results are shown in Figure 3.3. There was no significant difference in any of the heart parameters measured over the course of the day ($p>0.05$).

3.3.2.2 Functional analysis of the circadian mutant, per^{01}, revealed no diurnal rhythm, but a significant difference in heart rate at one time-point compared to background control line

To study diurnal cardiac rhythms in *Drosophila*, circadian clock-mutant (*period*-null – per^{01}) flies were also functionally assessed over the course of a single diurnal/circadian cycle. The results are shown in Figure 3.4. Like wildtype flies, clock-mutant ($yper^{01}w$) flies and their background control line (*yw*) individually did

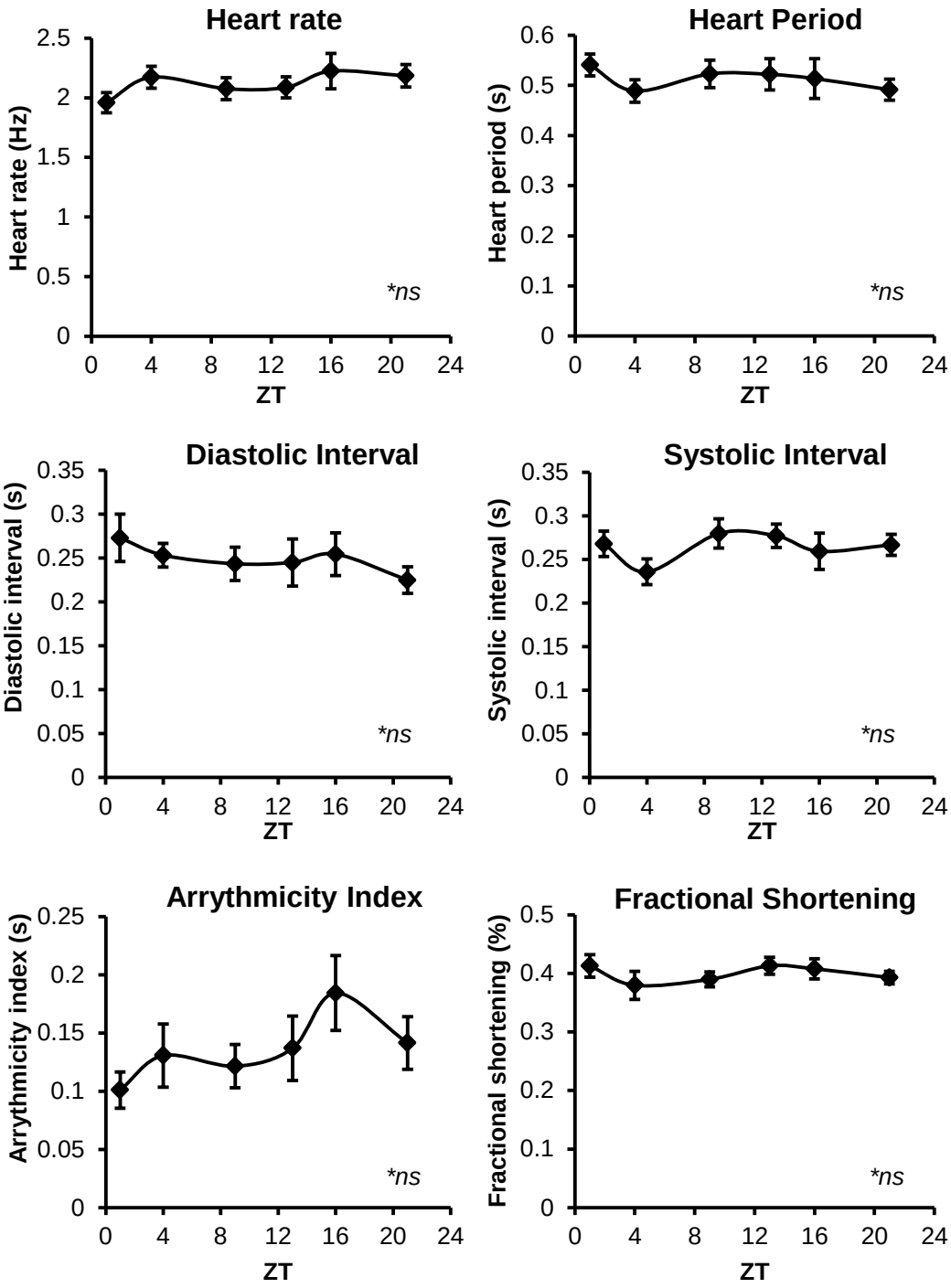

Figure 3.3. Heart function parameters in wildtype adult flies do not exhibit a diurnal rhythm.

Heart function was assessed at six time points over the course of the day in adult female *Drosophila*. There was no significant difference in any of the functional parameters measured over the day. Results are mean ± SEM, *n* = 16-24 flies per time point. One-way ANOVA with Tukey's post-hoc test was performed.

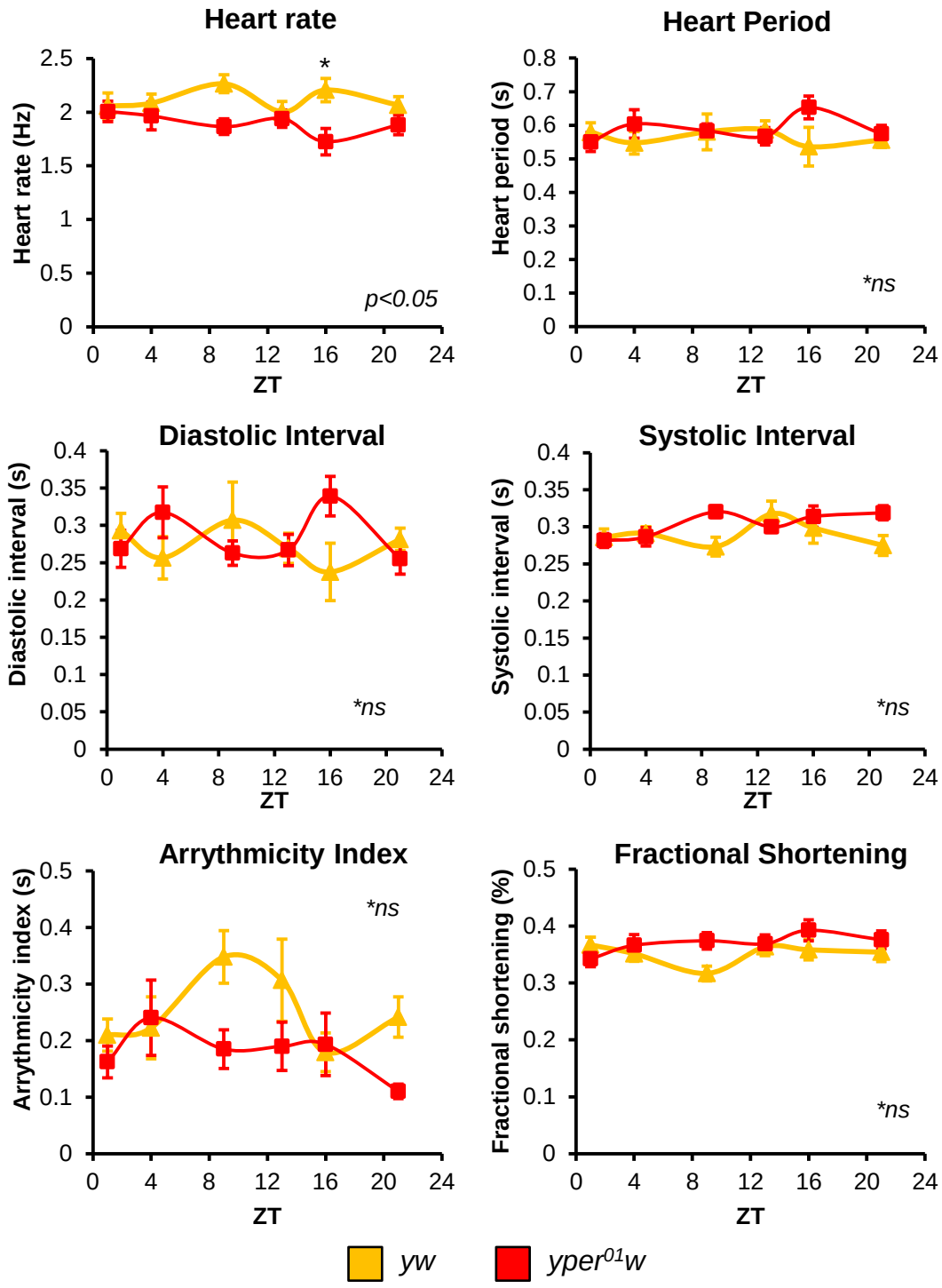

Figure 3.4. The clock mutant, *yper^{01}w*, differs from its background control, *yw*, in only one parameter at a single time point.
Heart function was assessed at six time points over the course of the day in adult female *yw* and *yper^{01}w* flies. Each genotype individually did not exhibit a significant diurnal rhythm in heart function. Heart rate was significantly lower in *yper^{01}w* flies at ZT16 compared to *yw* controls. There was no significant difference between any other time point, in any of the functional parameters measured over the day between these genotypes. Results are mean ± SEM, for *yw, n* = 22-24 flies per genotype per time point; for *yper^{01}w, n* = 17-24 flies per genotype per time point. *p<0.05, one-way ANOVA with Tukey's post-hoc test.

not show significant differences in any of the heart function parameters over the course of the day. In other words, in all three of the genotypes tested over the course of the light/dark cycle, none exhibited a diurnal rhythm in heart function. When the *yw* and *yper*^{01}*w* lines are compared, however, there did appear to be a small yet significant difference in heart rate at a single time-point in the middle of the night (ZT16), with *yper*^{01}*w* flies displaying a lower heart rate compared to *yw* background controls (2.21Hz (±0.11) *yw* vs. 1.72Hz (±0.12) *yper*^{01}*w*, $p<0.05$). There was no significant difference in any other measured heart parameter between these two genotypes, however.

3.3.3 Assessing heart morphology of circadian-knockdown adults

To examine the effect of abolishing individual circadian clock components in a cardiac-specific manner, the GAL4-UAS system was utilised to overexpress dominant-negative versions of the Clock and Cycle proteins (a kind gift from Paul Hardin: e.g. *UAS-Clk*^{DN} and *UAS-Cyc*^{DN}) or by depleting RNA levels by overexpressing RNAi targeted against endogenously expressed RNA (obtained from the Vienna *Drosophila* Research Center: e.g. *UAS-Clk*^{VDRC} and *Per*^{VDRC}). To limit the ectopic GAL4 expression to the heart, UAS lines were crossed to *TinCΔ4-GAL4* or *HandC-GAL4* lines (kind gifts from Manfred Frasch and Achim Paululat, respectively). The aim was to individually abolish each clock component in the heart of the fly and perform morphological analysis by staining open-heart preparations with phalloidin (to visualise structural F-actin) and anti-βPS-integrin antibody (to highlight alterations in cardiomyocyte-cardiomyocyte junctional integrity, as well as any deleterious effects on associated PNs).

3.3.3.1 Cardiomyocyte-specific ablation (using the *TinCΔ4-GAL4* driver) of core circadian clock components

The aforementioned clock-ablating UAS lines were overexpressed in the *Drosophila* heart using the cardiomyocyte-specific *TinCΔ4-GAL4* driver (LO and FRASCH 2001). The results are displayed in Figure 3.5. In control hearts (w^{1118}; *TinCΔ4-GAL4*), the *Drosophila* cardiac tube consists of cardiomyocytes that contain transverse spiralling myofibrils, covered by a layer of ventral longitudinal muscle, with PNs flanking the heart.

There was a noticeable effect of cardiac-specific Clk^{DN} overexpression on viability – with only 2-3 flies eclosing (out of hundreds of pupae) and appearing severely unhealthy, while the remainder died as pharate adults during late-stage pupation. Those flies that did emerge as adults were severely deformed (e.g. misshapen legs, with some failing to fully emerge from their pupal case). In *TinCΔ4-GAL4>*Clk^{DN} hearts, the heart is severely abnormal – with wisp-like phalloidin-stained structures present where the conical chamber is situated, at the anterior end of the abdomen. The lack of phalloidin staining along the rest of the heart appears to indicate an absence of filamentous actin, and thus, any contractile muscle structures. βPS-integrin staining highlighted the cell boundaries along the heart tube in these flies indicating the cardiac tube is still present. This result was not repeated in *TinCΔ4>*Clk^{VDRC} hearts - which were similar to wildtype controls. Hearts of *TinCΔ4>*Cyc^{DN} and *TinCΔ4>*Per^{VDRC} flies were also similar to wildtype.

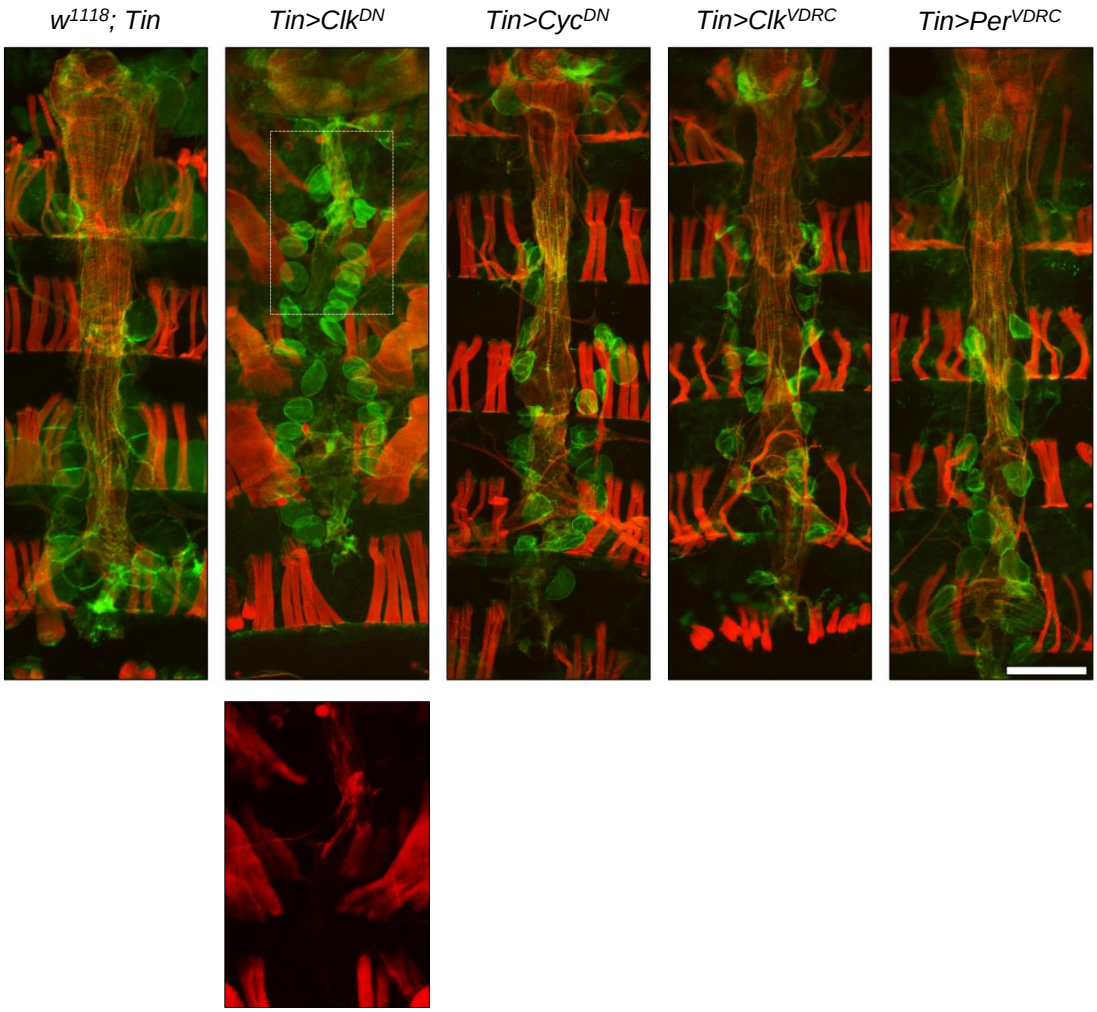

Figure 3.5. Screening selected clock genes for changes in cardiomyocyte morphology in the fly heart using the *TinCΔ4-GAL4* driver.
Overexpression of a dominant negative form of *Clk* in fly cardiomyocytes led to significant disruption of cardiac syncytium development. There was also ectopic body wall muscle expression in these flies. There was no significant effect from any of the other clock-disrupting UAS lines on cardiomyocyte morphology. Hearts are stained with Alexa-conjugated phalloidin (red), and anti-βPS integrin antibody (green). Scale bar = 100μm.

3.3.3.2 Cardiomyocyte ablation (using the *HandC-GAL4* driver) of core circadian clock components

The effect of these clock-disrupting UAS lines on adult heart morphology was further tested using another heart GAL4 driver, *HandC-GAL4*, which strongly drives developmental gene expression in the heart, but also in the PNs, and lymph glands (SELLIN *et al.* 2006). The results are displayed in Figure 3.6.

There were no surviving progeny from the *HandC>Clk*^{DN} crosses indicating a deleterious effect of this UAS line on *Drosophila* development. βPS-integrin staining in *HandC>Per*^{VDRC} PNs also appeared weaker compared to controls (*w*^{1118}*; HandC-GAL4*). For the remainder of the UAS lines, there was no significant effect on heart morphology after overexpression of *Clk*^{VDRC}, *Cyc*^{DN}, or *Per*^{VDRC} using the *HandC* driver.

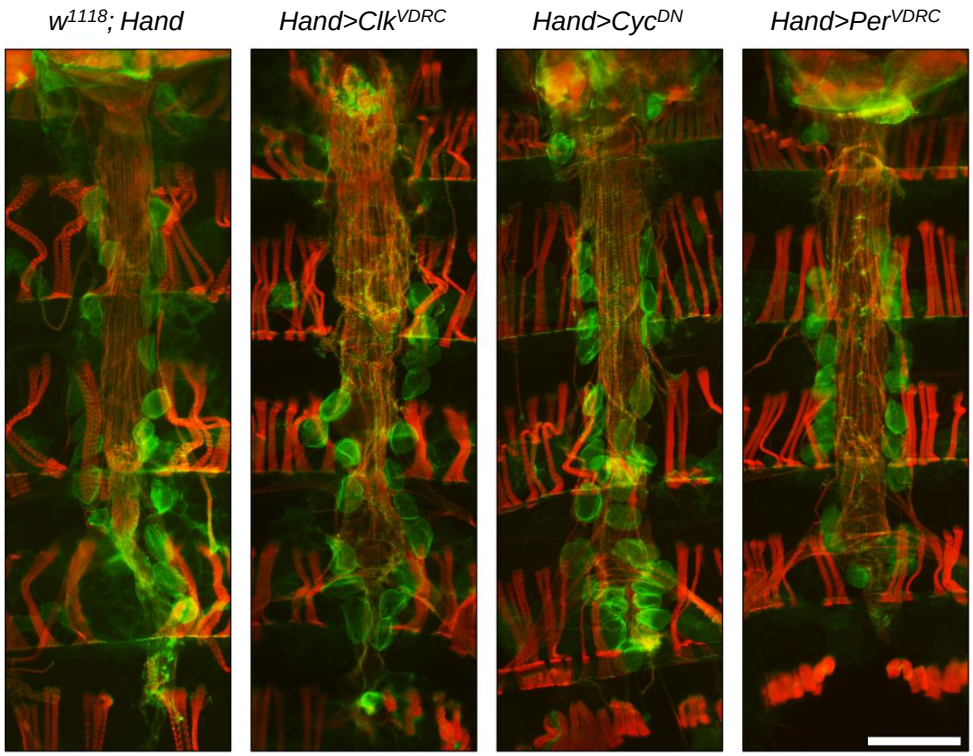

Figure 3.6. Screening selected clock genes for changes in pericardial nephrocyte as well as cardiomyocyte morphology in the fly heart using the *Hand-GAL4* driver.

There was no significant effect from any of the clock-disrupting UAS lines on cardiomyocyte or pericardial cell morphology, however, the β-integrin staining appears less intense in *Hand>Per^{VDRC}* hearts. Hearts are stained with Alexa-conjugated phalloidin (red), and anti-βPS integrin antibody (green). Scale bar = 100µm.

3.4 Discussion

The aim was to develop and characterise the adult *Drosophila* heart as a model of human heart function, by assessing measures which have previously been used to confirm the usefulness of *Drosophila* as a model. Effects of ageing and time-of-day on heart function were assessed, and while some results agreed with previously published data, others did not. These factors will be discussed, as well as the appropriateness of the adult *Drosophila* heart as a model of human heart function.

3.4.1 *Drosophila* heart function declined with age

In agreement with previously published findings concerning the ageing *Drosophila* heart (WESSELLS *et al.* 2004), heart rate declined as the flies aged. Functional decline was characterised by an increased diastolic interval. Unlike in elderly humans, where a higher resting heart rate is viewed as a predictor of cardiovascular and all-cause mortality (FOX *et al.* 2007), in *Drosophila*, heart rate declines with increasing age – and is seen as a sign of functional senescence (OCORR *et al.* 2007a; OCORR *et al.* 2007b; WESSELLS *et al.* 2004).

The process of visualising the beating adult fly heart for video recording is useful for identifying genetic, dietary and environmental factors that affect cardiomyocyte contractility but it disrupts neuronal inputs that may influence how the heart beats *in vivo*. Therefore, even the process of visualising the beating adult fly heart may adversely affect quantified heart function. One way around this would be to utilise optical coherence tomography (OCT) in conjunction with the videomicroscopy. This method obviates the need for invasive surgery, and can be

performed on intact, live flies, and has successfully been used to analyse and identify a variety of cardiomyopathies (CASAD *et al.* 2012; KIM and WOLF 2009; KIM *et al.* 2010).

Contrary to published data which states that arrhythmicity increases with increasing age (OCORR *et al.* 2007a; OCORR *et al.* 2007c), arrhythmicity was higher in younger flies. In humans, cardiac arrhythmias increase with age – with higher incidences of atrial fibrillation and ventricular arrhythmias in the elderly (LAKATTA 2003). The discrepancy between the present arrhythmicity values and those from the Bodmer lab may be due to different fly food used – the Bodmer lab used yeast/molasses/cornmeal food whereas the present work used yeast/sucrose/cornmeal food (OCORR *et al.* 2007c).

It is possible the higher arrhythmicity seen in younger flies may not necessarily be detrimental, demonstrating the dynamic ability of the young heart to adapt to fluctuating conditions. By increasing *n* numbers at each time point, the rigid (i.e. less adaptive) cardiac rhythm phenotype in older flies may be confirmed – mimicking the decrease in beat-to-beat variability in elderly humans (TSUJI *et al.* 1996; TSUJI *et al.* 1994). A decreased beat-to-beat variability is also prognostic of cardiovascular mortality (CHATTIPAKORN *et al.* 2007). Additionally, it may be informative to assess Ca^{2+}-signalling and morphological differences between younger and older hearts. It is possible that morphological changes, such as decreased myofibril content or disorganised myofibril patterning, may correlate with age-dependent changes to function.

3.4.2 A diurnal rhythm in heart function was not detected in *Drosophila*

Unlike the mammalian heart, which anticipates and adapts to oscillations within its environment over the course of the day (YOUNG *et al.* 2001), a diurnal rhythm in function was not detected in the wildtype adult *Drosophila* heart. Since it was possible that daily fluctuations in heart function may have been attenuated via tight regulation by the circadian clock, the heart function of a clock mutant (per^{01}) was also assessed – i.e. the strict regulation of heart function may be abolished if the fly has no internal timing mechanism – to reveal no significant diurnal rhythm. Therefore, subsequent heart function recordings could be taken at any time of the day in the knowledge that there would not be a confounding time-of-day factor.

For heart function studies to be performed during the subjective night, flies were housed in incubators set up on phase-shifted 12:12-hr LD schedules, so that heart function analysis could be performed during the day rather than the middle of the night. A drawback of this method, however, may be that any potential difference in heart function during the night would be minimised/lost after stimulating the flies to awaken by exposure to light/movement of vial/banging of the vial/anaesthetisation. In other words, as soon as you waken the fly from night-time sleep, any diurnal effect may be lost. However, it would be extremely difficult to expose the fly heart, without light, or by stressing the fly in some manner. A non-invasive technique that does not disturb the fly would be better system for analysing diurnal variation.

By utilising per^{01} flies, it was hypothesised that a potential diurnal rhythm in heart function may be disrupted. per^{01} flies display arrhythmic locomotor behaviour in constant conditions, but have also been shown to exhibit slightly rhythmic

locomotor activity in LD conditions (CERIANI *et al.* 2002), although this has been disputed (COLLINS *et al.* 2005). Therefore, it is possible any potential difference revealed by a dysfunctional circadian clock would be negated by these per^{01} flies still exhibiting a diurnal rhythm (however slight) – although the activity of these flies was not tested.

Future experiments would address these issues (i.e. measuring heart function in *Drosophila* over the course of the day) and would probably have live, but immobile flies (with access to food/water) under a variety of lighting regimens (e.g. 12:12-hr LD, constant darkness, etc.) analysed every 5-30 minutes by a non-invasive heart function measuring system (e.g. OCT). This way, any confounding effects caused by increased exertion (i.e. climbing, flying) would be minimal, and 'resting' basal heart function parameters could be measured.

3.4.3 Heart morphology of circadian-knockdown adults was similar to wildtype

Abolishing individual circadian clock components in a cardiac-specific manner, did not significantly affect heart morphology in the lines tested. Although morphological analysis generates a lot of useful information, functional analysis will also be important to rule out effects on heart rate, contractility, and rhythmicity among other parameters. The only notable phenotypes caused by clock ablation using heart-GAL4 drivers, to be discussed below, were: weaker βPS-integrin-staining of PNs in *Hand-GAL4>*Per^{VDRC} adults; and an almost complete loss of cardiac muscle in *TinCΔ4-GAL4>*Clk^{DN} adults.

The phenotype in *Per*-ablated PNs confirms previous observations in per^{01} flies which exhibited a "wrinkled and shrunken" surface morphology (CURTIS *et al.*

1999; LIVINGSTONE 1981). It is presently unknown exactly why a mutation in a gene primarily known for its effects on the circadian clock would cause this PN phenotype, although it is possible that the disrupted diurnal rhythms disproportionately affects the functioning of the PNs compared to other cells in the fly. It is also possible the *period* gene performs a different function in these cells, other than its already well-studied role in circadian timing. Additionally, heart function appeared normal in *period*-null individuals (DOWSE *et al.* 1995). Haem metabolism is a potential downstream process mediated by Period. The rate-limiting enzyme in heme biosynthesis and degradation, δ-aminolevulinate synthase (*Alas*), and heme oxygenase (*Ho*), respectively, have been demonstrated to cycle in *Drosophila* heads, indicating a role for the clock in haem metabolism (CERIANI *et al.* 2002). In Chapter 4, knockdown of the heart-enriched gene, *Alas*, in PNs is shown to cause an aberrant morphological phenotype. It is also worthwhile noting that in humans, the haem sensor, *Rev-erbα*, coordinates metabolic and circadian functions (YIN *et al.* 2007).

Clock protein is not required for cardiogenesis or any other developmental process in flies. Therefore, the severe effects of ectopic dominant-negative *Clock* expression in the fly heart is likely due to an off-target effect of the mutant Clock protein on another protein (potentially another basic helix-loop-helix (bHLH) protein, e.g. Hand, Twist) important for heart development (Paul Hardin, personal communication) (SELLIN *et al.* 2006; YIN *et al.* 1997). However, the severe phenotype of these flies demonstrated that knockdown of certain genes could have drastic consequences for the hearts of these flies, and that they could be easily visualised and scored.

In the adult *Drosophila*, it seems possible to dramatically ablate heart function without necessarily affecting viability, a finding noted by the Bodmer lab who state "the survival of the organism [*Drosophila*] is not as tightly coupled to heart function as it is in vertebrates" (OCORR *et al.* 2007b). While the fate of the heart in *Drosophila* may be somewhat independent of viability, an apparent disadvantage of the model, instead it should be considered an opportunity to scrutinise genetic pathways in the mature *Drosophila* that would otherwise prove lethal in mature mammals.

The following chapter (Chapter 4) further develops the idea of using the adult *Drosophila* to screen for genes relevant to human cardiovascular disease.

Chapter 4

Identifying genes involved in cardiomyocyte adhesion in *Drosophila*

4.1 Introduction

4.1.1 Utilising the *Drosophila* heart as a platform to identify conserved genes and pathways involved in human cardiovascular diseases

The *Drosophila* heart has been studied as a model of cardiovascular development for more than two decades (AZPIAZU and FRASCH 1993; BODMER 1993; BODMER *et al.* 1990), and although the fly heart differs from the human heart in many respects (e.g. size and structure), the function is conserved between species. Indeed, much of the regulatory genetic network controlling heart differentiation is conserved from flies to mammals (OCORR *et al.* 2007b). An example is the *tinman* gene, discovered in *Drosophila* when it was established that mutants for this gene failed to form the cardiac tube (AZPIAZU and FRASCH 1993; BODMER 1993), while mice mutant for its ortholog, *Nkx2-5*, die at the embryonic stage (LYONS *et al.* 1995; TANAKA *et al.* 1999). Additionally, heterozygous human mutations in *Nkx2-5* resulted in congenital heart disease (SCHOTT *et al.* 1998). Therefore, the fruit fly is an excellent genetic model with which to elucidate the function of uncharacterised genes for their role in the development of the heart. Though the *Drosophila* heart differs from the human heart in many respects (MEDIONI *et al.* 2009; SERLUCA and FISHMAN 2006), it shares many of the features of mammalian cardiac function, which appear to be conserved between species (WOLF *et al.* 2006).

The simplicity of the *Drosophila* genome has meant unbiased genome-wide screens can be performed with the aim of discovering genes important, not only for heart development (KIM *et al.* 2004), but also the establishment and maintenance of adult heart function. A recent genome-wide RNAi screen uncovered *not3* (and other

members of the CCR4-Not complex) as an essential regulator of adult heart function – a finding that the authors confirmed was conserved in mice and humans (NEELY *et al.* 2010b). Other researchers have used the availability of deficiency lines (i.e. mutant *Drosophila* that harbour very large genome deletions (COOK *et al.* 2012)) to screen the genome for genes involved in heart function – genes identified via this method include *Siah-interacting protein* (SIP) and *weary* (CASAD et al. 2012; KIM et al. 2010).

4.1.2 Cardiomyocyte-cardiomyocyte junctions in *Drosophila*

In the human cardiovascular system, billions of cardiomyocytes are separated from the circulatory system by endothelial cells (MOLLOVA *et al.* 2013). These cardiomyocytes join together to form a functional syncytium and are mechanically, chemically, and electrically connected to each other. Intercalated discs are the adhering structures that connect adjacent cardiomyocytes, and transmit the force of contraction from cell to cell (NOORMAN *et al.* 2009). In humans, intercalated discs are comprised of different types of junctions characterised by their protein compositions - adherens junctions (e.g. cadherin, integrin), desmosomal junctions (e.g. desmoglein-2, desmocollin-2), and gap junctions (e.g. connexion-43) (PERRIARD *et al.* 2003). Many cardiomyopathies are characterised by alterations in cell-cell adhesion (KOSTIN *et al.* 2003; MATSUSHITA *et al.* 1999; SMITH *et al.* 1991), increased integrin expression (HELING *et al.* 2000; TERRACIO *et al.* 1991), leading to arrhythmia pathogenesis (LI *et al.* 2006), indicating efficient electromechanical coupling requires appropriately-organised cardiomyocyte adhesion (KLEBER and RUDY 2004).

It has been hypothesised that during development integrin-based focal adhesions are the primary force-bearing/transmitting connections between cardiomyocytes, while mature cardiomyocytes favour cadherin-based adhesion. In pathological circumstances (e.g. fibrosis), however, integrin-based adhesions appear to compensate for the increased forces generated (McCain *et al.* 2012). Therefore, there appears to be a "developmentally regulated hierarchy of adhesion" responsible for assembly and maintenance of junctions between cardiomyocytes. In agreement with this, conditional loss of N-cadherin in the heart led to a compensatory upregulation of β1-integrin (Kostetskii *et al.* 2005).

In the adult *Drosophila* heart, similar intercalated disc-like junctions have been identified between adjacent cardiomyocytes (Lehmacher *et al.* 2012) – junctional β-integrin staining between cardiomyocytes is highlighted in Figure 4.1. During embryonic heart development, cadherin dependent junctions form between opposing cardiomyoblasts and seal the lumen (Medioni *et al.* 2008). Recently, it was also demonstrated that during heart development, integrins are required for cardioblast polarisation and likely play a stabilising role prior to cadherin reinforcement (Vanderploeg *et al.* 2012). Therefore, *Drosophila* offers a simple model with which to screen orthologous genes for their involvement in cardiomyocyte adhesion, and information generated may offer insights into human cardiac pathophysiology associated with intercalated disc dysfunction.

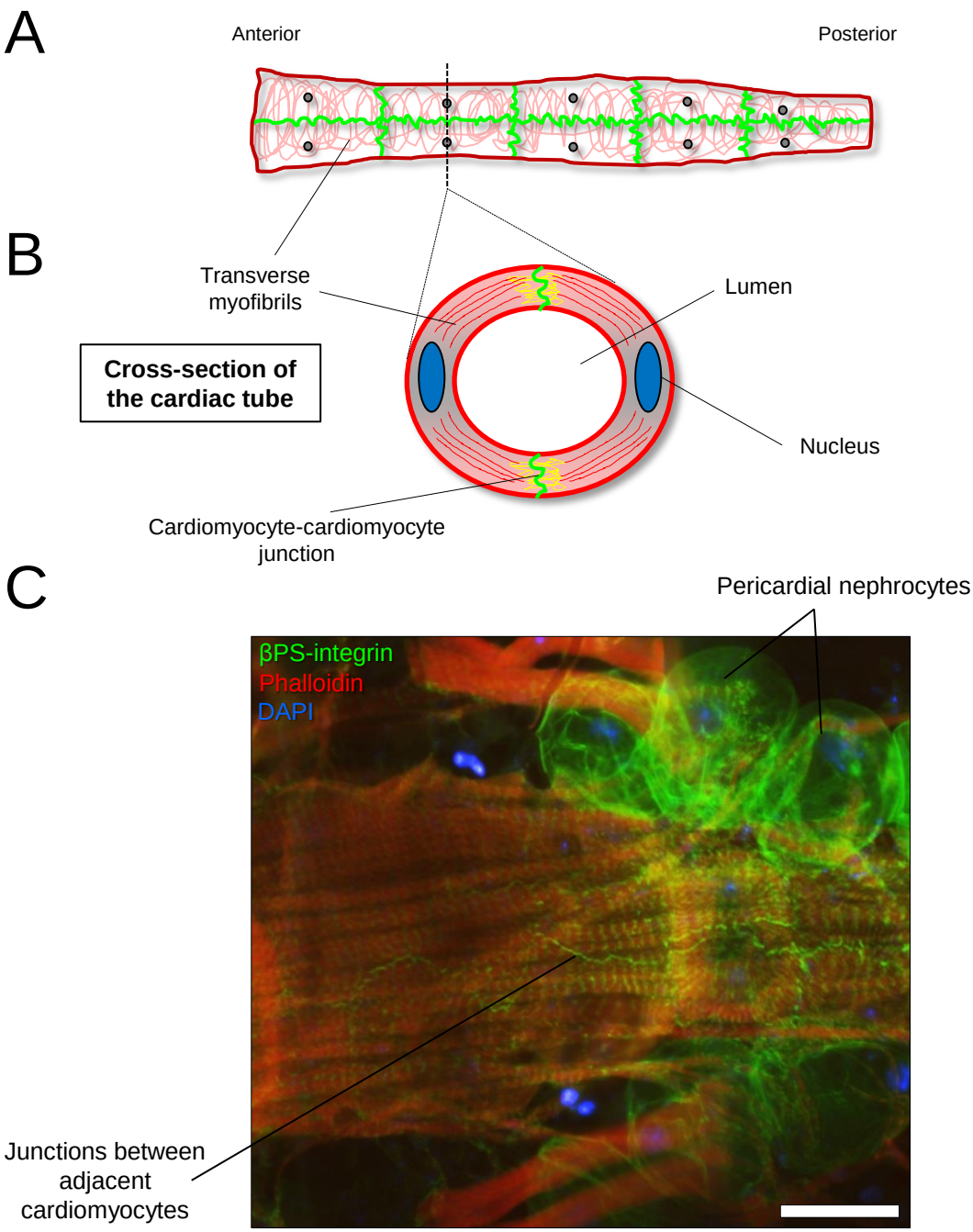

Figure 4.1. Cell junctions in the adult heart of *Drosophila melanogaster*.
A, layout of the adult *Drosophila* heart and position of the junctions between adjacent cardiomyocytes. The cardiac tube is formed from a single layer of opposing cardiomyocytes. **B**, a cross-section through the cardiac tube. Two opposing cardiomyocytes have formed a lumen for the flow of haemolymph, and are attached to each other via intercalated disc-like junctions. **C**, fluorescent image of the cardiac tube, with the thread-like intercalated disc-like junctions (highlighted with βPS-integrin staining) along the length of the heart. Pericardial nephrocytes are also labelled with βPS-integrin antibody (green), but not phalloidin (red) since these are not muscular structures. DAPI (blue) staining highlights the large nuclei of the pericardial nephrocytes. Scale bar = 25μm.

4.1.3 Utilisation of FlyAtlas dataset to discover enriched, orthologous genes relevant to human cardiovascular physiology

Chintapalli and colleagues generated the FlyAtlas to facilitate the delineation of the adult *Drosophila* genome into tissue-enriched gene sets so relevant information gained could be applied to human disease models (CHINTAPALLI *et al.* 2007). One of the *Drosophila* tissues this group dissected and analysed was the adult heart (i.e. the cardiac tube, and attached tissues necessarily including PNs, alary muscles, and probably some fat body). Therefore, the FlyAtlas dataset was utilised to create a list of enriched, orthologous genes with which to generate hypotheses regarding the effect of these genes on development of the functional cardiac syncytium in the adult fly.

4.2 Hypothesis

The hypothesis was that depletion of homologous, heart-enriched genes by ectopic RNAi expression in the *Drosophila* heart via the GAL4/UAS system may have adverse effects on the development of the functional cardiac syncytium.

4.2.1 Aims

1. Utilising heart-expressing GAL4 drivers, perform gene knockdown studies with selected RNAi lines to assess functional relevance of conserved heart-enriched genes.
    a. Assess effects of gene depletion by
        i. Phalloidin to examine cardiomyocyte structural integrity
        ii. β-integrin to assess effects on junctional integrity and PN morphology
        iii. Functional analysis of adult hearts utilising videomicroscopy

4.3 Results

4.3.1 Utilising FlyAtlas dataset to obtain genes enriched in adult *Drosophila* heart tissue

To examine genes that are important for adult heart function, and relevant to human heart function, the previously published tissue-specific microarray atlas of *Drosophila* gene expression (CHINTAPALLI *et al.* 2007) was used to sort genes that were enriched in *Drosophila* adult heart tissue. This list was generated and annotated by **Dr. Paul Hartley**.

Selected genes were then ordered from the VDRC, and an *a priori* mini-screen was performed to overexpress RNAi in the heart of the fruit fly. In the first instance, the heart- and PN-driver *HandC-GAL4* was used to drive expression since the extracted adult fly heart tissue for the FlyAtlas experiment also contained the closely associated PNs (CHINTAPALLI *et al.* 2007; SELLIN *et al.* 2006). Consequently, some of the 'highly enriched' genes may be specific for the PNs and have little or no involvement in the adult heart. Thus, PN morphology was also assessed. Subsequent assessment of the effect of knockdown of various genes on the cardiomyocytes alone (using *TinCΔ4-GAL4*) and PNs alone (using *Dot-GAL4*) was also performed for some genes (KIMBRELL *et al.* 2002; LO and FRASCH 2001). The expression patterns of all the GAL4 lines used to examine effects on heart morphology are shown diagrammatically in Figure 4.2.

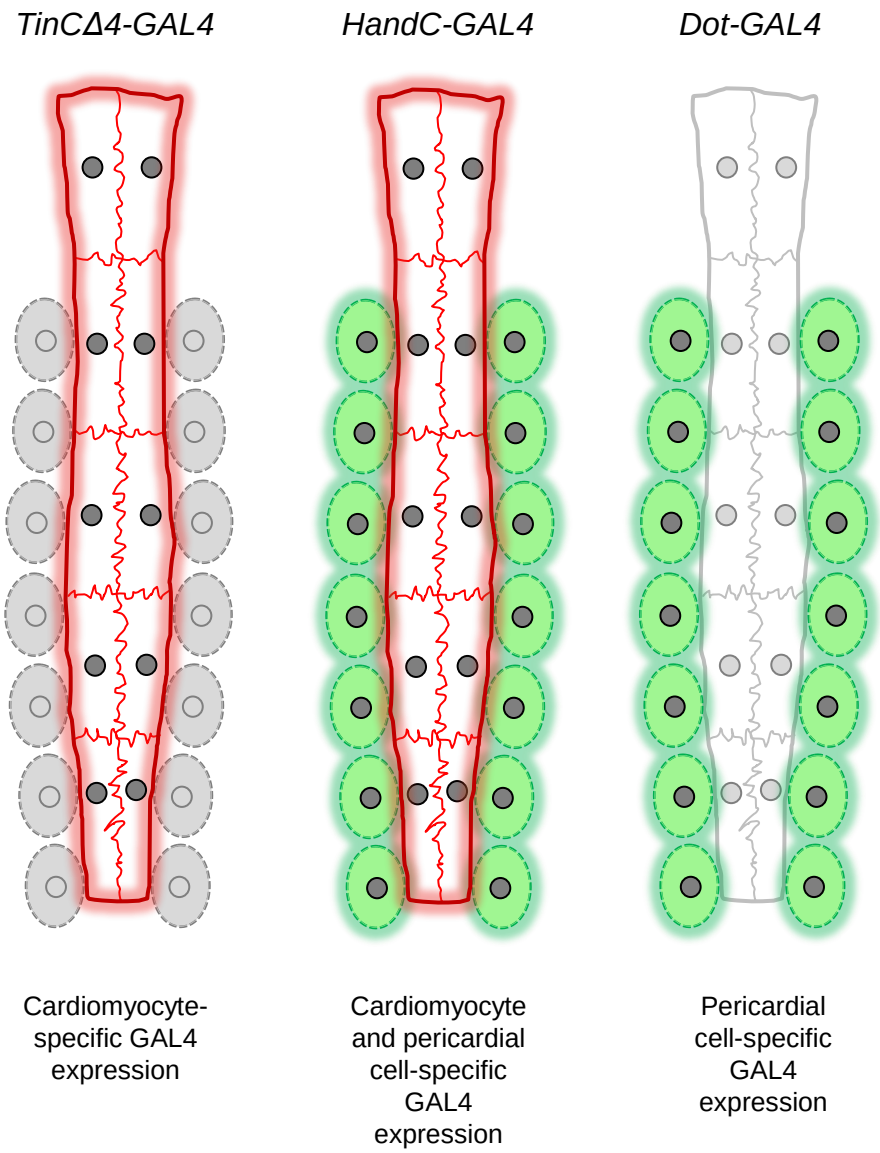

Figure 4.2. GAL4 expression patterns in different 'heart-specific' drivers in *Drosophila*.

TinCΔ4-GAL4 drives expression specifically in cardiomyocytes. *HandC-GAL4* drives expression in both cardiomyocytes and pericardial nephrocytes. *Dot-GAL4* drives expression in pericardial cells but not cardiomyocytes.

4.3.2 Performing a RNAi mini-screen on selected heart-enriched genes homologous to human orthologs in adult heart

The list of adult 'heart' genes from the FlyAtlas list was ranked according to heart enrichment – i.e. genes that appeared to be involved in the function of the adult dorsal vessel and/or its associated tissues (e.g. PNs) – and then according to how similar they were to human orthologs. Instead of randomly selecting genes from this list, genes were selected on the basis of previously published information (or lack thereof) that made them promising candidates for knockdown in the fly heart. These candidate 'orthologous' genes were then ordered from the VDRC, and a highly focused screen was performed with the aim of overexpressing RNAi in the heart of the fruit fly and assessing adult cardiac morphology, using orthologs with a potential or known role in heart function, based either on predicted gene function or expression pattern - this process is summarised in Figure 4.3. The genes were, in order of percentage sequence identity compared to the human protein ortholog: *Steamer duck* (*Stck*, 58% identity), *Aminolevulinate synthase* (*Alas*, 49%), *Fermitin 1* (*Fit1*, 48%), *Tolloid* (*Tld*, 42%), *Syntrophin-like 1* (*Syn1*, 41%), *Ninjurin A* (*NijA*, 32%), *Checkpoint suppressor homologue* (*Ches1*, 31%), *Ninjurin B* (*NijB*, 30%), *Tissue inhibitor of metalloproteases* (*Timp*, 21%), and *Basic transcription element-binding protein 2* (*Bteb2*, 18%).

Week-old adult progeny from each cross were collected (4 hearts from each cross), their hearts prepared and stained to highlight heart (phalloidin) and PN (β-integrin) morphology. The results of RNAi knockdown of these enriched and orthologous 'heart' enriched genes and their effect of heart morphology are shown in Figure 4.4, and scored in Table 4.1. The $Stck^{VDRC}$, $Fit1^{VDRC}$ and $Ches1^{VDRC}$ RNAi

A

Sort the FlyAtlas dataset according to…

Highly enriched genes

	A	B	C	D	E	
1	Enrichment in heart	ID	Ensembl Gene ID	Human % Identity	Human Ensembl Gene ID	
2	2045	1623953_at	FBgn0025686	17	ENSG00000166126	amnionless homolog (mouse) [S
3	159	1635028_s_at	FBgn0036169	49	ENSG00000001036	fucosidase, alpha-L- 2, plasma [S
4	135	1641037_at	FBgn0052702	23	ENSG00000157211	CUB domain containing protein 1
5	58	1635913_at	FBgn0033830	33	ENSG00000129151	butyrobetaine (gamma), 2-oxoglu
6	49	1640374_at	FBgn0051823	31	ENSG00000121064	serine carboxypeptidase 1 [Sourc
7	40	1630486_at	FBgn0025679	19	ENSG00000163884	Kruppel-like factor 15 [Source:HG
8	35	1639479_a_at	FBgn0001319	59	ENSG00000221818	early B-cell factor 2 [Source:HGN
9	26	1636158_at	FBgn0035813	37	ENSG00000090382	lysozyme [Source:HGNC Symbol
10	22	1634551_at	FBgn0038074	56	ENSG00000124713	glycine N-methyltransferase [So

	A	B	C	D	E	
1	Enrichment in heart	ID	Ensembl Gene ID	Human % Identity	Human Ensembl Gene ID	
2	5	1628779_a_at	FBgn0003651	75	ENSG00000175745	nuclear receptor subfamily 2, group
3	6	1634403_at	FBgn0015567	69	ENSG00000183020	adaptor-related protein complex 2, al
4	5	1625686_s_at	FBgn0086450	65	ENSG00000188641	dihydropyrimidine dehydrogenase [
5	8	1639956_at	FBgn0033756	62	ENSG00000156052	guanine nucleotide binding protein (
6	5	1635227_at	FBgn0001258	62	ENSG00000111716	
7	12	1625279_a_at	FBgn0003896	61	ENSG00000016082	ISL LIM homeobox 1 [Source:HGNC
8	5	1633523_at	FBgn0036271	60	ENSG00000148218	aminolevulinate dehydratase [Sourc
9	35	1639479_a_at	FBgn0001319	59	ENSG00000221818	early B-cell factor 2 [Source:HGNC S
10	22	1634551_at	FBgn0038074	56	ENSG00000124713	glycine N-methyltransferase [Source

Highly homologous genes

B

Perform RNAi mini-screen using heart-GAL4 driver

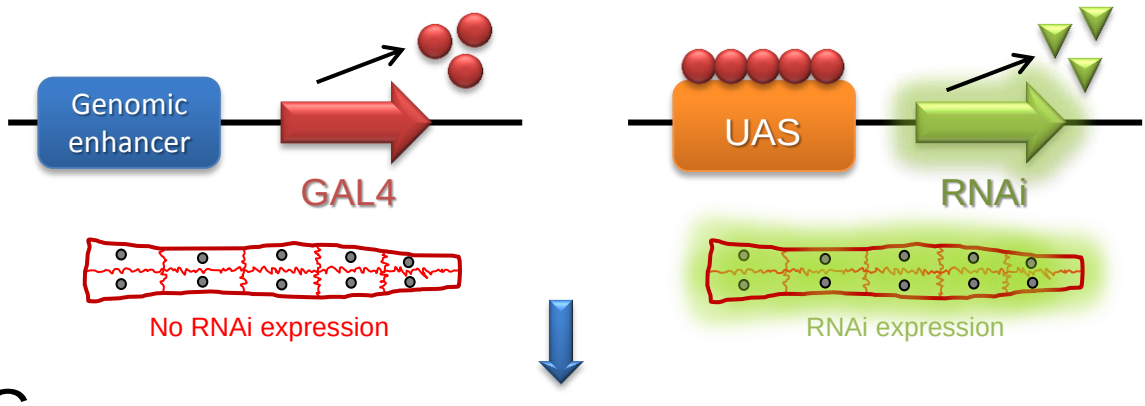

C

Screen adults for effects on heart morphology

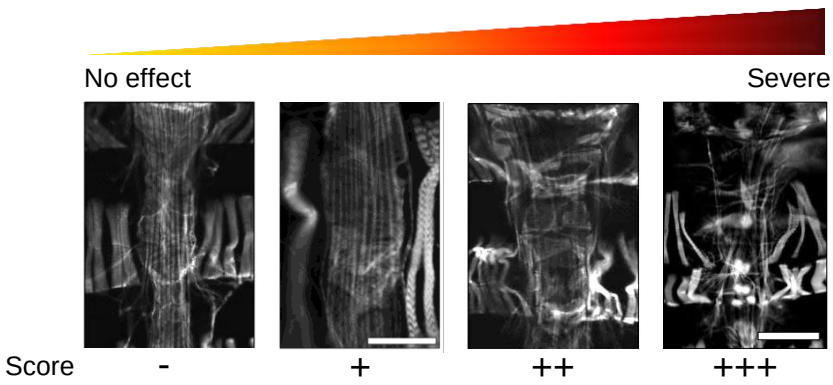

Figure 4.3. From FlyAtlas dataset to screening heart genes in the fly.
A, The FlyAtlas dataset obtained from http://www.flyatlas.org/ was sorted by heart enrichment, then by sequence identity to human orthologs. **B**, selected RNAi lines were then ordered from the VDRC, and subsequently crossed with heart-GAL4 drivers (e.g. *Hand-GAL4*). **C**, progeny from the mini-screen were examined and scored (+/++/+++) for effects on heart morphology.

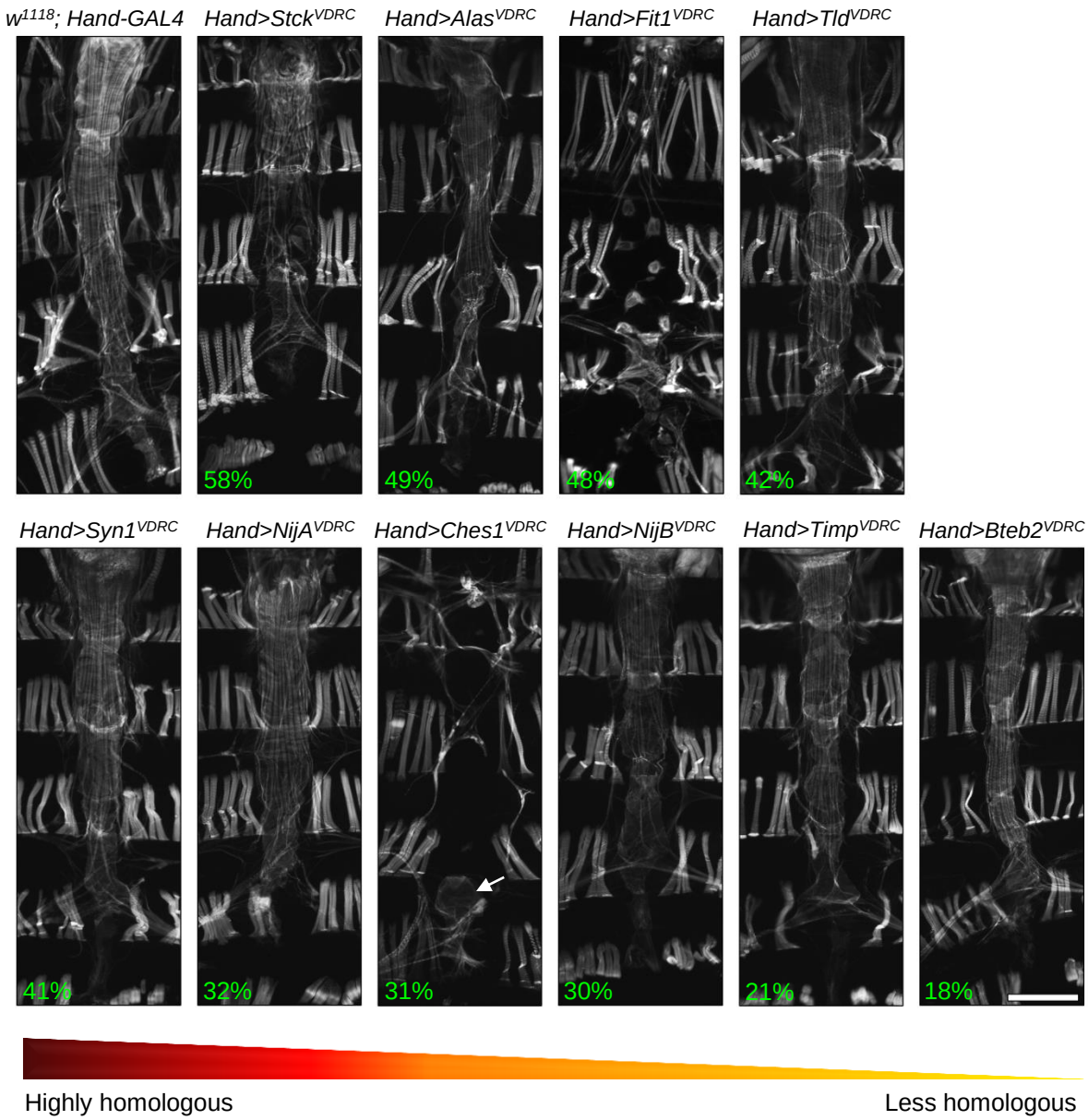

Figure 4.4. Screening homologous heart-enriched genes for changes in cardiomyocyte morphology.

There were a few RNAi lines that exerted a dramatic effect on cardiomyocyte morphology when driven by the *Hand-GAL4* driver. Sequence identities (i.e. the percentage similarity to the human ortholog) are annotated in green for each gene. *Hand>Stck^{VDRC}* and *Hand>Fit1^{VDRC}* hearts appeared to exhibit cardiomyocyte uncoupling, with *Hand>Fit1^{VDRC}* hearts particularly severely affected. However, the most severe cardiomyocyte phenotype was the 'absent adult heart' phenotype seen in *Hand>Ches1^{VDRC}* hearts – the remnant of the larval heart, the terminal chamber, can still be seen (white arrow). Scale bar = 100µm.

Genotype	Heart score	Pericardial nephrocyte score
w^{1118}; Hand-GAL4	-	-
Hand-GAL4>Stck^{VDRC}	++	-
Hand-GAL4>Alas^{VDRC}	-	++
Hand-GAL4>Fit1^{VDRC}	+++	+++
Hand-GAL4>Tld^{VDRC}	-	-
Hand-GAL4>Syn1^{VDRC}	-	-
Hand-GAL4>NijA^{VDRC}	-	-
Hand-GAL4>Ches1^{VDRC}	+++	+++
Hand-GAL4>NijB^{VDRC}	-	-
Hand-GAL4>Timp^{VDRC}	-	-
Hand-GAL4>Bteb2^{VDRC}	-	+++

Table 4.1. Scored heart and pericardial nephrocyte phenotypes from the *Hand>RNAi* mini-screen.
Results of the *Hand>RNAi* mini-screen were scored and show that overexpression of *Stck, Fit1,* and *Ches1* RNAi using the Hand-GAL4 driver deleteriously affected heart morphology. Effects of RNAi overexpression on pericardial nephrocyte morphology was also assessed and it was found that *Alas, Fit1, Ches1,* and *Bteb2* RNAi caused deleterious effects. Heart images were scored thusly: - = no effect, + = small effect, ++ = moderate effect, +++ = severe/strong effect.

lines exhibited profound effects on the adult *Drosophila* cardiac morphology, while the remaining RNAi lines did not appear to significantly affect morphology. *Hand>Stck*^{VDRC} adult cardiomyocytes appear dissociated from each other, with gaps between cells clearly visible. Similarly, but to a more severe extent, *Hand>Fit1*^{VDRC} cardiomyocytes also exhibited severe dissociation, such that cardiomyocyte F-actin architecture appeared highly condensed. The strongest adult heart phenotype came from *Hand>Ches1*^{VDRC} flies – with any semblance of a heart vessel completely missing, and a large empty area where the adult fly heart would normally be. However, these flies did appear to harbour the vestigial terminal heart chamber – a remainder of the larval heart, superseded by the remodelled adult heart: formed via the differentiation of the larval posterior aorta during metamorphosis (ZEITOUNI *et al.* 2007). Additionally, *Ches1* has recently been demonstrated to be vital for the division of cardiac progenitor cells in the *Drosophila* embryo (AHMAD *et al.* 2012).

PN morphology was additionally assessed in these progeny using the βPS-integrin antibody to stain PNs and highlight morphological features of PNs such as size and shape – the results of which are shown in Figure 4.5, and scored in Table 4.1. While *Hand>Fit1*^{VDRC} and *Hand>Ches1*^{VDRC} hearts displayed aberrant cardiomyocyte morphology, the PNs in these adults were also deleteriously affected - in this case, the PNs were not present in the adult. Although the cardiomyocytes of *Hand>Stck*^{VDRC} cardiomyocytes were dissociated, the PNs of these flies were morphologically similar to wildtype. Some of the PNs of *Hand>Alas*^{VDRC} adults were significantly larger (39.2µm (±3.5) *w*^{1118}*; Hand-GAL4* vs. 66.7µm (±3.2) *Hand>Alas*^{VDRC}, $p<0.01$) than wildtype – this is demonstrated in Figure 4.6.

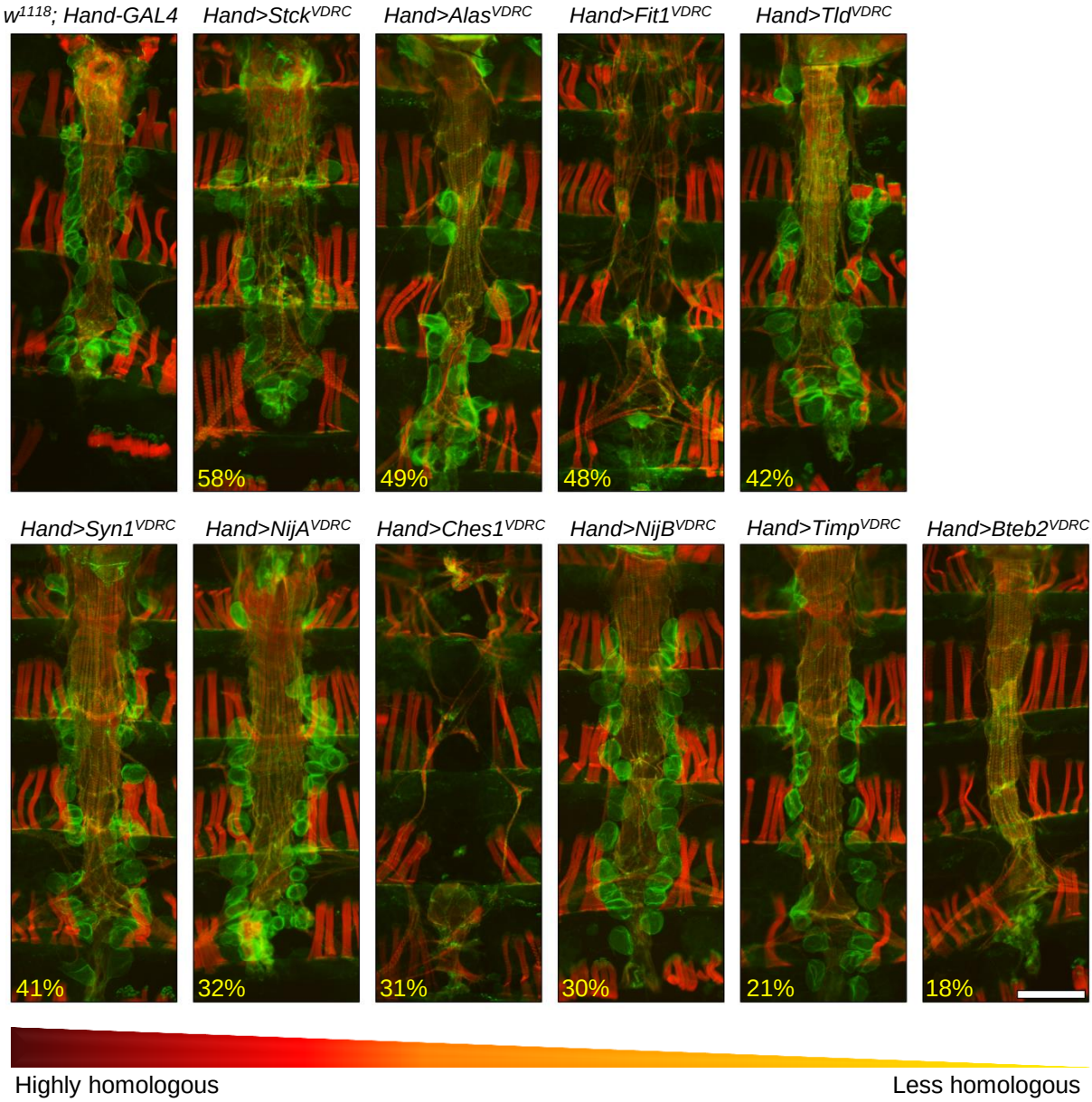

Figure 4.5. Screening homologous heart-enriched genes for changes in pericardial nephrocyte as well as cardiomyocyte morphology in the fly heart.

Pericardial nephrocytes were completely absent in *Hand>Fit1^{VDRC}*, *Hand>Ches1^{VDRC}*, and *Hand>Bteb2^{VDRC}* adult hearts, while in *Hand>Alas^{VDRC}* hearts these cells appeared abnormal – with some appearing unusually large. Sequence identities (i.e. the percentage similarity to the human ortholog) are annotated in yellow for each gene. Hearts are stained with Alexa-conjugated phalloidin (red), and anti-βPS integrin antibody (green). Scale bar = 100µm.

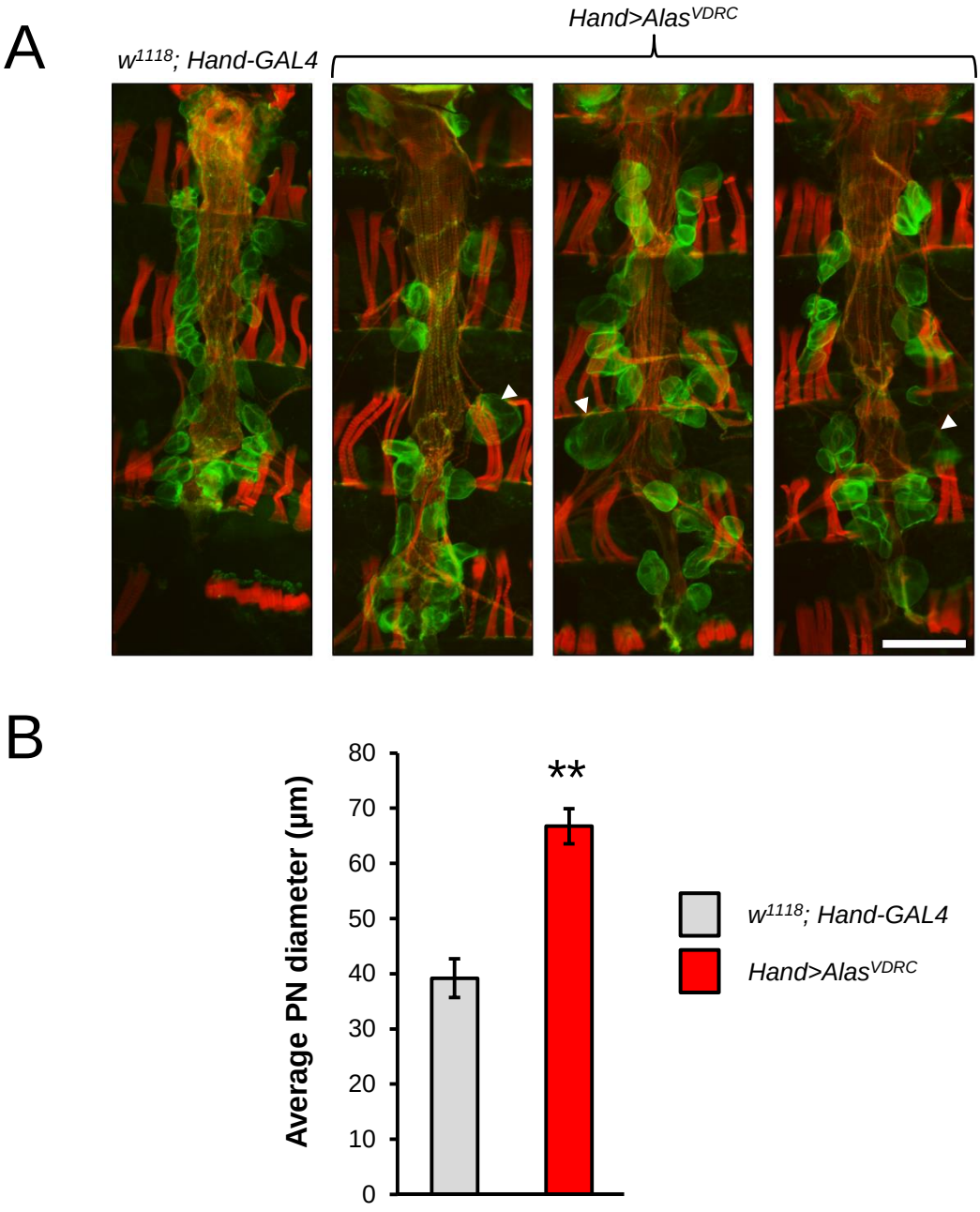

Figure 4.6. The pericardial nephrocytes are significantly larger in *Hand>Alas^{VDRC}* flies compared to controls.

A, pericardial nephrocytes in *Hand>Alas^{VDRC}* hearts were larger than wildtype controls (arrowheads indicate giant cells). Hearts are stained with Alexa-conjugated phalloidin (red), and anti-βPS integrin antibody (green). Scale bar = 100µm. **B**, the diameter of 15 PNs per fly was quantified - 4 flies per genotype (i.e. 60 measurements/genotype). The mean was then plotted for each genotype, and a Student's t-test was performed. **p<0.01, error bars indicate ±SEM.

Strikingly, while the hearts of *Hand>Bteb2*^{VDRC} mutants were similar to wildtype, the PNs of these flies were not present in the adult.

Stck was a previously characterised protein required for integrin-dependent cell adhesion (CLARK *et al.* 2003). *Ches1* was also recently characterised as vital for the cardioblast differentiation in the developing *Drosophila* embryo (AHMAD *et al.* 2012; ZHU *et al.* 2012). Although the *Bteb2* phenotype was interesting, and there were no previous publications that characterised this gene, the phenotype concerned the PNs, and not the heart. Therefore, it was decided that *Fit1* would be further characterised. The effect of *Fit1* knockdown in the heart was severe, and this observation had not been previously published. Additionally, since the sequence identity of *Fit1* to the human ortholog (*Kind2*) was relatively high, the likelihood of these genes having similar functions in the human was considerably increased.

4.3.3 Identification of cell adhesion proteins important for adult heart morphology

Since *Fit1* (and *Stck*) was predicted to be involved in cell adhesion, it was hypothesised that the coupling of the cardiomyocytes in the *Drosophila* to form the heart was essential for its function. Bai *et al*. had also previously observed that *Fit1* appeared to be involved in muscle assembly – but crucially, this group showed that the *Fit1* paralog, *Fit2*, was also important for this process and that depletion of both Fermitins mimicked loss of β-integrin function (BAI *et al.* 2008). Thus, another mini-screen was performed in the *Drosophila* heart, this time targeting genes known to be important for integrin-related cell adhesion, to examine effects of their knockdown on cardiomyocyte junctional integrity. The RNAi lines used were: *Fermitin 1* (*Fit1*,

both VDRC and TRiP lines), *Fermitin 2* (*Fit2*), *Fit1+Fit2* (this line was generated from the individual VDRC lines using standard crosses), *Myospheroid* (*Mys*, βPS-integrin), *Multuple edematous wings* (*Mew*, αPS1-integrin), *Inflated* (*If*, αPS2-integrin), *Armadillo* (*Arm*, β-catenin – important in cell-cell adhesion, particularly adherens junctions), and *Focal adhesion kinase* (*Fak56D*). The results of RNAi knockdown of these 'cell adhesion' genes and their effect of heart morphology are shown in Figure 4.7, and scored in Table 4.2.

The hearts of *Hand>Fit1*^{TRiP} flies were aberrant compared to wildtype, with hearts appearing thinner and with gaps seen between neighbouring cardiomyocytes, however the phenotype was not as severe as the cardiomyocyte dissociation phenotype seen in *Hand>Fit1*^{VDRC} flies. Similarly, gaps between neighbouring cardiomyocytes in *Hand>Fit2*^{VDRC} hearts were noticeable. The *Fit1*^{VDRC}*+Fit2*^{VDRC} (*Fit1+Fit2*^{VDRC}) double RNAi line was generated via standard crosses, and *Hand>Fit1+Fit2*^{VDRC} cardiomyocytes were fully dissociated from their neighbours – appearing spherical with F-actin appearing highly condensed within the cardiomyocyte. This 'rounded-up' cardiomyocyte phenotype mimicked the result also seen in *Hand>Mys*^{VDRC} hearts. The ventral longitudinal muscles are also present in both *Hand>Fit1+Fit2*^{VDRC} and *Hand>Mys*^{VDRC} hearts, indicating these are not significantly affected by RNAi knockdown of these genes. *Hand>If*^{VDRC} hearts also affected cardiomyocyte-cardiomyocyte adhesion, with gaps between cells similar to *Hand>Fit2*^{VDRC} hearts. *Mew*, and *Fak56D* RNAi knockdown had no significant effect on cardiomyocyte morphology compared to wildtype. The cardiomyocyte morphology of *Hand>Arm*^{VDRC} mutants were irregular, with myofibrils arranged longitudinally as opposed to transversely in wildtype. The effects of *Arm* knockdown

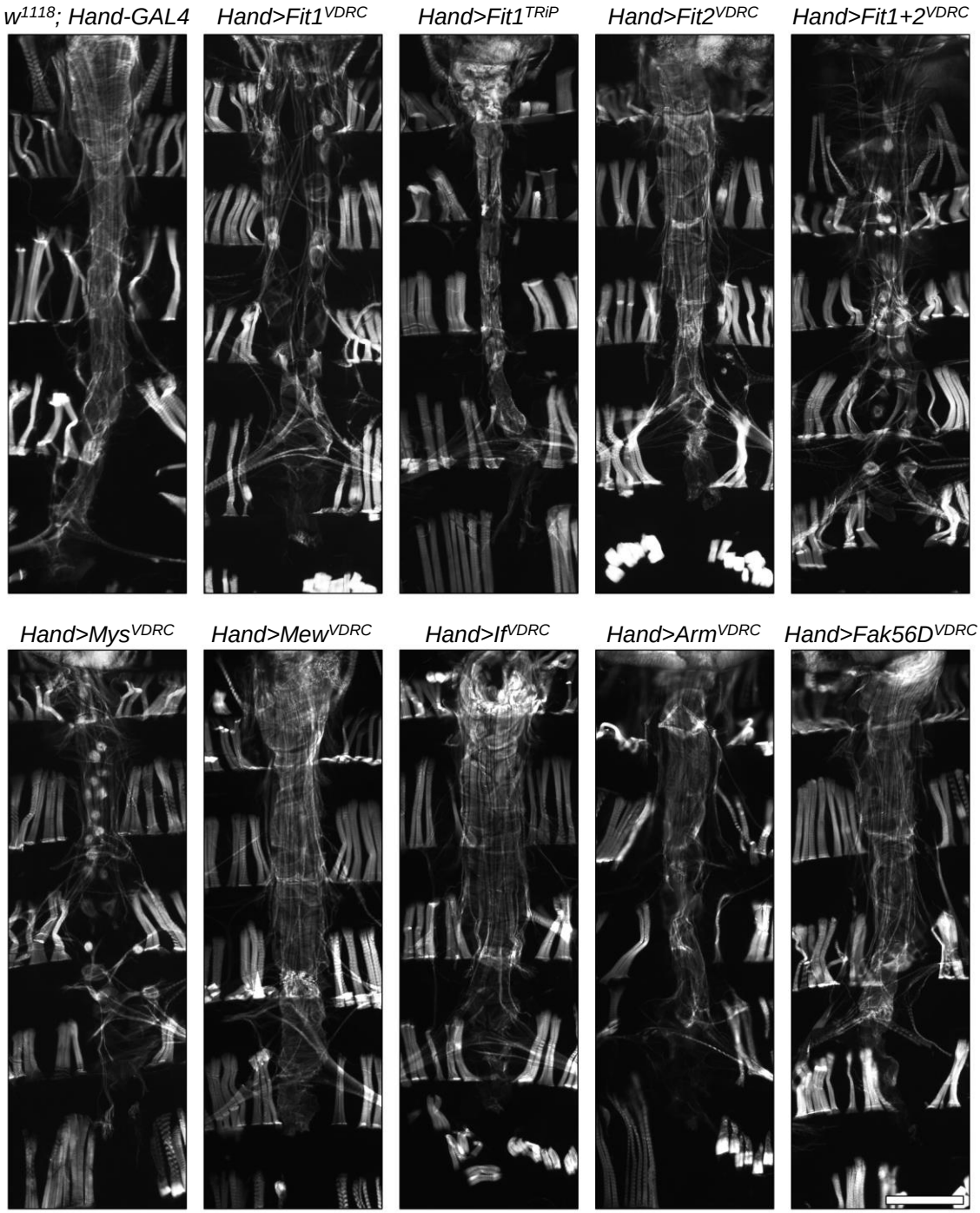

Figure 4.7. Screening cell adhesion genes for changes in cardiomyocyte morphology in the fly heart.

Since *Fit1*^{VDRC} had such a dramatic phenotype from the mini-screen of enriched heart genes, RNAi lines for several other known/predicted cell adhesion proteins – including the *Fit1* paralog, *Fit2* - were also screened for their effect on cardiomyocyte morphology. The most severe cardiomyocyte phenotype was the 'rounded-up' cardiomyocyte phenotype seen in *Hand>Fit1*^{VDRC}, *Hand>Fit1+2*^{VDRC}, and *Hand>Mys*^{VDRC} adult flies. Scale bar = 100µm.

Genotype	Heart score	Pericardial nephrocyte score
w^{1118}; Hand-GAL4	-	-
Hand-GAL4>Fit1^{VDRC}	+++	+++
Hand-GAL4>Fit1^{TRiP}	+	-
Hand-GAL4>Fit2^{VDRC}	+	+
Hand-GAL4>Fit1+2^{VDRC}	+++	+++
Hand-GAL4>Mys^{VDRC}	+++	+++
Hand-GAL4>Mew^{VDRC}	-	+++
Hand-GAL4>If^{VDRC}	++	-
Hand-GAL4>Arm^{VDRC}	++	+
Hand-GAL4>Fak56D^{VDRC}	-	-

Table 4.2. Scored heart and pericardial nephrocyte phenotypes from the *Hand>RNAi* cell-adhesion mini-screen. Results of the *Hand>RNAi* cell-adhesion mini-screen were scored and show that overexpression of *Fit1, Fit1+2, and Mys* RNAi using the *Hand-GAL4* driver had the most severe affect on heart morphology. Effects of RNAi overexpression on pericardial nephrocyte morphology was also assessed and it was found that *Fit1, Fit1+2, Mys,* and *Mew* RNAi caused the strongest PN phenotypes. Heart images were scored thusly: - = no effect, + = small effect, ++ = moderate effect, +++ = severe/strong effect.

will be discussed below. The distances between neighbouring cardiomyocytes was quantified for each genotype – these results are summarised in Figure 4.8.

PN morphology was additionally assessed in these progeny – the results of which are shown in Figure 4.9, and scored in Table 4.2. Unlike *Hand>Fit1*^{VDRC} flies, *Hand>Fit1*^{TRiP} flies had PNs that were similar to wildtype, but that were abnormally separated from the dorsal vessel. *Hand>Fit2*^{VDRC} flies also had PNs. PNs were not present in either *Hand>Fit1+Fit2*^{VDRC} or *Hand>Mys*^{VDRC} adult hearts. Interestingly, these cells were also absent in *Hand>Mew*^{VDRC} hearts, but were present in *Hand>If*^{VDRC} hearts – indicating a possible cell-specific role and divergence of function for these α-integrns. *Arm* and *Fak56D* RNAi overexpression had no significant effect on PN morphology compared to wildtype.

4.3.4 Verification of heart-specific effects of RNAi lines using cardiomyocyte-specific and PN-specific GAL4 drivers

Although the *HandC-GAL4* enhancer line is a strong driver of expression, it may be causing potentially unwanted side-effects on heart morphology by also affecting PN function. For example, if a specific RNAi, knocked-down only in PNs, appears to cause a heart phenotype, a secondary effect on heart physiology would be indicated. Pericardin, a collagen-like protein secreted mainly from PNs, is important for heart vessel morphogenesis, therefore affecting PN function may have unwanted consequences for heart development (CHARTIER *et al.* 2002). To avoid this problem, and in an attempt to resolve the effects of individual RNAis on both cardiomyocytes and PNs, the 'cell adhesion' mini-screen was also performed using the cardiomyocyte-specific *TinCΔ4-GAL4* driver and the PN-specific *Dot-GAL4* driver.

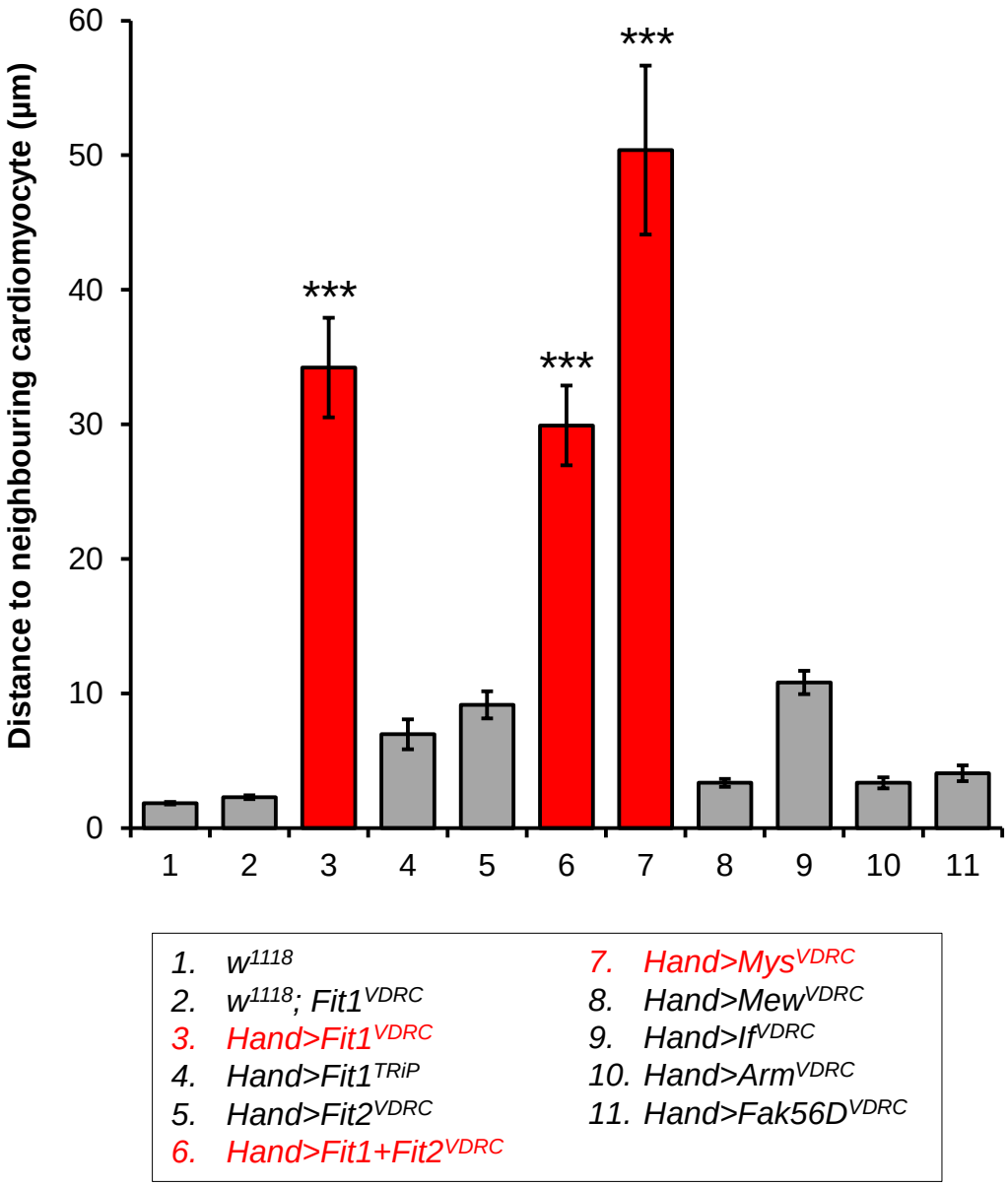

Figure 4.8. Quantification of the average distance between neighbouring cardiomyocytes from the different 'cell adhesion' RNAi.

Distances between adjacent cardiomyocytes were quantified for each genotype tested in the screen (including two controls – *w*^{1118} and *w*^{1118}*; Fit1*^{VDRC} flies). The distance between neighbouring cardiomyocytes was significantly greater in *Hand>Fit1*^{VDRC}, *Hand>Fit1+Fit2*^{VDRC}, and *Hand>Mys*^{VDRC} mutant hearts compared to all other lines. Four measurements were taken for each fly heart, with 4 flies were used for each genotype (i.e. 16 measurements per genotype). Means were calculated and plotted. One-way analysis of variance (ANOVA) followed by Tukey's post-hoc test was used to identify differences between the means derived from uneven sample sizes. ***p<0.001, error bars indicate ±SEM.

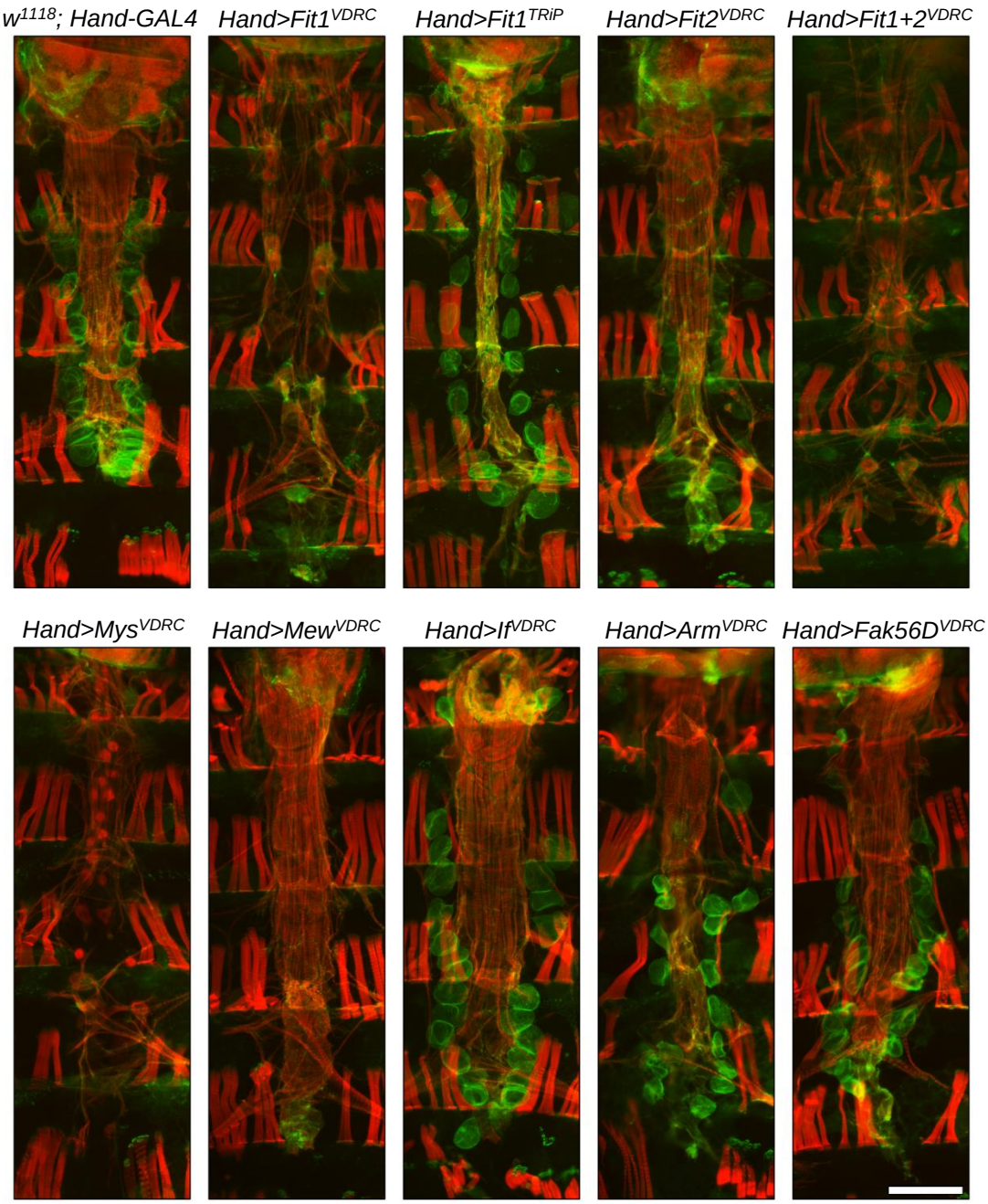

Figure 4.9. Screening cell adhesion genes for changes in pericardial nephrocyte as well as cardiomyocyte morphology in the fly heart.

Most of the RNAi lines that exhibited a cardiomyocyte morphology phenotype also resulted in deleterious effects on pericardial nephrocyte morphology. The pericardial cells in *Hand>Fit1*^{VDRC}, *Hand>Fit1+2*^{VDRC}, *Hand>Mys*^{VDRC}, and *Hand>Mew*^{VDRC} hearts appeared to be completely ablated. There was no significant effect from the other RNAi lines on pericardial cell morphology, however, the β-integrin staining appears less intense in *Hand>Fit2*^{VDRC} hearts. Hearts are stained with Alexa-conjugated phalloidin (red), and anti-βPS integrin antibody (green). Scale bar = 100μm.

The effects of the 'cell adhesion' RNAi lines on heart morphology after *TinCΔ4-GAL4* expression are shown in Figure 4.10, and scored in Table 4.3. This mini-screen was performed before the *Fit1+Fit2*^{VDRC} double RNAi line had been generated. Uncoupling of cardiomyocytes was most noticeable in *Tin>Fit1*^{VDRC}, *Tin>Mys*^{VDRC} and *Tin>If*^{VDRC} hearts, while *Tin>Fit1*^{TRiP} and *Tin>Fit2*^{VDRC} hearts did not exhibit any significant morphological defects. PN morphology was also examined in these hearts – shown in Figure 4.11, and scored in Table 4.3. PNs in these *Tin-GAL4* driven hearts were similar to wildtype controls.

The effects of the 'cell adhesion' RNAi lines on heart morphology after *Dot-GAL4* expression are demonstrated in Figure 4.12, and scored in Table 4.4. There was no effect of any of the 'cell adhesion' RNAi lines on cardiomyocyte morphology under the control of *Dot-GAL4* expression. PNs, however, were absent in *Dot>Fit1*^{VDRC}, *Dot>Fit1+Fit2*^{VDRC}, *Dot>Mys*^{VDRC} flies, and *Dot>Mew*^{VDRC} mutants - shown in Figure 4.13, and scored in Table 4.4. There was no significant effect on PNs in the remaining RNAi lines tested.

4.3.5 Functional analysis of *Fit1*^{VDRC} RNAi using *Tin*- and *Hand-GAL4* drivers

Due to the significant damage caused to *Hand>Fit1*^{VDRC} hearts, functional analysis was also performed in these flies to assess the effect of *Fit1* silencing on cardiac function. *Tin>Fit1*^{VDRC} hearts were also functionally assessed since these hearts also exhibited cardiomyocyte dissociation, but to a lesser extent. The results are shown in Figure 4.14. There was no significant difference in heart rate, heart period, diastolic interval, or systolic interval between the genotypes tested. *Hand>Fit1*^{VDRC} hearts exhibited significantly (0.15 (±0.04) *w*^{1118}*; Fit1*^{VDRC} vs. 0.52

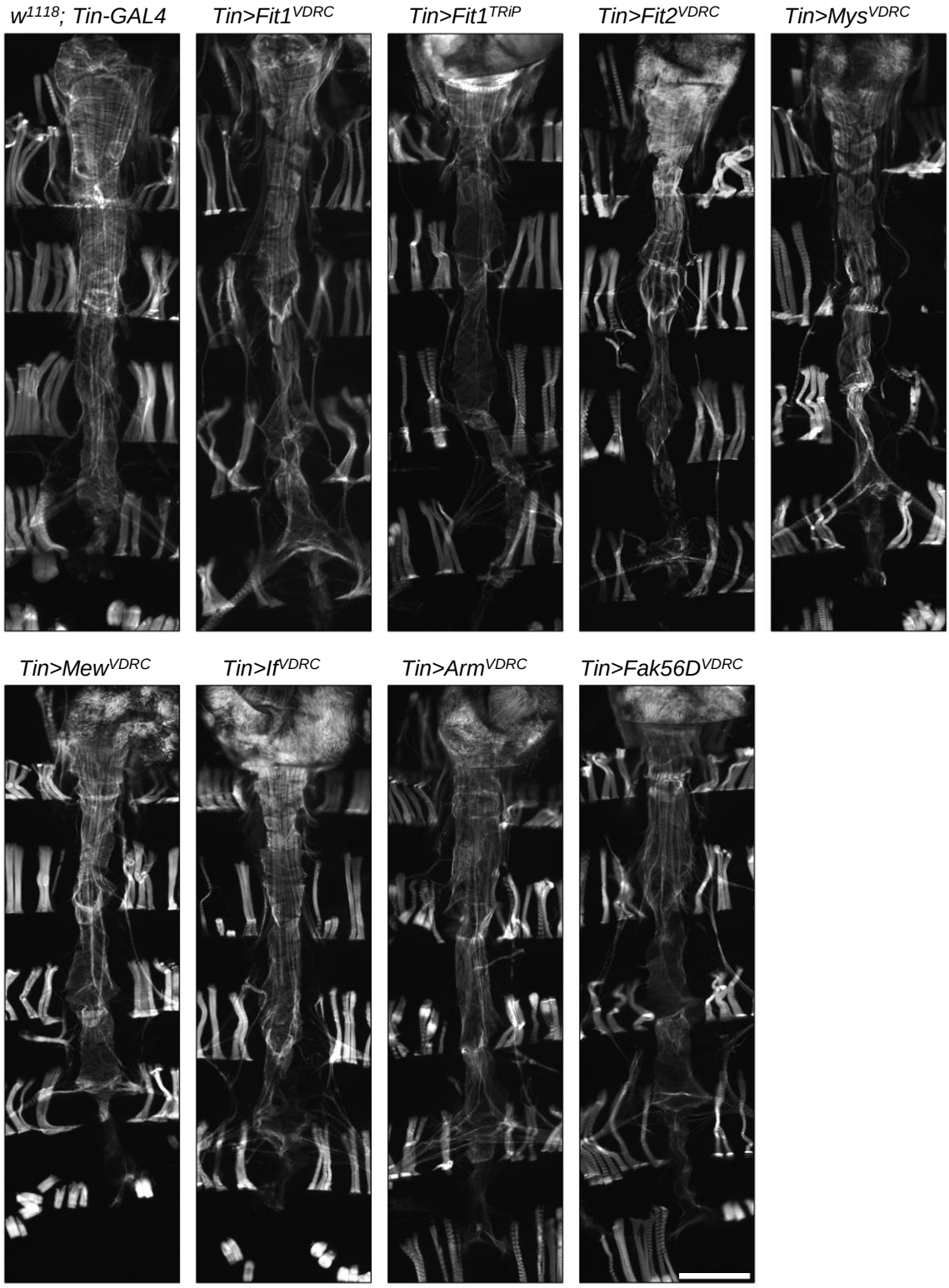

Figure 4.10. Screening cell adhesion genes for changes in cardiomyocyte morphology in the fly heart using the *TinCΔ4-GAL4* driver.
There is significant uncoupling of cardiomyocytes in *Tin>Fit1^{VDRC}*, *Tin>Fit2^{VDRC}*, *Tin>Mys^{VDRC}*, and *Tin>If^{VDRC}* hearts. There was no significant effect from the other RNAi lines on cardiomyocyte morphology. Scale bar = 100µm.

Genotype	Heart score	Pericardial nephrocyte score
w^{1118}; TinCΔ4-GAL4	-	-
TinCΔ4-GAL4>Fit1^{VDRC}	++	-
TinCΔ4-GAL4>Fit1^{TRiP}	-	-
TinCΔ4-GAL4>Fit2^{VDRC}	+	-
TinCΔ4-GAL4>Mys^{VDRC}	++	-
TinCΔ4-GAL4>Mew^{VDRC}	-	-
TinCΔ4-GAL4>If^{VDRC}	+	-
TinCΔ4-GAL4>Arm^{VDRC}	+	-
TinCΔ4-GAL4>Fak56D^{VDRC}	-	-

Table 4.3. Scored heart and pericardial nephrocyte phenotypes from the *TinCΔ4>RNAi* cell-adhesion mini-screen. Results of the *TinCΔ4>RNAi* cell-adhesion mini-screen were scored and show that overexpression of *Fit1, and Mys* RNAi using the *TinCΔ4-GAL4* driver had the most severe affect on heart morphology. There was no effect on pericardial nephrocyte morphology in any of the lines tested. Heart images were scored thusly: - = no effect, + = small effect, ++ = moderate effect, +++ = severe/strong effect.

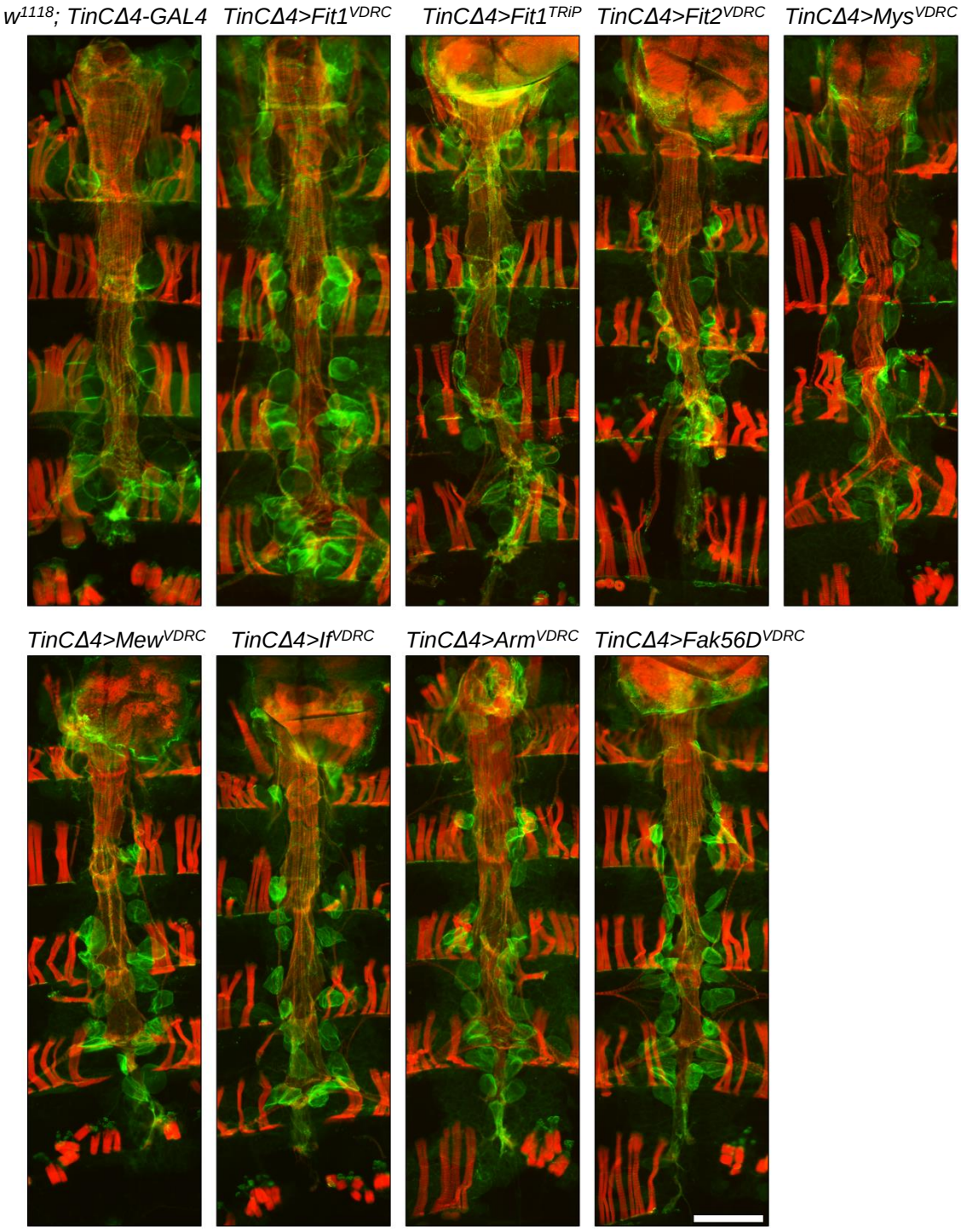

Figure 4.11. Screening cell adhesion genes for changes in pericardial nephrocyte as well as cardiomyocyte morphology in the fly heart using the *TinCΔ4-GAL4* driver.

There is significant uncoupling of cardiomyocytes in *Tin>Fit1*^{VDRC}, *Tin>Fit2*^{VDRC}, *Tin>Mys*^{VDRC}, and *Tin>If*^{VDRC} hearts. There was no significant effect from the other RNAi lines on cardiomyocyte morphology. Pericardial cells are remain unaffected in lines since the cardiomyocyte-specific *TinCΔ4-GAL4* does not drive expression in these cells. Hearts are stained with Alexa-conjugated phalloidin (red), and anti-βPS integrin antibody (green). Scale bar = 100μm.

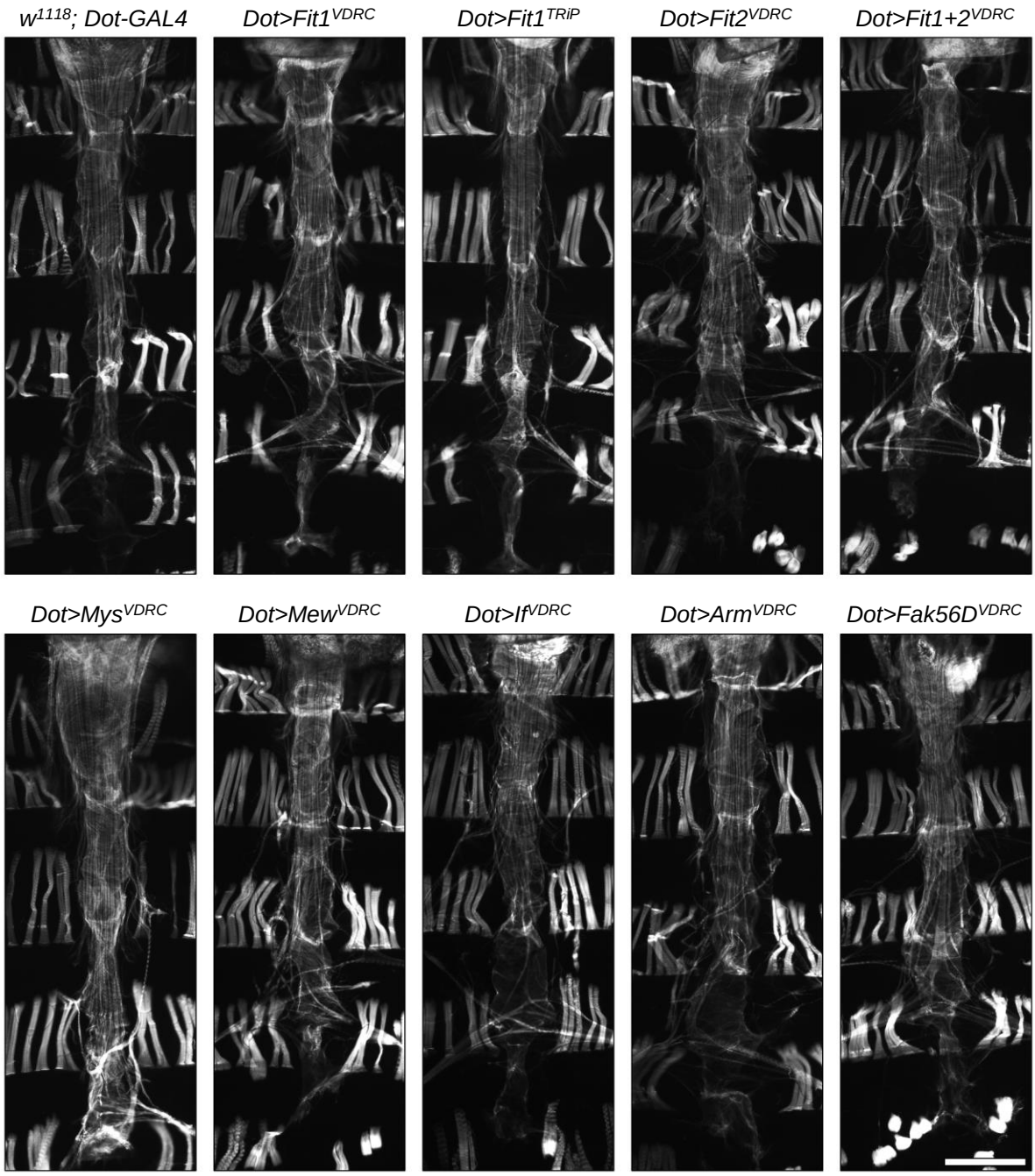

Figure 4.12. Screening cell adhesion genes for changes in cardiomyocyte morphology in the fly heart using the pericardial cell-driver, *Dot-GAL4*.
There was no effect on cardiomyocyte morphology from any of the 'cell adhesion' RNAi lines driven by the pericardial cell-driver, *Dorothy-GAL4*. Scale bar = 100µm.

Genotype	Heart score	Pericardial nephrocyte score
w^{1118}; Dot-GAL4	-	-
Dot-GAL4>Fit1^{VDRC}	-	+++
Dot-GAL4>Fit1^{TRiP}	-	-
Dot-GAL4>Fit2^{VDRC}	-	+
Dot-GAL4>Fit1+2^{VDRC}	-	+++
Dot-GAL4>Mys^{VDRC}	-	+++
Dot-GAL4>Mew^{VDRC}	-	+++
Dot-GAL4>If^{VDRC}	-	-
Dot-GAL4>Arm^{VDRC}	-	-
Dot-GAL4>Fak56D^{VDRC}	-	-

Table 4.4. Scored heart and pericardial nephrocyte phenotypes from the *Dot>RNAi* cell-adhesion mini-screen.
Results of the *Dot>RNAi* cell-adhesion mini-screen were scored and show that there was no effect on heart morphology. Effects of RNAi overexpression on pericardial nephrocyte morphology was also assessed and it was found that *Fit1, Fit1+2, Mys,* and *Mew* RNAi caused the strongest PN phenotypes. Heart images were scored thusly: - = no effect, + = small effect, ++ = moderate effect, +++ = severe/strong effect.

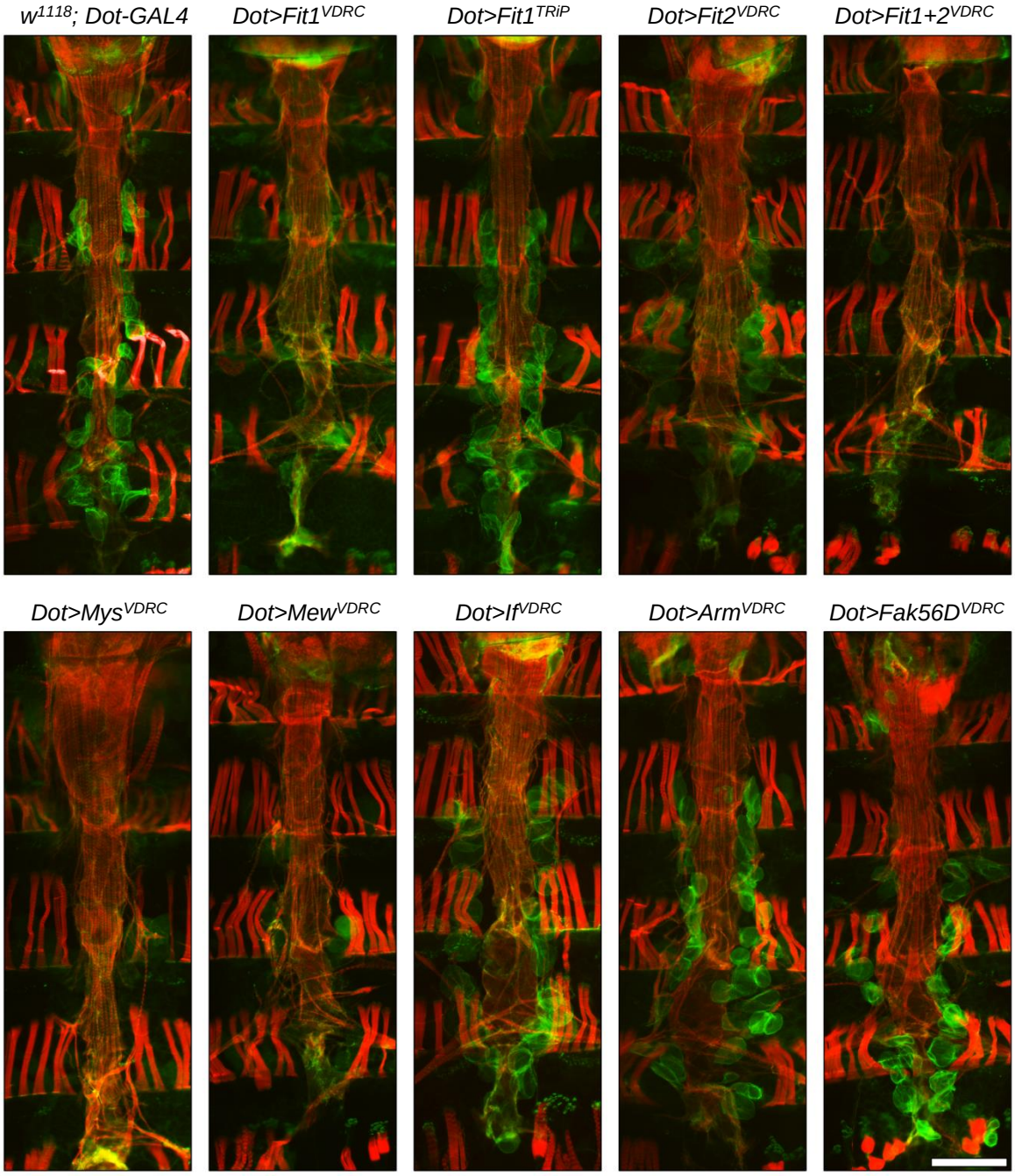

Figure 4.13. Screening cell adhesion genes for changes in pericardial nephrocyte morphology in the fly heart using the pericardial cell-driver, *Dot-GAL4*.

There were a few RNAi lines that exerted a dramatic effect on pericardial nephrocyte morphology when driven by the *Dot-GAL4* driver. The pericardial cells in *Dot>Fit1^{VDRC}*, *Dot>Fit1+2^{VDRC}*, *Dot>Mys^{VDRC}*, and *Dot>Mew^{VDRC}* hearts appeared to be completely ablated. There was no significant effect from the other RNAi lines on pericardial cell morphology, however, the β-integrin staining appears less intense in *Dot>Fit2^{VDRC}* hearts. Hearts are stained with Alexa-conjugated phalloidin (red), and anti-βPS integrin antibody (green). Scale bar = 100μm.

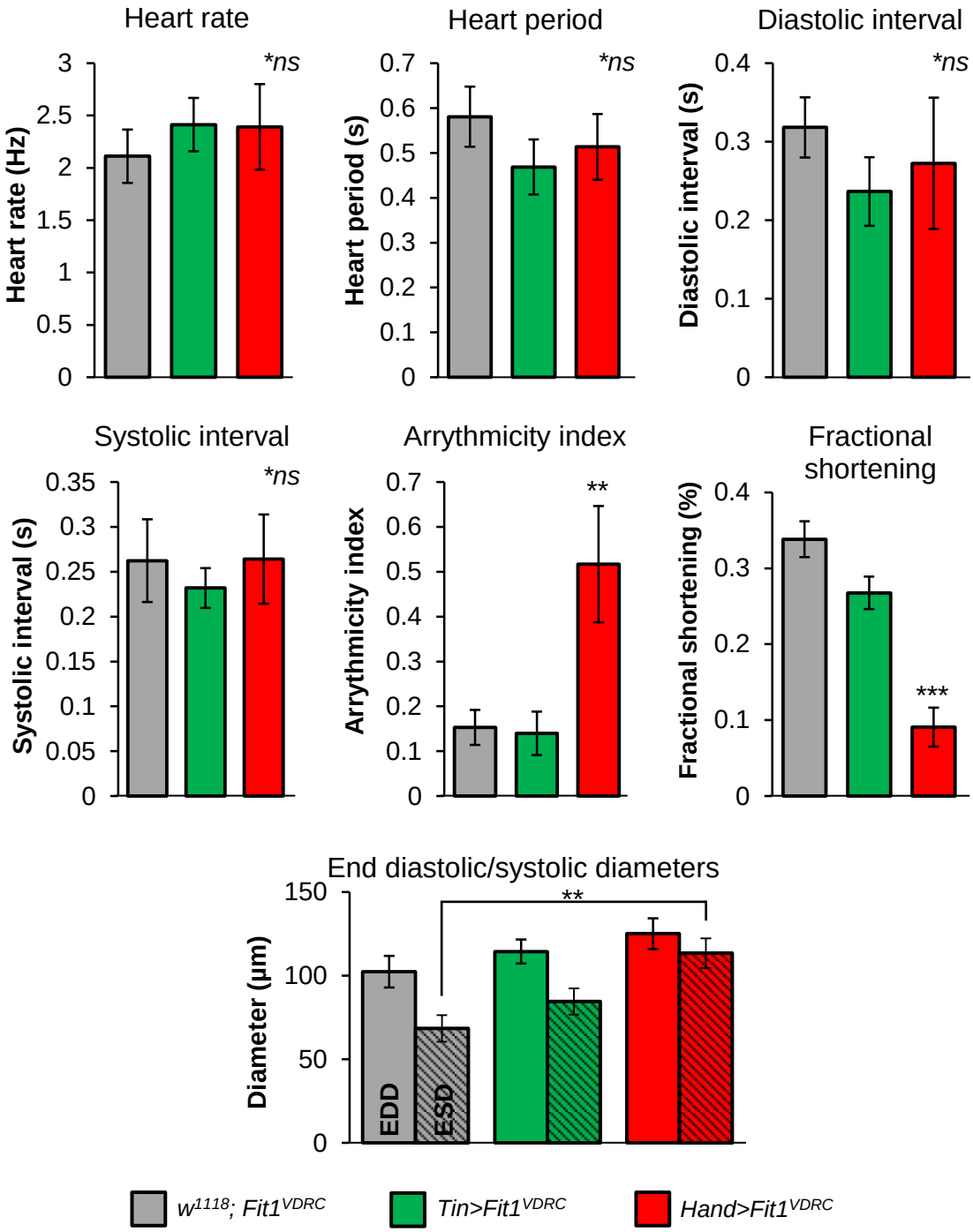

Figure 4.14. Heart function of *Fit1*^{VDRC} flies using different heart-GAL4 drivers.

There was no significant difference in heart rate, heart period, diastolic interval, or systolic interval between all genotypes. However, *Hand>Fit1*^{VDRC} hearts exhibited significantly greater arrhythmicity, and a significantly lower degree of fractional shortening compared to *w*^{1118}*; Fit1*^{VDRC} controls. There was no difference in end diastolic diameter (non-shaded) values between genotypes, however, *Hand>Fit1*^{VDRC} hearts exhibited significantly larger end systolic diameter (shaded) values compared to controls. Results are mean ± SEM, *n* = 6-8 flies per genotype. **p<0.01, ***p<0.001, one-way ANOVA with Tukey's post-hoc test.

(±0.13) *Hand>Fit1*^{VDRC}, *p<0.01*) greater arrhythmicity, and a significantly (0.34 (±0.02) *w*^{1118}*; Fit1*^{VDRC} vs. 0.09 (±0.03) *Hand>Fit1*^{VDRC}, *p<0.001*) lower degree of fractional shortening compared to *w*^{1118}*; Fit1*^{VDRC} controls. There was no difference in end diastolic diameter values between genotypes, however, end systolic diameters from *Hand>Fit1*^{VDRC} hearts were significantly (68.5µm (±7.98) *w*^{1118}*; Fit1*^{VDRC} vs. 113.5µm (±8.87) *Hand>Fit1*^{VDRC}, *p<0.01*) larger compared to controls.

4.3.6 Silencing *Arm* in cardiomyocytes

As mentioned previously, knockdown of *Arm* RNA affected myofibril patterning in the cardiomyocytes – with longitudinal actin staining instead of transverse. The effect of *Arm* knockdown after GAL4 knockdown in the three GAL4 drivers is summarised in Figure 4.15A. Knockdown of *Arm* RNA in the cardiomyocytes (i.e. *Hand* and *Tin* GAL4 lines) resulted in cardiomyocyte myofibrils aligning parallel to the anterior-posterior axis, instead of transversely aligned myofibrils in wildtype hearts. Additionally, the valve-like ostial cells were lacking in these hearts (highlighted in Figure 4.15B) – possibly indicating a failure to differentiate. There was no such phenotype in the hearts of *Dot>Arm*^{VDRC} mutants.

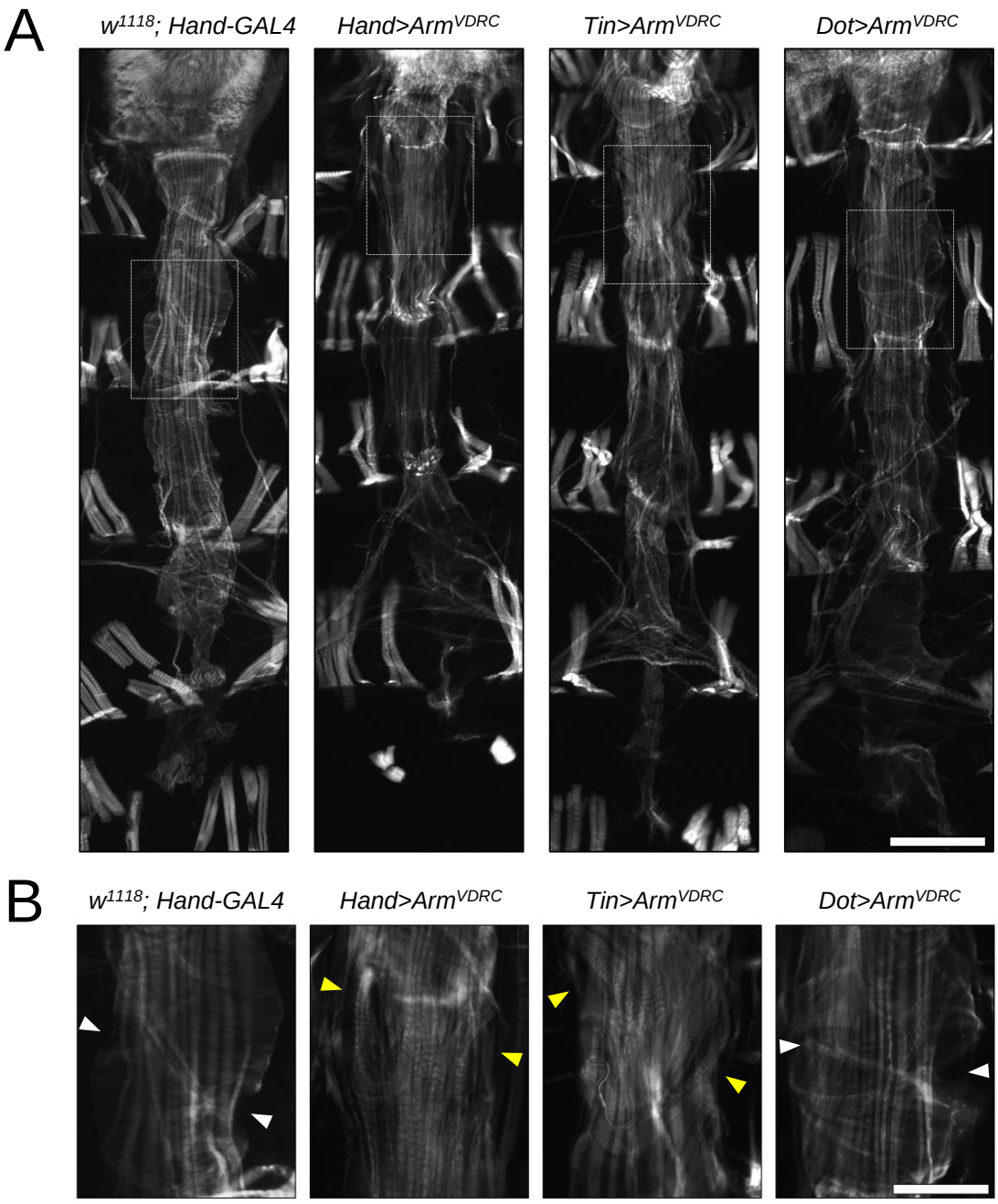

Figure 4.15. Depletion of *Arm* RNA in the *Drosophila* heart results in cardiomyocytes that fail to differentiate.

A, hearts of wildtype adults (*Hand>w^{1118}*) have characteristic transverse spiralling actin myofibrils, and ostial cells (i.e. valve-like openings) periodically along the length of the heart. In the hearts of *Hand>Arm^{VDRC}* and *Tin>Arm^{VDRC}* mutants, hearts appear similar in width to wildtype, but cardiomyocyte myofibrils are orientated longitudinally instead of transversely – indicating failure to properly differentiate. *Dot>Arm^{VDRC}* hearts appear normal. **B**, higher magnification images of the dashed boxes in **A**. Ostial cells (white arrowheads) are present in *Hand>w^{1118}* and *Dot>Arm^{VDRC}* hearts, while these openings appear to be absent in *Hand>Arm^{VDRC}* and *Tin>Arm^{VDRC}* mutant hearts – yellow arrowheads indicate apparently undifferentiated ostial cells. Hearts were stained with Alexa-conjugated phalloidin. Scale bar = 100µm (upper panels), 50µm (lower panels).

4.4 Discussion

The aim was to screen genes chosen based on their expression and homology with human orthologs, for their involvement in the development of the adult *Drosophila* cardiac syncytium. Candidate genes were extracted from the FlyAtlas dataset (CHINTAPALLI *et al.* 2007) by ranking genes according to those with the highest 'heart' enrichment, then performing an RNAi mini-screen with these candidates, focussing on orthologs with a potential or known role in heart function, based either on predicted gene function or expression pattern.

4.4.1 PNs likely skewed the adult 'heart' gene list

The term 'heart' is in inverted commas since the adult heart tissue extracted for microarray analysis by Chintapalli *et al*. would "necessarily include some adherent tissues" (About & FAQ, FlyAtlas - http://www.flyatlas.org/). The "adherent tissues" mentioned would invariably have included PNs – which, undoubtedly skewed this list of genes. The PNs are relatively large cells compared to the heart itself, and, from experience with heart extractions, could potentially constitute ~30-50% of extracted tissue. The PNs are pinocytotic (DAS *et al.* 2008a; MILLS and KING 1965) and are evolutionarily related to vertebrate podocytes (WEAVERS *et al.* 2009) – and have a reticuloendothelial functions, ancestral to that of the mammalian kidney and hepatic system, with dual roles in haemolymph homeostasis and toxin clearance/sequestration, respectively. In agreement with this, high on the 'heart'-enriched gene list were genes predicted to be involved in processes not typically associated with cardiomyocytes, including lysosomal activity (*Lectin-33A*, *Lectin-24Db*, *CG31823*, *Fuca*), and vitamin B12 transport (*CG11592*, *CG42255*,

CG32702). The genes involved in vitamin B12 transport, in particular, were very highly expressed and highly specific to the FlyAtlas adult 'heart' tissue fraction, and appear to be orthologous components of the Cubam receptor - a multi-ligand receptor complex involved in reabsorption of various proteins from the glomerular ultrafiltrate, a process observed in the proximal tubules of the kidney (BIRN *et al.* 2000; PEDERSEN *et al.* 2010). The PNs are inherently closely associated with the heart and removal of these cells without damage to the adult cardiac tissue (and sample loss) is incredibly difficult. Therefore, the microarray signal from adult fly hearts is cardiomyocyte and pericardial in origin. Future studies aiming to ascertain heart-enriched genes should aim to avoid this PN contamination of extracted heart tissue – i.e. potentially utilising flies that have had their pericardial cells removed (DAS *et al.* 2008b). Additionally, to obtain cardiomyocyte-specific signal it may be possible to use laser capture microdissection to isolate the heart, or FACS sorting of labelled cell types.

Since the list of 'heart'-enriched genes also contained genes that appeared to be nephrocytic in origin, it was decided to utilise the cardiomyocyte- and PN-enhancer, *HandC-GAL4*, to drive RNAi expression in these cells, in an effort to deduce the consequences of selected RNAi knockdown on both cell types. The *HandC-GAL4* driver is also a stronger driver of expression in the adult compared to the cardiomyocyte-specific *TinCΔ4-GAL4* driver (LO and FRASCH 2001; SELLIN *et al.* 2006). Indeed, while the *TinCΔ4-GAL4* driver is excellent for embryonic heart overexpression, it may not be the most appropriate for overexpression in the adult as enhancer expression is mainly localised in the valve-like ostial cells of the adult heart (ZEITOUNI *et al.* 2007).

In the primary screen, effects of the selected RNAis on heart (and PN) morphology was chosen as a read-out. Phalloidin was used to highlight structural changes to actin-architecture of the cardiomyocytes, while βPS-integrin antibody was used to highlight effects on cardiomyocyte-cardiomyocyte junctions and PNs – an excellent marker for both these purposes (BROWER *et al.* 1984). Heart immunostaining can generate excellent information regarding cell morphology, including detail of multiple structures at the subcellular level. Heart function analysis needs 4-5 times as many heart dissections/heart video recordings/heart video analyses compared to just 4 heart stainings that can be performed in the same well of a 96-well plate. However, by solely relying on differences in morphology between groups (some of which may be subtle), there may be an increase in false negatives – i.e. hearts that appear morphologically identical to wildtype, but which may be functionally abnormal (e.g. dilated cardiomyopathy, disrupted Ca^{2+}-signalling, arrhythmic heart). Quantitative PCR to confirm genetic knockdown, and functional analysis would be useful differentiate between these false negatives and true negatives.

4.4.2 Knocking down heart-enriched, orthologous genes produced severe cardiac phenotypes

The FlyAtlas genes were the ranked according to their percentage sequence identity with their human orthologs, and selected RNAi lines were screened via a heart-specific RNAi mini-screen. This list contained orthologous genes there had significant, deleterious effects on cardiac and PN morphology. Knockdown of *Steamer duck* (*Stck*) a.k.a. the *Drosophila* ortholog of Particularly Interesting New Cysteine-Histidine rich protein (PINCH), in the fly heart resulted in cardiomyocytes

that were moderately dissociated from each other, indicating a role for PINCH protein in cardiomyocyte-cardiomyocyte adhesion in *Drosophila*. PINCH is an important cell adhesion protein, and is known to indirectly interact with ECM-ligated integrins via the integrin-linked kinase, PINCH, parvin (IPP) ternary complex, regulating signalling and connecting the ECM to the actin cytoskeleton (CLARK *et al.* 2003; LEGATE *et al.* 2006). In animal models, morpholino-knockdown of both PINCH isoforms in zebrafish resulted in loss of cardiac contractility (MEDER *et al.* 2011), while ablation of PINCH in mice caused dilated cardiomyopathy with concurrent disruption of intercalated discs (LIANG *et al.* 2009). Therefore, the cardiomyocyte uncoupling that occurs after depletion of *Stck* mRNA highly suggests that the function of this protein is conserved from flies to mice. No studies have, as yet examined functional consequences of PINCH ablation in human cardiomyocytes, but it has been observed that PINCH expression was significantly upregulated in failing heart tissue (SOPKO *et al.* 2011). It was also noted that knockdown of *Stck* had no significant effect on PN morphology – potentially indicating a muscle-specific primary role in βPS-integrin/ILK signalling at sites of actin filament anchorage (CLARK *et al.* 2003).

Knockdown of *δ-Aminolevulinate synthase* (*Alas*) did not appear to affect cardiac morphology in the fly, but did result in significantly enlarged PNs. *Alas* is a mitochondrial enzyme important for heme biosynthesis, while *Alas*-null *Drosophila* larvae exhibit significant water loss due to breakdown in skin impermeability (SHAIK *et al.* 2012). The reason for this increase in PN size is presently unknown.

The strongest adult heart phenotype came from *Hand>Ches1*^{VDRC} flies. These adults completely lacked an abdominal cardiac tube and the associated pericardial

cells – yet these flies did appear to harbour the vestigial terminal heart chamber (ZEITOUNI *et al.* 2007). It has recently been reported that loss of the forkhead transcription factor, *Ches1*, results in aberrant division of cardiac progenitor cells in the *Drosophila* embryo (AHMAD *et al.* 2012). However, although these authors utilised the same heart-driver (*Hand-GAL4*) to drive *Ches1* RNAi expression in the developing embryo, they did not examine the hearts of adults. These authors also speculate that phenotypes caused by loss of *Ches1* could be due to a downstream effect on the kinase *Polo* – an important protein implicated in cellular mitosis, meiosis and cytokinesis (ARCHAMBAULT and GLOVER 2009). Therefore, the phenotype of these adult *Ches1*-knockdown hearts confirms the observations seen by Ahmad *et al*. about the importance for this protein in *Drosophila* heart development.

Hand>Ches1 Drosophila can survive to adulthood even though the heart appears to have undergone complete ablation. The terminal heart chamber is still present, which suggests that the larval heart was not severely affected – since *Hand-GAL4* expression is strong in larval cardiomyocytes (SELLIN *et al.* 2006) – and the *Hand-GAL4* driver does not drive expression in these cells in the adult. Some residual beating of the terminal heart chamber, therefore, may also be keeping the flow of haemolymph strong enough to sustain the adult fly. Similarly, inactivating Calmodulin or L-type Ca2+-channels specifically in the cardiac tube, stopped the beating of the heart yet resulted in viable and apparently healthy animals (MEDIONI *et al.* 2009). It is possible, then, that this strong *Ches1* phenotype arises during metamorphosis. Ideally, tracking the development of the hearts of these mutants throughout development would be necessary to pinpoint when these cardioblasts/cardiomyocytes fail to thrive. But the strong phenotype of these *Ches1*

mutants reiterates the question of the requirement of a functioning cardiac syncytium at all in the adult fly.

Knockdown of *Bteb2* in the hearts did not significantly affect heart morphology, but did cause complete ablation of the PN, in agreement with published information (IVY *et al.* 2012). *Bteb2* is a zinc-finger transcription factor related to human Krüppel-like factor, KLF15 – known for its role in kidney podocyte differentiation, as well as renal and cardiac hypertrophy (FISCH *et al.* 2007; MALLIPATTU *et al.* 2012). Additionally, *Bteb2* was one of the most 'heart'-specific genes from the FlyAtlas list with 40-fold enrichment compared to the rest of the fly. Lineage-tracing experiments tracking the development of PNs in *Hand>Bteb2*^{VDRC} animals throughout development will be important to elucidate at which point these cells are lost.

One of the most severe cardiac phenotypes occurred with *Fermitin 1* (*Fit1*) knockdown. There was significant cardiomyocyte dissociation after *Fit1* RNA depletion, with cardiomyocytes appearing severely detached from adjacent cardiomyocytes. PNs of these mutants were also ablated – indicating an essential role of *Fit1* in these cells. *Fit1* is a highly expressed, heart enriched gene which was demonstrated to be important for embryonic heart development (KIM *et al.* 2004) – embryos injected with *Fit1* dsRNA displayed an aberrant heart phenotype. The Fit1 protein is predicted to be involved in cell adhesion due to its high sequence homology with the human Kindlin protein family – namely Kindlin 2, a heart enriched protein essential for viability in mice, and important for heart development and angiogenesis in mice and zebrafish (DOWLING *et al.* 2008a; PLUSKOTA *et al.* 2011). The only study in *Drosophila* thus far to identify a function of *Fit1* was by

Bai *et al*. who identified, in a screen to identify genes involved in muscle assembly, that knockdown of *Fit1* in the *Drosophila* embryo via dsRNA injection led to some body wall muscles 'rounding-up', while knockdown of both *Fit1* and its paralog in the fly, *Fit2*, phenocopied the severe muscle rounding phenotype seen in *myospheroid*-knockdown embryos (BAI *et al.* 2008). This link between the Fermitins and β-integrins (Fit1/Mys) is relevant since the same link is seen in other model organisms from *C. elegans* (UNC-112/PAT3) to humans (KIND2/β1-integrin) (LARJAVA *et al.* 2008; ROGALSKI *et al.* 2000).

There were no significant effects on heart or PN morphology from the remainder of the RNAi lines – i.e. *Tld*, *Syn1*, *NijA*, *NijB*, and *Timp*. However, qPCR was not performed and it may be the case that genetic knockdown was insufficient. Future studies should address this issue.

4.4.3 Integrin-related cell adhesion genes play an important role in the development of the *Drosophila* cardiac syncytium

Since *Stck* and *Fit1* depletion caused similar phenotypes, it was reasoned that other proteins known to be involved in integrin-associated cell adhesion may also be important for development of the cardiac syncytium, therefore a final targeted mini-screen was performed. From this selection of genes known/hypothesised to be important for cell adhesion (*Fit1*, *Fit2*, *Mys*, *Mew*, *If*, *Arm*, and *Fak56D*), there were a few lines that demonstrated significant deleterious effects on cardiac and PN morphology.

Fit1 RNAi from both the VDRC and TRiP stock collections were assessed for their effects on heart morphology – with differing results. Whereas $Fit1^{VDRC}$

knockdown caused a significant breakdown of cardiomyocyte-cardiomyocyte adhesion and PN ablation, $Fit1^{TRiP}$ knockdown hearts did not reproduce this severe phenotype – with gaps between cardiomyocyte visible in some areas, but cells still connected, and the presence of PNs. It will be necessary to reconcile the difference in effects on the fly hearts between these two RNAi lines. Regardless, it highly suggests that *Fit1* is involved in cardiomyocyte adhesion. *Fit2* knockdown in the heart also appeared to result in loss of cardiomyocyte junctional integrity – with increased β-integrin staining clearly visible between cardiomyocytes compared to wildtype. PNs of *Fit2* knockdown adults were also present but β-integrin staining appeared dim. Therefore it appeared that both Fermitins were important for cardiomyocyte adhesion. This was confirmed when the $Fit1{+}Fit2^{VDRC}$ double RNAi knockdown line was expressed in the heart. Cardiomyocytes of these mutants were completely spherical and mimicked the heart phenotype of Mys^{VDRC} mutants – confirming the observation of rounding-up of embryonic body wall muscles, noted by Bai and colleagues, also applies to *Drosophila* cardiomyocytes (BAI *et al.* 2008). PNs were also absent in both $Fit1{+}Fit2^{VDRC}$, and Mys^{VDRC} mutants – indicating these proteins are required for PN viability. What was unclear was if there was a compensatory role that each *Fermitin* was performing in the absence of its paralog. This is answered and discussed at length in Chapter 6.

The severity of cardiomyocyte dissociation between each RNAi line was also quantified - with $Fit1^{VDRC}$, $Fit1{+}Fit2^{VDRC}$, and Mys^{VDRC} lines exhibiting a significantly greater level of dissociation between cardiomyocytes. $Fit1^{TRiP}$, $Fit2^{VDRC}$, and If^{VDRC} RNAi lines also appeared to be significantly more dissociated compared to

wildtypes – but this apparent difference was negated by the weighted influence of the severely dissociated RNAi lines on the statistical test.

Interestingly, knockdown of *Mew* and *If* indicated distinct roles for each in cardiomyocytes and PNs. *Mew* is essential for PN viability, but has no effect on cardiomyocyte morphology. Conversely, *If* is important for adhesion of adjacent cardiomyocytes, but has no apparent effect on PNs. This was confirmed after RNAi analysis using three 'heart'-GAL4 drivers (*HandC-GAL4, TinCΔ4-GAL4,* and *Dot-GAL4*) – summarised in Figure 4.16). It has previously been shown that *Mew* (αPS1-integrin) and *If* (αPS2-integrin) are involved in discrete functions in *Drosophila* – with *If* essential for somatic muscle morphogenesis, and *Mew* apparently dispensable (BROWER *et al.* 1995; PROKOP *et al.* 1998). Indeed, the integrin heterodimer in muscles is αPS2βPS (αPS2 is the ortholog of vertebrate α5, IIb, V and 8 integrins) (TANENTZAPF and BROWN 2006). It would also seem to be the case with cardiac muscle – with *Mew* and *If* dispensable and essential, respectively, for cardiac development in *Drosophila*. Conversely, *If* is dispensable for PN development, while *Mew* is essential – this is summarised in Figure 4.17.

There were no significant effects on heart or PN morphology from the *Fak56D* RNAi line. Knockdown of *Arm* RNA in the heart will be discussed below.

4.4.4 Screening these cell adhesion genes using 3 different 'heart' drivers confirmed the importance of the Fermitins for cardiac tissue development

To assess whether the severe cardiomyocyte phenotypes observed (e.g. *Hand>Fit1+Fit2*^{VDRC}) were due to expression of RNAi in PNs, or in the cardiomyocytes, two other GAL4 drivers were utilised – the *HandC* promoter drives

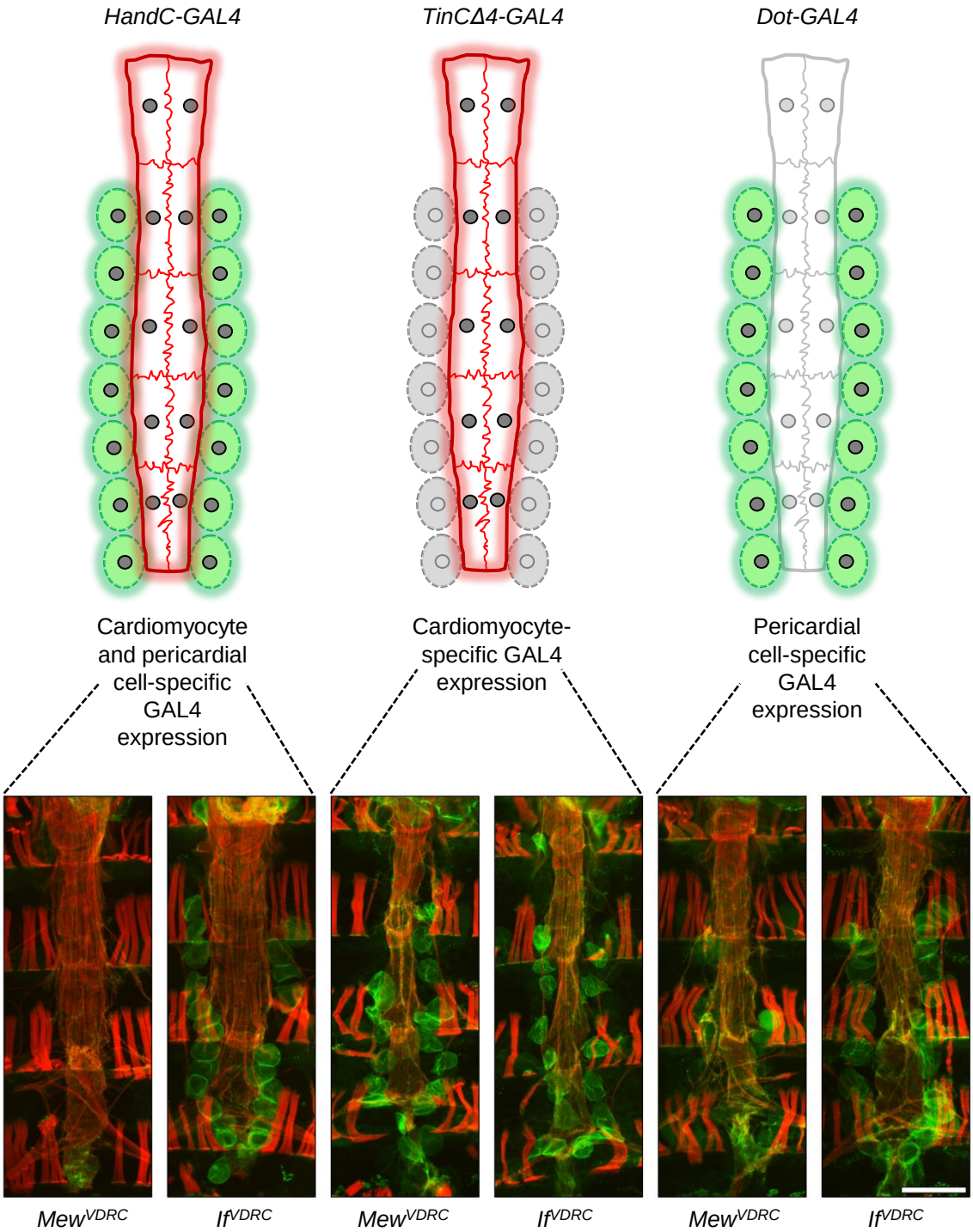

Figure 4.16. Depletion of *Mew* and *If* generates different phenotypes in cardiomyocytes and pericardial nephrocytes.
By driving *Mew* and *If* RNAi expression via three different 'heart' GAL4 drivers in the fly, it was demonstrated that *Mew* is important for the presence of pericardial nephrocytes in the adult fly, and depletion has no effect on cardiac morphology. Conversely, *If* is important for cardiac morphology, while having no impact on pericardial nephrocytes. Scale bar = 100µm.

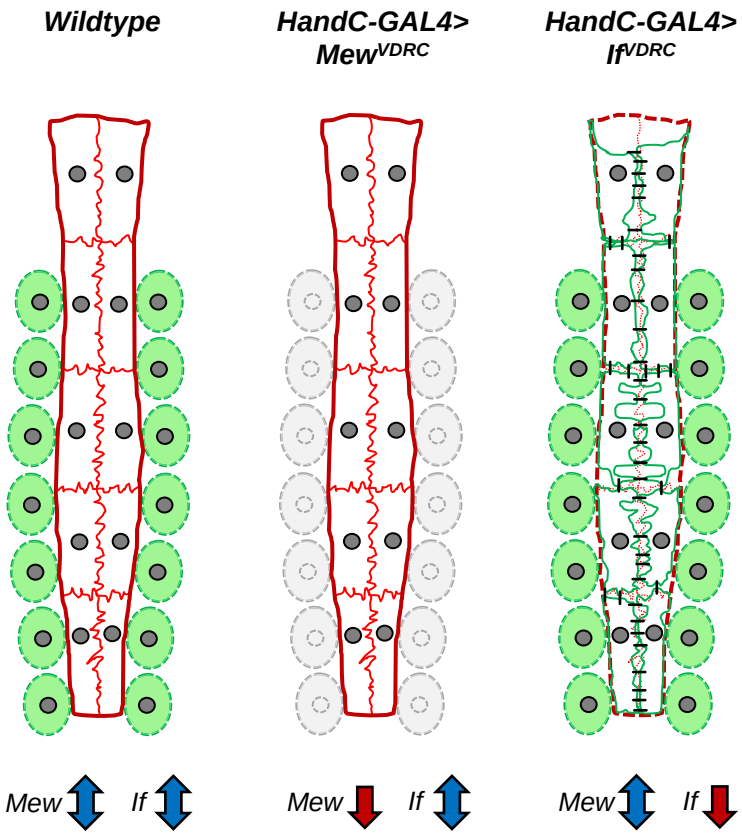

Figure 4.17. *Mew* and *If* have different functions in cardiomyocytes and pericardial nephrocytes.

Mew is important for the presence of pericardial nephrocytes in the adult fly, and depletion has no effect on cardiac morphology. Conversely, *If* is important for cardiac morphology, while having no impact on pericardial nephrocytes.

GAL4 expression in both the cardiomyocytes and PNs (SELLIN *et al.* 2006); the *TinCΔ4* enhancer drives GAL4 expression solely in the cardiomyocytes (LO and FRASCH 2001); and the *Dot* enhancer drives GAL4 expression solely in the PNs (KIMBRELL *et al.* 2002).

The dissociative cardiomyocyte phenotype of *Fit1* RNAi (both VDRC and TRiP lines) was also observed after cardiomyocyte-specific overexpression, although to a much lesser extent compared to *HandC*-driven RNAi. Similarly, *Fit2* knockdown resulted in noticeable joins between cardiomyocytes. *Mys* knockdown had the most significant effect on cardiomyocytes, with apparent large gaps between these cells. This mini-screen using the *TinCΔ4* enhancer was performed prior to the *Fit1+Fit2*^{VDRC} double RNAi line had been generated. However, it would be expected that *Fit1+Fit2*^{VDRC} hearts would have exhibited the same phenotype as *TinCΔ4>Mys*^{VDRC} hearts. The discrepancy between the severity of cardiomyocyte phenotypes between *Tin* and *Hand* enhancers is likely down to strength of enhancer expression. *TinCΔ4-GAL4* is a slightly weaker GAL4 driver in the adult – at least compared to *HandC* (TOGEL et al. 2008). *TinCΔ4-Gal4* drives expression in differentiating cardioblasts from embryonic stage 11 to 12 onwards, but is missing the early *tin* expression domain (LO and FRASCH 2001; PERRIN *et al.* 2004), while *HandC* is expressed from stage 12 onwards in both cardioblasts and pericardial cells (KOLSCH and PAULULAT 2002; SELLIN *et al.* 2006). However, a possible advantage of this 'half-way house' in cardiomyocyte-dissociation phenotypes between these GAL4 drivers means that it may be possible to compare and contrast RNAi dosage – with greater RNAi expression resulting in more severe phenotypes, e.g. *TinCΔ4>Mys*^{VDRC} hearts compared to *HandC>Mys*^{VDRC} hearts.

RNAi overexpression using the *Dot-GAL4* driver did not result in morphological damage to the hearts of any of the lines tested. However, similar to *HandC*-driven RNAi, PNs were ablated in $Fit1^{VDRC}$, $Fit1{+}2^{VDRC}$, Mew^{VDRC}, and Mys^{VDRC} hearts. Therefore, the Fermitins, αPS1, and βPS are required for PN viability in the adult *Drosophila*. The *Dot* mini-screen also confirms that loss of PNs does not affect the viability of the fly – confirming previous observations (DAS *et al.* 2008b) – nor does loss of these cells affect cardiac morphology. There were no significant effects on heart or PN morphology from the *Fak56D* RNAi line.

4.4.5 Cardiomyocyte-overexpression of $Fit1^{VDRC}$ also caused defects in heart function parameters

Since the hearts of $Hand{>}Fit1^{VDRC}$ and $Tin{>}Fit1^{VDRC}$ exhibited significant cardiomyocyte-dissociation compared to controls hearts, functional analysis was also performed in these flies to assess the effect of *Fit1* silencing on cardiac function. Given the severity of the cardiomyocyte dissociation in $Hand{>}Fit1^{VDRC}$ hearts, however, it may be more accurate to describe the hearts of these flies as (mostly) isolated cardiomyocytes. Similarly, qualifying the rhythmic beating of these cardiomyocytes as heart function in the wildtype 'functional syncytium' sense, is inappropriate. The heart function analysis software can detect the rhythmic nature of these beating cardiomyocytes and registers these as correct function – even if many heart parameters exhibit similar properties to $w^{1118}; Fit1^{VDRC}$ hearts – including heart rate, heart period, and diastolic/systolic intervals. However, due to many of the $Hand{>}Fit1^{VDRC}$ recordings containing hearts that had independently beating cardiomyocytes (i.e. not functionally connected) this increased the degree of arrhythmicity in this genotype. However, not all $Hand{>}Fit1^{VDRC}$ heart recordings had

completely separated cardiomyocytes and some of these adult hearts appeared functionally connected (to an extent), likely explaining the large error bars in this group. Importantly, the degree of fractional shortening was significantly reduced in *Hand>Fit1*^{VDRC} hearts, highlighting these significantly dissociated cardiomyocytes as lacking the ability to form a functional syncytium. Additionally, the EDD and ESD values were not significantly different in *Hand>Fit1*^{VDRC} hearts.

Tin>Fit1^{VDRC} hearts were also functionally assessed since these hearts also exhibited cardiomyocyte dissociation, but to a lesser extent. However, there was no significant difference in any of the heart function parameters compared to w^{1118}; *Fit1*^{VDRC} hearts. It may be the case that the cardiomyocytes in the hearts of *Tin>Fit1*^{VDRC} flies were not significantly dissociated enough to exhibit a significant functional phenotype – other than the obvious morphological differences. In other words, the hearts of *Tin>Fit1*^{VDRC} flies still formed a functional syncytium. This lack of functional effect in hearts that would otherwise appear functionally compromised, is explored further in Chapter 5.

4.4.6 Inhibition of the Wnt signalling pathway via *Arm* RNAi resulted in cardiomyocyte differentiation failure

The adult *Drosophila* heart is formed by the remodelling of the posterior larval aorta during metamorphosis. The remodelling process significantly widens the heart tube (regions A1-A4), with a concurrent increase in the number of contractile myofibrils in each differentiating cardiomyocyte, while the larval heart (region A5) is histolysed (MOLINA and CRIPPS 2001; MONIER *et al.* 2005; SELLIN *et al.* 2006). In the canonical Wnt signalling pathway in the fruit fly, stabilised Arm protein (i.e.

Drosophila β-catenin) translocates to the nucleus, where, in conjunction with Pangolin (i.e. *Drosophila* TCF) it activates transcription of downstream target genes (DASGUPTA *et al.* 2005).

Knockdown of *Arm* RNA in the cardiomyocytes (i.e. using the *Hand* and *Tin* GAL4 drivers) resulted in irregular myofibril arrangement and an absence of the valve-like ostial cells that characterise the adult dorsal vessel, while pericardial cells were unaffected after knockdown (using *Hand* and *Dot* GAL4 lines). In agreement with this, downregulation of the Wnt pathway via ectopic expression of a dominant negative form of dTCF, resulted in hearts with longitudinally arranged myofibrils, and a lack of ostial cell formation – the authors interpreted this aberrant cardiac phenotype as a transformation of these normally destined A1-A4 cardiomyocytes into A5 terminal chamber-like myocytes (ZEITOUNI *et al.* 2007). Additionally, a different group studying heart function, found *Arm* knockdown resulted in reduced end diastolic dimension (CASAD *et al.* 2012). Therefore, downregulation of the Wnt pathway in the *Drosophila* heart appears to inhibit correct cardiac differentiation, and prevents ostial cell formation.

4.4.7 Conclusions from the cardiac screening of RNAi lines and possible roles of the Fermitins in the *Drosophila* heart

4.4.7.1 Remarkable phenotypes and missed opportunities

There were a variety of phenotypes exhibited from most of the RNAi lines that were screened - from adult flies that lacked a cardiac tube altogether (*Ches1*) to giant PNs. However, proteins involved in cell adhesion that resulted in similar cardiomyocyte-dissociation were focussed on. From the hearts of *Fit1* and *Stck*-

knockdown mutants, further known/hypothesised binding partners and signalling molecules were selected and targeted by RNAi. Integrin-related proteins such as Talin (*rhea*), Integrin-linked kinase (*ilk*), Parvin (*parvin*), and αPS3-integrin (*scb*), and cadherin-related proteins such as E-cadherin (*shg*), and α-catenin (*α-Cat*) should also be tested for their effects on cardiac syncytium development. Talin is a well-studied β-integrin-binding protein essential for cell adhesion and would likely result in a similar 'rounded-up' cardiomyocyte phenotype as *Fit1+2*, or *Mys*-knockdown (BROWN *et al.* 2002; BULGAKOVA *et al.* 2012). Similarly, ILK is another vital component of the integrin signalling and adhesion complex. Studies have shown that ILK, similar to PINCH, does not bind directly to β-integrins (ZERVAS and BROWN 2002; ZERVAS *et al.* 2001) – therefore, it would be predicted that knockdown would result in a phenotype not as extreme as *Mys*-knockdown, but more akin to *Stck* knockdown. Scab (αPS3-integrin), in particular, should be examined since it was previously shown to be involved in heart formation and binding to βPS-integrin (STARK *et al.* 1997). All the cell adhesion genes tested were on the cytoplasmic side of the cell and predicted to link in some way to the Fermitins, but extracellular matrix proteins such as the integrin-binding Laminin A, and Perlecan – mutations in which have previously been demonstrated to result in heart malformations (HAAG *et al.* 1999; MEDIONI *et al.* 2008) – should also be assessed.

Interestingly, Medioni and colleagues described the formation of the cardiac tube in the *Drosophila* embryo and noted the localisation of *Arm* (β-catenin), and other cell adhesion proteins such as DE-Cadherin, at the adherens junctions connecting cardiomyocytes. It is likely these proteins are still present at the junctions between contiguous cardiomyocytes in the adult *Drosophila*, but knockdown of the

Fermitins is sufficient to cause cell dissociation that cannot be compensated for by other important cell adhesion proteins – e.g. integrins, cadherins.

In adult *Drosophila* hearts, β-integrin staining highlighted the thread-like junction between adjacent cardiomyocytes and staining was clearly visible in cardiomyocytes that were slightly uncoupled – however, junctional staining in wildtype hearts appeared weaker compared to uncoupled hearts. It is possible that β-integrin expression is increased in these mutants as a compensatory mechanism to prevent complete dissociation and maintain connection between cardiomyocytes. This will be discussed at length in Chapter 5.

4.4.7.2 Relevance to heart formation in the *Drosophila* embryo

Cardioblasts in the *Drosophila* embryo migrate medially from the lateral mesoderm and converge at the midline to form the heart vessel – a functional syncytium (VANDERPLOEG *et al.* 2012). Integrins and related adhesion proteins (ILK, Talin, Laminin A, Syndecan, Robo, and Slit) are necessary for heart assembly and lumen formation in *Drosophila* cardiogenesis (KNOX *et al.* 2011; MACMULLIN and JACOBS 2006; VANDERPLOEG *et al.* 2012). βPS-integrin, in particular, is concentrated at spot adherens junctions linking contralateral cardioblasts during lumen formation (i.e. the side where both cardioblasts connect to each other to form the heart) (LEHMACHER *et al.* 2012; VANDERPLOEG *et al.* 2012).

4.4.7.3 Intercalated discs in *Drosophila*? A role for Fermitins

The plaque-bearing adherens junctions that connect contiguous cardiomyocytes in vertebrates are known as intercalated discs (FRANKE *et al.* 2006). Mutations in proteins important for intercalated disc function can lead to deleterious

heart pathologies – e.g. dilated cardiomyopathy (EHLER *et al.* 2001; PERRIARD *et al.* 2003). Human heart diseases attributed to intercalated disc dysfunction include arrhythmogenic right ventricular cardiomyopathy caused by mutations in D proteins (e.g. Desmoplakin, Plakophilin-2, and Desmoglein-2) (BASSO *et al.* 2006), and hypertrophic and dilated cardiomyopathy caused by a missense mutation in the integrin-binding adhesion protein, Vinculin (VASILE *et al.* 2006). Integrins and related binding proteins (e.g. Vinculin and Talin) were also identified at intercalated discs in adult human cardiac tissue (ANASTASI *et al.* 2009; DI MAURO *et al.* 2009), while expression of these is increased in cardiomyopathy (HAUSELMANN *et al.* 2011; TERRACIO *et al.* 1991).

Thus, there is a need to develop genetically tractable models with which to study the role of these proteins in cardiac development and function. Intercalated disc-like structures resembling the vertebrate equivalents have been identified in adult *Drosophila* cardiomyocytes, but so far there have been no empirical studies examining the role of this structure in the heart (LEHMACHER *et al.* 2012). A hypothetical model of intercalated disc-like structure and its components is summarised in Figure 4.18.

Studies of vertebrate hearts suggest a role for *Kind2* in cardiac development and function, however these studies are limited by the embryonic lethality of *Kind2* knock-out in the mouse model, and the lack of tissue specific *Kind2* silencing in the fish model (DOWLING *et al.* 2008a; MONTANEZ *et al.* 2008). The aberrant phenotype caused by silencing orthologs of *Kind2* in the cardiomyocytes of an invertebrate demonstrates that the protein's role in cardiac development has been evolutionarily

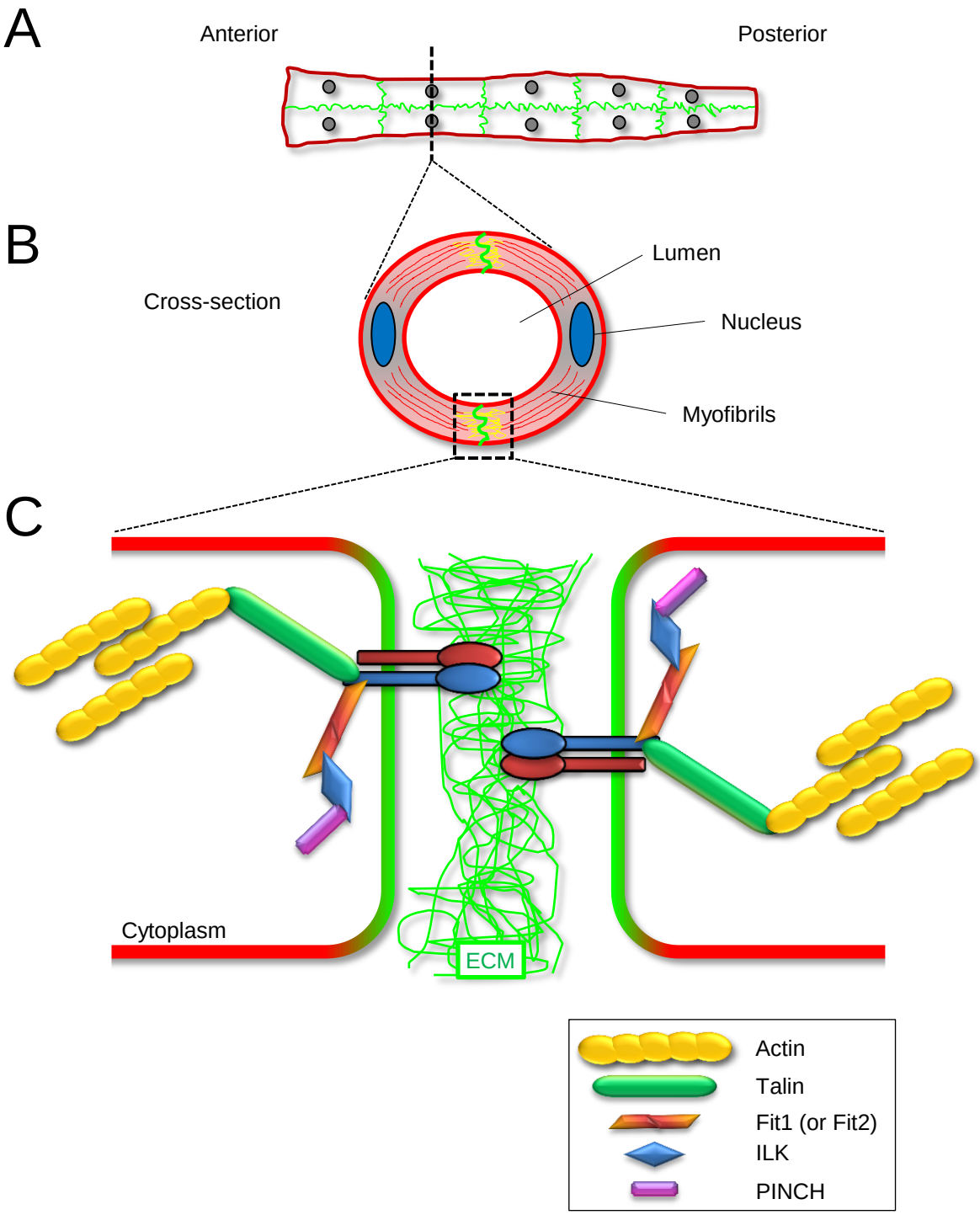

Figure 4.18. Hypothetical model of the role of integrins and their binding partners at the intercalated disc-like junction between cardiomyocytes in *Drosophila*.

A, **B**, the adult *Drosophila* heart and a cross-sectional view of two opposing cardiomyocytes indicating the location of the junctions between them. **C**, close-up view of the intercalated disc-like structure between the adult cardiomyocytes. Integrins tether themselves to the extracellular matrix and are helped to secure the connection to the actin cytoskeleton by integrin-associated proteins – including Fit1 (or Fit2), Talin, ILK, and PINCH.

conserved and also reiterates the validity of using *Drosophila* to study genes relevant to mammalian cardiac physiology.

The aberrant heart phenotype caused by *Fermitin* knock-down in *Drosophila* reproduces many aspects of the cardiomyopathy caused by morpholino knock-down of *Kind2* in zebrafish (DOWLING *et al.* 2008a), and supports the authors' conclusion that *Kind2* regulates heart development. Morpholino-knockdown in zebrafish disrupted angiogenesis but also affected intercalated disc formation in cardiomyocytes and significantly reduced fractional shortening.

4.4.7.4 A model of integrin-based adhesion at the junction between contiguous cardiomyocytes in adult *Drosophila*

Previous studies in *Drosophila* have identified the *Fermitins* as mediators of muscle assembly (BAI *et al.* 2008), and the current findings extend this observation to include the assembly of a functional cardiac syncytium. The current data provide evidence that the β-integrin encoded by *myospheroid* is localised at the boundaries between adjacent cardiomyocytes, and also indicate that the development of a functional cardiac syncytium is strictly dependent on *myospheroid* as well as the expression of *Fermitins*. The cardiomyopathy caused by silencing *Fit1* and *Fit2* phenocopied *myospheroid* knock-down and is therefore consistent with the *Fermitins* regulating β-integrin signalling and promoting cardiomyocyte coupling during development (LEHMACHER *et al.* 2012; VANDERPLOEG *et al.* 2012). There is evidence from mammalian models that Kindlins, via the FERM F3 subdomain, interact directly with the cytoplasmic tail of β-integrins (MONTANEZ *et al.* 2008; SHI *et al.* 2007).

The FERM domain of *Drosophila* Fermitins is conserved from worms to humans and it is therefore speculated that Fermitins directly interact with the β-integrin *myospheroid* to form a signalling complex required for cardiomyocyte coupling. Indeed, it was demonstrated that Kindlin-2 binds to the extreme C terminus of β-integrin, allowing accommodation of both Kindlin-2 and Talin to enhance integrin signalling (BLEDZKA *et al.* 2012).

No study has yet manipulated the expression of mammalian *Kind2* solely in the cardiomyocytes, however it is predicted that a phenotype would develop that is similar to that seen in ventricular cardiomyocyte-targeted β1-integrin knockout mice (SHAI *et al.* 2002). Histological studies of the β1-integrin KO hearts revealed significant disruption of myofibrils and intercalated discs, with subsequent onset of dilated cardiomyopathy. Additionally, differentiation and integrity of cardiac muscle cells are impaired in the absence of β1 integrin (FASSLER *et al.* 1996).

In summary, the findings identify *Fermitins* as important mediators of cardiomyocyte coupling and heart function in *Drosophila*. Given the evolutionary conservation between invertebrate *Fermitins* and mammalian Kindlins, the evidence supports the hypothesis that disruption of cardiomyocyte *KIND2* may lead to abnormal intercalated discs and cardiomyopathies in humans.

Chapter 5

Generation and characterisation of *Fermitin* deletion mutant flies via P-element mobilization, and their effects on the morphology and function of the *Drosophila* heart.

5.1 Introduction

The severe cardiomyocyte dissociation phenotype of *Fit1*^{VDRC}, and *Fit1*^{VDRC}/*Fit2*^{VDRC} cardiac-specific knockdown adult flies (Chapter 4) was novel and was previously unreported, therefore efforts were undertaken to further elucidate the function of the Fermitins and their effect on heart development and adult heart function.

5.1.1 The Fermitins are orthologous to the Kindlin cell-adhesion proteins

The Kindlin family of cell adhesion proteins, orthologous to fly Fermitins, are evolutionarily conserved from worms to humans (ROGALSKI *et al.* 2000; WHITE and MCLEAN 2005), and mediate cell-cell and cell-matrix adhesion by regulating integrin function (LARJAVA *et al.* 2008). Findings from several animal models suggest that the formation of junctions between neighbouring cardiomyocytes (intercalated discs) may require integrins and integrin binding proteins (EHLER *et al.* 2001; KNOLL *et al.* 2007; PERRIARD *et al.* 2003; SHAI *et al.* 2002; WHITE *et al.* 2006). It is important to understand the role of these proteins because mutations and polymorphisms that affect intercalated disc formation may be associated with the development of cardiomyopathies in humans (BASSO *et al.* 2006; PERRIARD *et al.* 2003; VASILE *et al.* 2006).

The Kindlin family comprises 3 members – Kindlin 1, an epithelial-specific Kindlin associated with the skin-blistering genetic disorder Kindler syndrome (SIN *et al.* 2011); Kindlin 2, the ubiquitous Kindlin that is highly enriched in smooth/striated muscle (including cardiac tissue) (DOWLING *et al.* 2008a; MONTANEZ *et al.* 2008); and Kindlin-3, found to be present in haematopoietic and endothelial cells (BIALKOWSKA *et al.* 2010; USSAR *et al.* 2006).

5.1.2 Kindlin 2 is essential for life and crucial for heart development

Murine KIND2 protein is detected at intercalated discs, however genetic ablation of *Kind2* in mice causes early embryonic lethality at the peri-implantation stage, before cardiogenesis (DOWLING *et al.* 2008a; MONTANEZ *et al.* 2008). In zebrafish, the global knock-down of *Kind2* causes cardiac hyperplasia, disrupts intercalated disc formation and significantly reduces cardiac contractility (DOWLING *et al.* 2008a). Additionally, angiogenesis in morpholino-knockdown zebrafish and heterozygous mice is aberrant – with mice displaying immature neovascularisation (DOWLING *et al.* 2008a; MONTANEZ *et al.* 2008; PLUSKOTA *et al.* 2011). Dowling *et al*. also demonstrated that Kindlin 2 protein was enriched at intercalated discs in mice, and morpholino-knockdown in zebrafish disrupted intercalated disc formation leading to a failure in myofibril attachment to membrane complexes. Since Kindlin-2 protein is highly heart-enriched and is present at the junctions between adjacent cardiomyocytes, it suggests this protein may have a role in cardiomyocyte adhesion and function. Embryonic lethality precludes the study of the Kindlin 2 in mice, and no tissue-specific conditional knockdown system is currently available for study in zebrafish. These findings link *Kind2* with the development of a functional cardiac syncytium; however a cardiomyocyte-specific test of this hypothesis is yet to be conducted.

Kindlin 2 has also been shown to be important in the growth of certain cancers including increased expression in uterine leiomyomas (KATO *et al.* 2004), gastric cancer (SHEN *et al.* 2012), and the invasion front of malignant mesothelioma – where it was also noted to have significant nuclear localisation (AN *et al.* 2010). Indeed, aside from its crucial role at the cell membrane, Kindlin 2 has recently been

shown to act as a transcriptional co-activator of the Wnt pathway alongside β-catenin and TCF4 (YU *et al.* 2012). Therefore, Kindlin 2 appears to play a variety of roles in the cell – from integrin signalling at the cell membrane and its importance for cell adhesion, to transcriptional activation of evolutionarily conserved genes crucial for morphogenesis.

5.1.3 The importance of integrins, and their binding partners, for cardioblast adhesion in the developing *Drosophila* embryo

Cardioblasts in the *Drosophila* embryo migrate medially from the lateral mesoderm and converge at the midline to form the heart vessel – a functional syncytium (VANDERPLOEG *et al.* 2012). Integrins and related adhesion proteins (ILK, Talin, Laminin A, Syndecan, Robo, and Slit) are necessary for heart assembly and lumen formation in *Drosophila* cardiogenesis (KNOX *et al.* 2011; MACMULLIN and JACOBS 2006; VANDERPLOEG *et al.* 2012). One β-integrin (*Myospheroid* in *Drosophila*), in particular, is concentrated at spot adherens junctions linking contralateral cardioblasts during lumen formation (i.e. the side where both cardioblasts connect to each other to form the heart) (LEHMACHER *et al.* 2012; VANDERPLOEG *et al.* 2012). The plaque-bearing adherens junctions that connect contiguous cardiomyocytes in vertebrates are known as intercalated discs (FRANKE *et al.* 2006). Mutations in proteins important for intercalated disc function can lead to deleterious heart pathologies – e.g. dilated cardiomyopathy (EHLER *et al.* 2001; PERRIARD *et al.* 2003). Intercalated disc-like structures resembling the vertebrate equivalents have been identified in *Drosophila* cardiomyocytes, but so far there have been no empirical studies examining the role of this structure in the heart (LEHMACHER *et al.* 2012).

5.1.4 Using the *Drosophila* heart to assess functional consequences of *dKindlin* knockdown

The *Drosophila melanogaster* heart is a model of cardiovascular development, sharing many features of mammalian cardiac function (WOLF *et al.* 2006), and while the fly heart differs from the human heart in many respects, the function is conserved between species (MEDIONI *et al.* 2009; SERLUCA and FISHMAN 2006). *Drosophila melanogaster* is an important model for the identification and study of genes that have relevance to mammalian cardiovascular development and function (BIRSE *et al.* 2010; KIM and WOLF 2009; MEDIONI *et al.* 2009; NEELY *et al.* 2010b; WOLF *et al.* 2006). Recent genetic screens identified novel candidate genes (e.g. SIP, Wry, Not3) that directly translate into conserved mammalian orthologs essential for normal heart function (CASAD *et al.* 2012; KIM *et al.* 2010; NEELY *et al.* 2010b). The abdominal heart in *Drosophila* consists of individual cardiomyocytes that form a contractile syncytium and pump haemolymph from the abdomen, through the thorax towards the head.

A schematic of the *Drosophila* equivalents of the Kindlin proteins is illustrated in Figure 5.1A. *Drosophila* expresses two orthologs of human KIND2, *Fermitin1* (*Fit1*) and *Fermitin2* (*Fit2*) that contain a highly conserved FERM (4.1, Ezrin, Radixin, Moesin) domain which is required for binding to the cytoplasmic tail of β-integrins (SHI *et al.* 2007) - specifically, the FERM F3 subdomain which contains the β-integrin-binding motif. Clustal alignments of the FERM F3 subdomains from humans, mice, and zebrafish, are compared to the fruit fly orthologs, shown in Figure 5.1B. The *Drosophila* Fermitin protein family share a high degree of homology (48 and 45% protein identity, for Fermitin 1 (*Fit1*) and

A

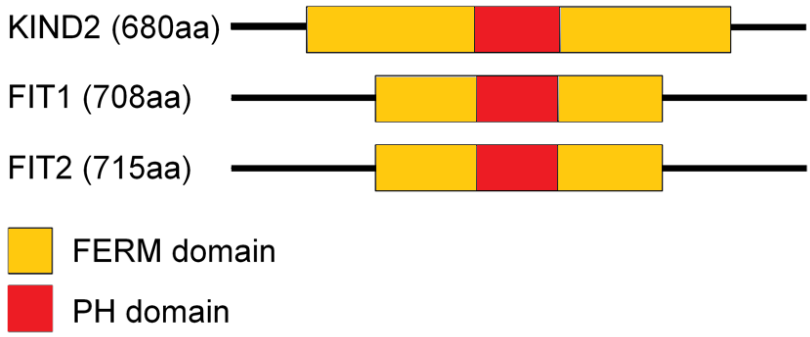

B

```
Hs_KIND2_F3      LPEFGITHFIARFQGGKKEELIGIAYNRLIRMDASTGDAIKTWRFSNMKQWNVNWEIKMV
Mm_KIND2_F3      LPEFGITHFIARFQGGKREELIGIAYNRLIRMDASTGDAIKTWRFSNMKQWNVNWEIKMV
Dr_KIND2_F3      LPEFGITHFLAKFQGGKKDELIGITYNRLIRMDAGTGDAIKTWRFSNMKQWNVNWEIKMV
Dm_FIT1_F3       LPDFGVTLFIIKFDGHKKEELLGVANNRIMRMDLNTGDHIKTWRYNTMKAWNVNWGIKCM
Dm_FIT2_F3       LPDFGVSLFIIKFDGHRKEELLGVAHNRIMRMDLSSGDHIKTWRYNTMKAWNVNWNIKCM
                 **:**:: *: :*:* :::**:*:: **::***  :** *****:..** ***** ** :

Hs_KIND2_F3      TVEFADEVRLSFICTEVDCKVVHEFIGGYIFLST
Mm_KIND2_F3      TVEFADEVRLSFICTEVDCKVVHEFIGGYIFLST
Dr_KIND2_F3      TVEFADEPSLAFICAEVDCKVVHEFIGGYIFLST
Dm_FIT1_F3       MIQLQDE-NIVFSVQSADCKVVHEFIGGYIFMSM
Dm_FIT2_F3       MIQFEDE-NVVFSCHSADCKVVHEFIGGYIFMSM
                  ::: **  : *   ..**************:*
```

Figure 5.1. The Kindlin-2 FERM F3 subdomain, important for integrin-binding, is highly conserved in *Drosophila* Fermitins.

A, The integrin binding FERM domain of human Kind2 is present in both Fit1 and Fit2. **B**, Clustal Omega alignments of human, mouse, and zebrafish KIND2 FERM F3 subdomain with *Drosophila* orthologs Fit1 and Fit2. The FERM F3 subdomain common to all three human Kindlin proteins, which is required for binding to the cytoplasmic tail of β-integrins, is conserved in *Drosophila* Fit1 and Fit2. Shaded grey areas show exact matches, while dots show similar amino acids.

Fermitin 2 (*Fit2*) respectively) with human Kindlin 2, and were previously identified in a genetic screen for genes involved in muscle assembly (BAI *et al.* 2008). Both *Fit1* and *Fit2* message and protein are detected in adult heart tissue, consistent with a role in cardiac function (CAMMARATO *et al.* 2011; CHINTAPALLI *et al.* 2007). Therefore, the Fermitins may be relevant to the development and function of the adult fly heart.

To explore the role of Fermitins in the *Drosophila* heart we silenced their expression in cardiomyocytes and analysed the function of the adult heart. It was found that cardiomyocyte expression of *Fermitins* is critical for the development of a functional syncytium in *Drosophila* and that the genes can functionally compensate for each other. The findings support the hypothesis that disruption of cardiomyocyte *KIND2* may lead to abnormal intercalated discs and cardiomyopathies in humans.

5.2 Hypothesis

The hypothesis was that removal of either *Fit1* or *Fit2* may have an adverse effect on heart development and adult heart function in *Drosophila*.

5.2.1 Aims

1. To generate individual *Fit1* and *Fit2* deletion (Δ) mutants via P-element mobilisation.
    a. To characterise and phenotype these ΔFit1 and ΔFit2 mutants.
2. To generate double *Fit1 Fit2*-null flies and characterise these mutants.
3. To generate flies that are null in *Fit1* that also silence *Fit2* in the cardiomyocytes.
    a. To phenotype the hearts of these mutants.

5.3 Results

5.3.1 Generating *Fit1* and *Fit2* deletion mutants via imprecise excision of an existing P-element

In order to understand the role of the Fermitins in *Drosophila melanogaster*, I aimed to generate null mutants for each paralog (i.e. *Fit1* and *Fit2*) via imprecise excision of an already existing P-element mutant, otherwise known as Δ2-3 mutagenesis. Appropriate crosses were set up for both $Fit1^{KG05576}$ and $Fit2^{EY08530}$ P-element lines (shown in Figure 5.2) and possible deletion mutants were screened by PCR using primers designed to flank the P-element insertions ($Fit1^{KG05576}$ Figure 5.3A, and $Fit2^{EY08530}$ Figure 5.3B respectively). To confirm the primer sets were successful in amplifying the desired gene-spanning regions (for *Fit1* and *Fit2*), PCRs were performed using genomic DNA from wildtype *CaS* flies and *Fit* P-element flies. The elongation time in the PCR reactions was set at 4 mins – i.e. long enough so the wildtype fragment could be amplified, but too short to also amplify the genome-region containing the large (>10kb) P-element. As shown in Figure 5.4A+B, both *Fit1* and *Fit2* genomic targets were amplified in wildtype flies but were not amplified in each respective P-element line. As a positive genomic and loading control, *RP49* was amplified to demonstrate the presence of DNA in *Fit* P-element samples. Since the *RP49* PCR product in Figure 5.4A is relatively small (128 base pairs), it is possible the bands may have overlapped, and may be confused on a gel with primer dimers. It is for this reason that, when using this *RP49* primer pair, a DNAse treatment control was also performed on both wildtype and *Fit1* P-element DNA (Figure 5.4A, bottom panel). The *RP49* PCR product in Figure 5.4B (bottom

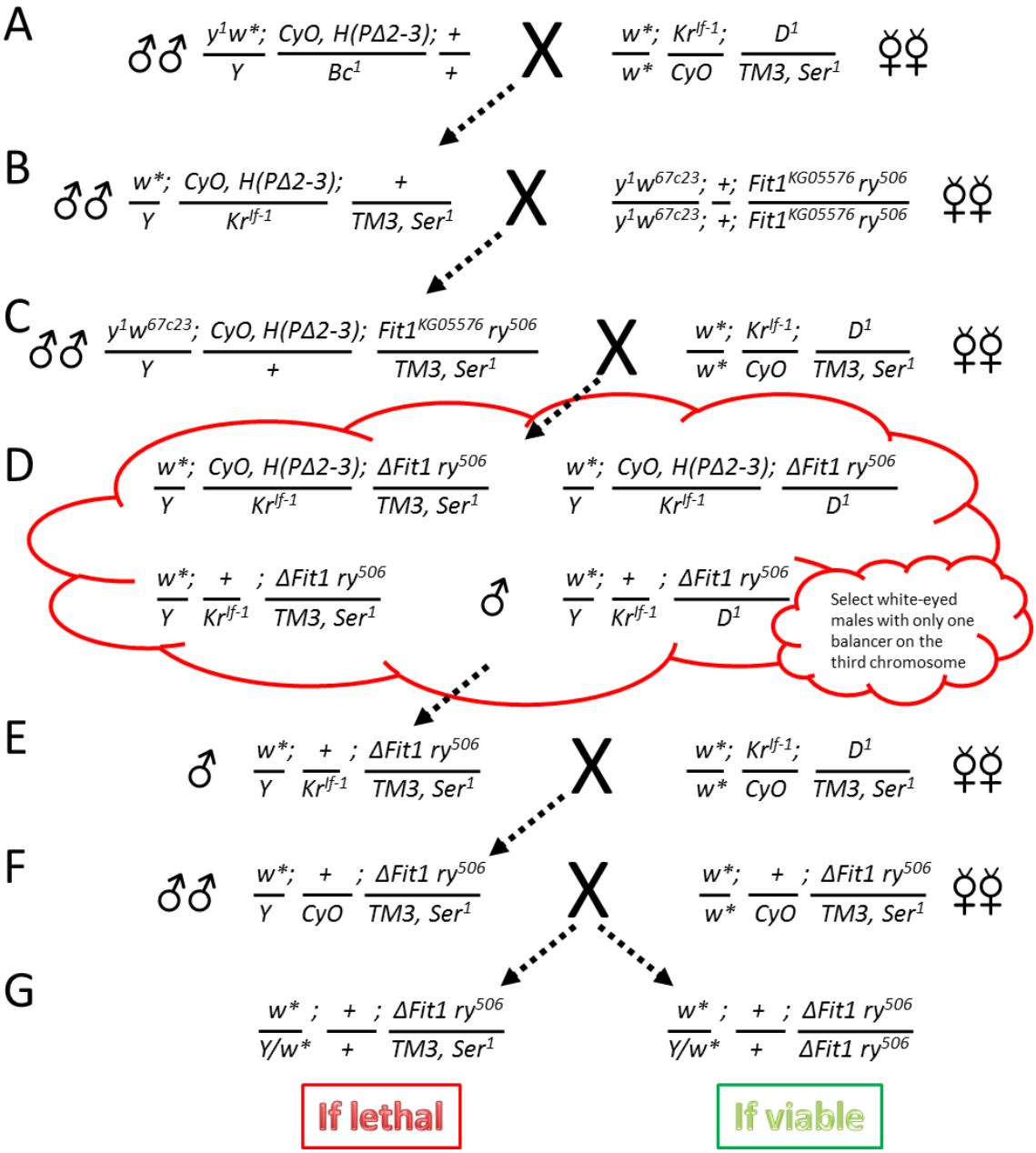

Figure 5.2. Crossing scheme for the generation of Fit1 deletions using imprecise excision of the P-element via Δ2-3 transposase.
The *Fit1*^{KG05576} line was used as the P-element that was 'hopped out'. The same crossing scheme was used to generate deletions in *Fit2*^{EY08530} flies. ♂/♀ indicates single male/female crossings. ♂♂/♀♀ indicates en masse crossings.

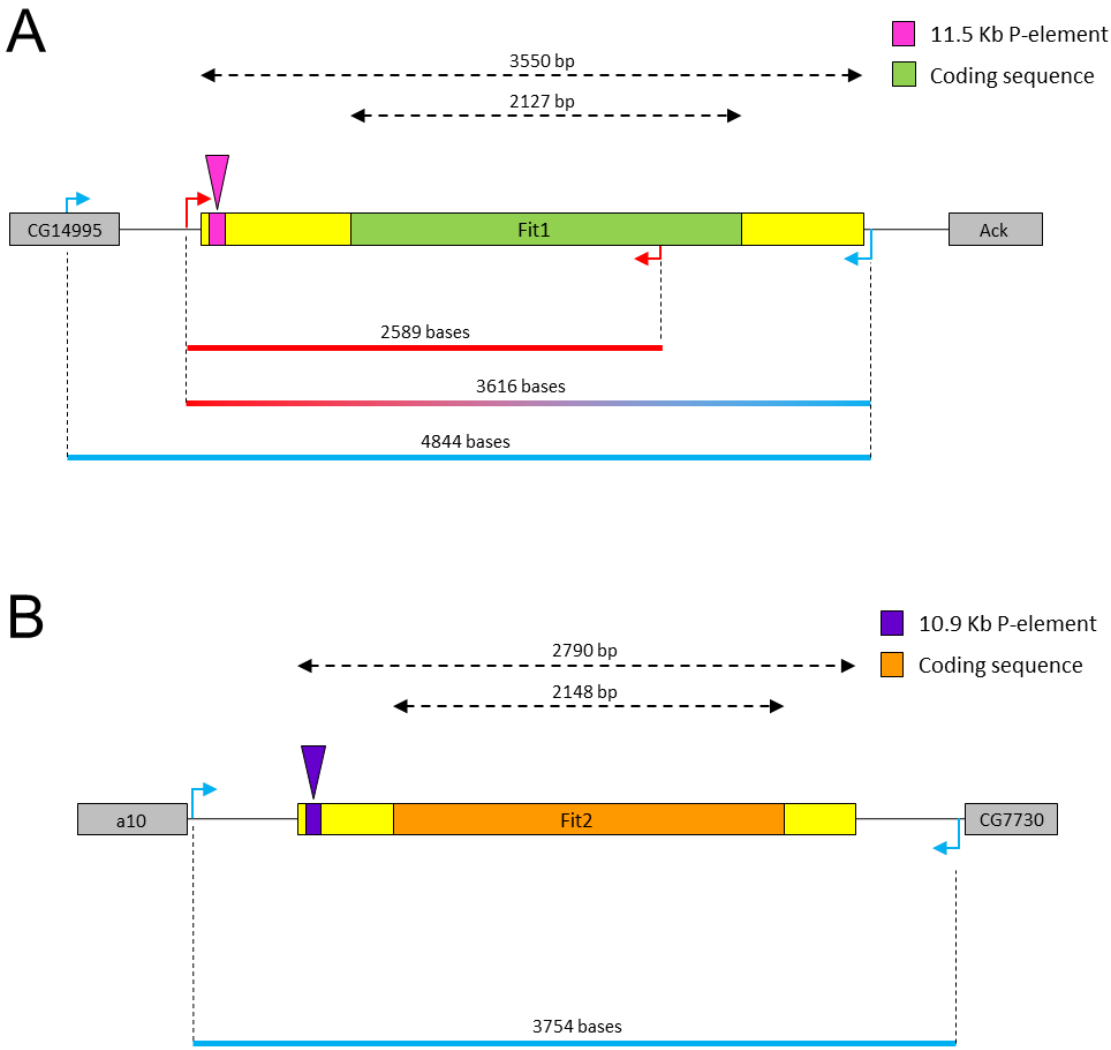

Figure 5.3. Location of primers used to check for imprecise excision events.
A,**B**, primers spanning length of *Fit1* and *Fit2* were designed on Primer3 website (http://frodo.wi.mit.edu/).

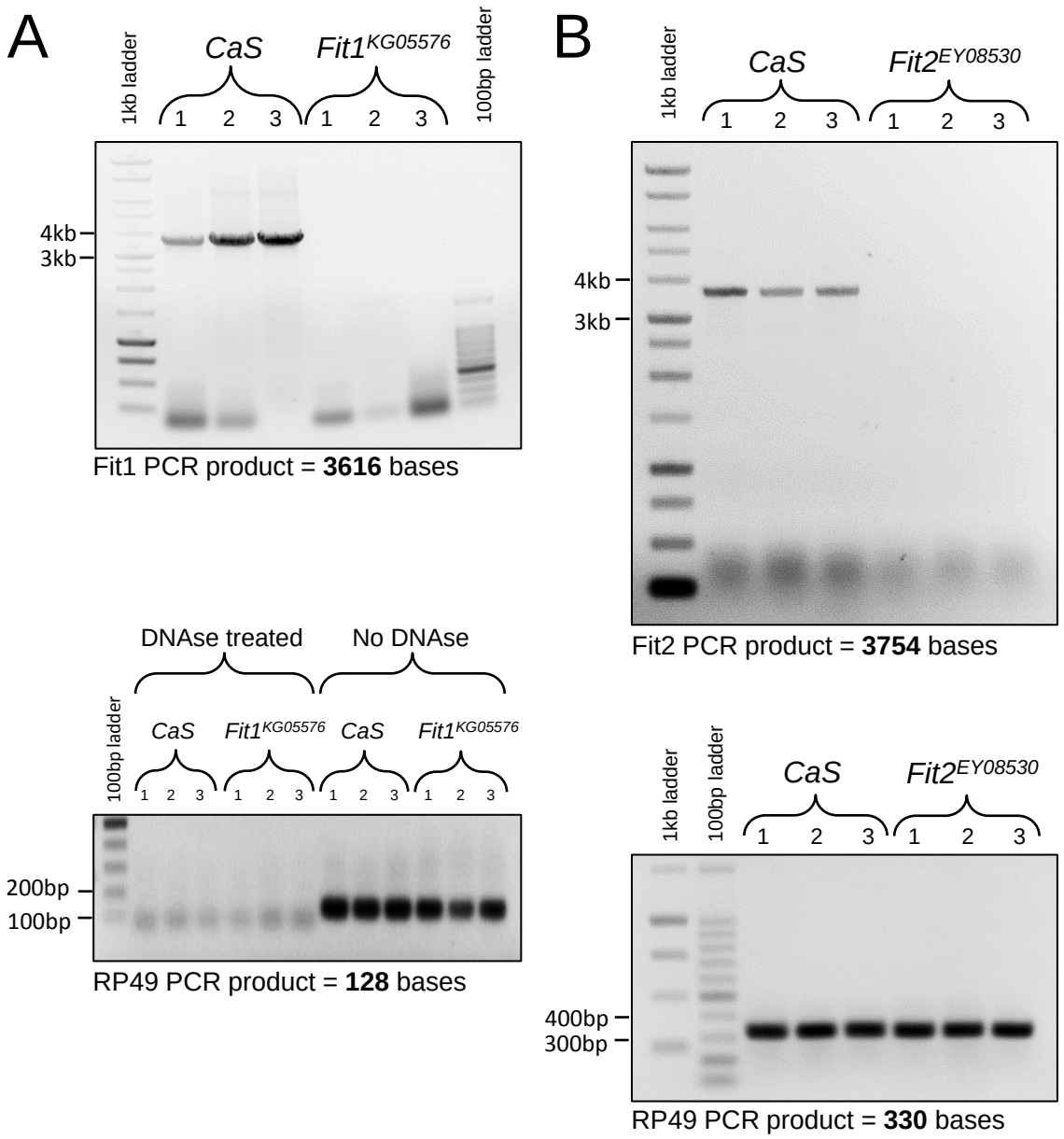

Figure 5.4. PCR of Fit1 and Fit2 in *CaS* and *Fit1* or *Fit2* P-element flies. **A+B**, samples in triplicate show that the wild-type (*CaS*) version of the gene is amplified at the expected molecular weight, while *Fit1*^{KG05576} and *Fit2*^{EY08530} (containing 11.5kb and 10.9kb P-elements respectively) are not. Elongation time in the PCR reaction (4mins) was enough that the wild-type copy of the gene could be amplified but not enough to cover the gene and P-element. The bottom panels for **A** and **B** are the respective RP49 controls. To make sure the small 128bp RP49 product band was not random primer dimers, a DNAse treatment was performed before the PCR reaction.

panel) is sufficiently large (330 base pairs) so that it can be distinguished from primer dimers.

Genomic DNA was extracted from a total of 227 potential *Fit1* deletion (Δ) lines and was screened for the presence of a genetic deletion. It should be noted that due to the nature of some vials of flies containing very few flies, it was reasoned that heterozygous flies (that carried the potential deletion over a balancer chromosome) could also be included when extracting DNA from each potential deletion line. A deletion was suspected when there was a band on the gel that was smaller than the wildtype band. Using the same primers as used in Figure 5.4A (top panel), PCRs were performed on each potential ΔFit1 line, and samples were run on DNA electrophoresis gels. For an unknown reason, most of the PCR samples that were run on the first 3 gels (panels labelled 1-3 in Figure 5.5) did not work. However, samples run on gels 4 and 5 (Figure 5.5), displayed more wildtype bands, that were to be expected. On gel 4 (Figure 5.5), there were two noticeable genetic deletions in ΔFit1 lines 134 and 161.

To ensure the majority of the ΔFit1 DNA samples were intact, a different set of primers was used to check for the presence of a genomic deletion – the positions of which are shown in Figure 5.3A. To confirm the primers were successful in amplifying the desired gene-spanning region of *Fit1*, PCRs were performed using genomic DNA from wildtype *CaS* flies and $Fit1^{KG05576}$ flies. Again, the elongation time in the PCR reactions was set at 4 mins. As shown in Figure 5.6A, the *Fit1* genomic target was amplified in wildtype flies but not in $Fit1^{KG05576}$ flies. *RP49* was used as a control. Using these same primers, PCRs were performed on each potential ΔFit1 line, and PCR samples were run on DNA electrophoresis gels. It should be

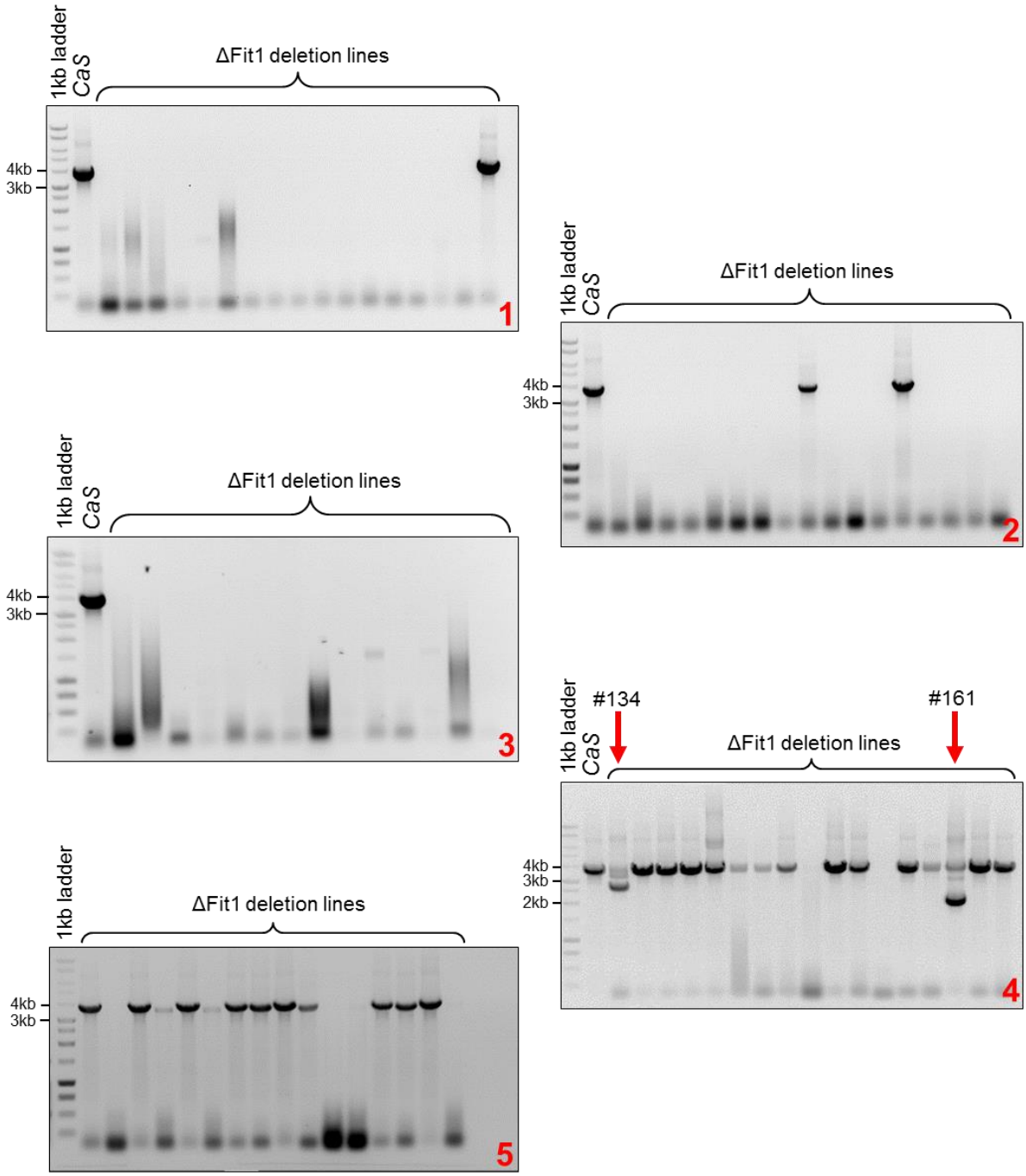

Figure 5.5. Genotyping via PCR of *Fit1* in *CaS* and *ΔFit1* deletion lines. PCRs of *CaS* and 81 *ΔFit1* deletion lines (heterozygous for the deletion over a balancer on the 3rd chromosome) spread over 5 DNA gels. In gels 1-3, the annealing T_m may have been too low, so was increased for gels 4 and 5. There were 2 noticeable deletions using these primers – lines #134 and #161 – in gel 4.

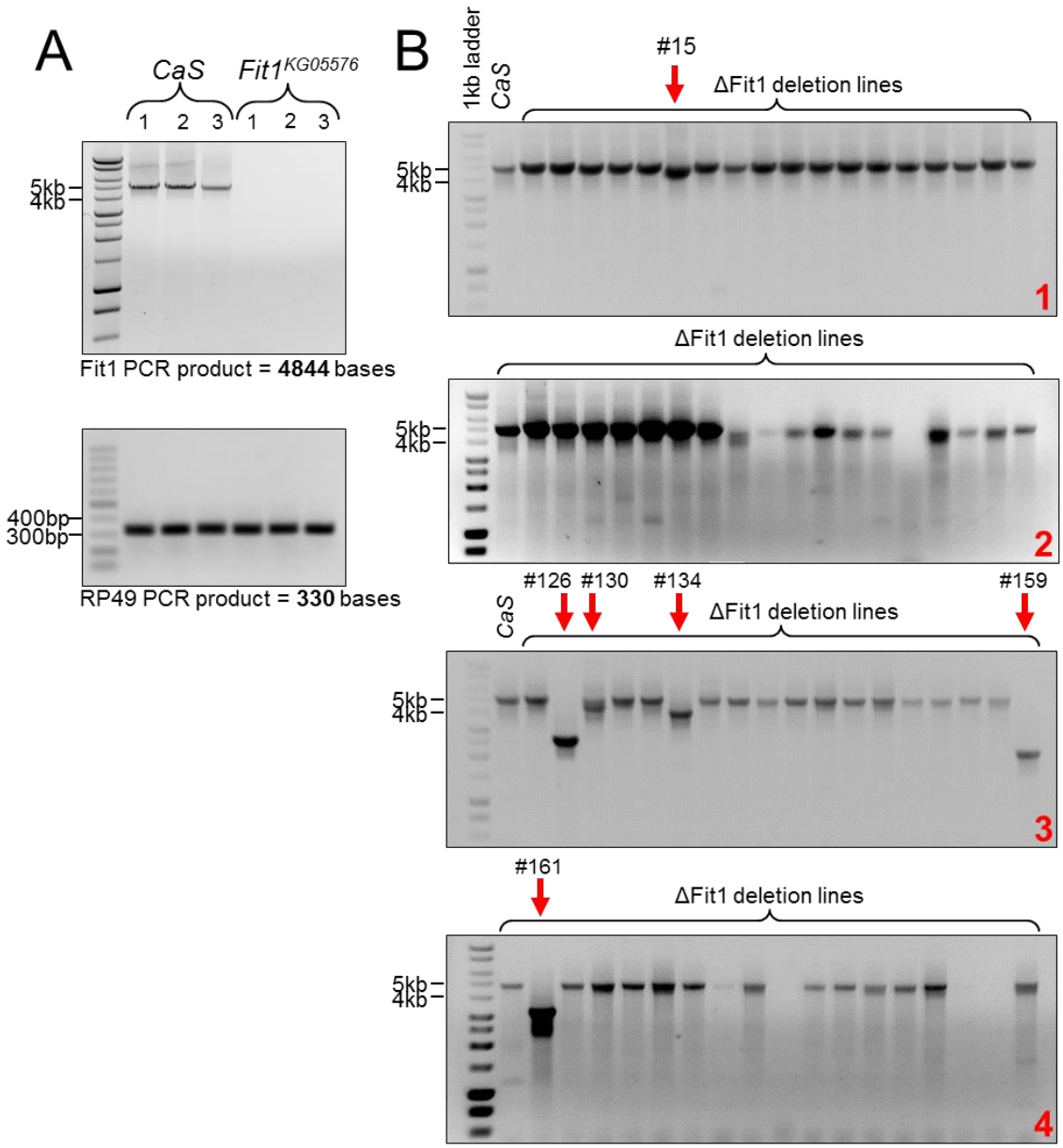

Figure 5.6. Genotyping via PCR of *Fit1* in *CaS* and *ΔFit1* deletion lines using different primers.

A, triplicate samples show wild-type (*CaS*) version of *Fit1* is amplified at expected molecular weight, while *Fit1*^{KG05576} (containing 11.5kb P-element) is not. Elongation time in the PCR reaction (4mins) was enough that the wild-type copy of the gene could be amplified but not enough to cover the gene and P-element. The figure below shows RP49 control. **B**, PCR of *CaS* and 73 *ΔFit1* deletion lines (heterozygous for the deletion over a balancer on the 3rd chromosome) spread over 4 DNA gels. There were 6 noticeable deletions using these primers – lines #15, 126, 130, 134, 159, 161.

noted that during the time between the first PCR screen of ΔFit1 lines and the second screen (Figure 5.6B) a few of the lines perished – either due to being 'sick' or apparently not breeding. In panels 1-4 (Figure 5.6B), it can be seen that in this round of PCRs, most samples displayed a band at the wildtype size, demonstrating that the samples were not compromised in any way. In this screen, the 134 and 161 genomic deletions were confirmed, and further genomic deletions were discovered (including #15, 126, 130 and 159). Unfortunately, lines 126, 134 and 159 perished meaning that was as far as the genetic analysis was explored in these lines. The ΔFit1 161 line – which contained a large, approximately 1.6kb genome deletion - was 'healthy' and was used for subsequent analysis.

The $Fit1^{\Delta 161}$ line was bred to homozygosity and was, again, genotyped to confirm a genetic deletion. A different set of primers were used to confirm the deletion and the w^{1118} line was this time used as a more appropriate background control (Figure 5.7). After sequencing, it was found that $Fit1^{\Delta 161}$ resulted from the imprecise excision of the P-element and created an out-of-frame deletion which removed 1685bp (629bp from 5' UTR region and 1055bp from coding sequence - deletion corresponds to nucleotides 67-1752) and retains a 12bp fragment (CATGATGAAATA) from the start of the 11,467bp KG05576 P-element – this is demonstrated diagrammatically in Figure 5.7C.

Genomic DNA was extracted from a total of 165 potential *Fit2* deletion (Δ) lines and was screened for the presence of a genetic deletion. Similar to ΔFit1 lines, it should be noted that due to the nature of some vials of flies containing very few flies, it was reasoned that heterozygous flies (that carried the potential deletion over a balancer chromosome) could also be included when extracting DNA from

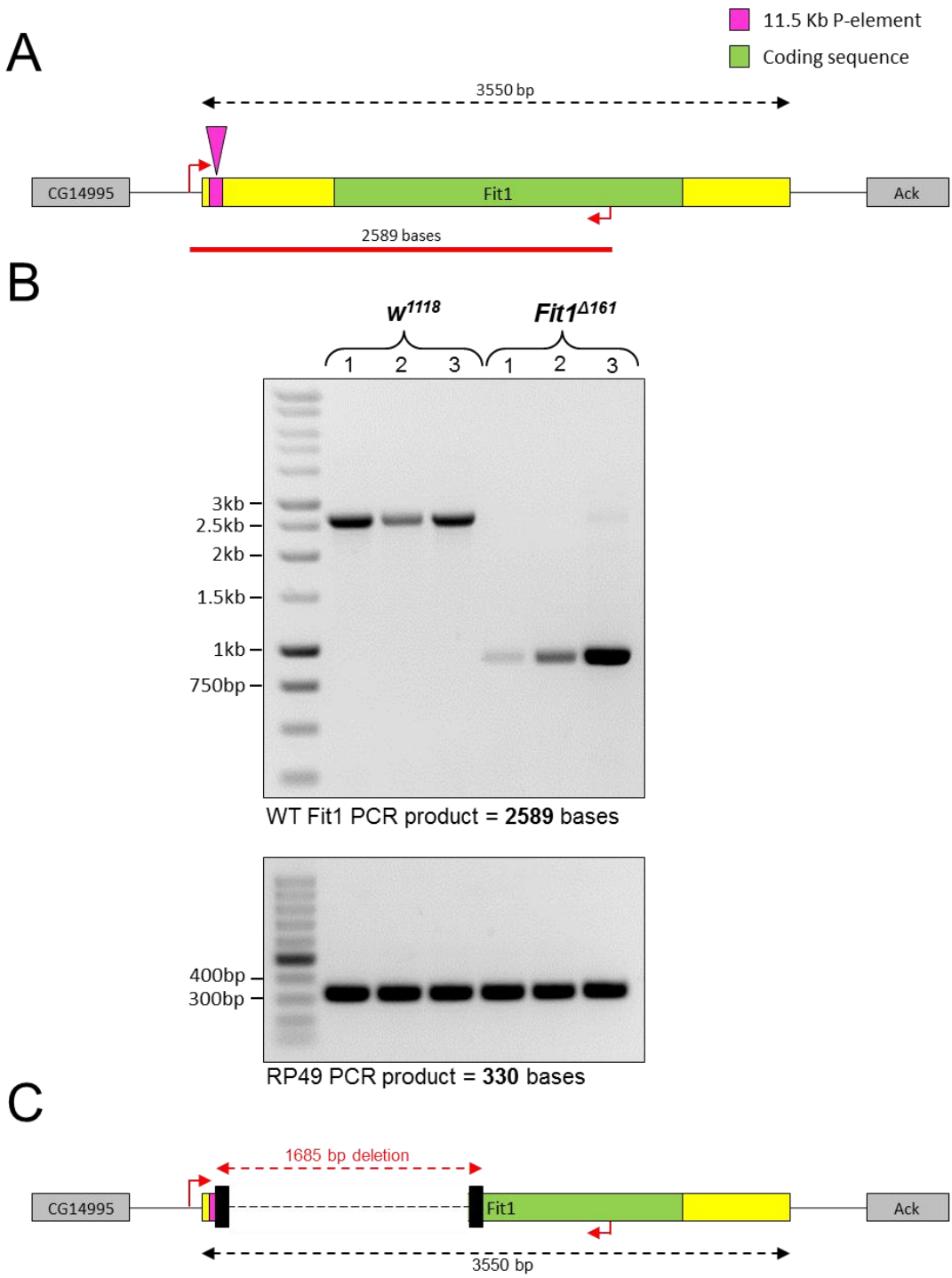

Figure 5.7. PCR of Fit1 and RP49 in *w*^{1118} and *Fit1*$^{\Delta 161}$ flies.
A, schematic showing the location of the respective primers and size of the predicted PCR product. **B**, samples in triplicate show that the wild-type (*w*^{1118}) version of the gene is amplified at the expected molecular weight, while *Fit1*$^{\Delta 161}$ flies show a band at ~900bp – i.e. a ~1.7kb deletion. The figure below shows the RP49 controls. **C**, schematic showing the predicted size and location of the deletion in the Fit1 gene in *Fit1*$^{\Delta 161}$ flies.

each potential deletion line. A deletion was suspected when there was a band on the gel that was smaller than the wildtype band. Using the same primers as used in Figure 5.3B and 5.4B (top panel), PCRs were performed on each potential ΔFit2 line, and samples were run on DNA electrophoresis gels. In both gels shown in Figure 5.8, it can be seen that in this round of PCRs, most samples displayed a band at the wildtype size, with the exception of sample #8 which displayed a second band approximately 500bp higher than the wildtype band – most likely indicating a remnant of the P-element that was imprecisely excised. In this screen for Fit2 deletions, there were no genomic deletions were confirmed. This was as far as the PCR screening process went for the ΔFit2 lines.

In the process of generating a deletion using imprecise excision of a P-element, one can also generate precise excisions – and animals that have had their P-element excised precisely can act as excellent background 'wildtype' controls to the animals which carry a deletion. Possible precise excisions (i.e. homozygous lines that appeared healthy) were screened for both ΔFit1 and ΔFit2 lines, and the results are shown in Figure 5.9B. Most of the homozygous (i.e. non-balanced) ΔFit1 lines appeared to have a band the same size as the w^{1118} controls, indicating that the P-elements in these lines were precisely excised. However, lines #123 and 130 have a slightly lower molecular weight band and no band, respectively – no further experiments were performed with these lines. $Fit1^{\Delta 130}$ flies may have a deletion that covers the forward primer shown in Figure 5.9A, since in Figure 5.6B (third panel) a band (of lower molecular weight than wild-type) is present.

To check for the presence of *Fit1* gene product in $Fit1^{\Delta 161}$ flies, RT-PCR was performed and compared with other ΔFit1 lines – as shown in Figure 5.10. As can be

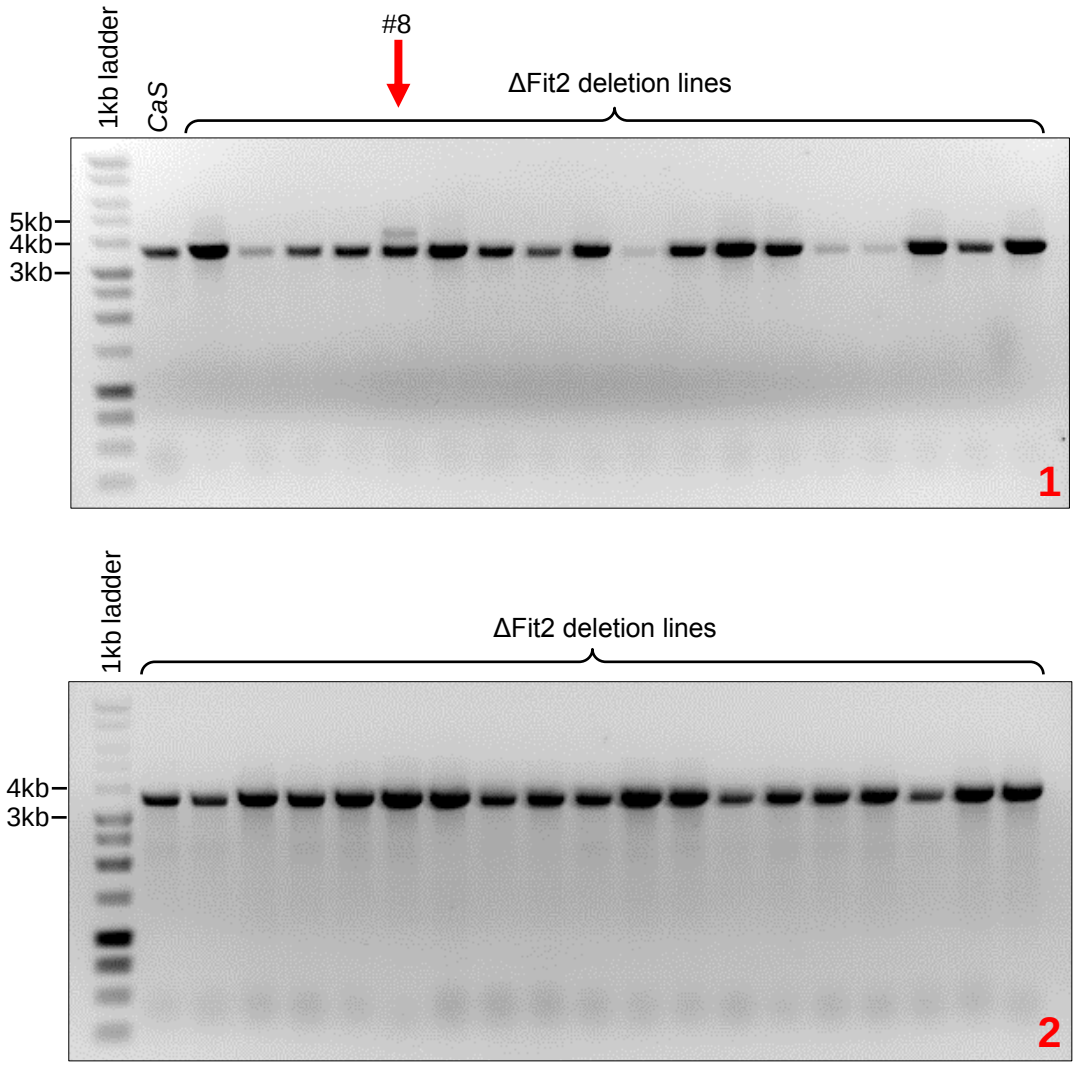

Figure 5.8. Genotyping via PCR of Fit2 in *CaS* and *ΔFit2* deletion lines. PCRs of *CaS* and 37 *ΔFit2* deletion lines (heterozygous for the deletion over a balancer on the 3rd chromosome) spread over 2 DNA gels. There appeared to be no noticeable deletions using these primers – line #8 in gel 1 appears to have a ~500bp remnant of the P-element.

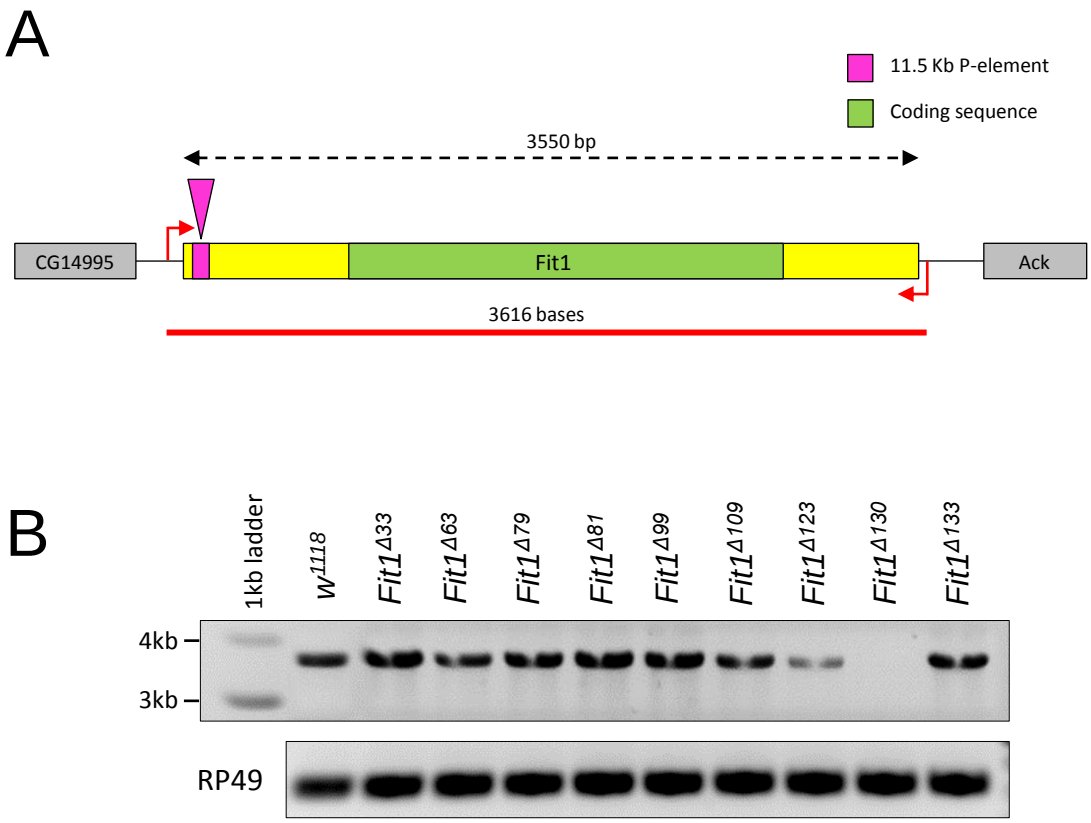

Figure 5.9. Genotyping precise excisions. PCR of Fit1 and RP49 in homozygous *ΔFit1* deletion lines.
A, schematic showing the location of the respective primers and size of the predicted PCR product. **B**, PCR of 9 suspected precise ΔFit1 deletion lines (homozygous). Every sample (except $Fit1^{\Delta 130}$) showed a band around the predicted full-length size. $Fit1^{\Delta 130}$ flies have a deletion that covers the above forward primer, since in Figure 5.6B a band (of lower molecular weight than wild-type) is present in the $Fit1^{\Delta 130}$ line. RP49 controls are shown.

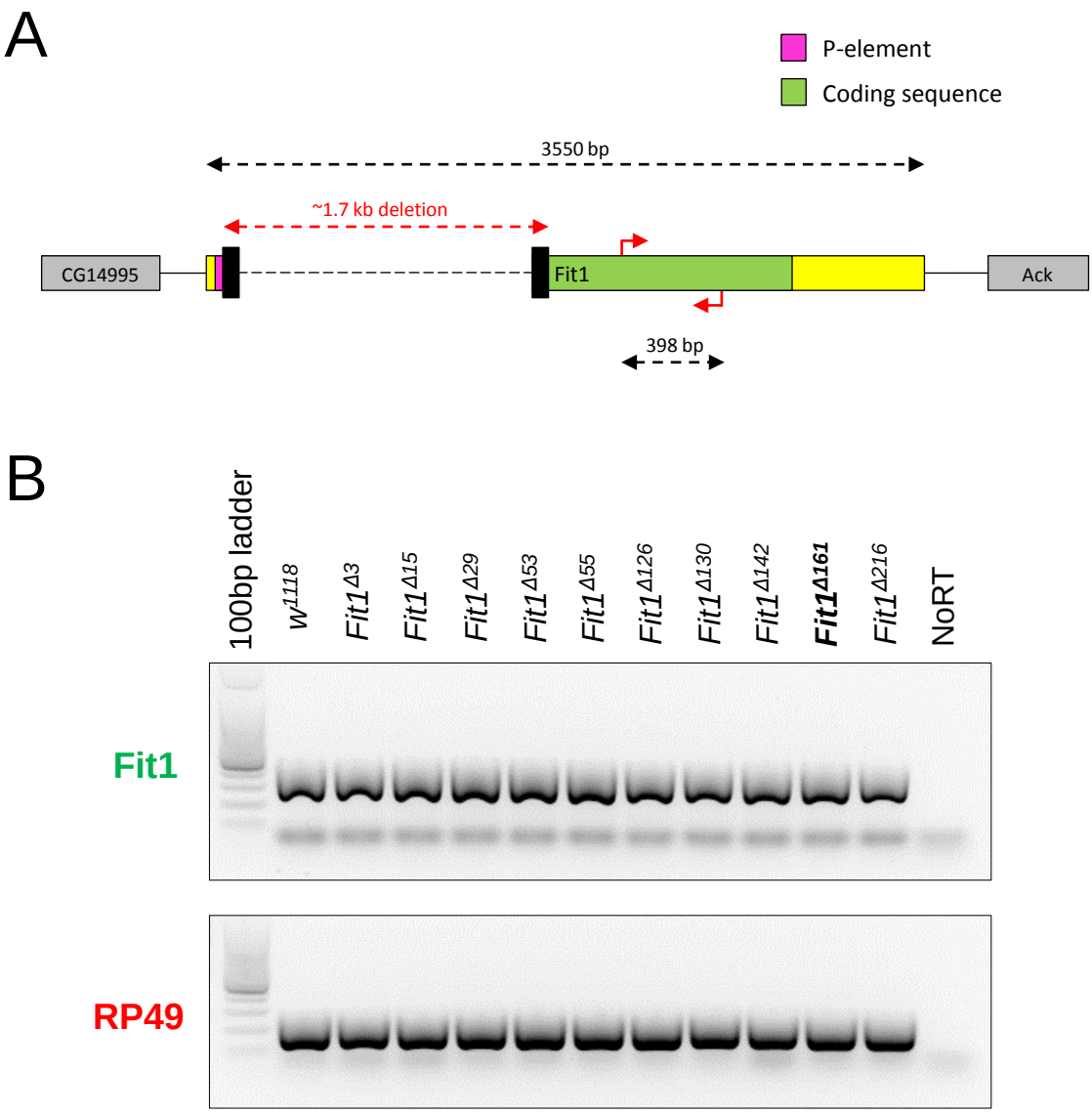

Figure 5.10. RT-PCR of Fit1 and RP49 in w^{1118} and $Fit1^{\Delta}$ flies.
A, schematic of the *Fit1* gene arrangement in $Fit1^{\Delta 161}$ flies showing the location of the respective primers and size of the predicted PCR product. **B**, all of the deletion lines tested, including $Fit1^{\Delta 161}$, show *Fit1* gene expression – *Rp49* gene expression was used as a control. NoRT samples show no band, meaning only cDNA is being amplified.

seen in Figure 5.10B, each ΔFit1 line tested exhibited *Fit1* gene expression to match the w^{1118} controls. Therefore, although $Fit1^{\Delta 161}$ flies have a deletion of ~1.7kb into the beginning of the Fit1 gene, the remainder of the gene is still being expressed, most likely explained by the presence of the transcription start site. Since the $Fit1^{\Delta 161}$ flies were sequenced, it was reasoned that even though *Fit1* message is still being generated (likely due to the 12bp remainder fragment from the excised P-element creating an artificial transcription start site), the deletion it carries is predicted to be out-of-frame and so the translated message would be nonsense. Additionally, even if the message was found to be in-frame, there is a stop codon three amino acids after the 'start' Methionine, and the protein would not be generated. Therefore, it is highly probable that the $Fit1^{\Delta 161}$ line is a 'genetic-null' line and Fit1 protein cannot be synthesised. An attempt was made to sequence this *Fit1* message from $Fit1^{\Delta 161}$ flies, but the experiment was unsuccessful. Similarly, Western blots using an antibody raised against Fit1 were inconclusive.

Since the $Fit1^{\Delta 161}$ deletion appeared to only affect the *Fit1* gene, the genes flanking *Fit1* were also examined to verify that they were still producing mRNA. Shown in Figure 5.11A, *CG14995* and *Ack* appear to be produced in all of the ΔFit1 lines tested. Additionally, *Fit2* and genes flanking *Fit2* (*a10* and *CG7730*) were also examined for their ability to produce mRNA in selected ΔFit2 lines. Shown in Figure 5.11B, each of the ΔFit2 lines tested appeared to produce *a10*, *Fit2*, and *CG7730*.

As the process of genotyping the ΔFit1 lines was carried out, one line, $Fit1^{\Delta 193}$, did not produce unbalanced homozygous flies – i.e. flies were only $Fit1^{\Delta 193}$/*TM3, Ser*^{1}. These flies were then bred onto a GFP balancer (*TM3, Act5C-GFP, Ser*^{1}) that could be used to sort unbalanced homozygous embryos from

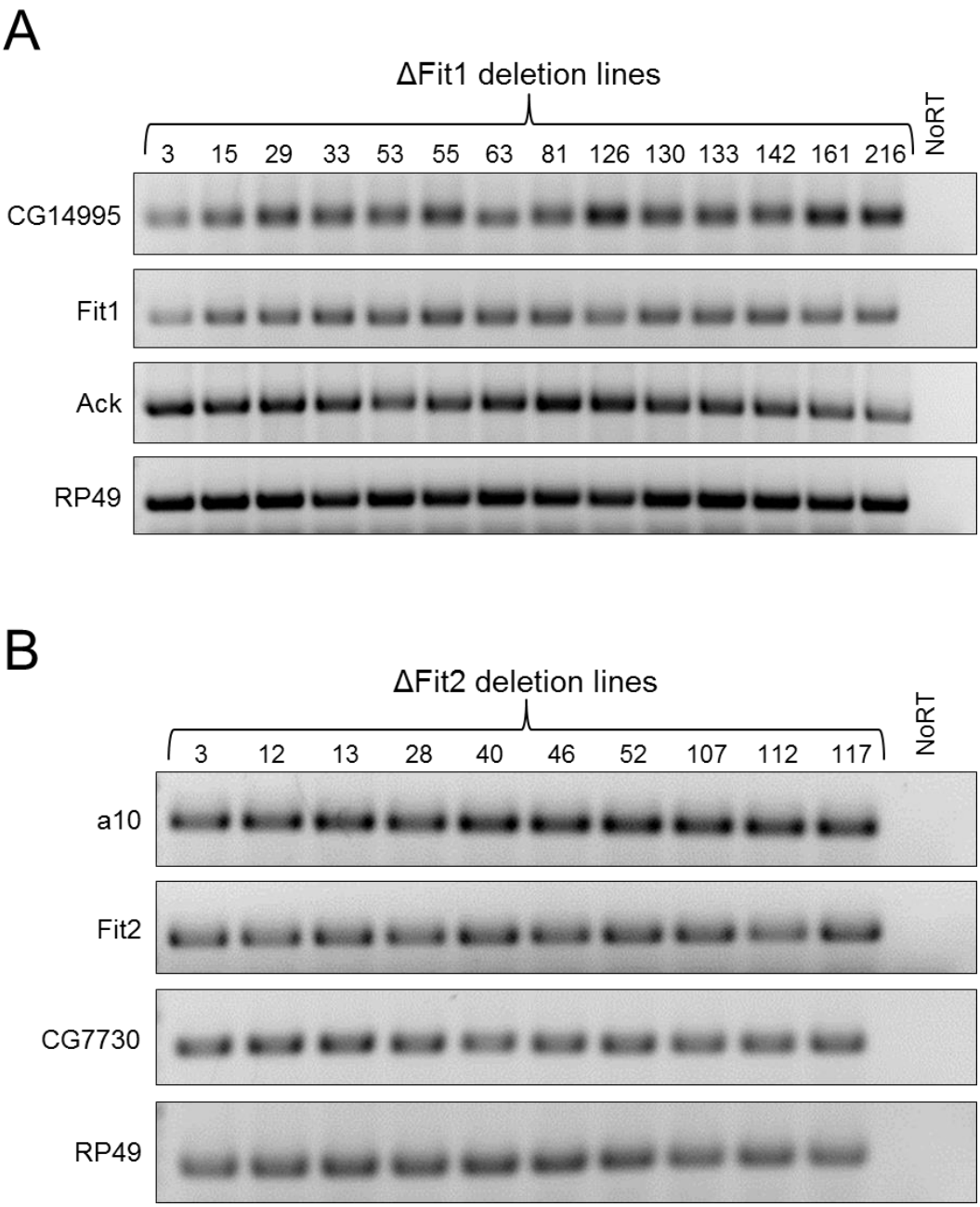

Figure 5.11. RT-PCR of Fit1, Fit2 and flanking genes in remaining *ΔFit1* and *ΔFit2* deletion lines show there are no genetic null mutants.
A, *ΔFit1* deletion lines have mRNA message for CG14995, Fit1 and Ack. **B**, *ΔFit2* deletion lines have mRNA message for a10, Fit2 and CG7730. NoRT samples show no band, meaning only cDNA is being amplified.

heterozygous balanced embryos under UV illumination. Homozygous (i.e. without GFP) *Fit1*$^{\Delta 193}$ embryos were collected for RT-PCR, as well as heterozygous embryos (*Fit1*$^{\Delta 193}$*/TM3, Act5C-GFP, Ser*^{1}) to act as a positive control – and were tested for the presence of *Fit1* and *Fit2* mRNA, shown in Figure 5.12. Compared to heterozygotes, *Fit1*$^{\Delta 193}$ embryos produced no *Fit1* message and can be described as true *Fit1*-null animals. Interestingly, *Fit2* appears to be upregulated in *Fit1*$^{\Delta 193}$ embryos compared to *Fit1*$^{\Delta 193}$*/TM3, GFP, Ser*^{1} embryos, indicating it may be attempting to compensate for the loss of *Fit1*. The experiment was repeated, this time probing for genes that flank *Fit1* in *w*^{1118}, *Fit1*$^{\Delta 193}$, and *Fit1*$^{\Delta 193}$*/TM3, GFP, Ser*^{1} embryos – shown in Figure 5.13A. From Figure 5.13B, it was confirmed that *Fit1*$^{\Delta 193}$ embryos do not generate *Fit1* mRNA, but they also appear to have lower amounts of *CG14989* mRNA compared to controls, while there appears to be no message produced from *CG14990* or *CG14995*. Message is produced from *Ack* (the gene directly downstream of *Fit1*) suggesting *Fit1*$^{\Delta 193}$ embryos carry a deletion spanning from (at least) *CG14989* to *Fit1*, although this was not confirmed.

Therefore, since the *Fit1*$^{\Delta 161}$ deletion line is highly likely to be a *Fit1*-null mutant, and since this deletion only affects *Fit1*, and does not appear to negatively affect the flanking genes (unlike *Fit1*$^{\Delta 193}$ mutants), the *Fit1*$^{\Delta 161}$ line was used in subsequent experiments comparing *Fit1*-null flies with controls.

5.3.2 Phenotyping *Fit1*$^{\Delta 161}$ mutant flies

5.3.2.1 Semi-lethality of *Fit1*$^{\Delta 161}$ mutants at the 1st-2nd instar larval stage

It had been noticed that, although the *Fit1*$^{\Delta 161}$ line was viable, there was a noticeable amount of dead 1st-2nd instar larvae in these vials. To address this issue of

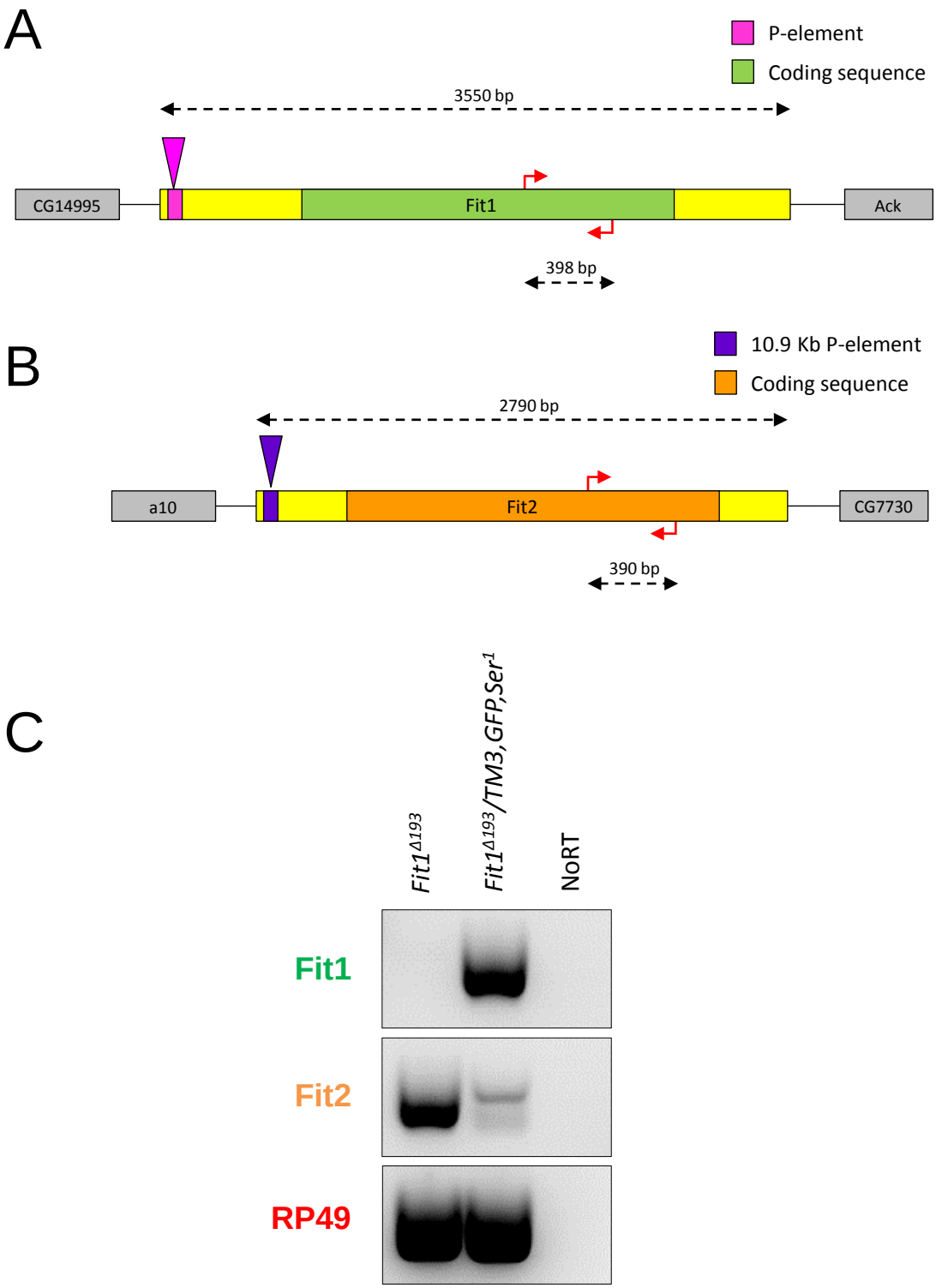

Figure 5.12. RT-PCR of Fit1, Fit2 and RP49 in *Fit1$^{\Delta 193}$* and *Fit1$^{\Delta 193}$/TM3, GFP, Ser^{1}* flies.

A,**B**, schematic showing the location of the respective primers and size of the predicted PCR products for Fit1 and Fit2. **C**, *Fit1$^{\Delta 193}$* embryos have no Fit1 gene expression but show Fit2 and RP49. *Fit1$^{\Delta 193}$/TM3,GFP,Ser^{1}* embryos show Fit1 expression and Fit2 expression but at a lower level. NoRT samples show no band, meaning only cDNA is being amplified.

A

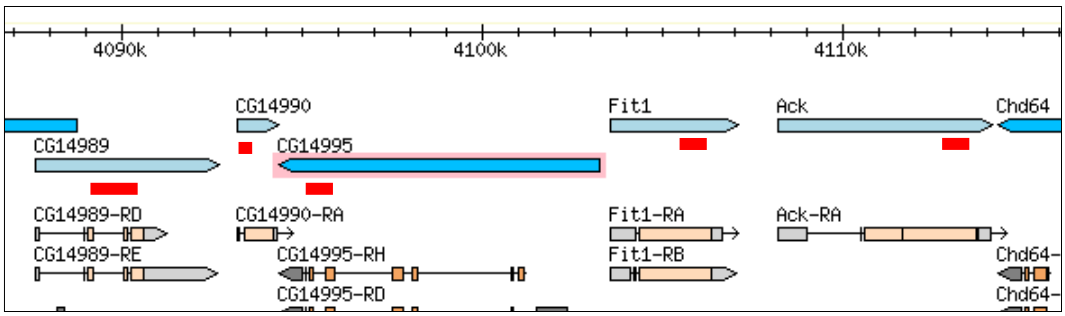

B

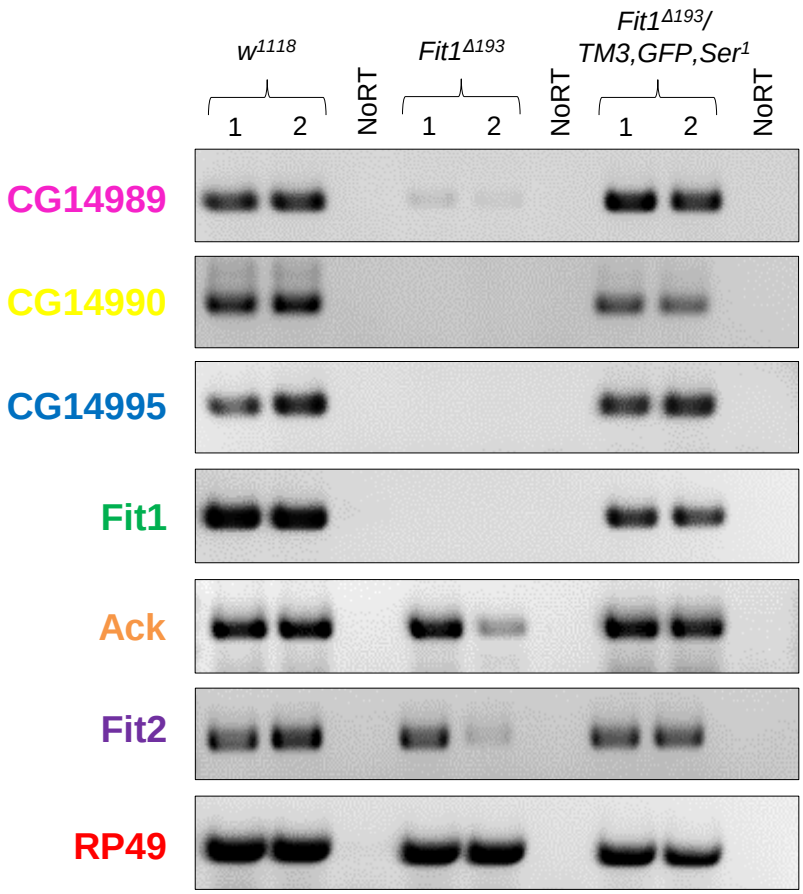

Figure 5.13. RT-PCR of CG14995, Fit1, Ack and RP49 in *w*^{1118}, *Fit1*$^{\Delta 193}$, and *Fit1*$^{\Delta 193}$*/TM3, GFP, Ser*^{1} flies.

A, schematic showing the location of the respective PCR amplicons (red band) for CG14989, CG14990, CG14995, Fit1, and Ack. **B**, *Fit1*$^{\Delta 193}$ embryos show lowered expression of CG14989 and have no CG14990, CG14995 or Fit1 gene expression but show Ack and RP49. Fit2 shows no sign of up regulation *Fit1*$^{\Delta 193}$ embryos compared to controls. NoRT samples show no band, meaning only cDNA is being amplified.

possible semi-lethality, it was determined that the best way to study this phenotype was to follow the fly population size throughout development. Flies (w^{1118} and $Fit1^{\Delta 161}$) were left to lay eggs in egg cages and the number of embryos were counted after 4 hours. Fertilised eggs normally hatch after around 24 hours (at 25°C), so the eggs were left for 30 hours before counting the number of eggs that remained unhatched – this value was then subtracted from the total number of eggs laid to get the number of fertilised eggs (i.e. hatched larvae). It is possible that any eggs, from $Fit1^{\Delta 161}$ flies, remaining unhatched after this period of time may have still been developing due to the effect of the mutation, but since there was no difference in the number of unhatched eggs between $Fit1^{\Delta 161}$ and w^{1118} controls, the unhatched eggs are most likely unfertilised eggs. Since it would be extremely difficult to try to count the number of larvae (especially when there are hundreds writhing about/on top of each other), the number of pupae were counted – with the reasoning that every hatched larva should grow and develop into a pupa. It was at this point that the semi-lethal phenotype of the $Fit1^{\Delta 161}$ mutation revealed itself, with more than 50% of $Fit1^{\Delta 161}$ larvae perishing during the larval stages compared to w^{1118} controls – shown in Figure 5.14A+B. The number of $Fit1^{\Delta 161}$ adults that eclosed from their pupae was not different compared to w^{1118} controls. Further in-depth analysis of the precise instar stage at which these $Fit1^{\Delta 161}$ mutants are dying, was not performed but it was observed that there were no brown/black 3rd instar larvae, which would indicate lethality at this stage. Therefore, it is likely that the semi-lethality of $Fit1^{\Delta 161}$ mutants is occurring at the 1st-2nd instar stage.

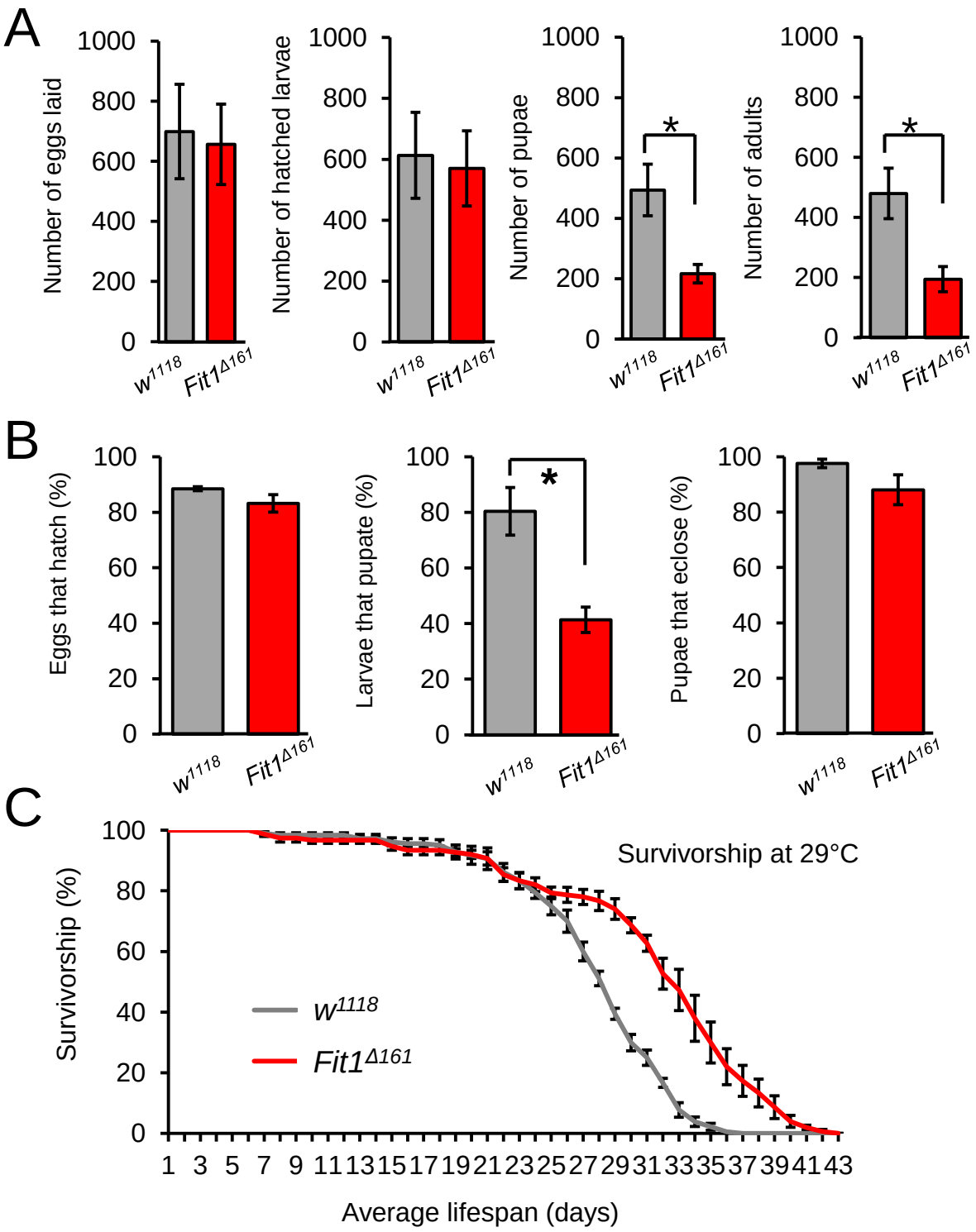

Figure 5.14. The *Fit1$^{\Delta 161}$* mutation is semi-lethal during the larval stage, yet survivors live longer than *w^{1118}* controls.
A, *w^{1118}* and *Fit1$^{\Delta 161}$* flies were allowed to lay in egg cages for 4 hours and number of eggs were counted. Subsequently, number of hatched larvae, pupae, and adults were counted. The experiment was replicated 3 times, and means ± SEM were calculated. **B**, using data from A, percentages were calculated to show that the number of eggs that hatched, and the number of pupae that eclosed were similar to wildtype, whereas during the larval stage, approx. 50% of *Fit1$^{\Delta 161}$* larvae perished. C, the *Fit1$^{\Delta 161}$* animals that survived to adulthood showed an unexpected extension of lifespan compared to *w^{1118}* controls. Animals were kept on standard medium at 29°C and tipped onto fresh food twice a week. *p<0.05

5.3.2.2 Lifespan extension in *Fit1*$^{\Delta 161}$ mutant survivors

Since there was a semi-lethal phenotype in *Fit1*$^{\Delta 161}$ mutants during the early-mid larval stages, we decided to assess whether there were detrimental effects to the lifespan of the 'escapers' – i.e. the *Fit1*$^{\Delta 161}$ mutants that managed to survive to adulthood. For all intents and purposes, *Fit1*$^{\Delta 161}$ adults resembled that of their *w*^{1118} control counterparts, with no apparent difference in size/shape/behaviour. The lifespan of *Fit1*$^{\Delta 161}$ survivors was then measured by placing flies in vials (20 females and 10 males per vial, with 6 vials for *w*^{1118} and 5 vials for *Fit1*$^{\Delta 161}$ = 180 and 150 flies in total, respectively) at 29°C on standard medium, with tipping twice a week. The results of this lifespan study, displayed in Figure 5.14C, show that up to around the 25 day mark, *Fit1*$^{\Delta 161}$ survivors have the same death rate as *w*^{1118} controls. After the 25th day, however, the death rates begin to diverge, and result in the *Fit1*$^{\Delta 161}$ survivors living almost a week longer than their *w*^{1118} counterparts (43 days versus 37 days, respectively).

Developmental lethality and lifespan measurement was the extent of the phenotypic analysis of these *Fit1*$^{\Delta 161}$ mutants. All subsequent phenotypic analysis of *Fit1*$^{\Delta 161}$ mutants was concerned with the effects of the mutation on heart function physiology, and morphology in the adult survivors.

5.3.2.3 Normal heart morphology and function in *Fit1*$^{\Delta 161}$ mutant survivors

Since knockdown of *Fit1* in the *Drosophila* heart appeared to show different phenotypes depending on which RNAi line was used (VDRC elicited a severe cell-dissociation phenotype, while TRiP phenotype was mainly indistinguishable from wildtype), the hearts of *Fit1*$^{\Delta 161}$ mutant adults were stained with Alexa-conjugated

phalloidin to establish any effect of the null mutation on heart morphology. As shown in Figure 5.15, morphology of the hearts of $Fit1^{\Delta 161}$ adults appeared indistinguishable from w^{1118} control hearts. $Fit1^{KG05576}$ and $Fit2^{EY08530}$ hearts were also phalloidin-stained, and these hearts were also no different from wildtype controls.

Since the $Fit1^{\Delta 161}$ adult hearts appeared morphologically similar, this did not rule out potential deleterious effects of the mutation on adult heart function. Thus, the heart function of these adult flies was subsequently assessed. As shown in Figure 5.16, heart function in $Fit1^{\Delta 161}$ flies was identical to w^{1118} controls in each functional parameter measured (i.e. heart rate, fractional shortening, arrhythmicity index etc. were all identical).

5.3.2.4 $Fit1^{VDRC}$ RNAi has off-target effect by depleting *Fit2* mRNA as well as *Fit1*

The fact that the hearts of $Fit1^{\Delta 161}$ adults appeared morphologically indistinguishable and functionally identical to controls, appeared to suggest that the severe cardiomyocyte-dissociation phenotype seen in hearts from VDRC *Fit1*-knockdown flies was not due to the depletion of *Fit1*. A possible explanation for this discrepancy was that the *Fit1* VDRC line was having off-target effects and the RNAi was possibly affecting another gene's function. To address this, the $Fit1^{VDRC}$ RNAi sequence was entered into a program designed to predict off-target effects of RNAi (http://www.flyrnai.org/RNAi_find_frag_free.html). It was found that $Fit1^{VDRC}$ RNAi can also target *Fit2* mRNA and recognises a 27bp sequence of *Fit2* mRNA – shown in Figure 5.17A. To test this hypothesis, RT-PCRs were performed on hearts

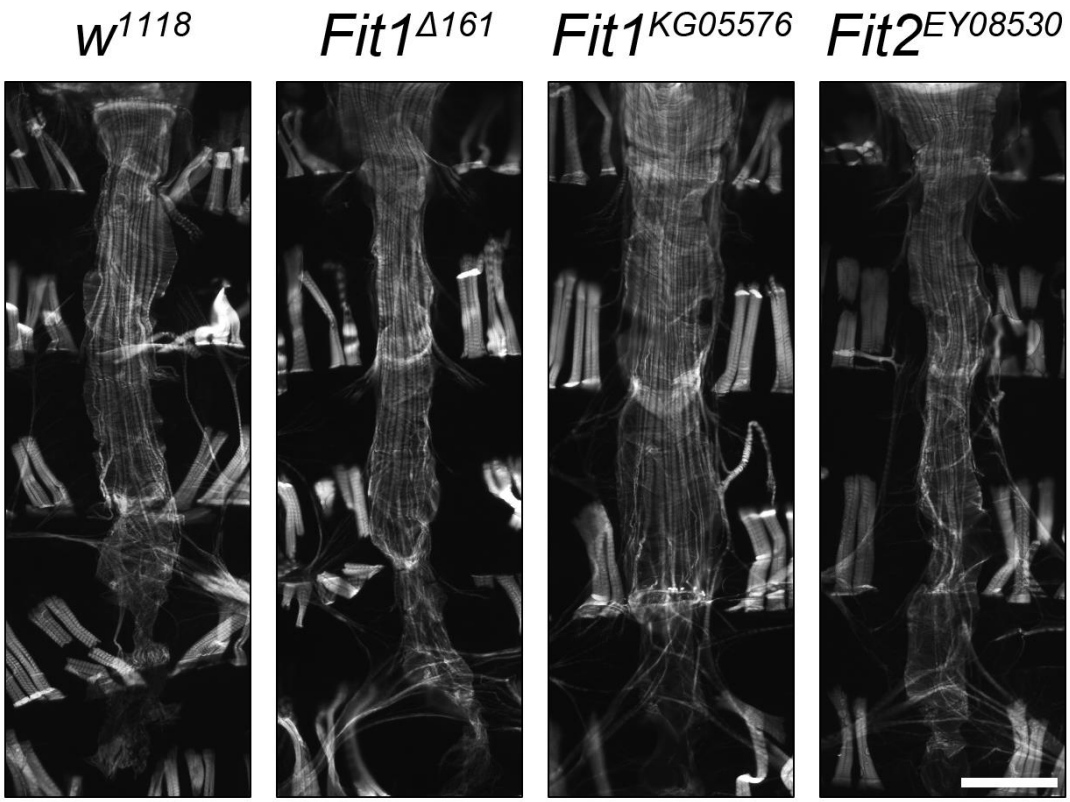

Figure 5.15. The hearts of *Fit1$^{\Delta 161}$* adults appear morphologically similar to *w^{1118}* controls.
Adult hearts were stained with Alexa-conjugated phalloidin to reveal the cardiac muscle structure. Overlying the heart proper is a layer of striated muscle called the ventral longitudinal muscle. Underneath, the heart exhibits a spiralling myofibrillar architecture. The hearts of *w^{1118}*, *Fit1$^{\Delta 161}$*, *Fit1^{KG05576}*, and *Fit2^{EY08530}* flies were virtually identical with no gross abnormalities. Scale bar = 100µm.

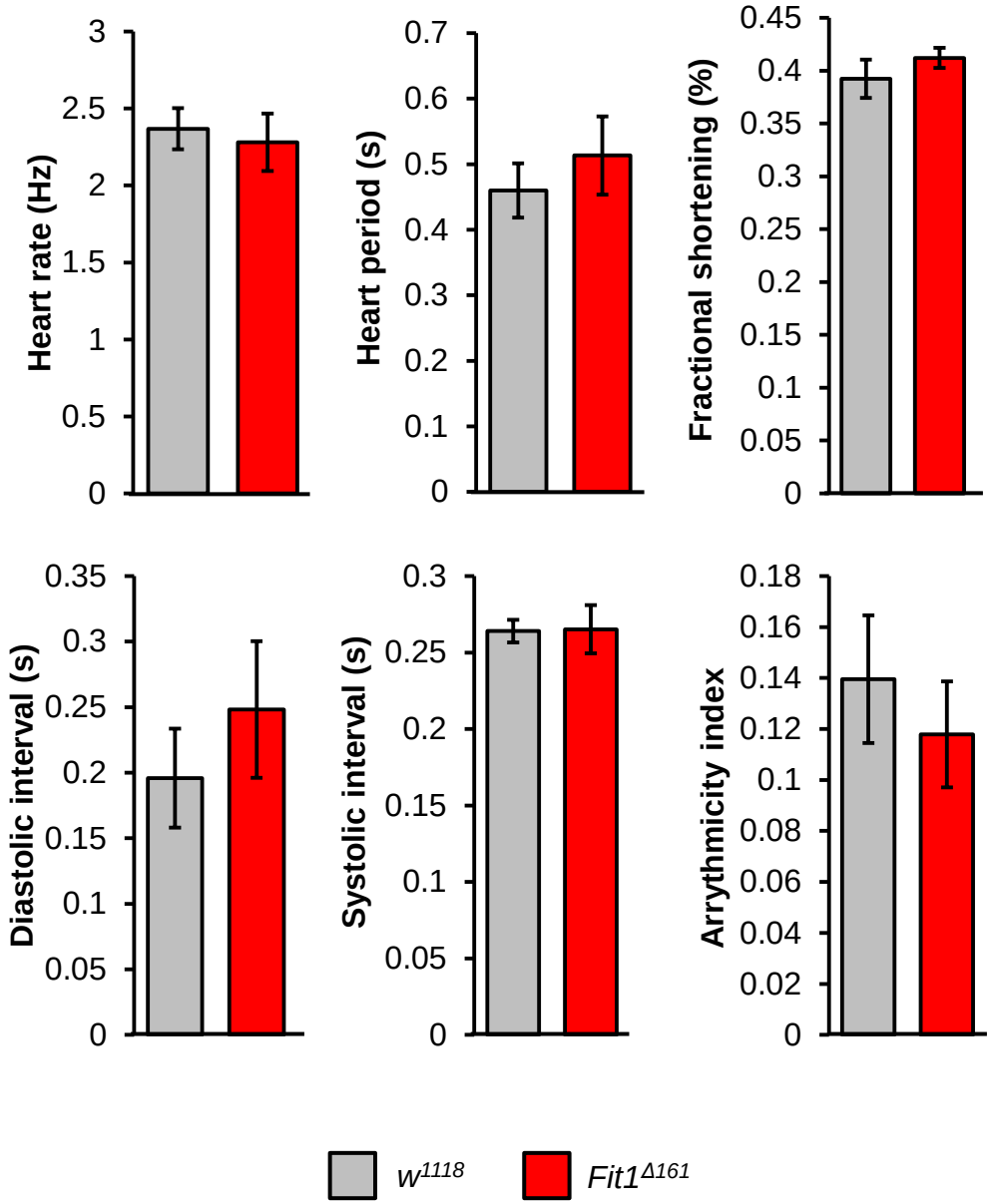

Figure 5.16. The *Fit1$^{\Delta 161}$* mutation has no effect on adult heart function.

w^{1118} and *Fit1$^{\Delta 161}$* flies were dissected a week after eclosion and their heart function was analysed using videomicroscopy and analysis of these videos using a MatLab-based heart analysis program. Heart function in *Fit1$^{\Delta 161}$* flies was identical to *w^{1118}* controls for all parameters measured. Error bars represent SEM, *n* = 13-15 flies per genotype.

A

Sequences indicating Predicted Off-Targets

Sequence: unknown

The following are potential primary targets:

Fit1: covers 351 bp out of 351 bp

There is 1 potential secondary target.

It is:

27 bp Fit2

The following is a color-coded map to indicate where targets lie: Black indicates target-free regions. Blue indicates primary target regions. Red indicates secondary target (Off-Target) regions or regions that are both secondary and primary target.

GTCCGATCACGCCCTGTGGTGGCCCGCCAAGAATATCTGGCTGACCAGGACGCGGTCCACTTTGGACCAGGCCGGAGTTC
AATCGGATTCCTTTCTGCACTTCACGCCCATGCACAAGACACTGAGGGTGCAGATGCCCGATCTTCGTTATCTGGACTAC
CGCGTCAACTTTTCGGCCAAAACTTTCGGAGCCGTTGTGAGCTTGTGCAAGGACCTGGACATTCGCTATCCGGAGGAACT
GTCTTTCTGCAAGCCCCTGGAACCGGAGCATCTGAAGAAGAACTTCTCCAAGCTGCCGCAGCGAAAGATTCCGGTGGCGG
AGGCAAATGGAATCGCATACGTGCAGCCAGC

Click here for sequence text for cutting and pasting or saving

```
>unknown region 1
GTCCGATCACGCCCTGTGGTGGCCCGCCAAGAATATCTGGCTGACCAGGACGCGGTCCACTTTGGACCAGGCCGGAGTTC
AATCGGATTCCT
>unknown region 2
CACTGAGGGTGCAGATGCCCGATCTTCGTTATCTGGACTACCGCGTCAACTTTTCGGCCAAAACTTTCGGAGCCGTTGTG
AGCTTGTGCAAGGACCTGGACATTCGCTATCCGGAGGAACTGTCTTTCTGCAAGCCCCTGGAACCGGAGCATCTGAAGAA
GAACTTCTCCAAGCTGCCGCAGCGAAAGATTCCGGTGGCGGAGGCAAATGGAATCGCATACGTGCAGCCAGC
```

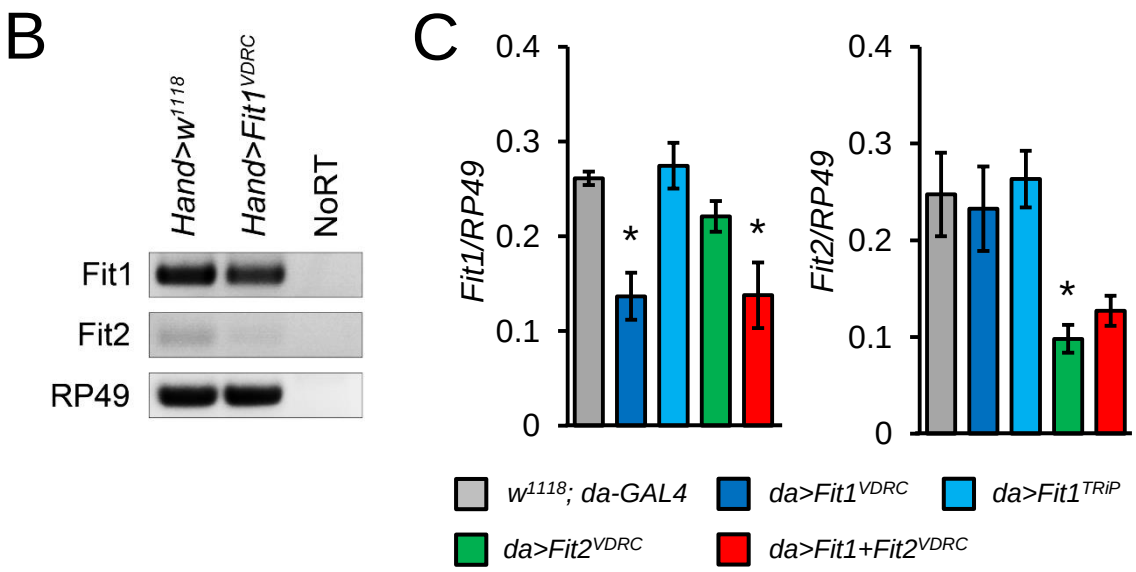

Figure 5.17. The Fit1^{VDRC} RNAi targets both *Fit1* and *Fit2* gene expression in the *Drosophila* heart.

A, the *Fit1^{VDRC}* RNAi (construct ID 17050) was predicted to affect *Fit2* gene expression as well as *Fit1*. Off-target prediction was performed using the 'Find OTEs' program on the DRSC website (http://www.flyrnai.org/RNAi_find_frag_free.html). **B**, micrographs show *Fit1* and *Fit2* gene expression data from adult *Drosophila* heart tissue. Expression of both *Fit1* and *Fit2* was detected in cDNAs prepared from *Hand>w^{1118}* hearts (though *Fit2* expression was difficult to detect in the heart), whereas *Fit1* and *Fit2* were both affected in *Hand>Fit1^{VDRC}* flies. The housekeeping gene *RP49* was used as a positive control. NoRT – No Reverse transcriptase. **C**, qPCR was performed on embryos over-expressing RNAi via the ubiquitous *daughterless*-GAL4 driver. *Fit1* was significantly reduced in *da>Fit1^{VDRC}* and *da>Fit1+Fit2^{VDRC}* embryos, while *Fit2* was significantly reduced in *da>Fit2^{VDRC}* embryos. Results are mean ± SEM, *p<0.05. *RP49* was used as a control.

extracted from *Hand>w*^{1118} and *Hand>Fit1*^{VDRC} adult flies, with the aim of amplifying *Fit1* and *Fit2* to assess if both were being targeted by Fit1^{VDRC} RNAi. As shown in Figure 5.17B, *Fit1* and *Fit2* appear to be downregulated in *Hand>Fit1*^{VDRC} hearts compared to *Hand>w*^{1118} controls. Therefore, it would suggest that knockdown of *Fit1* function alone does not have any noticeable effect on heart morphology, and only with the depletion of both *Fit1* and *Fit2* can a heart phenotype be exhibited – in other words, *Fit2* may be compensating for the loss of *Fit1*.

To further assess the ability of the *Fit1*^{VDRC} line to deplete *Fit2* mRNA levels, the ubiquitously expressed *daughterless* GAL4 driver (*da-GAL4*) was used to drive expression of the *Fit1*^{VDRC}, *Fit1*^{TRiP}, *Fit2*^{VDRC}, and *Fit1+2*^{VDRC} RNAi lines in embryos. qPCR was then performed to assess the effects on *Fit1* and *Fit2* mRNA levels - the results are shown in Figure 5.17C. *Fit1* was significantly reduced (~50%) in both *da>Fit1*^{VDRC} and *da>Fit1+2*^{VDRC} embryos, while there was no significant effect on *Fit1* levels in *da>Fit1*^{TRiP} or *da>Fit2*^{VDRC} embryos. *Fit2* was significantly reduced (~60%) in *da>Fit2*^{VDRC} embryos, while *Fit2* was similarly reduced in *da>Fit1+2*^{VDRC} embryos but this did not reach significance. There was no significant effect on *Fit2* levels in *da>Fit1*^{VDRC} or *da>Fit1*^{TRiP} embryos.

5.3.3 Generating and phenotyping *Fit1*$^{\Delta 161}$ *Fit2*^{EY08530} and *Fit1*$^{\Delta 161}$ *UAS-Fit2*^{VDRC} mutant flies

5.3.3.1 Generating *Fit1*$^{\Delta 161}$ *Fit2*^{EY08530} and *Fit1*$^{\Delta 161}$ *UAS-Fit2*^{VDRC} mutant flies

To test the hypothesis that *Fit2* is compensating for the loss of *Fit1* in both *Fit1*$^{\Delta 161}$ and Fit1^{VDRC}-knockdown flies, flies carrying mutations in both *Fit1* and *Fit2* (*Fit1*$^{\Delta 161}$ *Fit2*^{EY08530}), and flies carrying a mutation in *Fit1* and a Fit2 RNAi transgene

(*Fit1*$^{\Delta 161}$ *UAS-Fit2*^{VDRC}), were generated – the crossing scheme, and primer positions used for the positive identification of lines containing the *Fit1*$^{\Delta 161}$ mutation in both lines is shown in Figure 5.18A+B.

Since *Fit1*$^{\Delta 161}$, *Fit2*^{EY08530}, and *UAS-Fit2*^{VDRC} are all on the 3rd chromosome, these mutations/insertions had to be recombined onto the same chromosome via homologous recombination. Briefly, virgin females carrying the *Fit1*$^{\Delta 161}$ deletion over a balancer (in this case *Sb*^{1}) were crossed to males carrying the *Fit2*^{EY08530} P-element insertion over the same balancer (in a parallel mating scheme, these virgins were crossed to males carrying the *UAS-Fit2*^{VDRC} P-element insertion over *Sb*^{1}). Unbalanced virgin female progeny from this mating were crossed to balanced males (i.e. *Sb*^{1}*/TM3, GFP, Ser*^{1}), and the non-white eyed male progeny from this mating were collected and mated individually with balanced virgins (i.e. *Sb*^{1}*/TM3, GFP, Ser*^{1}). This resulted in vials containing flies that may or may not have contained the *Fit1*$^{\Delta 161}$ deletion, but did contain the *Fit2*^{EY08530} P-element insertion (or the *UAS-Fit2*^{VDRC} P-element insertion) due to the flies having non-white eye colour (i.e. due to the presence of the mini-white marker in the P-element). Genetic linkage rules state that the further away genes are on a chromosome, then the higher the likelihood of a crossover event. *Fit1*$^{\Delta 161}$ and *Fit2*^{EY08530} are far from each other on the 3rd chromosome (3L:4103564..4107116 and 3L:17017428..17020217, respectively), while there is no information on the precise location of the *UAS-Fit2*^{VDRC} insertion. Therefore the likelihood that there would be a crossover event between *Fit1*$^{\Delta 161}$ and *Fit2*^{EY08530}, was relatively high and so fewer vials (in this case 10) would need to be set up to screen for recombination events, and since the genetic location of the *UAS-Fit2*^{VDRC} insertion was unknown, more vials were used (in this case 15). The progeny

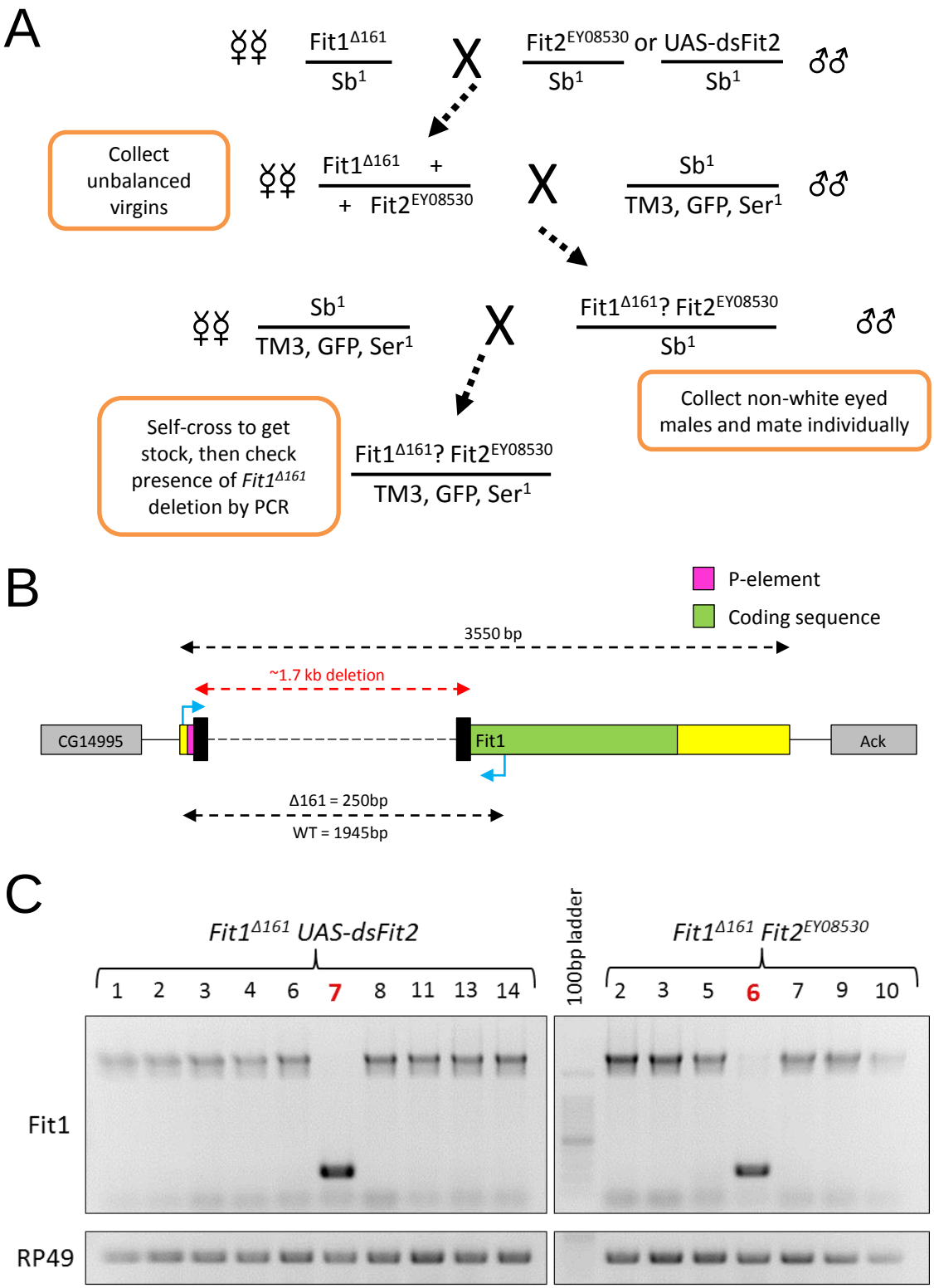

Figure 5.18. Generation of *Fit1$^{\Delta161}$*, *UAS-dsFit2* and *Fit1$^{\Delta161}$*, *Fit2^{EY08530}* flies.

A, crossing scheme to achieve desired fly stocks. Non-white eyed males were selected due to the presence of the mini-white marker P-element indicating the presence of either *UAS-dsFit2* or *Fit2^{EY08350}*. **B**, schematic showing the location of the Fit1 primers (blue arrows) and size of the predicted PCR products for *Fit1$^{\Delta161}$* and wildtype. **C**, PCR using the Δ161 primers show that only one fly line in each genotype (highlighted in red) have the *Fit1$^{\Delta161}$* deletion. RP49 was used as a control.

from these crosses were then screened for the presence of the *Fit1*$^{\Delta 161}$ deletion by PCR – the results are shown in Figure 5.18C. It should be noted that a few of the lines perished before they could be screened – thus 10 out of 15 *UAS-Fit2*^{VDRC} lines, and 7 out of 10 *Fit2*^{EY08530} lines were screened for the presence of *Fit1*$^{\Delta 161}$. From these, a single line for each desired genotype (i.e. *Fit1*$^{\Delta 161}$ *Fit2*^{EY08530} (Line #7) and *Fit1*$^{\Delta 161}$ *UAS-Fit2*^{VDRC} (Line #6)) was achieved.

5.3.3.2 Phenotyping *Fit1*$^{\Delta 161}$ *Fit2*^{EY08530} and *Fit1*$^{\Delta 161}$ *UAS-Fit2*^{VDRC} mutant flies

5.3.3.2.1 The *Fit1*$^{\Delta 161}$ *Fit2*^{EY08530} double mutant line is embryonic lethal

The *Fit1*$^{\Delta 161}$ *Fit2*^{EY08530} double mutants did not breed to homozygosity, and homozygotes did not progress past the late embryonic stage, indicating that both *Fit1* and *Fit2* are required for viability in *Drosophila*. When viewed under the sorting UV microscope, dechorionated *Fit1*$^{\Delta 161}$ *Fit2*^{EY08530} homozygotes appeared fully developed and some could be seen slowly writhing inside their vitelline membrane cases. Mutant embryos also appeared to have punctate lesions in and around the gut area that heterozygous embryos lacked, possibly indicating sites of apoptosis. It was hypothesised that loss of both *Fit1* and *Fit2* would result in a phenotype similar to *myospheroid* (βPS-integrin) mutant embryos (BAI *et al.* 2008) – i.e. severely rounded-up body wall musculature – and it was this adverse effect on the late-stage embryo that resulted in the embryo being unable to escape its egg-case. Several attempts were made to image these embryos, with the aim of staining the body wall musculature to assess any damage and compare to heterozygote controls, but each was unsuccessful.

5.3.3.2.2 A targeted second-site non-complementation mini-screen, crossing *ΔFit* mutants to amorphic 'cell-adhesion' mutants, revealed that these transheterozygotes could fully complement one another

The embryonic lethality of the double $Fit1^{\Delta 161}$ $Fit2^{EY08530}$ mutants indicated the importance of these genes for viability, and mimicked the embryonic lethality seen in other *Drosophila* cell adhesion mutants – e.g. *mys*, *rhea*, *if*, *ilk* (BULGAKOVA *et al.* 2012). In an effort to determine if the Fermitins were genetically linked to the other essential cell adhesion proteins in the fly, a second-site non-complementation (SSNC) test was performed. The SSNC test assesses the ability of transheterozygote mutations - i.e. mutations which lie in different genes, to complement each other (HAWLEY and GILLILAND 2006). For example, if flies carrying a null *mys* mutation were crossed to flies carrying a null *rhea* mutation this would result in flies heterozygous for each mutation (i.e. transheterozygotes - *mys*/+ *rhea*/+). If the mutations in *trans* resulted in a reduction in viability it could be said that these mutations failed to complement one another, and that a genetic interaction was present. Therefore, a targeted 'cell adhesion' SSNC test was performed using newly generated *ΔFit* mutants (including $Fit1^{\Delta 161}$, $Fit1^{\Delta 193}$, and $Fit1^{\Delta 161}$ $Fit2^{EY08530}$ mutants) as well as existing *Fit* P-element lines and a predicted 'precise excision' revertant (i.e. $Fit1^{KG05576}$, $Fit2^{EY08530}$, and $Fit1^{\Delta 81}$). The 'cell adhesion' lines included null alleles of integrins and related binding partners/interactors (including *mys* (βPS-integrin), *mew* (αPS1-integrin), *if* (αPS2-integrin), *rhea* (Talin), *ilk* (ILK), and *stck* (PINCH)), as well as null alleles of cadherin binding partners (including *arm* (β-catenin), and *pan* (TCF)). The relevant flies were crossed and the resultant progeny were sorted according to their genotype and counted, with observed/expected

calculations performed. The results are shown in Table 5.1, with full results of the mini-screen, including absolute numbers, in the Appendix.

The results from this targeted 'cell adhesion' SSNC mini-screen showed that there was no effect on viability in any of the transheterozygotes tested. In fact, many of the potentially deleterious transheterozygotes from each cross, made up a higher proportion of the progeny than their 'single mutation/balancer' counterparts (see Appendix). Therefore, each *Fit* mutant line managed to fully complement each 'cell adhesion' mutant – in other words, there appeared to be no genetic interaction.

5.3.3.2.3 Driving *UAS-Fit2^{VDRC}* RNAi in the hearts of *Fit1$^{\Delta 161}$* homozygous flies causes a cardiomyocyte-dissociation phenotype and adversely affects fractional shortening and cardiac synchrony

To test the hypothesis that *Fit2* was compensating for the loss of *Fit1* in the hearts of *Fit1$^{\Delta 161}$* flies, *Hand-GAL4; Fit1$^{\Delta 161}$ UAS-Fit2^{VDRC}* flies were generated through standard crosses. *Fit2* was depleted via *Hand*-driven RNAi in the hearts of these *Fit1*-null flies. The hearts of week-old *Hand-GAL4; Fit1$^{\Delta 161}$ UAS-Fit2^{VDRC}* mutant adults were stained with Alexa-conjugated phalloidin to establish any effect of *Fit2* RNAi knockdown on heart morphology. As shown in Figure 5.19A, morphology of the hearts of *Hand-GAL4; Fit1$^{\Delta 161}$ UAS-Fit2^{VDRC}* adults was severely affected compared to *Fit1$^{\Delta 161}$ UAS-Fit2^{VDRC}* control hearts – i.e. without *Hand*-driven GAL4 expression. The hearts of these flies displayed a similar cardiomyocyte-dissociation phenotype to the hearts of *Hand*-driven double *Fit1/Fit2* RNAi knockdown flies (as shown in Figure 4.7). This dissociation phenotype was quantified and the results are shown in Figure 5.19B. The distance between

	Second-site non-complementation screen	Observed/Expected Trans-Het*100							
		***mys*^{1}**	***mew*^{M6}**	***if*^{B2}**	***rhea*^{1}**	***Ilk*^{1}**	***stck*$^{3R-17}$**	***arm*^{4}**	***pan*^{2}**
1	***w*^{1118}**	81.99	158.49	141.98	111.76	107.67	137.76	151.54	113.18
2	***Fit1*^{KG05576}**	122.29	151.56	146.13	97.05	116.57	112.30	147.10	101.20
3	***Fit2*^{EY08530}**	141.64	161.54	150.82	135.98	108.22	122.08	163.27	101.56
4	***Fit1*$^{\Delta 81}$**	127.34	156.61	195.38	114.91	112.18	120.32	175.74	100.80
5	***Fit1*$^{\Delta 161}$**	134.77	160.00	179.87	121.95	111.87	119.04	148.29	104.24
6	***Fit1*$^{\Delta 193}$**	170.97	265.31	188.07	134.53	169.20	147.42	149.69	104.56
7	***Fit1*$^{\Delta 161}$ *Fit2*^{EY08530}**	147.13	243.81	160.91	112.12	132.85	131.53	175.61	101.30

Table 5.1. Targeted second-site non-complementation mini-screen using null mutants for integrins and related proteins. Results of the second-site non-complementation screen show that there was no deleterious genetic interaction that affected viability between the different *Fit* alleles and integrins or their interacting proteins. *Mys*^{1} = βPS-integrin, *mew*^{M6} = αPS2-integrin, *if*^{B2} = αPS1-integrin, *rhea*^{1} = talin, *Ilk*^{1} = integrin-linked kinase, *stck*$^{3R-17}$ = PINCH, *arm*^{4} = β-catenin, *pan*^{2} = TCF. Full results of the screen with absolute numbers are listed in the Appendix.

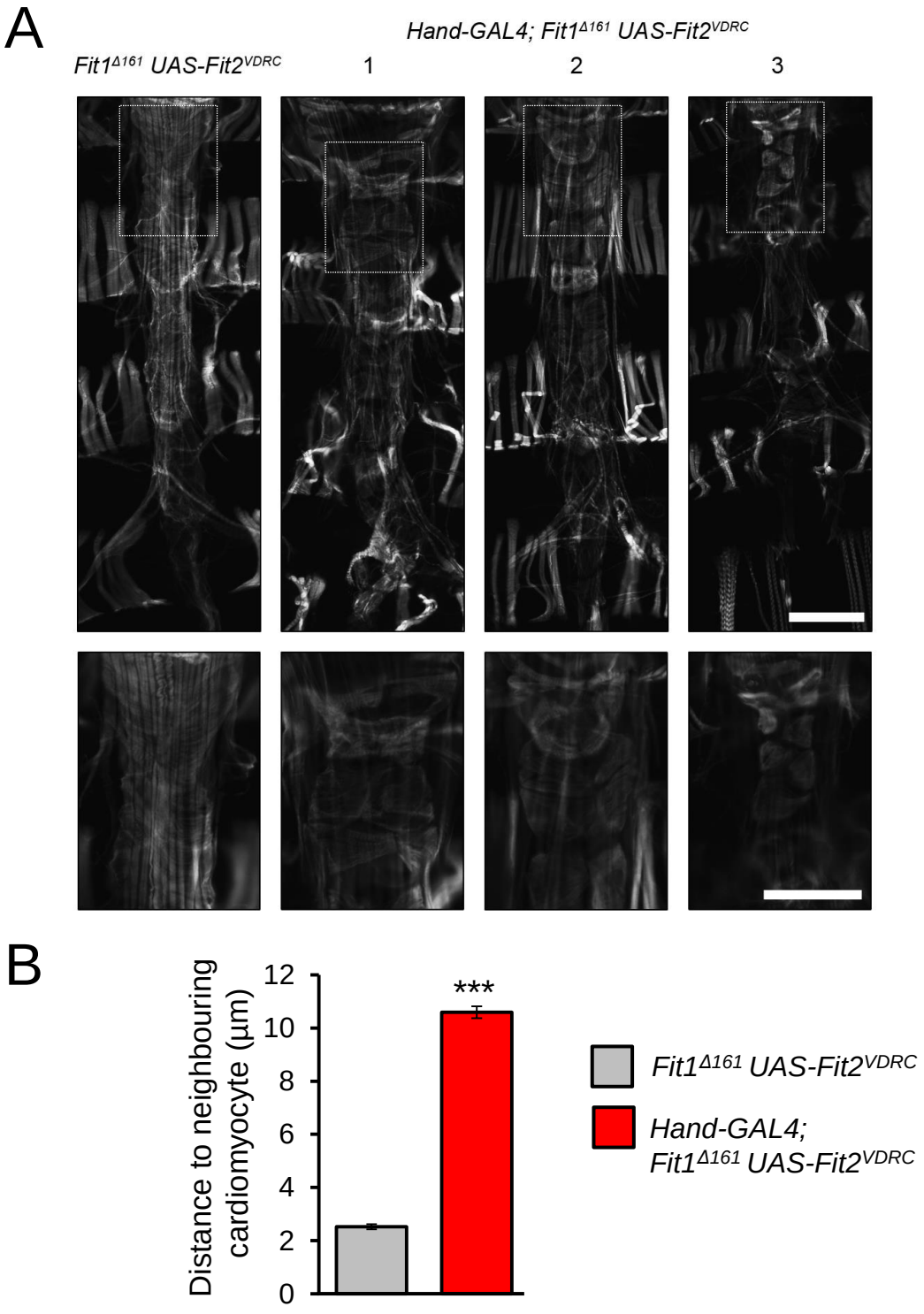

Figure 5.19. Cardiomyocyte *Fit2* compensates for the loss of *Fit1* to establish the cardiac syncytium.

A, micrographs of adult hearts stained with Alexa-conjugated phalloidin. Three examples of *Hand-GAL4; Fit1$^{\Delta161}$ UAS-Fit2^{VDRC}* hearts are shown to express the severe nature of the phenotype. White dashed boxes indicate magnified regions in micrographs below. Scale bar = 100µm. **B**, mean (±SEM) distance between neighbouring cardiomyocytes. *n* = 12-16 measurements from four independent flies for each genotype, ***P<0.001.

neighbouring cardiomyocytes was significantly greater in *Hand-GAL4; Fit1$^{\Delta 161}$ UAS-Fit2^{VDRC}* hearts compared to *Fit1$^{\Delta 161}$ UAS-Fit2^{VDRC}* controls. Therefore, *Fit2* appears to be compensating for the loss of *Fit1* in *Fit1$^{\Delta 161}$* cardiomyocytes, and in agreement with the phenotype seen in *Fit1$^{\Delta 161}$ Fit2^{EY08530}* mutants, only depletion of both *Fit1* and *Fit2* is sufficient to cause a deleterious phenotype.

In order to assess the damage caused by *Fit2*-knockdown in *Fit1*-null hearts, functional heart analysis was also performed on these week-old adults - the results are shown in Figure 5.20. The hearts of *Hand-GAL4; Fit1$^{\Delta 161}$ UAS-Fit2^{VDRC}* adults were not significantly different for most functional parameters compared to *Fit1$^{\Delta 161}$ UAS-Fit2^{VDRC}* controls, however, fractional shortening was significantly (0.35 (±0.01) *Fit1$^{\Delta 161}$ UAS-Fit2^{VDRC}* vs. 0.23 (±0.02) *Hand-GAL4; Fit1$^{\Delta 161}$ UAS-Fit2^{VDRC}*, $p<0.001$) decreased in *Hand-GAL4; Fit1$^{\Delta 161}$ UAS-Fit2^{VDRC}* hearts. It was also observed that *Hand-GAL4; Fit1$^{\Delta 161}$ UAS-Fit2^{VDRC}* hearts appeared to have a higher degree of arrhythmicity, but this did not reach significance ($p=0.06$). It was noticed there were slower action potential depolarization waves along the heart tube – but this could not be quantified using the existing MatLab-based video analysis software (CATTERSON *et al.* 2013; OCORR *et al.* 2009).

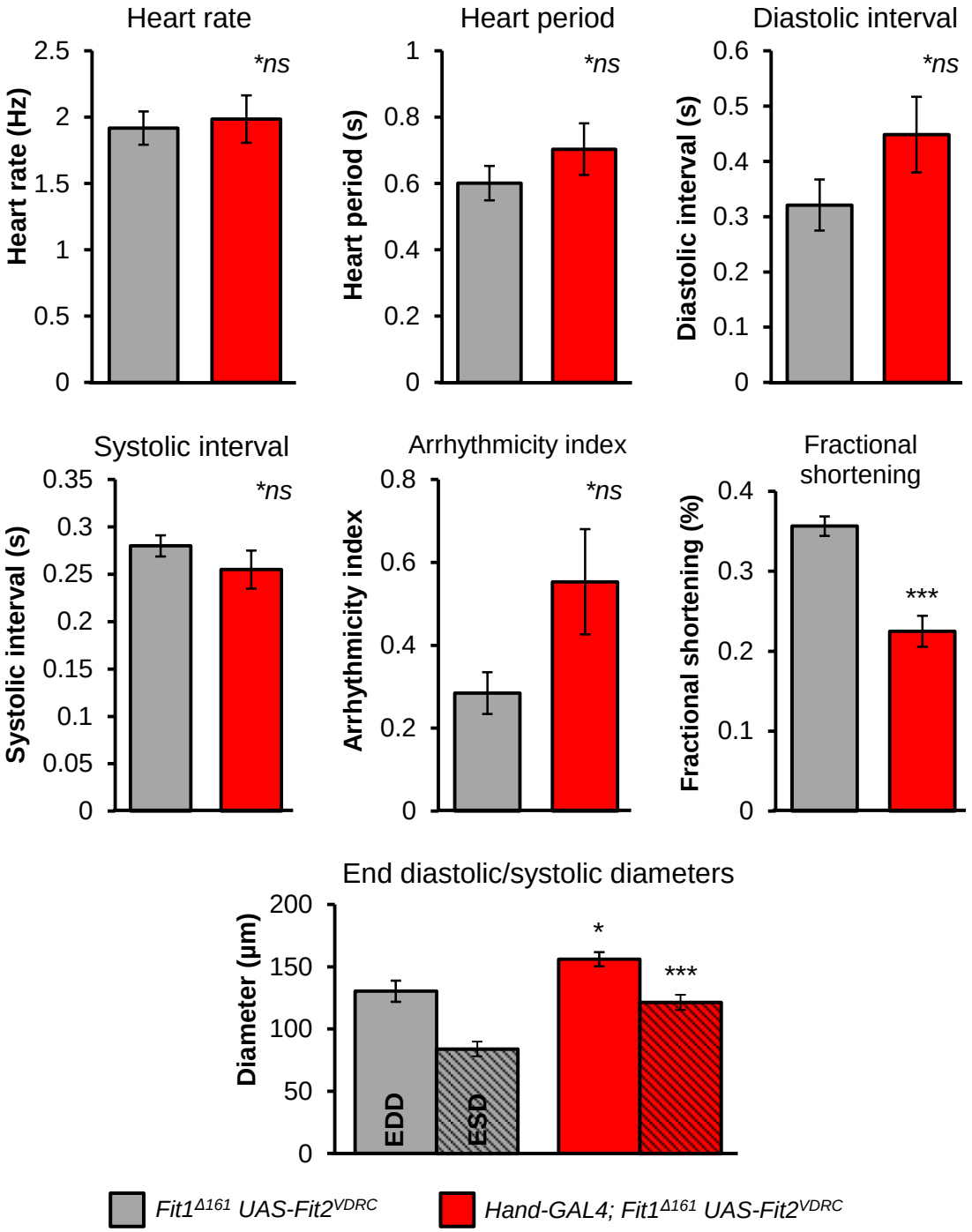

Figure 5.20. Heart function of *Fit1$^{\Delta 161}$ UAS-Fit2^{VDRC}* flies with/without *Hand-GAL4* activation in the cardiomyocytes.
There was no significant difference in heart rate, heart period, diastolic interval, systolic interval, or arrhythmicity index between genotypes. However, *Hand-GAL4; Fit1$^{\Delta 161}$ UAS-Fit2^{VDRC}* hearts exhibited a significantly lower degree of fractional shortening compared to *Fit1$^{\Delta 161}$ UAS-Fit2^{VDRC}* hearts. End diastolic diameter (non-shaded) and end systolic diameter (shaded) values were significantly greater in *Hand-GAL4; Fit1$^{\Delta 161}$ UAS-Fit2^{VDRC}* hearts compared to *Fit1$^{\Delta 161}$ UAS-Fit2^{VDRC}* hearts. Results are mean ± SEM, *n* = 15-16 flies per genotype. *p<0.05, ***p<0.001, one-way ANOVA with Tukey's post-hoc test.

5.4 Discussion

Work carried out in Chapter 4 illustrated the importance of the *Fermitins* and related cell adhesion proteins for the development of the adult *Drosophila* heart. What was unclear was whether there was a compensatory role that each *Fermitin* was performing in the absence of its paralog. It was demonstrated that hearts driving overexpression of $Fit1^{VDRC}$ resulted in severely dissociated cardiomyocytes, while heart-specific overexpression of $Fit1^{TRiP}$ did not reproduce this extreme phenotype, yet heart morphology still appeared to be negatively affected. *Hand-GAL4>*$Fit1^{TRiP}$ hearts were also functionally identical to controls – indicating that though cardiac morphology can be disrupted to a certain extent without adversely affecting heart function. Knockdown using $Fit2^{VDRC}$ also appeared to noticeably affect cardiac morphology, to a similar extent as that produced in *Hand-GAL4>*$Fit1^{TRiP}$ hearts. Cardiac-specific knockdown of both *Fit1* and *Fit2* (i.e. overexpression of both $Fit1^{VDRC}$ and $Fit2^{VDRC}$ RNAi) produced the most severe phenotype, with fully rounded-up cardiomyocytes, mimicking those seen in *Hand-GAL4>*Mys^{VDRC} mutants.

This rounded-up musculature phenotype was also previously observed in *Drosophila* embryos injected with dsRNAs against both *Fit* and *Fit2* – mimicking the result seen in embryos injected with dsRNA against *Mys* (BAI et al. 2008). Similarly, Bai *et al*. found that injection of *Fit1* or *Fit2* individual dsRNAs resulted in rounding up of only some muscles. The authors suggest that *Fit1* and *Fit2* may have "overlapping roles *in vivo*" – a hypothesis in agreement with unpublished data from Nick Brown's lab (DEVENPORT and BROWN 2005; MAITRA *et al.* 2009).

However, injecting whole embryos with dsRNAs affects the global development of the embryo, and potential embryonic phenotypes may be masked by maternally loaded proteins (PERRIMON *et al.* 2010).

Existing P-element stocks obtained from Bloomington for both *Fit1* (*Fit1*^{KG05576}) and *Fit2* (*Fit2*^{EY08530}) appeared to be healthy, with each P-element insertion appearing to have no significant effect on the transcription of the respective gene. It is possible that translation may have been affected in these genes, but without a reliable antibody to assess the levels of protein produced, this would be purely speculative. Therefore, to further elucidate the function of the *Fermitins* in the development of the *Drosophila melanogaster* heart, it was necessary to generate individual *Fit1* and *Fit2* mutants via mobilization of the P-element in these existing lines, with the aim of generating null deletion mutants by the imprecise excision of the P-element from the genome of these lines. Creating a null mutant was the only way to be sure that production of Fit1 and Fit2 proteins was impossible.

5.4.1 Generating genome deletions via P-element mobilisation

With hindsight, the method used to generate deletions via P-element mobilisation was unnecessarily laborious and probably detrimental to the experimental outcome. Instead of utilising a line that harboured a Δ2-3 transposase on the same chromosome as the P-element intended to be excised (i.e. both *Fit1* and *Fit2*, and their respective P-elements are on the 3rd chromosome), a transgenic line that carried the Δ2-3 transposase on a different chromosome was utilised. Not only did this result in extra crosses using a multiply balanced – and extremely unhealthy – stock (*w***; Kr*$^{If-1}$*/CyO; D*^{1}*/TM3, Ser*^{1}) so the P-element and the Δ2-3 transposase

could be followed, but it also meant any resulting potential ΔFit1 deletion line would also carry a balancer that would be deleterious to the health of the line. There is no question that this is a probable reason for the loss of so many of the ΔFit1 (and ΔFit2) lines – with the balancer either causing ill-health and/or fertility problems (GREENSPAN 1997). It is also possible that many more ΔFit lines could have been produced if not for both 2nd and 3rd chromosome being balanced, increasing the chance of creating a desirable deletion. Additionally, after a deletion is identified, any balancers still remaining on other chromosome have to be crossed out – meaning more unnecessary crossing schemes/collections. Therefore, for any future experiments involving P-element mobilisation, it would be simpler and less time-consuming to use a line that harbours the Δ2-3 transposase on the same chromosome as the P-element to be mobilised.

5.4.2 Screening ΔFit deletions

Before screening of the ΔFit lines (for both *Fit1* and *Fit2*) began, it was necessary to design primers that would span a large enough area to uncover a genetic deletion, but small enough so the PCR reaction would still be possible – PCR becomes increasingly unstable when amplifying larger pieces of DNA. It is important to note, therefore, that any negative results obtained from the PCR screen may show up as false negatives – i.e. there may be a large deletion that extends outwith the region being amplified by the selected primers. Additionally, since heterozygotes were used in most cases for the deletion screen, there is a wildtype band indicating the presence of a wildtype copy of the gene amplified from the balancer chromosome. Depending on the size of the deletion generated, this wildtype band can aid in the determination of the deletion size. However, if the deletion is

small it may be masked by the dominant wildtype band, again indicating that some false negatives may have been overlooked.

The reason for so few amplifications in the first 3 sets of PCRs in Figure 6.4B is not certain, but a probable reason is that these PCR reactions were performed in 0.5ml eppendorf tubes rather than 50µl PCR tubes – PCR tubes are thinner and heat exchange is more efficient across the walls of the tubes – indicating these reactions could not carry on due to inefficient heat transfer to the reaction mixes. PCR tubes were used for all subsequent PCR reactions – as seen in the last 2 sets of PCRs in Figure 6.4B – and the problem appeared to be rectified.

The method of screening genetic deletions by identifying changes in the size of PCR amplicons was chosen because it only needed genomic DNA samples, which are highly stable, and because deletions are relatively easy to identify on a gel. However, just because there appears to be a deletion, does not mean it will have any effect on the function of the gene of interest – e.g. there may be an in-frame deletion which removes a large enough chunk of the genome to be identified on a PCR gel, but which only deletes a dispensible region such as the region downstream of the transcription start site but upstream of the translation start site.

Screening genetic deletions by RT-PCR (or even qPCR), instead of genomic PCR, and assessing the level of gene expression would be a better method to identify deletion lines that actually affected the expression of the gene of interest, and would include even apparently minor deletions, that would otherwise be missed by genomic PCR screening, and could potentially cut the number of false negatives. For example, an imprecise excision of the *Fit1*^{KG05576} P-element which deleted only 50bp (a

deletion small enough that it would have probably not been detected in the PCR screens performed here) in the 5' direction (i.e. towards the transcription start site) would have removed the transcription start site and potentially would have prevented the transcription of *Fit1* and, thus, creating a *Fit1*-null mutant without actually deleting any of the *Fit1* coding sequence. However, mRNA extractions would have to be performed on homozygotes – instantly increasing the amount of time and effort going into the screen, as potentially hundreds of lines would need to be homozygous, including deletion lines which are not viable without the presence of a balancer, these would need to be crossed onto a GFP balancer if not already on one, and homozygous embryos selected – not a simple job. Additionally, screening via RT-PCR would have missed the $Fit1^{\Delta 161}$ deletion as mRNA appears to be produced at the normal amount (Figure 7.9B).

Therefore, while screening via RT-PCR offers increased reliability of identifying deletion mutations that affect gene expression, this increase in fidelity may come at the expense of a substantially increased workload, whereas screening by PCR immediately identifies potential candidate deletions that can be further examined by RT-PCR, Western blotting etc.

5.4.3 A *Fit1*-null deletion mutant, $Fit1^{\Delta 161}$, was generated via P-element mobilization from $Fit1^{KG05576}$ flies, whereas there were no deleterious mutations generated by the mobilization of the P-element from $Fit2^{EY08530}$ flies

There appeared to be multiple candidate *Fit1*-null deletion lines from the 227 ΔFit1 vials that were originally produced, though unfortunately due to some lines being unhealthy and/or not breeding, some of these potential *Fit1*-null deletions were

lost (e.g. #126, 134 and 159 from Figure 6.5) and subsequently no further characterisation of these lines was carried out. It is also possible there were even more deletion lines than counted, since the size of the amplified PCR fragments to check for deletions were comparatively large (approximately 4.9kb) and were run on 0.8% agarose gels, meaning that unless the deletion was greater than approximately 100bp, spotting differences in PCR amplicon sizes between 4kb and 5kb on the 1kb ladder was challenging. For example, some of the deletion lines that appear to show a wildtype band, may actually carry a deletion of less than 100bp, but one that deletes the start of the *Fit1* transcription site and, therefore, a potential *Fit1* null. However, the primers used to screen deletions were designed to obtain the widest range that would include the most desirable deletions – i.e. within the open reading frame of the whole of *Fit1* - and would not extend into flanking genes - undesirable in a mutant in this case, with possible deleterious consequences.

One of the deletion lines, $Fit1^{\Delta 161}$, was confirmed to contain a deletion that eliminated almost half of the *Fit1* gene and, upon sequencing, was found to harbour a 1685bp deletion spanning from just after the *Fit1* transcription start site to approximately half way into the *Fit1* coding sequence, while also retaining a 12bp-fragment of the 5' end of the KG05576 P-element. This fragment contained two ATG start codon sequences, making it possible that translation could proceed and a truncated yet active Fit1 protein could still be generated, however the ATG sequences are out-of-frame with the predicted start site of transcription and so even a truncated form of *Fit1* could not be produced. Additionally, even if the ATG start sequences were in-frame, there is a STOP codon that lies two codons directly downstream of the second ATG site that would result in a 4 amino acid protein (i.e.

Met-Met-Lys-STOP) after translation. Therefore, it is highly likely the *Fit1*$^{\Delta 161}$ line is a null *Fit1* mutation, and no Fit1 protein is being produced. The *Fit1*$^{\Delta 161}$ line was also deemed appropriate to use since there appears to be no adverse effect of the deletion on flanking genes, which could otherwise complicate experimental interpretations and conclusions.

Unfortunately, there appeared to be no deletions in any of the ΔFit2 deletion lines that were screened. There was one deletion line (#8) that appeared to contain an approximately 500bp fragment of the EY08530 P-element but this appeared to have no significant effect on the health of the line. Similar to the screening of ΔFit1 mutant lines, it is possible there were undetected deletions in the ΔFit2 lines, since the size of the amplified PCR fragments to check for deletions were comparatively large (approximately 3.8kb), with subtle differences hard to identify on 0.8% agarose gels. Different (and possibly better) methods of generating null mutants, including using ends-out/ends-in homologous recombination were also considered (RONG and GOLIC 2000; XIE and GOLIC 2004), but due to time constraints this was deemed unjustified.

5.4.4 A *Fit1*-null deletion mutant, *Fit1*$^{\Delta 193}$, that completely abolished *Fit1* mRNA transcription was also generated but this deletion also ablated neighbouring genes

The *Fit1*$^{\Delta 193}$ deletion line was also a good candidate for further analysis, what with it being a true genetic *Fit1*-null deletion line, however the deletion in these flies appeared to span not only *Fit1* but also at least 3 other genes upstream of *Fit1*'s transcription start site – namely, *CG14989*, *CG14990*, and *CG14995*. Thus, any

further analysis of the effect of the deletion of *Fit1* in these flies would be complicated by the effects of deletion of these other potentially crucial genes. In agreement with this, the $Fit1^{\Delta 193}$ deletion line did not breed to homozygosity, with homozygous embryos perishing at the late embryonic stage. Additionally, the $Fit1^{\Delta 161}$ deletion was only semi-lethal, indicating that the late embryonic lethality of the $Fit1^{\Delta 193}$ deletion can be attributable to loss of function of one (or more) of the other deleted genes. The fact that an imprecise P-element excision can remove a large region of the genome (in the case of the $Fit1^{\Delta 193}$ deletion, up to 18kb), again highlights the advantages of targeted methods of genetic knockout in *Drosophila* (e.g. ends-out/ends-in homologous recombination) that would be specific for the targeted gene and would not affect neighbouring genes (RONG and GOLIC 2000; VENKEN and BELLEN 2005; XIE and GOLIC 2004).

5.4.5 The $Fit1^{\Delta 161}$ mutation is semi-lethal indicating *Fit1* and *Fit2* are partially redundant

With the $Fit1^{\Delta 161}$ line selected as the *Fit1*-null mutant, experiments aiming to phenotype these animals were performed. It was found that the $Fit1^{\Delta 161}$ line was semi-lethal and that around 50% of animals survived til adulthood – with death occurring during the early-mid larval stages. It is presently unknown exactly why this *Fit1*-null mutation is semi-lethal, as opposed to viable or lethal, but the most likely explanation is due to the presence of *Fit2*. With the absence of *Fit1*, the paralog of *Fit1* in *Drosophila*, *Fit2*, may be playing a compensatory role. In agreement with this, it was shown that $Fit1^{\Delta 161}$ $Fit2^{EY08530}$ double mutants died at the embryonic stage, indicating a requirement of both for viability. Therefore, the incomplete nature of the rescue, and the apparent compensatory role of *Fit2* in *Fit1*-null mutants

indicated a partial genetic (and functional) redundancy – in agreement with previous observations (BAI *et al.* 2008; DEVENPORT and BROWN 2005; MAITRA *et al.* 2009). Additionally, it was also recently demonstrated that *Kind2* can functionally compensate for loss of *Kind1* in the developing zebrafish (POSTEL *et al.* 2013).

Fit2 shares 76% protein identity with Fit1, but when similar amino acids are factored in this number increases to 87% - so although the Fit proteins are highly similar, they remain dissimilar enough to be able to perform divergent functions. It is likely the semi-lethality seen in $Fit1^{\Delta 161}$ homozygotes is, therefore, due to the inability of *Fit2* to completely rescue the function of *Fit1*. In other words, Fit2 protein may be able to perform many similar functions as Fit1, but not all, and the function(s) that Fit2 cannot perform may be important but not necessary to avoid lethality at the larval development stage. This functional divergence of gene paralogs is not uncommon in *Drosophila* and has been studied in genes important for eye development (PUNZO *et al.* 2004), and immunity (YANG *et al.* 2006). Indeed, gene duplication events and subsequent functional divergence of paralogs have been established as vital for the development of novel innovations – with two possible potentials for duplicate genes, subfunctionalisation (i.e. duplicate genes undergo a division of labour by maintaining different functions of the original gene – for example, haemoglobins (STORZ *et al.* 2008)), or neofunctionalisation (i.e. duplicate genes acquire a novel function – for example, antifreeze protein (DENG *et al.* 2010)) over a period of time (LONG *et al.* 2003; OHNO 1970; ZHAN *et al.* 2012).

In the nematode worm, *Caenorhabditis elegans*, there is only one Fermitin-like protein called UNC-112 which, when ablated, causes a paralysed phenotype with impairments in muscle assembly (WILLIAMS and WATERSTON 1994). In a more

closely related species, the European honey bee (*Apis mellifera*, Order: Hymenoptera) there appears to be only one Fermitin-like protein – and this protein shares 60 and 58% identity with Fit1 and Fit2, respectively. It is thought the Hymenoptera-Diptera divergence occurred ~300 million years ago (GRIMALDI and ENGEL 2005), while the mosquitos' and fruit flies' common ancestors – belonging to the Diptera order – diverged ~250 million years ago (NENE *et al.* 2007). The malaria vector mosquito (*Anopheles gambiae*) also appears to harbour only one Fermitin-like protein – this protein shares 70 and 65% identity with Fit1 and Fit2, respectively. Therefore, *Drosophila melanogaster* (and other members of the *Drosophilidae* family) are the only dipterans identified thus far that harbour two Fit genes (according to OrthoDB (WATERHOUSE *et al.* 2013)). Since Fit1 is more similar to Fit-like proteins in nematodes, honey bees, and mosquitos, it is likely *Fit2* emerged after a gene duplication event sometime after the divergence of the dipteran common ancestor of fruit flies and mosquitos. Therefore, the semi-lethality of *Fit1*-null flies potentially indicate that the Fit2 protein can perform similar roles and functions as Fit1 (subfunctionalisation), but not all – and a possible novel function(s) (neofunctionalisation).

Alternatively, Fit2 has the ability to entirely compensate for the loss of Fit1 and rescue the semi-lethal phenotype but cannot due to the insufficient expression of the gene in certain mutants – since around half of these survive to adulthood. This could be tested via overexpression of *Fit2* in the *Fit1*-null background. If overexpression of *Fit2* rescued the semi-lethality then the semi-lethality is likely due to insufficient expression of Fit2, however if overexpression did not rescue the semi-lethality then *Fit2* must have diverged sufficiently enough from *Fit1* to perform

many of its functions but also enough to perform distinct role(s). Thus *Fit1* and *Fit2* exhibit partial functional redundancy.

5.4.6 The *Fit1$^{\Delta 161}$* mutation is semi-lethal, yet mutants that survive to adulthood have an extended lifespan

It seems almost counter-intuitive that *Fit1$^{\Delta 161}$* mutants that make it to adulthood live longer than their wildtype (*w^{1118}*) counterparts. It might be expected that flies with a mutation in a cell adhesion protein would die, if not during larval development, then at least within a few days of eclosion – especially since half of the *Fit1$^{\Delta 161}$* progeny die during the larval stage.

Loss-of-function *myospheroid* (βPS-integrin) mutants have also been shown to exhibit delayed functional senescence and an increased mean lifespan (GODDEERIS *et al.* 2003). Additionally, studies in *C. elegans* have demonstrated a previously unidentified role for *Integrin-linked kinase* (*pat-4* in *C. elegans*) and *actopaxin* (*pat-6* – known to bind to integrin-linked kinase) in lifespan extension (HANSEN *et al.* 2005). Further, studies on the human interactome and potential signalling pathways regulating lifespan have identified a significant over-representation of cell-cell/cell-matrix, and focal adhesion proteins – for example, fibronectin, focal adhesion kinase (FAK), paxillin, and vinculin (WOLFSON *et al.* 2009). The authors of these studies offer no explanation/mechanism for the lifespan extension other than to say there might be a novel regulatory pathway that influences ageing. Thus, it may be the case that loss of *Fit1* may extend lifespan of the adult escapers via the same novel pathway as these other cell adhesion proteins.

5.4.7 The hearts of *Fit1*$^{\Delta 161}$ adults are morphologically and functionally similar to wildtypes

Since RNAi knockdown of *Fit1* (via both VDRC and TRiP RNAi lines) in the fly heart significantly disrupted the morphology of the cardiomyocytes (see Chapter 5), it was hypothesised that the hearts of *Fit1*$^{\Delta 161}$ adults would be similarly affected. However, these mutant hearts were morphologically indistinguishable from w^{1118} controls. *Fit1*^{KG05576} and *Fit2*^{EY08530} hearts were also examined for morphological differences but none were identified. Functional analysis was also performed on week-old *Fit1*$^{\Delta 161}$ hearts and these hearts were functionally identical to w^{1118} controls. The contrast between the apparently healthy hearts of *Fit1*$^{\Delta 161}$ adults and the grossly abnormal hearts of those overexpressing *Fit1* RNAi indicates that there may be another factor important for the development of the cardiac syncytium and its function in the adult fly heart.

5.4.8 The *Fit1*^{VDRC} RNAi also targets *Fit2* mRNA

It was subsequently identified that the *Fit1*^{VDRC} RNAi may have had an off-target effect – a feature of this RNAi that had been previously overlooked – targeting a 27bp sequence that downregulated the levels of *Fit2* mRNA. This result then could help explain why the *Fit1*^{VDRC} RNAi had such a dramatic effect on cardiomyocyte morphology compared to *Fit1*^{TRiP} RNAi – which is predicted to target *Fit1* alone. However, when overexpressed in the heart, the *Fit1*^{TRiP} RNAi line still appeared to affect heart morphology to an extent, however slight. Since the hearts of *Fit1*$^{\Delta 161}$ adults are normal, it would suggest the varied phenotype seen in *Fit1*^{TRiP} RNAi hearts was possibly due to another (albeit, unpredicted) off-target effect of the RNAi

– a phenomenon not uncommon to *Drosophila* RNAi screens (KULKARNI *et al.* 2006; MA *et al.* 2006) – or, alternatively, reflects some general toxicity associated with RNAi production.

Since qPCR analysis of *Fit* depletion in *Hand>Fit1*^{VDRC} heart tissue was difficult to achieve, the ability of the 'Fit' RNAi lines to instead deplete *Fit* mRNA levels ubiquitously, was assessed in *da>GAL4* embryos (due to the lethality involved at later stages). It was demonstrated that both *Fit* VDRC RNAi lines could significantly deplete their respective paralogs, while the TRiP RNAi line did not affect *Fit1* mRNA expression. Therefore, the *Fit1*^{VDRC} and *Fit2*^{VDRC} RNAi lines would be predicted to be functioning correctly when driven by cardiac GAL4 drivers. In this data set the *Fit1*^{VDRC} RNAi did not appear to affect *Fit2* levels. Ideally, qPCR would be performed on extracted heart tissue from these adults.

5.4.9 *Fit1*$^{\Delta 161}$ *Fit2*^{EY08530} double mutants die at the embryonic stage

Therefore, it was hypothesised *Fit2* was compensating for the lack of *Fit1* in the hearts of *Fit1*$^{\Delta 161}$ adults and that only genetic ablation of both *Fit1 and Fit2* would cause the severe cardiomyocyte dissociation phenotype exhibited in double *Fit1*^{VDRC}/*Fit2*^{VDRC} RNAi knockdown hearts. It was also hypothesised that loss of both *Fit1* and *Fit2* would result in a phenotype similar to *myospheroid* (βPS-integrin) mutant embryos (BAI *et al.* 2008).

Fit1$^{\Delta 161}$ *Fit2*^{EY08530} double mutants were generated and were found to be embryonic lethal – with embryos appearing to struggle exiting their vitelline cases, likely due to insufficient force produced from the musculature. This phenotype also mimicked that seen in *mys* embryos, but unfortunately attempts to establish if double

Fit mutants developed severely rounded-up body wall musculature were unsuccessful. It is hypothesised that when properly stained, $Fit1^{\Delta 161}$ $Fit2^{EY08530}$ mutant embryos would display a similar rounded-up phenotype as *mys* embryos (DRYSDALE *et al.* 1993) and *Fit1/Fit2* double knockdown embryos (BAI *et al.* 2008). This embryonic lethality of these $Fit1^{\Delta 161}$ $Fit2^{EY08530}$ double mutants demonstrated three important findings: 1, the $Fit1^{\Delta 161}$ deletion is adversely affecting the expression of *Fit1*; 2, the $Fit2^{EY08530}$ P-element insertion must also be having some deleterious effect on the expression of *Fit2*, a result which was previously only suspected and; 3, *Fit2* is sufficient for viability since *Fit1*-null mutants can still reach adulthood, albeit with lethality for half the expected progeny.

At this time, since no appropriate antisera are available to verify the presence/absence of either Fit1 or Fit2, it is difficult to tell if the $Fit2^{EY08530}$ P-element insertion is causing a null or hypomorph mutation. P-elements frequently insert proximal to transcription start sites and can result in hypomorphic mutations (SPRADLING *et al.* 1995) – it has also been demonstrated that transcription can initiate from within the P-element itself, and may be responsible for some insertions causing hypomorphic alleles when otherwise expected to be null (LAFAVE and SEKELSKY 2011).

5.4.10 *ΔFit*/'cell adhesion' transheterozygotes fully complemented each other, indicating no genetic interaction between these genes

Since the embryonic lethality of the double $Fit1^{\Delta 161}$ $Fit2^{EY08530}$ mutants indicated the importance of these genes for viability, and mimicked the embryonic lethality seen in other *Drosophila* cell adhesion mutants, a targeted SSNC mini-

screen was performed to identify if the *Fit* mutants interacted genetically with selected 'cell adhesion' mutants. Viability was scored among transheterozygote progeny and it was found that there was no effect on the observed number of progeny compared to the expected Mendelian ratio. The results from this targeted 'cell adhesion' SSNC mini-screen not only showed that there was no effect on viability in any of the transheterozygotes tested (and that the mutations in *trans* fully complemented each other), but that many of the potentially deleterious transheterozygotes from each cross made up a higher proportion of the progeny than their 'single mutation/balancer' counterparts. A potential reason for this phenomenon may be explained by 'hybrid vigour' or heterosis – whereby fitness of the resulting progeny is enhanced as a result of mixing the genetic contributions of its inbred parents (BURKE and ARNOLD 2001).

Although there appeared to be no genetic interaction between the *Fit* mutants and any of the 'cell adhesion' mutants tested, this does not rule out a physical interaction between the proteins. Indeed, it is predicted that Fit1 and Fit2 proteins can bind to βPS-integrins, ILK, and β-catenin (QADOTA *et al.* 2012; YU *et al.* 2012). It is likely, therefore, that in the transheterozygous state for each cross in the SSNC mini-screen, a compensatory increase in gene expression/protein levels was sufficient to allow development to proceed. Future work identifying the binding partners of the Fit proteins, including co-immunoprecipitation studies, will help determine the function of these proteins in *Drosophila*.

5.4.11 Ablation of *Fit2* in the hearts of $Fit1^{\Delta 161}$ adults reproduces the cell dissociation phenotype seen with double *Fit1/Fit2* knockdown in the heart and highlights the importance of both Fermitins for heart development

Fit1$^{\Delta 161}$ *UAS-Fit2*^{VDRC} flies were generated in parallel with *Fit1*$^{\Delta 161}$ *Fit2*^{EY08530} flies and were viable – suggesting only P-element disruption of *Fit2* is sufficient to cause causes embryonic lethality in *Fit1*-null mutants – although the exact position of the P-element in *UAS-Fit2*^{VDRC} flies remains to be determined. The effect of the double *Fit* mutation on the adult heart could also not be assessed due to the embryonic lethality. Therefore, to assess the effect of downregulating *Fit2* in the *Fit1*-null background, *Hand-GAL4; Fit1*$^{\Delta 161}$ *UAS-Fit2*^{VDRC} flies were subsequently generated, and were also viable. The hearts of these flies were severely affected and showed a dramatic cardiomyocyte dissociation phenotype, echoing the disruption seen in double *Fit1*^{VDRC}*/Fit2*^{VDRC} heart-specific knockdown adults. However, the phenotype seen in these hearts appears weaker than the severely rounded-up cardiomyocyte phenotype seen in double *Fit*, and *mys* knockdown hearts. A likely reason for this discrepancy is that, in the *Fit1*^{VDRC}*/Fit2*^{VDRC} hearts, *Fit2* is getting a 'double whammy' knockdown hit from both the *Fit2*^{VDRC} RNAi, and the *Fit1*^{VDRC} which also targets *Fit2* mRNA – this is summarised in Figure 5.21.

The cardiomyopathy caused by silencing *Fit1* and *Fit2* phenocopied *myospheroid* knock-down and is therefore consistent with the *Fermitins* regulating β-integrin signalling and promoting cardiomyocyte coupling during development (LEHMACHER *et al.* 2012; VANDERPLOEG *et al.* 2012). There is evidence from mammalian models that Kindlins, via the FERM F3 subdomain, interact directly with the cytoplasmic tail of β-integrins (MONTANEZ *et al.* 2008; SHI *et al.* 2007). The FERM domain of *Drosophila* Fermitins is conserved from flies to humans and it is therefore speculated that Fermitins directly interact with the β-integrin *myospheroid* to form a signalling complex required for cardiomyocyte coupling. No study has yet

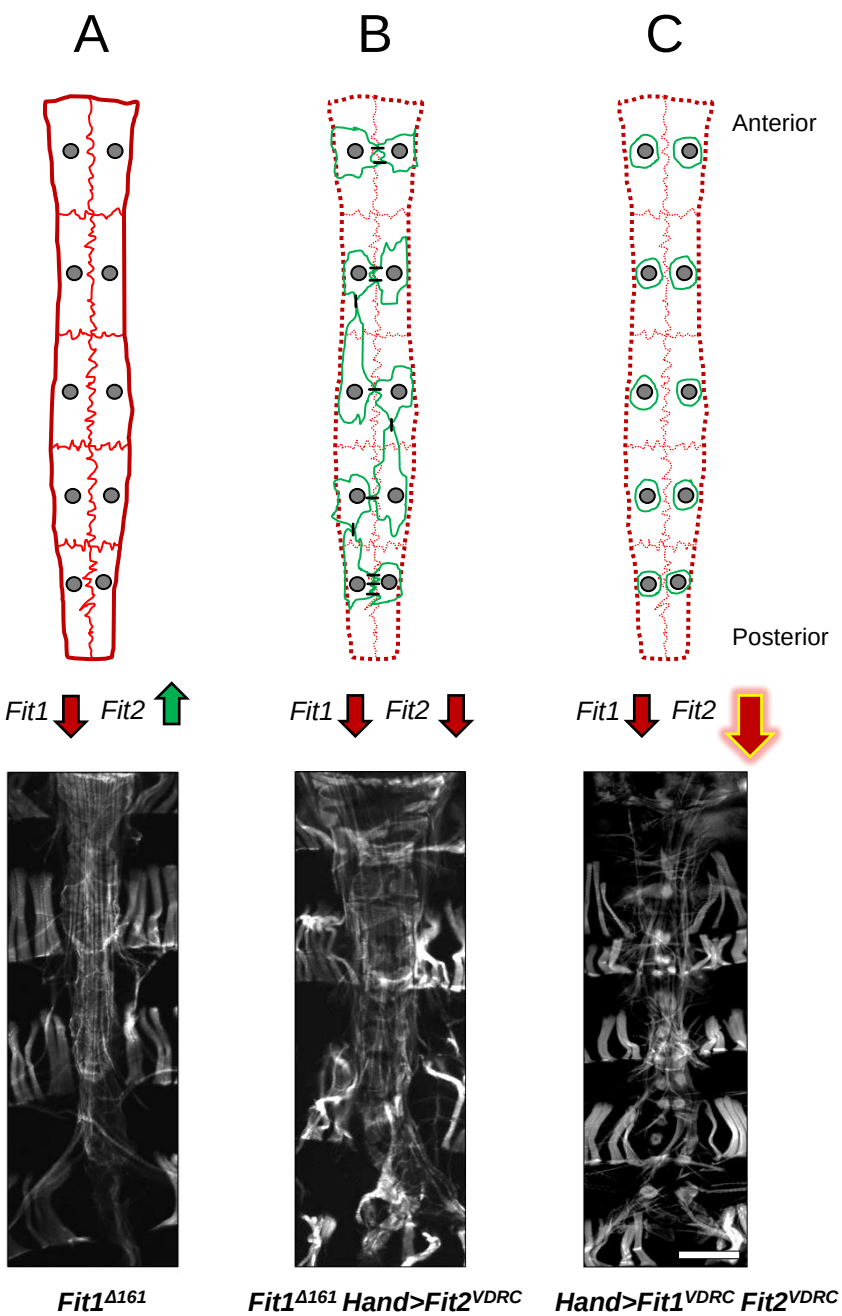

Figure 5.21. Model illustrating effects of *Fermitin* knockdown in the *Drosophila* heart.

A, the fully coupled fly heart with junctions between cardiomyocytes demonstrates *Fit2* can fully compensate for *Fit1* loss. **B**, a breakdown of cardiomyocyte junctional integrity with discrete regions of cell coupling via β-integrins due to knockdown of *Fit2* in the *Fit1*-null heart. Black bars represent junctional β-integrin localisation. **C**, complete loss of cardiomyocyte structure, cells appear as rounded-up spherical myocytes (myospheroid) and are fully dissociated from adjacent cardiomyocytes. *Fit1* mRNA is being depleted by $Fit1^{VDRC}$, while *Fit2* mRNA depletion is augmented by $Fit2^{VDRC}$ and $Fit1^{VDRC}$ (off-target effect). Scale bar = 100µm.

manipulated the expression of mammalian *Kind2* solely in the cardiomyocytes, however it is predicted that a phenotype would develop that is similar to that seen in ventricular cardiomyocyte-targeted β1-integrin knockout mice (SHAI *et al.* 2002). Histological studies of the β1-integrin KO hearts revealed significant disruption of myofibrils and intercalated discs, with subsequent onset of dilated cardiomyopathy.

5.4.12 Ablation of *Fit2* in the hearts of $Fit1^{\Delta 161}$ adults also led to significantly decreased contractile ability and highlighted a problem with cardiomyocyte synchrony

Heart function of *Hand-GAL4;* $Fit1^{\Delta 161}$ *UAS-*$Fit2^{VDRC}$ flies was subsequently assessed and the hearts were most parameters were found to be comparatively normal, while fractional shortening was significantly affected – with hearts unable to contract fully. This phenotype was similar to that seen in *Hand>*$Fit1^{VDRC}$ hearts (i.e. similar heart rate, and heart period values, but increased arrhythmicity and decreased fractional shortening values – see Figure 4.14). A distinctive feature of these hearts, however, was a noticeable decrease in the speed of contraction along the length of the heart – i.e. the wave of action potential that flows through the heart was slower. While the MatLab-based video analysis software designed to analyse heart function parameters was appropriate for measuring heart rate, fractional shortening, arrhythmicity index etc. (OCORR *et al.* 2009), it was not useful for analysis of heart synchrony, as this needed two points of reference at different ends of the heart. Cardiac synchrony analysis was subsequently performed by Dr. Paul Hartley utilising an ImageJ analysis method and it was found that the hearts of *Hand-GAL4;* $Fit1^{\Delta 161}$ *UAS-*$Fit2^{VDRC}$ flies were less synchronous compared to $Fit1^{\Delta 161}$ *UAS-*$Fit2^{VDRC}$ 'control' flies (data not shown) (CATTERSON *et al.* 2013).

The diminishment of cardiac synchrony in *Hand-GAL4; Fit1$^{\Delta 161}$ UAS-Fit2^{VDRC}* flies suitably illustrated the adverse effect of loss of cell-cell coupling and cardiomyocyte dissociation in the fly heart. There remained, however, enough contact and adequate connection between these cardiomyocytes to continue to function 'normally', with no obvious ill effect on the development or health of the fly.

5.4.13 Relevance to human cardiovascular diseases

Human heart diseases attributed to intercalated disc dysfunction include arrhythmogenic right ventricular cardiomyopathy caused by mutations in D proteins (e.g. Desmoplakin, Plakophilin-2, and Desmoglein-2) (BASSO *et al.* 2006), and hypertrophic and dilated cardiomyopathy caused by a missense mutation in the integrin-binding adhesion protein, Vinculin (VASILE *et al.* 2006). Integrins and related binding proteins (e.g. Vinculin and Talin) were also identified at intercalated discs in adult human cardiac tissue (ANASTASI *et al.* 2009; DI MAURO *et al.* 2009). Thus, there is a need to develop genetically tractable models with which to study the role of these proteins in cardiac development and function.

5.4.14 Summary

In summary, these results identify *Fermitins* as important mediators of cardiomyocyte coupling and heart function in *Drosophila*, and definitively demonstrate their role in the development of a functional cardiac syncytium. Abnormalities in the junctions between contiguous cardiomyocytes are known to contribute to cardiomyopathies in humans. Kindlin-2 (KIND2) is associated with these junctions but it remains unclear whether cardiomyocyte *Kind2* expression is

required for cardiomyocyte junction formation and the development of normal cardiac function. To address this question, the expression the two invertebrate orthologs of *Kind2*, was silenced in fruit fly cardiomyocytes. Cardiac knockdown led to a severe cardiomyopathy and loss of synchrony between cardiomyocytes. The findings also demonstrate that the Kindlin orthologs can functionally compensate for each other in order to control syncytium development. These findings support the concept that abnormalities in cardiomyocyte KIND2 expression or function may contribute to the pathogenesis of human cardiomyopathies.

Chapter 6

Generation of TARGET (GAL80^{ts}) flies to investigate the effects of *Fermitin* loss in the adult heart

6.1 Introduction

Age-related functional decline (i.e. senescence) of the human myocardium often accompanies an increased likelihood of conduction defects and cardiac arrhythmogenesis (KISTLER *et al.* 2004). The role of the intercalated disc in the pathogenesis of these cardiac abnormalities has come under increasing scrutiny due to its involvement in the pathogenesis of cardiomyopathies (BASSO *et al.* 2006; LI *et al.* 2006; LI and RADICE 2010; PERRIARD *et al.* 2003; SPRAGG and KASS 2005). From Chapter 5, it was demonstrated that ablation of both *Fermitins* in the fly heart led to severe cardiomyocyte-dissociation, mimicking β-integrin loss. However, this phenotype was generated using an ectopic gene expression system (GAL4/UAS) which depleted *Fermitin* RNA throughout development. This was assessment of an adult phenotype which may have had its origins during embryonic/larval/pupal development. Thus in this chapter, experiments were designed to address the developmental stage at which the *Fit* genes were required. An additional aim was to model the effects of aberrant *Kind2* function in the adult human myocardium, therefore the effects of *Fit*-knockdown after eclosion also had to be assessed in the *Drosophila* model. Therefore, in order to investigate the effects of *Fermitin* loss in the adult fly heart, an inducible cardiac-expressing method of genetic ablation was utilised.

6.1.1 Spatiotemporal control of gene expression using the temperature-sensitive (GAL4/UAS/GAL80^{ts}) TARGET system

One of the main advantages of using *Drosophila* as a model organism is the availability of various genetic tools that make it feasible to perform experiments that

would otherwise be difficult, time-consuming and expensive in higher organisms (VENKEN and BELLEN 2005). The yeast GAL4/UAS system was developed for *Drosophila* by Andrea Brand and Norbert Perrimon (BRAND and PERRIMON 1993) – shown in Figure 1.3. This system allows for the tissue-specific ectopic expression of transgenes (including RNAi) for effective silencing of genes/proteins. A caveat of using the GAL4/UAS system is the presence of GAL4 throughout development, and precludes investigation of the gene's relevance in adult tissues, independently of its role in development (KIM and WOLF 2009).

The GAL4/UAS system was updated to include a temperature-sensitive GAL80 ($GAL80^{ts}$) molecule also exploited from yeast – this new system was named the TARGET system (MCGUIRE *et al.* 2003; MCGUIRE *et al.* 2004). A schematic diagram indicating the mechanism of action of the spatiotemporal TARGET system is shown in Figure 6.1. In brief, when kept at 18°C (non-permissive) the temperature-sensitive $GAL80^{ts}$ protein inhibits the GAL4 protein and prevents it from binding to the upstream activation sequence (UAS) – and thus inhibits transcription of the transgene. If the temperature is then raised to 29°C (permissive), the $GAL80^{ts}$ protein is inactivated and can no longer inactivate GAL4 – allowing GAL4 to successfully bind to the UAS and initiate transcription. The main advantage of this method for use in *Drosophila* genetics is the ability to manipulate genes/proteins in a developmental stage-specific manner, thus avoiding any deleterious developmental effects – e.g. probing the function of genes during larval/pupal stages (GUTIERREZ *et al.* 2007). This system has also been used by other researchers investigating conserved genetic pathways in the adult fly heart (MELKANI *et al.* 2011; QIAN *et al.* 2011).

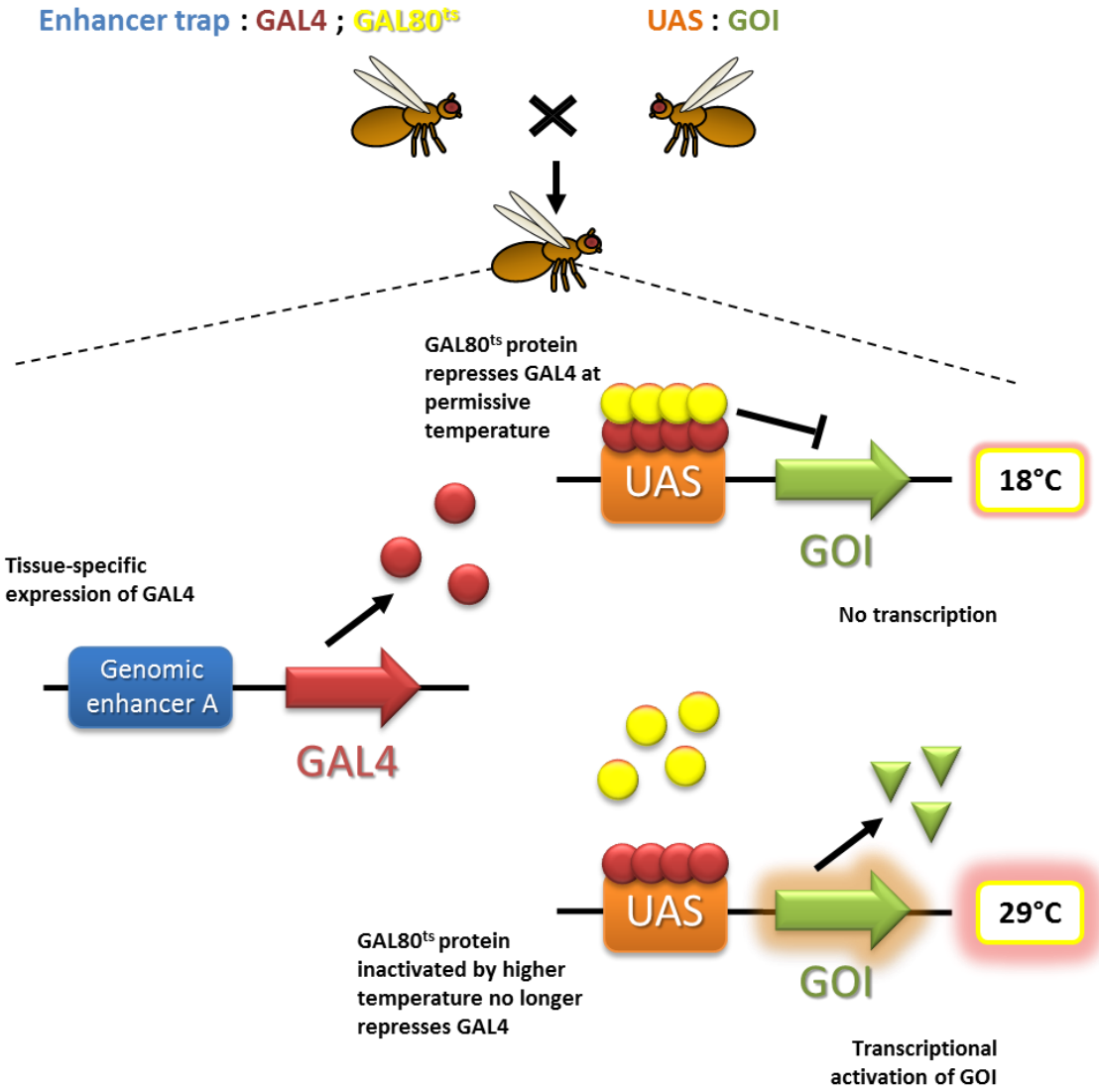

Figure 6.1. Spatiotemporal gene expression using the TARGET system.
In the TARGET system, the conventional GAL4-UAS system is conditionally controlled by the temperature-sensitive GAL80^{ts} repressor protein - expressed ubiquitously from the tubulin 1$^{\alpha}$ promoter. GAL80^{ts} (highlighted in yellow) represses the transcriptional activity of GAL4 at permissive temperatures (e.g. 18°C), but becomes inactive at 29°C, allowing GAL4 to drive expression of the gene of interest (GOI) in a tissue-specific manner. Therefore, the TARGET system provides spatial and temporal control of gene expression.

6.2 Hypothesis

Fermitin expression may contribute to adult heart function independently of their role in heart development.

6.2.1 Aims

1) Generate different temperature-sensitive TARGET fly lines from existing GAL4 lines (i.e. *Act5C*, *TinCΔ4*, *HandC*) by standard crosses, and verify TARGET line generation by PCR, and adult-only GFP expression.

2) Investigate the temporal requirement for *Fit* expression in controlling adult heart function.

3) Assess morphological and functional consequences of consequences of *Fit* gene depletion in the adult stage.

6.3 Results

6.3.1 Generation of TARGET flies and verification of their temperature-sensitivity

TARGET (*GAL4-GAL80^{ts}*) flies that have *GAL4* and *GAL80^{ts}* on different chromosomes were generated by using the crossing schemes shown in Figure 6.2 for Actin5C (*Act5C-GAL4; tubGAL80^{ts}*), Figure 6.3 for Tinman (*tubGAL80^{ts}; tinCΔ4-GAL4*), and Figure 6.4 for Hand (*handC-GAL4; tubGAL80^{ts}*) flies using previously generated lines (see Methods section). In brief, the GAL4-containing line and the GAL80^{ts} line were both crossed to multiply balanced stocks (in this case, *w*; Kr^{If-1}/CyO; D^{1}/TM3, Ser^{1}*) so both the 2nd and 3rd chromosome genotype could be followed in subsequent crosses. These [GAL4/Balancer; +/Balancer] and [+/Balancer; GAL80^{ts}/Balancer] lines were then crossed to each other in order to get flies that carry both GAL4 and GAL80^{ts} (e.g. GAL4/Balancer; GAL80^{ts}/Balancer). The resulting flies were then self-crossed and the balancers were selected against to achieve [GAL4/GAL4; GAL80^{ts}/ GAL80^{ts}] flies.

Genomic PCR was performed to check for presence/absence of GAL4/GAL80^{ts} transgenes in all lines generated. As can be seen from Figure 6.5A, GAL80^{ts} was not detected by PCR of genomic DNA in GAL4 lines and GAL4 was not detected in GAL80^{ts} lines. In Figure 6.5B, both GAL4 and GAL80^{ts} PCR products were detected in TARGET lines. Therefore, each TARGET line was generated successfully.

To confirm presence of both GAL4 and GAL80^{ts} and to show gene expression in the desired pattern, GAL4, and GAL4/GAL80^{ts} flies were crossed with

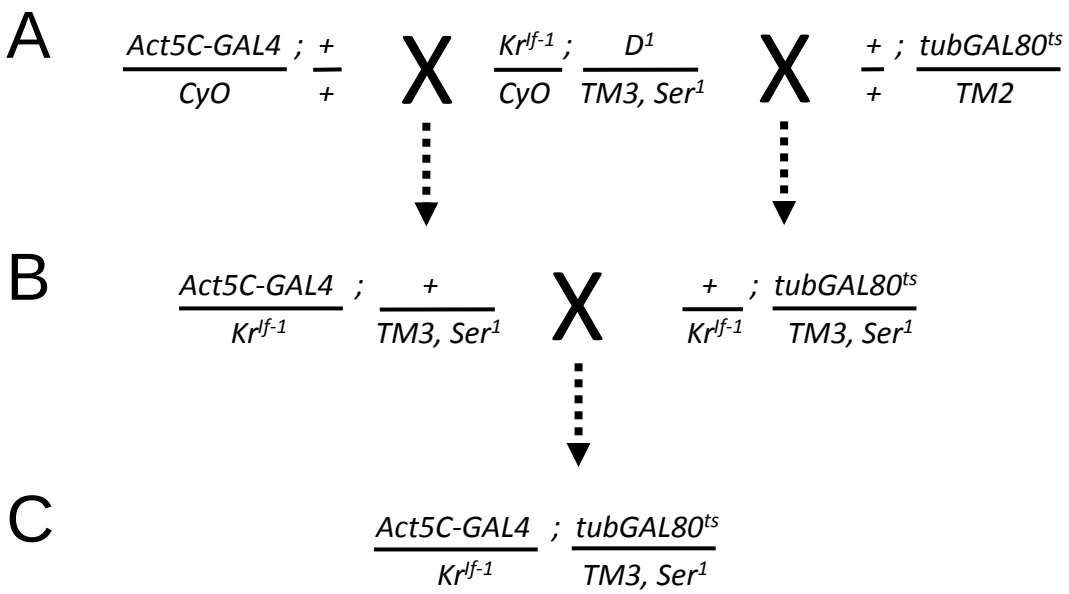

Figure 6.2. En masse crossing scheme for the generation of *Actin5C-TARGET* flies.

A, *Act5C4-GAL4/CyO* and *tubGAL80^{ts}/TM2* flies are crossed to multiply balanced flies, the aim is to balance both 2nd and 3rd chromosome so the genotype of each can be followed in subsequent crosses. **B**, selected progeny from each cross were then crossed together to achieve *handC-GAL4* and *tubGAL80^{ts}* in the same fly, both chromosomes balanced, **C**.

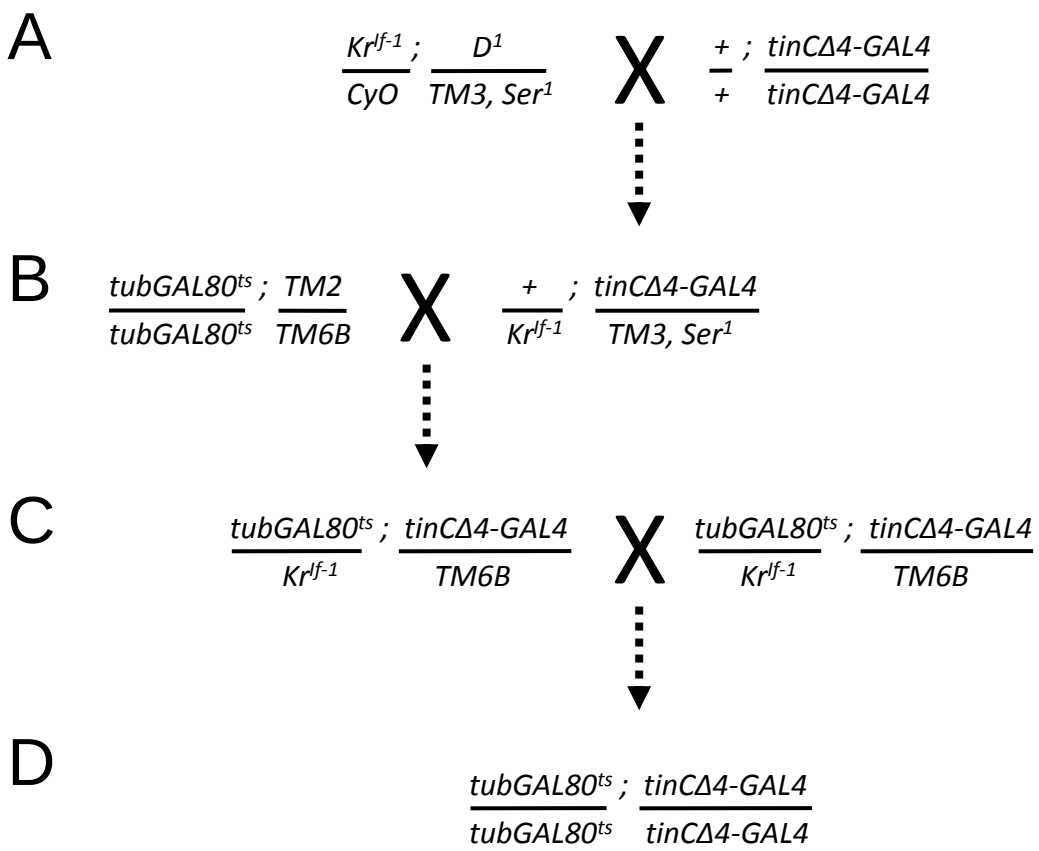

Figure 6.3. En masse crossing scheme for the generation of *Tinman-TARGET* flies.
A, *tinCΔ4-GAL4* flies are crossed to multiply balanced flies, the aim is to balance both 2nd and 3rd chromosome so the genotype of each can be followed in subsequent crosses. **B**, *tubGAL80^{ts}* flies already balanced on the 3rd chromosome are crossed to balanced *tinCΔ4-GAL4* flies. **C**, flies with both *tinCΔ4-GAL4* and *tubGAL80^{ts}* are self-crossed and progeny are selected without balancers (i.e. homozygous for both *tinCΔ4-GAL4* and *tubGAL80^{ts}*, **D**).

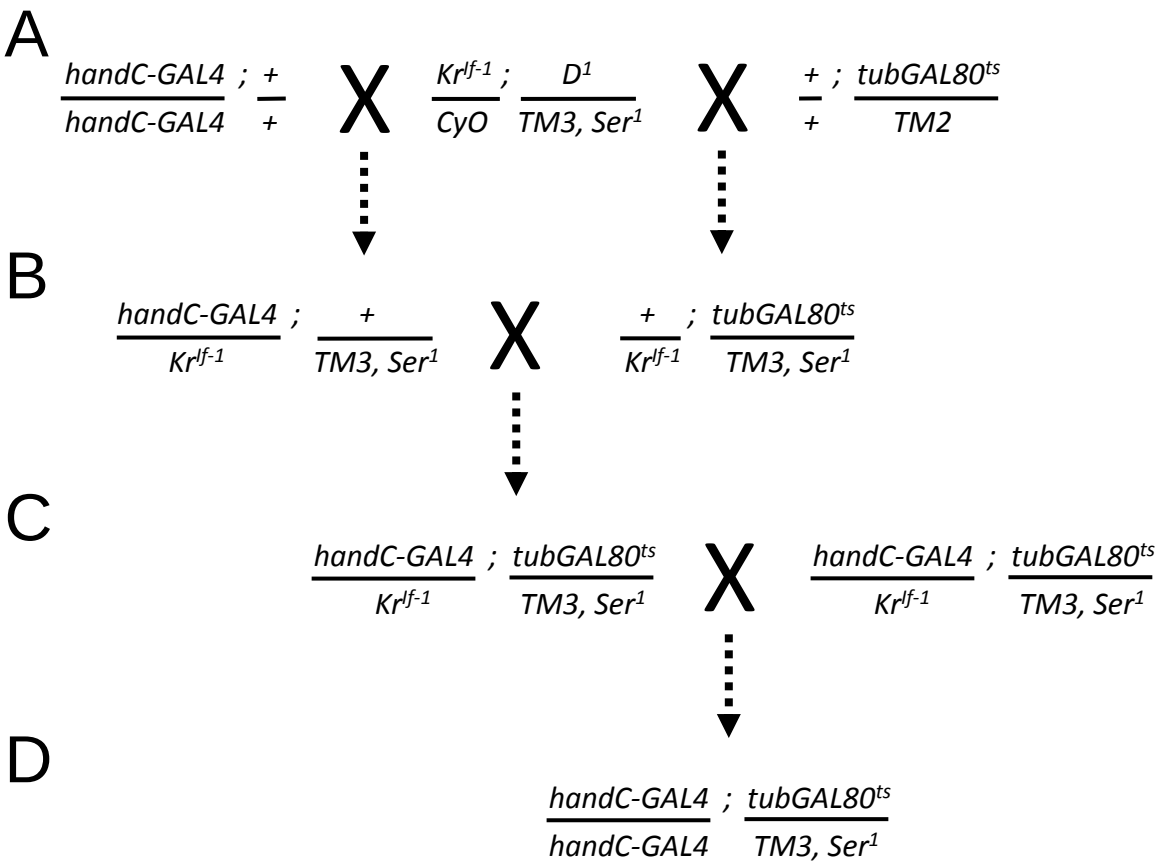

Figure 6.4. En masse crossing scheme for the generation of *Hand-TARGET* flies.

A, *handC-GAL4* and *tubGAL80^{ts}/TM2* flies are crossed to multiply balanced flies, the aim is to balance both 2nd and 3rd chromosome so the genotype of each can be followed in subsequent crosses. **B**, selected progeny from each cross were then crossed together to achieve *handC4-GAL4* and *tubGAL80^{ts}* in the same fly, both chromosomes balanced. **C**, flies with both *handC4-GAL4* and *tubGAL80^{ts}* are self-crossed and progeny are selected without balancers (i.e. homozygous for *handC4-GAL4* and *tubGAL80^{ts}/TM3, Ser^{1}*, **D**).

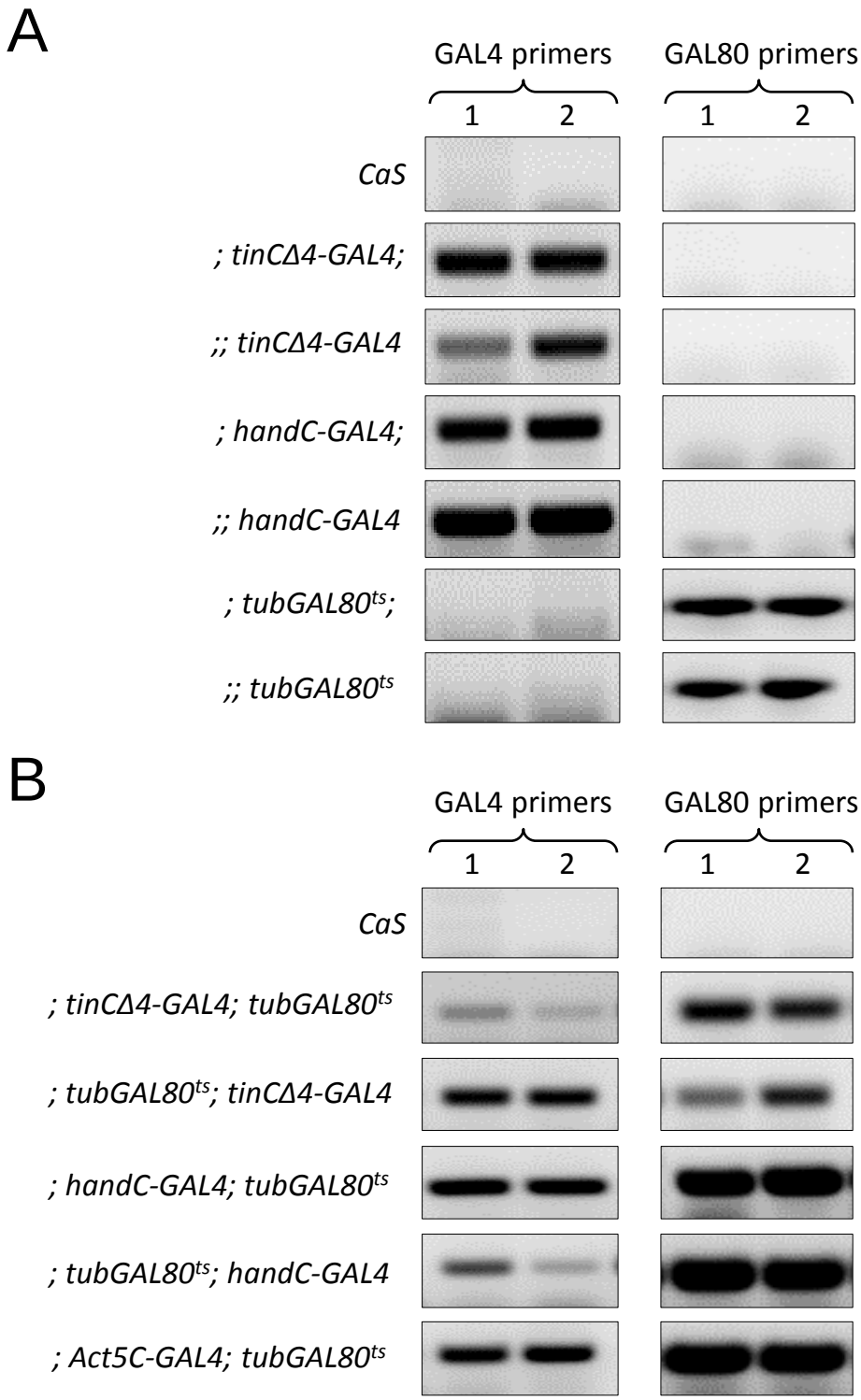

Figure 6.5. Genotyping via PCR of TARGET and non-TARGET flies using GAL4 and GAL80 primers.
A, Whole-fly PCR results (in duplicate) showing presence or absence of GAL4 and GAL80 in flies homozygous for either GAL4 ***OR*** tubGAL80^{ts}. *CaS* flies were used as a wild-type control. **B**, Whole-fly PCR results showing presence or absence of GAL4 and GAL80 in flies homozygous for GAL4 ***AND*** tubGAL80^{ts}. CaS flies were used as a wild-type control.

UAS-EGFP flies. Flies that harboured only GAL4 should express GFP protein in a manner corresponding to the pattern of expression regulated by the respective enhancer – i.e. tissue-specific – and should not dramatically change with temperature (DUFFY 2002). Flies that harboured both GAL4 and GAL80^{ts} will express GFP protein in a manner that corresponds to the expression of its enhancer, but only at the permissive temperature (i.e. 29°C). The following figures show *Actin5C-GAL4; tubGAL80^{ts}* (Figure 6.6), *tubGAL80^{ts}; tinCΔ4-GAL4* (Figure 6.7) and *handC-GAL4; tubGAL80^{ts}* (Figure 6.8, Figure 6.9 shows close-up view) respectively – also included are positive GAL4/UAS (i.e. without GAL80^{ts}) controls to show presence of GFP at both 18°C and 29°C.

GFP in adult *TinCΔ4* hearts was cardiomyocyte-specific, with particularly strong signal in the valve-like ostial cells. In *Tin-TARGET* hearts, GFP signal was less obvious in the non-ostial cardiomyocytes, with discontinuous GFP expression along the length of the heart. GFP in adult *HandC* hearts was restricted to the PNs (strong signal) and cardiomyocytes (weaker signal – confirmed in Figure 6.9-F), with additional staining in the lymph glands (noticeable in Figure 6.8, top left panel).

6.3.2 Knockdown of *Fermitin* expression during development/remodelling led to significant cardiomyocyte dissociation

Since TARGET flies had been successfully generated, and were verified to be temperature-sensitive, the effect of *Fermitin* knockdown on cardiac morphology was assessed at different stages during development. From Chapter 5, it was shown that ablation of both *Fermitins* was required to produce a cardiomyopathy. Using the newly developed *Hand-TARGET* line, the effect of *Fit1^{VDRC}* overexpression (since

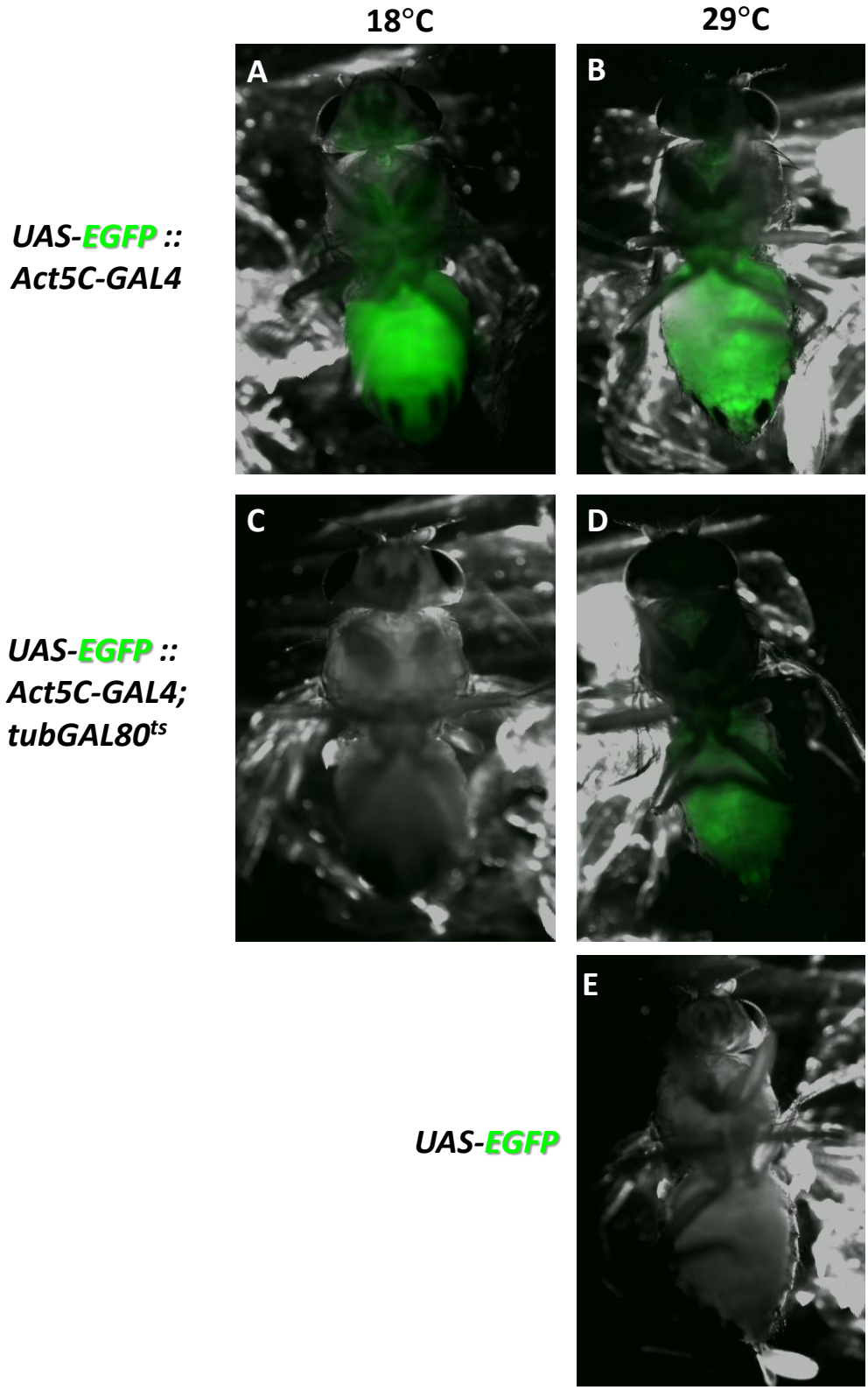

Figure 6.6. Utilisation of the TARGET GAL4/GAL80^{ts} system using *Act5C-GAL4* driver allows spatiotemporal control of global gene expression.

The temperature-sensitive GAL80 molecule represses GAL4 transcriptional activity at permissive temperatures, allowing the control of gene expression throughout development and/or adulthood. The temperature-sensitive repression/activation of GAL4 expressing EGFP is confirmed in the figures above. **A+B**) *UAS-EGFP/Act5C-GAL4*, **C+D**) *UAS-EGFP/Act5C-GAL4; tubGAL80^{ts}*, and **E**) *UAS-EGFP*.

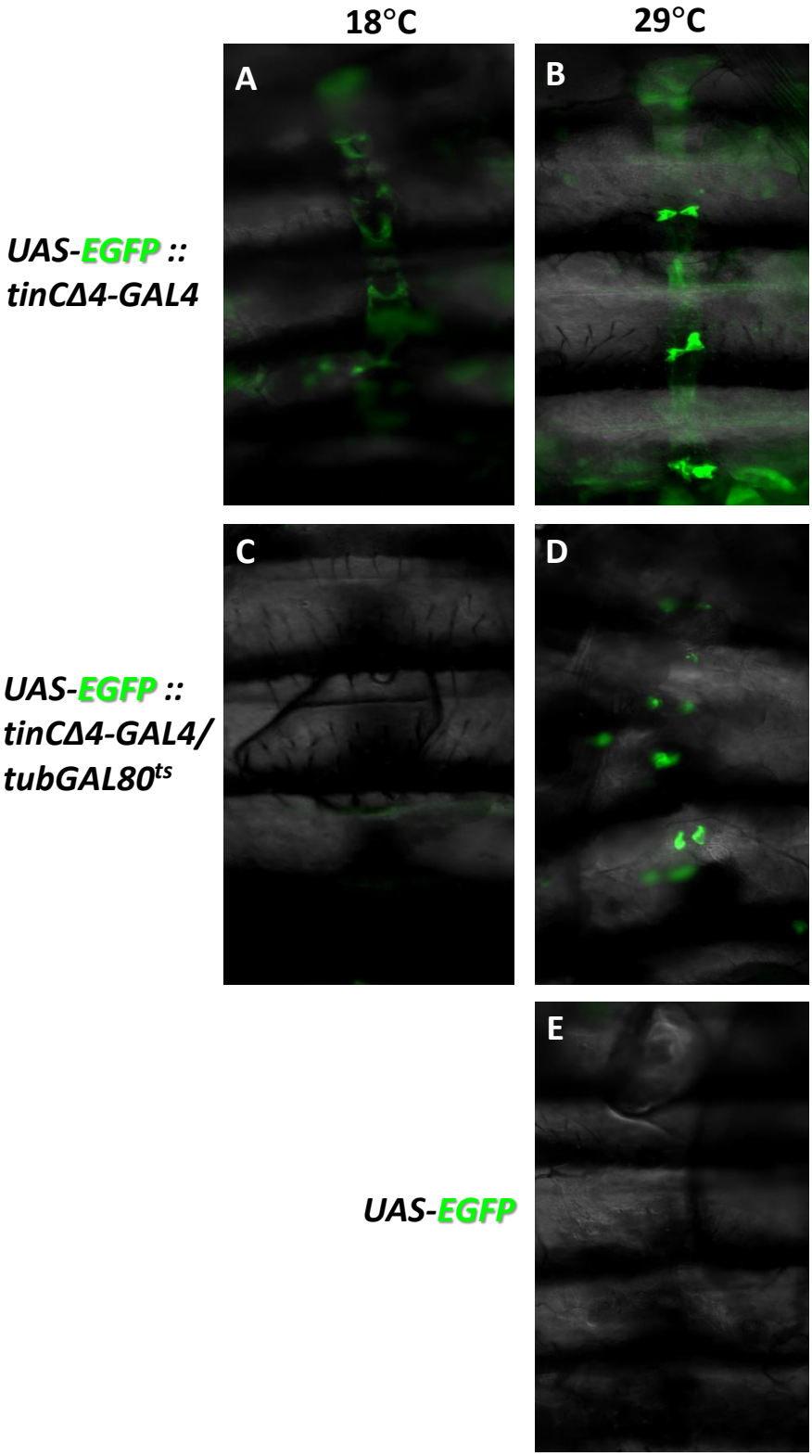

Figure 6.7. Cardiomyocyte-specific spatiotemporal control of gene expression using the *tinCΔ4-GAL4* driver.
The temperature-sensitive GAL80 molecule represses GAL4 transcriptional activity at permissive temperatures, allowing the control of gene expression throughout development and/or adulthood. The temperature-sensitive repression/activation of GAL4 expressing EGFP is confirmed in the figures above. **A+B**) *UAS-EGFP/tinCΔ4-GAL4*, **C+D**) *UAS-EGFP; tinCΔ4-GAL4/tubGAL80^{ts}*, and **E**) *UAS-EGFP*. GFP expression appears particularly strong in the valve-like ostial cells in the adult heart.

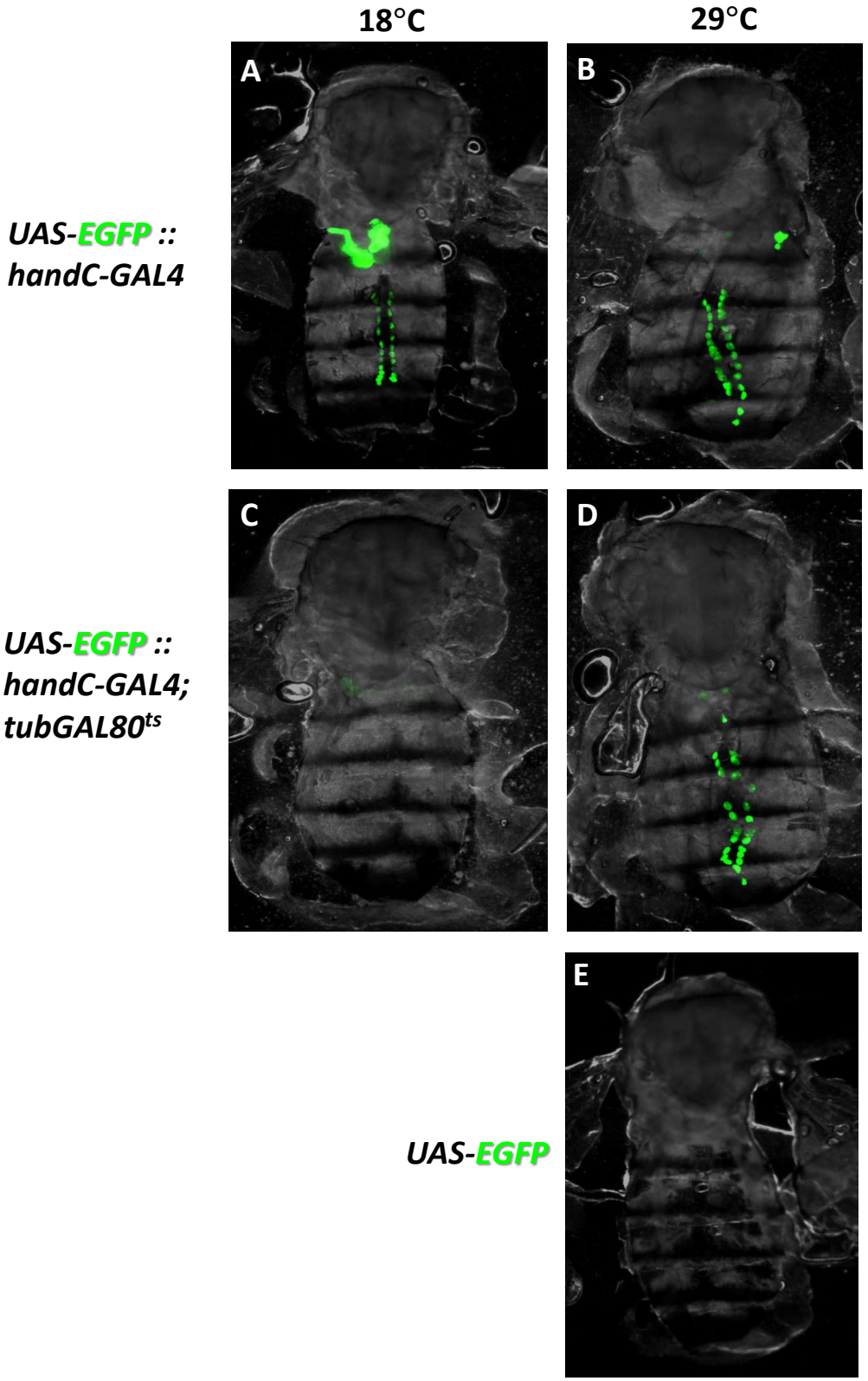

Figure 6.8. Heart- and haematopoeitic cell-specific spatiotemporal control of gene expression using the *handC-GAL4* driver.
The temperature-sensitive GAL80 molecule represses GAL4 transcriptional activity at permissive temperatures, allowing the control of gene expression throughout development and/or adulthood. The temperature-sensitive repression/activation of GAL4 expressing EGFP is confirmed in the figures above. **A+B**) *UAS-EGFP/handC-GAL4*, **C+D**) *UAS-EGFP/handC-GAL4; tubGAL80^{ts}*, and **E**) *UAS-EGFP*. GFP expression is particularly strong in the pericardial nephrocytes.

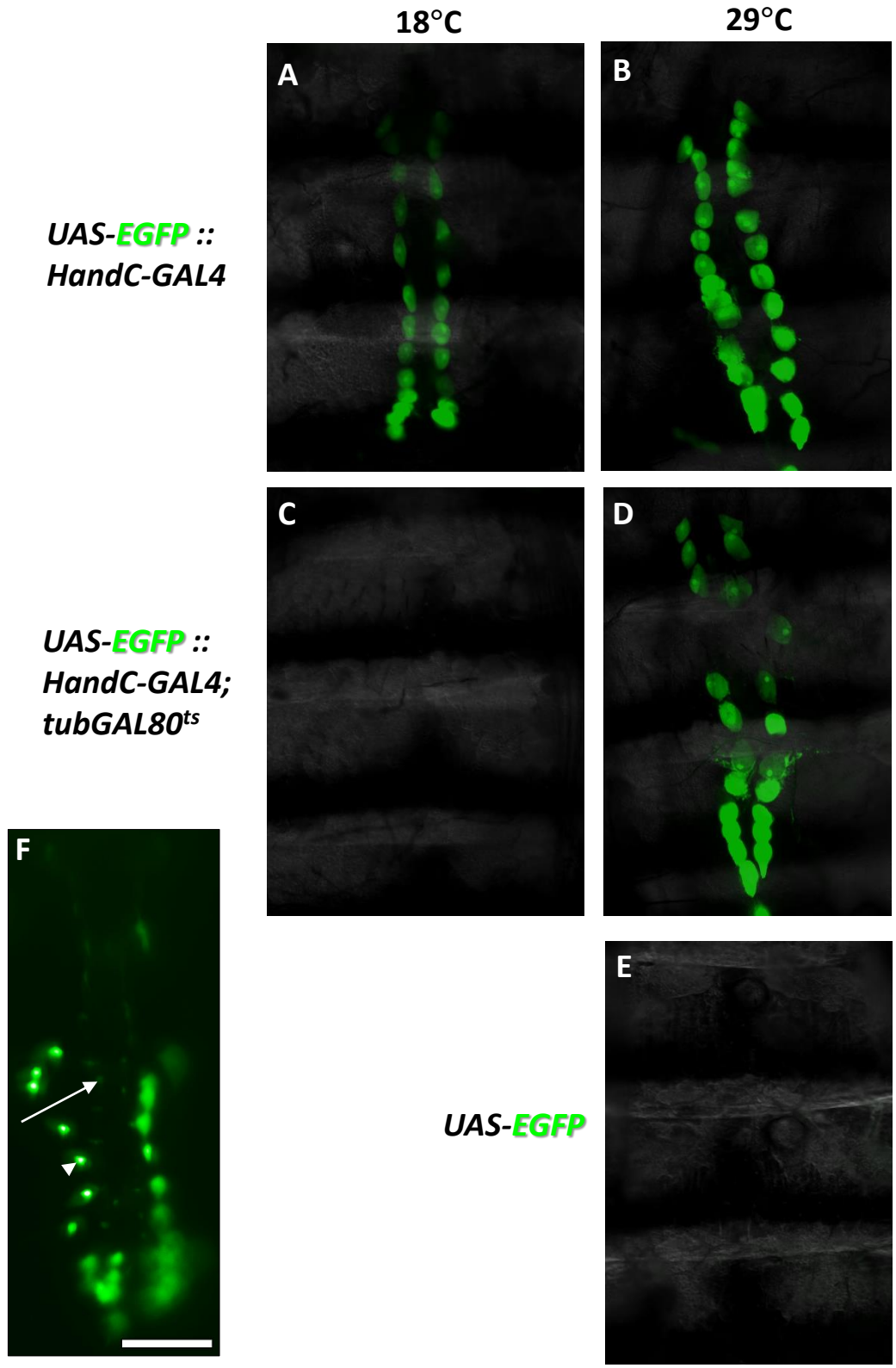

Figure 6.9. Closer view of the heart- and haematopoeitic cell-specific spatiotemporal control of gene expression using the *handC-GAL4* driver. The temperature-sensitive GAL80 molecule represses GAL4 transcriptional activity at permissive temperatures, allowing the control of gene expression throughout development and/or adulthood. The temperature-sensitive repression/activation of GAL4 expressing EGFP is confirmed in the figures above. **A+B**) *UAS-EGFP/handC-GAL4*, **C+D**) *UAS-EGFP/handC-GAL4; tubGAL80^{ts}*, and **E**) *UAS-EGFP*. F, overexposed heart image showing weaker GFP signal in cardiomyocytes (arrow) compared to pericardial nephrocytes (arrowhead), scale bar = 100µm.

the *Fit1*^{VDRC} line had been shown to affect both *Fermitins*, and since the double *Fit1+2*^{VDRC} line had not been generated at this point) on cardiac morphology during different stages of development was assessed. Figure 6.10 shows the experimental timeline with 5 different experimental groups, all flies were genetically identical (i.e. *Hand-GAL4/UAS-Fit1*^{VDRC}*; tubGAL80*^{ts}). As shown in Figure 6.11 (and quantified in Figure 6.12), flies raised at 18°C (i.e. without *Fit1*^{VDRC} RNAi overexpression) have hearts that were morphologically identical to wildtype, confirming the successful repression of GAL4 by the GAL80 protein at this non-permissive temperature. Similarly, flies raised at 18°C then *Fit1*^{VDRC} expression switched on after eclosion (and kept at 29°C for 7 days) had hearts that were not different compared to controls. Only when *Fit1*^{VDRC} was switched on during a developmental/remodelling stage did there appear to be cardiomyopathy. When *Fit1*^{VDRC} was switched on from the beginning of pupal stage through to eclosion and adulthood, there was a significant (p<0.05 vs 18°C 'OFF' control) disconnection of adjacent cardiomyocytes which appeared to affect the anterior portion (i.e. spanning A1-A2 abdominal segments) of the adult heart – i.e. one of the heart portions significantly remodelled during metamorphosis (Lo *et al.* 2007). When *Fit1*^{VDRC} was overexpressed during embryonic/larval development, then switched off subsequently from pupation/adulthood, the cardiomyocyte-dissociation phenotype caused significant cardiomyocyte dissociation (p<0.001 vs 18°C 'OFF' control) along the entire length of the heart – i.e. as opposed to just the A1-A2 anterior end. The most severe cardiomyocyte 'rounding-up' phenotype, however, occurred when *Fit1*^{VDRC} was overexpressed throughout development *and* metamorphosis – i.e. mimicking *Hand-*

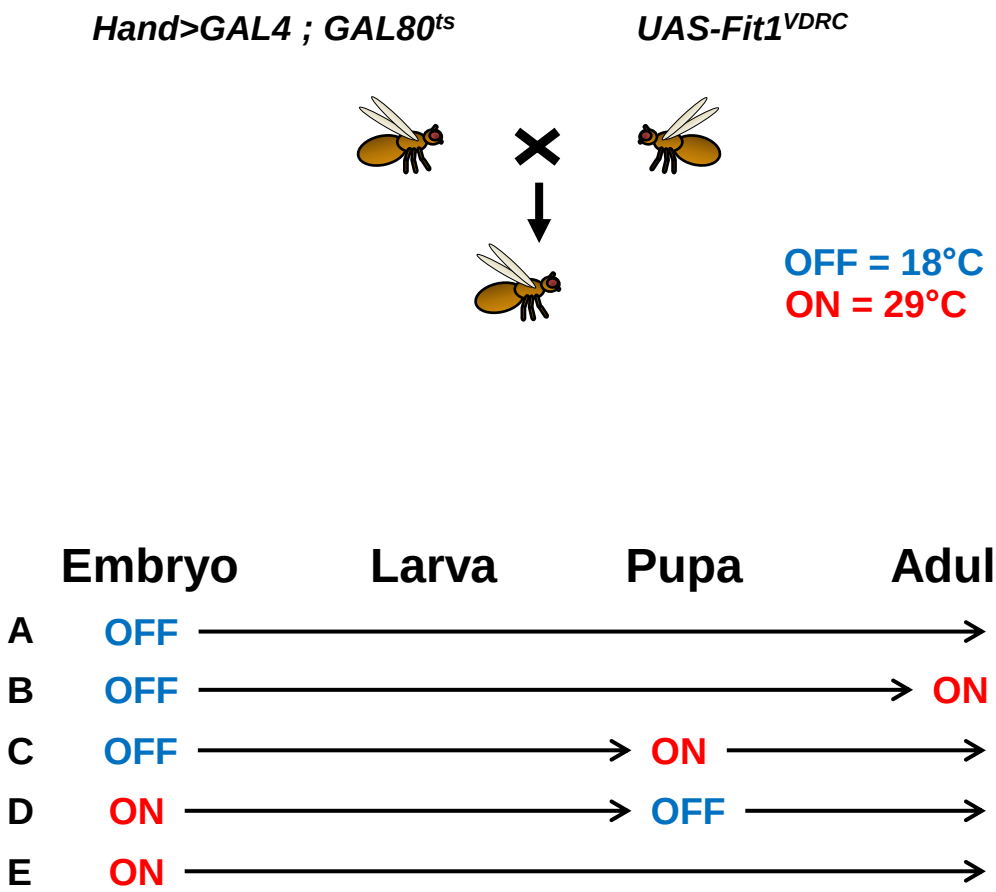

Figure 6.10. Controlling *Fit1* gene expression at different stages of development using the Hand-TARGET system.
Schematic showing when *Fit1* RNAi was switched ON (29°C)/OFF (18°C) in *Hand*-expressing cells during development.

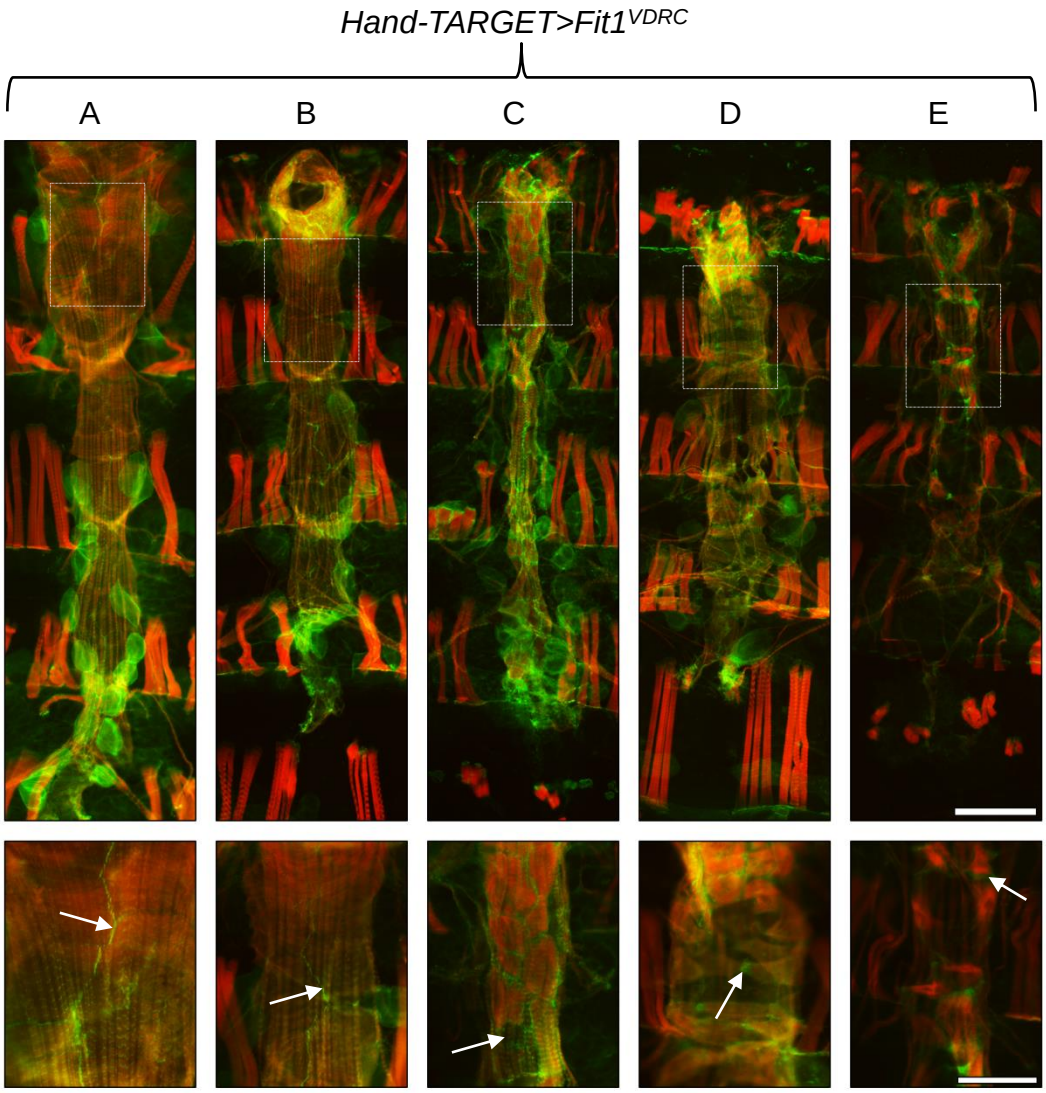

Figure 6.11. Disrupting *Fit1* expression is most damaging to cardiac morphology during development/remodelling.
Images correspond to the labels from the schematic in Figure 6.10, the lower panels are higher magnification images corresponding to the white dotted boxes in the upper panels. Wildtype heart morphology in hearts not exposed to *Fit1* RNAi (**A**). The junctions between opposing cardiomyocytes are indicated with the white arrow in the lower panel. Similarly, when *Fit1* RNAi was OFF until eclosion and ON thereafter (**B**), hearts appeared no different from wildtype. Heart morphology was significantly disrupted when *Fit1* RNAi was ON from early pupal stage (**C**), showing disrupted cardiomyocytes at the anterior end of the heart. White arrow in lower **C** panel indicates gap where cardiomyocyte should be. Cardiac disruption was even more pronounced when *Fit1* RNAi was ON during embryonic/larval development - affecting the entire length of the heart (**D**). White arrow in lower **D** (and **E**) panel indicates β-integrin staining between disrupted cardiomyocytes. The heart was most disrupted when *Fit1* RNAi was ON throughout development, with significant loss of cell contact between cardiomyocytes (**E**). Hearts are stained with Alexa-conjugated phalloidin (red), and anti-βPS integrin antibody (green). Scale bar = 100μm (upper panels), 50μm (lower panels).

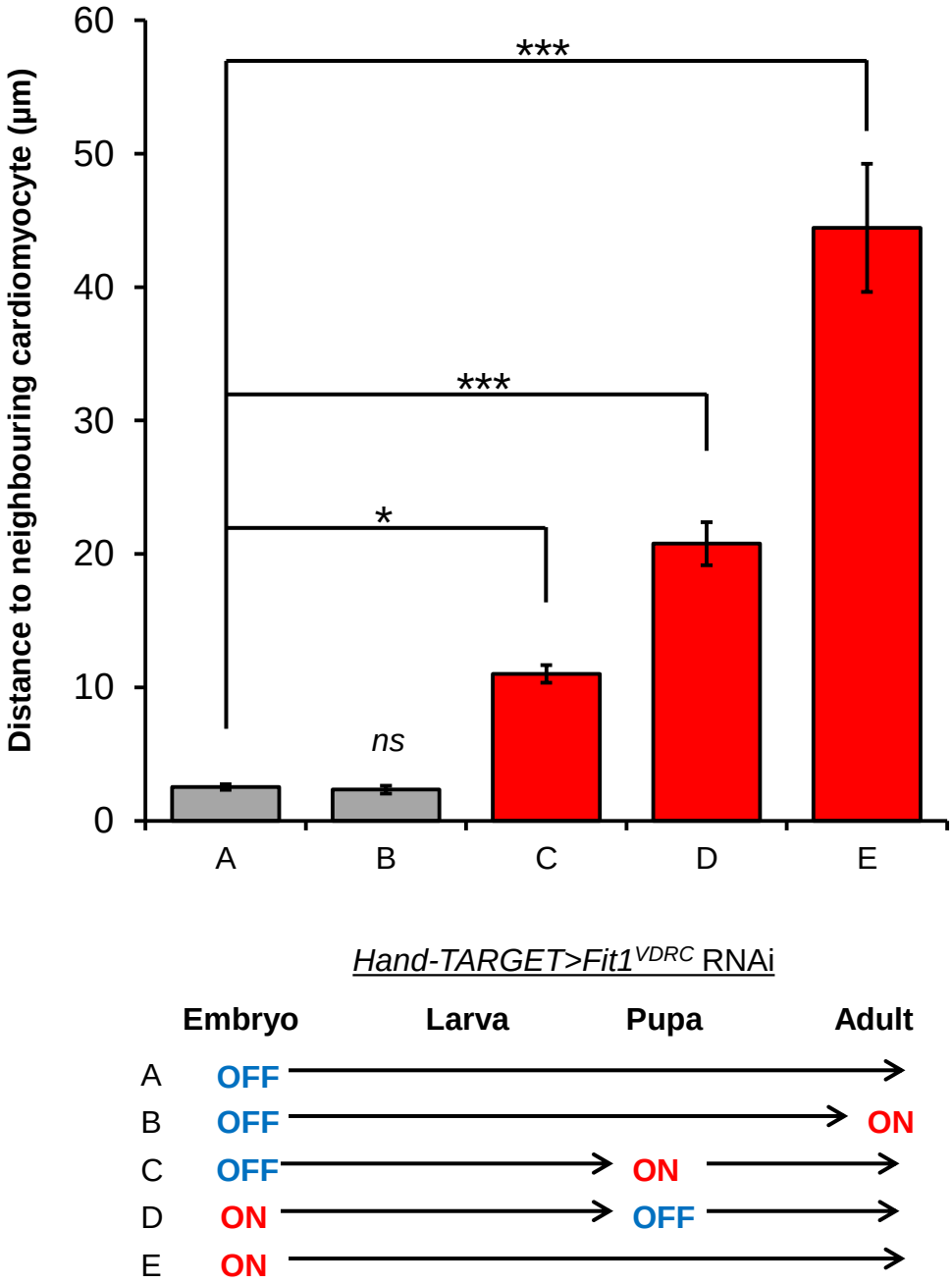

Figure 6.12. Quantification of the average distance between neighbouring cardiomyocytes from the different TARGET conditions.

There was no significant difference between hearts with *Fit1*^{VDRC} RNAi switched OFF throughout development, and those with RNAi switched ON after eclosion (**A** vs **B**). Distances between neighbouring cardiomyocytes were significantly greater in hearts with *Fit1*^{VDRC} RNAi switched on during developmental- (**C**) and remodelling (**D**) stages compared to controls. Cardiomyocyte distances were most pronounced in hearts that had *Fit1*^{VDRC} RNAi switched ON throughout development (**E**). Four measurements were taken for each fly heart, with 4 flies were used for each genotype (i.e. 16 measurements per genotype). Means were calculated and plotted. One-way analysis of variance (ANOVA) followed by Tukey's post-hoc test was used to identify differences between the means derived from uneven sample sizes. ***p<0.001, *p<0.05, error bars indicate ±SEM.

GAL4>UAS-Fit1^{VDRC} hearts without *GAL80*^{ts} – which caused significant (p<0.001 vs 18°C 'OFF' control) 'rounding up' of cardiomyocytes.

6.3.3 *Fermitin*-knockdown in the adult heart via the TARGET system resulted in cardiomyopathy

Since there appeared to be no significant effects caused to cardiac morphology after *Fit1*^{VDRC} overexpression during adulthood, it was hypothesised that 7 days of adult-only expression may not have been long enough for a phenotype to be revealed. Therefore, the effect of long-term (i.e. 3 weeks) *Fit* knockdown on cardiac morphology was examined and quantified in the adult heart. As a positive control for deleterious effects on the adult heart, the *UAS-Reaper* line was used. Overexpression of *Reaper* is a well-studied way of inducing apoptosis when it is overexpressed using the GAL4 system (WING *et al.* 1999). *Fit1*^{VDRC} was again utilised, and *Fit1+2*^{VDRC} (which had been generated by this point) was also used to ablate *Fit* expression in the adult heart.

As shown in Figure 6.13, there was no significant effect of *Reaper*-, and *Fit1*^{VDRC}-overexpression on cardiac morphology after 3-weeks compared to control hearts (i.e. *Hand-TARGET>w*^{1118}). However, there was significant (2.67µm (±0.30) *w*^{1118}*; Hand-TARGET* vs. 4.73µm (±0.50) *Hand-TARGET> Fit1+2*^{VDRC}, *p<0.001*) cardiomyocyte dissociation in *Hand-TARGET>Fit1+2*^{VDRC} hearts compared to control hearts. To verify TARGET>*Fit* knockdown in the adult heart after 3-weeks, RT-PCR on extracted heart tissue was performed. As shown in Figure 6.14, both *Fit1* and *Fit2* mRNA levels were knocked-down in *Hand-TARGET>Fit1*^{VDRC} hearts compared to *Hand-TARGET>w*^{1118} hearts.

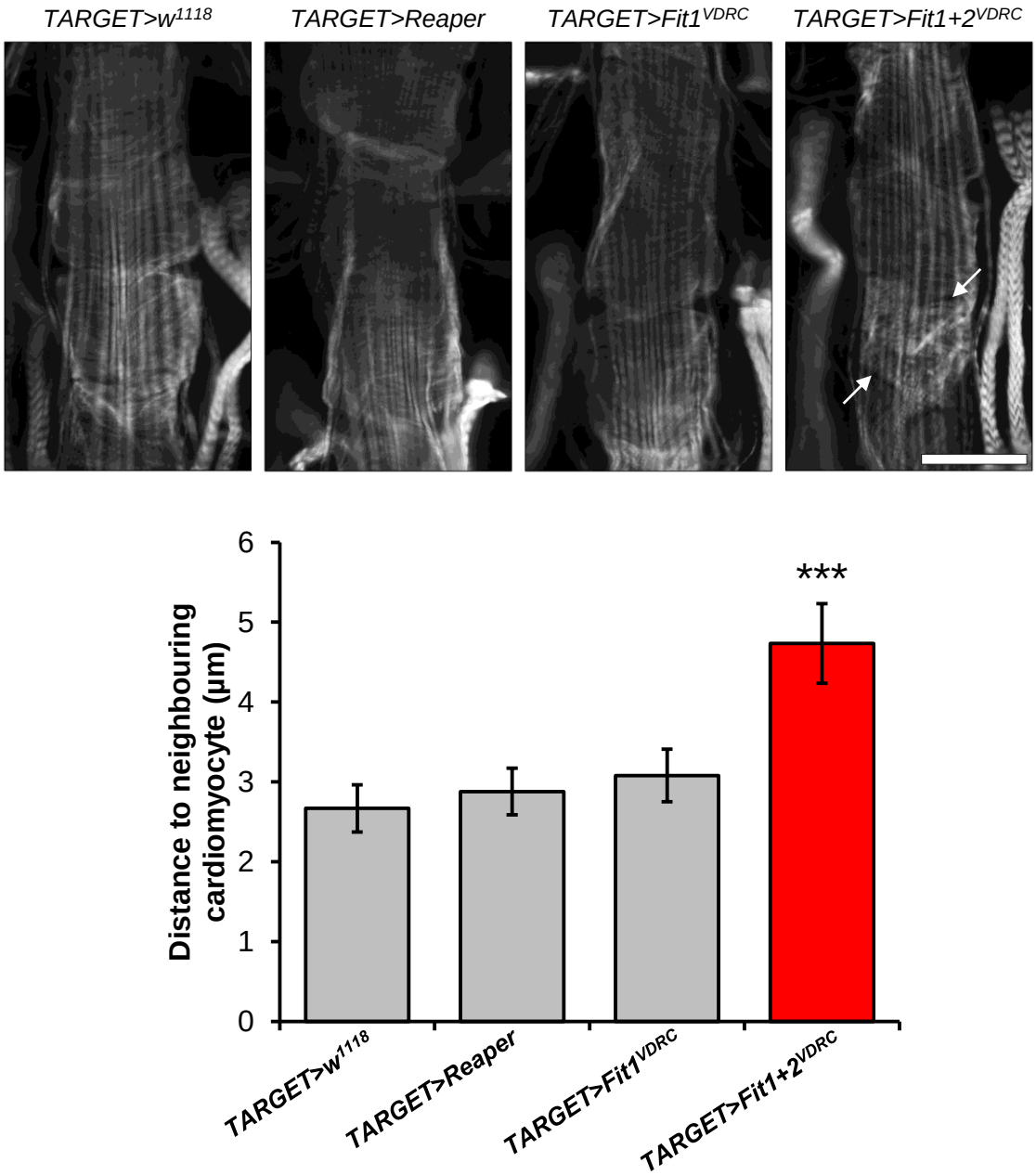

Figure 6.13. Only knockdown of both *Fermitins* in the adult heart using the TARGET system had an effect on cardiac morphology.
Since TARGET-knockdown of *Fit1*^{VDRC} had such a dramatic phenotype during development/remodelling, *Reaper*, *Fit1*^{VDRC}, and *Fit1+2*^{VDRC} were all ectopically expressed in the adult heart from eclosion for 3-weeks. *TARGET>Fit1+2*^{VDRC} hearts exhibited significant cardiomyocyte dissociation compared to *TARGET>w*^{1118} controls. There was no difference in cardiac morphology compared to controls in any of the other lines tested. Hearts were stained with Alexa-conjugated phalloidin. Arrows indicate gaps between neighbouring cardiomyocytes. Scale bar = 50µm. Four measurements were taken for each fly heart, with 4 flies were used for each genotype (i.e. 16 measurements per genotype). Means were calculated and plotted. One-way analysis of variance (ANOVA) followed by Tukey's post-hoc test was used to identify differences between the means derived from uneven sample sizes. ***p<0.001, error bars indicate ±SEM.

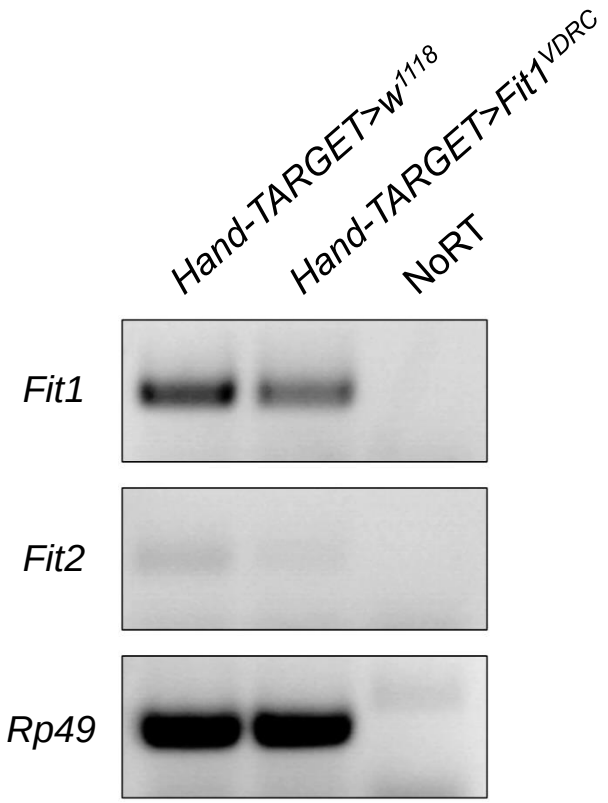

Figure 6.14. *Fit1*- and *Fit2*-knockdown in *Hand-TARGET>Fit1^{VDRC}* flies after 3 weeks at 29°C.
TARGET flies were raised at 18°C until eclosion, then kept for 3-wk at 29°C. Hearts were then removed from adult females (*n* = 15 per genotype) and RT-PCR was performed. Both *Fit1* and *Fit2* gene expression appears to be lower in *Hand-TARGET>Fit1^{VDRC}* flies compared to controls (*Hand-TARGET>w^{1118}*). NoRT samples show no band, meaning only cDNA is being amplified.

6.3.4 *Fermitin*-knockdown in the heart during adulthood via the TARGET system caused significant cardiac arrhythmia

Heart function was also tested in these flies, and the results of this experiment are shown in Figure 6.15. After 3-weeks of TARGET-overexpression, there was no significant difference in heart rate, diastolic interval, systolic interval, and end diastolic/systolic diameters (EDD/ESD) between genotypes. However, *Hand-TARGET>Reaper* flies had significantly shorter heart periods (0.60s (±0.07) w^{1118}*; Hand-TARGET* vs. 0.41s (±0.02) *Hand-TARGET>Reaper*, $p<0.05$), and a significantly lower degree of fractional shortening (0.44 (±0.01) w^{1118}*; Hand-TARGET* vs. 0.36 (±0.02) *Hand-TARGET>Reaper*, $p<0.05$) compared to controls. There was no significant difference in any functional parameters between *Hand-TARGET>Fit1*^{VDRC} hearts and controls. *Hand-TARGET>Fit1+2*^{VDRC} hearts, however, were significantly arrhythmic (0.20 (±0.03) w^{1118}*; Hand-TARGET* vs. 0.39 (±0.04) *Hand-TARGET> Fit1+2*^{VDRC}, $p<0.01$), and had a lower degree of fractional shortening (0.44 (±0.01) w^{1118}*; Hand-TARGET* vs. 0.37 (±0.02) *Hand-TARGET> Fit1+2*^{VDRC}, $p<0.05$) compared to controls.

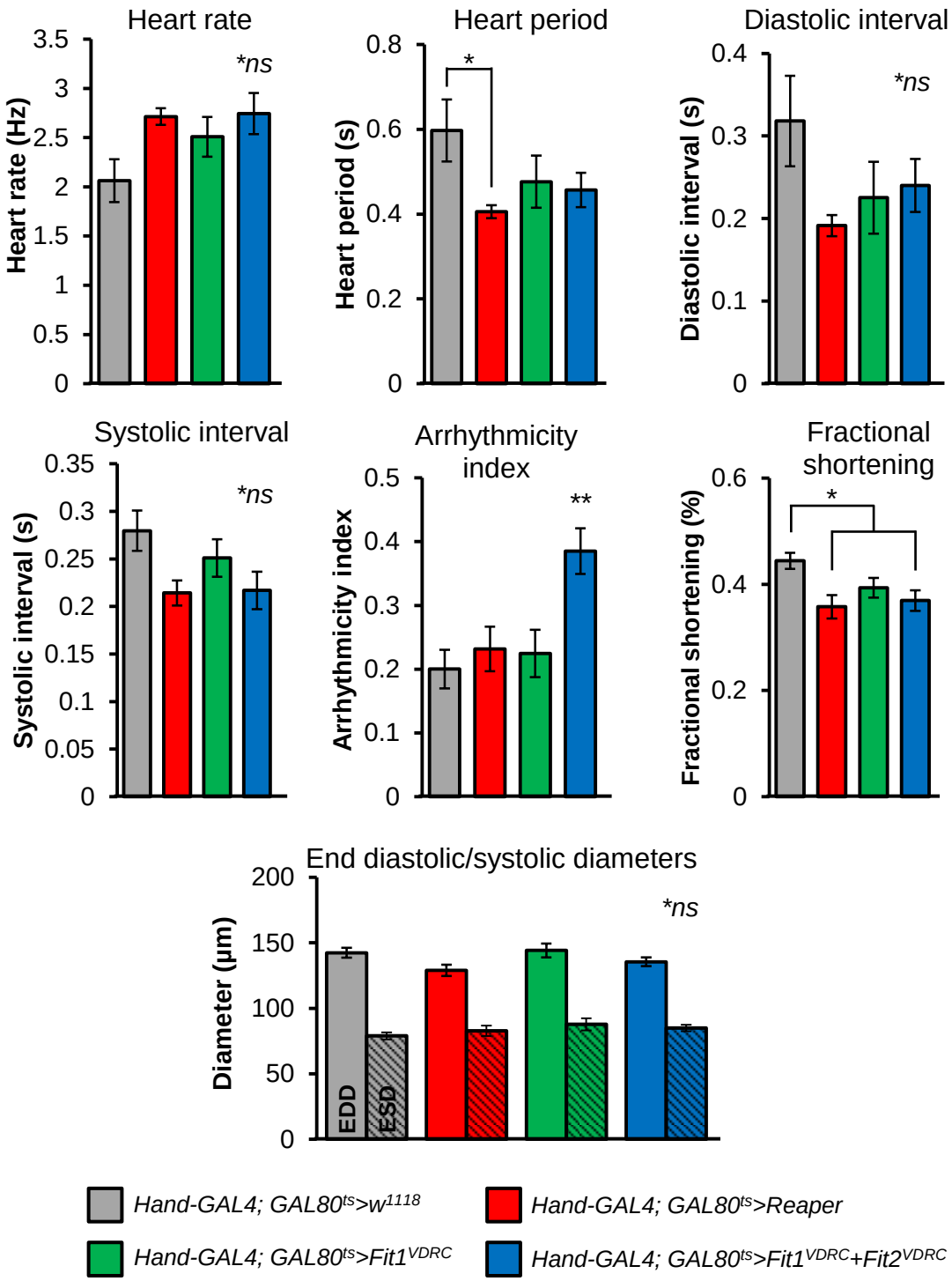

Figure 6.15. Heart function of different *Hand-GAL4; GAL80^{ts}* (TARGET) flies after 3 weeks at 29°C.

TARGET flies were raised at 18°C until eclosion, then kept for 3-wk at 29°C. There was no significant difference in heart rate, diastolic interval, or systolic interval between all genotypes. However, *TARGET>Reaper* hearts had a significantly shorter heart period, and degree of fractional shortening compared to *TARGET>w^{1118}* controls. *TARGET>Fit1^{VDRC}+Fit2^{VDRC}* flies exhibited significant arrhythmia, and reduced fractional shortening compared to controls. There was no difference in end diastolic diameter (non-shaded) and end systolic diameter (shaded) values between genotypes. Results are mean ± SEM, *n* = 13-16 flies per genotype. **p<0.01, *p<0.05, one-way ANOVA with Tukey's post-hoc test.

6.4 Discussion

The aim of the experiments in this Chapter was to knock down the *Fermitins* during different stages of the *Drosophila* life cycle to establish their relevance to cardiac syncytium development. This was done by generating and utilising a temporally controlled, cardiac-expressing model of gene expression. This also meant that since gene expression could be controlled during adulthood, and independently of developmental stages, it may potentially model the development of cardiac pathophysiology in ageing humans.

6.4.1 TARGET lines were successfully generated and verified

In summary, five different TARGET lines (i.e. one ubiquitous *Act5C-TARGET* line, two cardiomyocyte-specific *tinCΔ4-TARGET* lines (2^{nd} and 3^{rd} chromosome), and two heart and haematopoietic-specific *handC-TARGET* lines (2^{nd} and 3^{rd} chromosome)) were generated via standard crosses using pre-existing GAL4 and $GAL80^{ts}$ lines. The correct genotype was established by PCR, and the temperature-sensitivity verified by assessing GFP expression in adults.

In *Tin-TARGET>GFP* hearts, GFP expression was highly restricted to the cardiomyocytes – particularly enriched in three pairs of valve cells. These cells are known to be *Tin*-expressing cells, and develop from a discrete subset of aorta cells (ZEITOUNI *et al.* 2007). In *Hand-TARGET>GFP* hearts, GFP signal was restricted to the nuclei of cardiomyocytes, and PNs – and would also likely be expressed in garland cells and gut epithelial cells. GFP signal was noticeably much stronger in PNs compared to cardiomyocytes (ALBRECHT *et al.* 2006), and although GFP signal

was comparatively weaker, GFP was expressed in all cardiomyocytes (i.e. unlike *TinCΔ4*).

6.4.2 The *Fermitins* are critical for cardiac integrity during developmental and remodelling stages

Knockdown of the *Fermitins* led to the severe cardiomyocyte-dissociation phenotype – discussed at length in Chapter 5. *Fit1*^{VDRC} RNAi was shown to deplete both *Fit1* and *Fit2* mRNA (Chapter 5), and will henceforth be referred to as affecting both *Fit* RNA expression. To further investigate the temporal requirement of the *Fermitins* for the developmental of a functional cardiac syncytium, the newly generated *Hand-TARGET* flies were used to deplete *Fermitin* expression at different developmental stages by altering the temperature. *Hand-TARGET>Fit1*^{VDRC} animals were kept, at different stages of development, at either permissive (29°C) or non-permissive temperature (18°C) to dissect when *Fit*-knockdown exerted the most severe effects. An advantage of this experimental set-up was that, all of the flies tested were genetically identical – therefore any significant effects would be due to the conditions of the experiment rather than due to inherent differences in the genetic background of the flies. In essence, these flies acted as their own positive (29°C) and negative (18°C) controls. However, this experiment could still have benefited from genetic controls (e.g. *w*^{1118}*; Hand-TARGET* or *w*^{1118}*; Fit1*^{VDRC} flies) independent of temperature.

When raised throughout development at 18°C, these flies displayed no aberrant heart morphology (with hearts comparable to wildtypes), confirming the repressive action of GAL80^{ts} on GAL4. Conversely, when raised throughout

development at 29°C (i.e. with derepression of the inhibitory action of $GAL80^{ts}$ on GAL4), these hearts resembled the hearts of *HandC-GAL4>Fit1*^{VDRC} hearts (i.e. without $GAL80^{ts}$). When *Fit* RNAi was overexpressed from eclosion for 7 days there was no significant difference in cardiomyocyte morphology compared to controls. When *Fit* RNAi was overexpressed from pupal stage onwards (i.e. from metamorphosis through to adulthood), adjacent cardiomyocytes (particularly in the anterior section of the heart, including the conical chamber), dissociated from each other longitudinally as well as transversely. The cardiomyocyte-dissociation phenotype at the anterior portion of the heart may be explained by the fact that, although most of the adult heart is remodelled from the larval aorta during metamorphosis, the large conical chamber is significantly changed (both structurally and functionally) from the larval aorta cells from which it stems (CURTIS *et al.* 1999; ZEITOUNI *et al.* 2007). When *Fit* RNAi was overexpressed only during embryonic/larval stages, the cell adhesion phenotype affected the entire length of the heart, and cardiomyocytes did not appear as 'rounded-up' compared to hearts that had *Fit* RNA depleted throughout development, metamorphosis and adulthood – potentially indicating a slight rescue of the cardiomyocyte-dissociation phenotype during remodelling. Essentially, cardiomyopathy was significant when *Fit* RNAi was overexpressed during a developmental/remodelling stage.

At the time of performing these experiments, the double RNAi line *Fit1+2*^{VDRC} had yet to be generated, but *Fit1*^{VDRC} had been shown to affect both *Fit1* and *Fit2*. Further work using the *Fit1+2*^{VDRC} line should address the effect of more effective *Fit* knockdown on cardiac development. Most likely, the outcomes would be the same, but the cardiomyopathy phenotypes would be more severe – see

Hand>Fit1+2^{VDRC} images in Figure 4.7, and explanation in Figure 5.21. *In situ* hybridisation expression data for both *Fermitins* throughout development would help to elucidate when and where these genes are being expressed, and would highlight their importance at those times/in those areas. Many of the deleterious effects on the cardiac syncytium, apparently due to *Fit* depletion, could potentially be explained by varying levels of the GAL4 enhancer (in this case *Hand*) during development/metamorphosis, but this is unlikely as *Hand* expression is relatively constant throughout *Drosophila* development (GRAVELEY *et al.* 2011).

6.4.3 Expression of the pro-apoptotic gene, *Reaper*, during adulthood did not significantly affect cardiac morphology

It was possible that 7 days of adult-only expression may not have been long enough for a morphological phenotype to be revealed in adult-only *Hand-TARGET>Fit1*^{VDRC} hearts – see Figure 6.11. Therefore, the effect of long-term (i.e. 3 weeks) *Fit* knockdown in the adult heart was assessed – using both *Fit1*^{VDRC} and *Fit1+2*^{VDRC} lines. The pro-apoptotic gene, *Reaper*, was used as a positive control for deleterious effects on adult heart morphology – i.e. after 3-weeks of Reaper expression in these adults, hearts would likely be damaged.

Surprisingly, *Reaper* did not appear to have any significant effect on cardiac morphology after 3-weeks, but did appear to affect some aspects of cardiac function. Although, without adequate staining for apoptotic markers (e.g. TUNEL, cleaved-Caspase-3) that may highlight apoptotic cells, it is difficult to interpret these findings. It could be argued that the *Hand* enhancer driving GAL4 expression is too weak to induce apoptosis in adult cardiomyocytes (GRAVELEY *et al.* 2011). However,

there is still noticeable GFP signal in *Hand-TARGET>GFP* cardiomyocytes (see Figure 6.9), even though PN-GFP signal was stronger. Additionally, *Reaper*-overexpression appeared to have no effect on PN morphology, indicating there may be a compensatory mechanism preventing apoptosis in these cells. It is also possible, there is no effect of *Reaper* expression during adulthood as tissues (that require *Reaper* expression) have already been formed, a finding confirmed by studies testing the potencies of different effector genes (including *Reaper*) in the adult *Drosophila* neural system (THUM et al. 2006). Thum and colleagues found *Reaper*-dependent ablation in adults to be of limited use – especially when compared with more effective *Kir2.1*, *TNT*, and shi^{ts1} effector genes. However, adult-only *Reaper* expression has been shown to ablate glial cells effectively (GHOSH *et al.* 2011), though these authors used a different method of adult-only *Reaper* expression than the present data/Thum and colleagues.

6.4.4 Overexpression of *Fit* RNAi during adulthood resulted in significant cardiomyocyte-dissociation and arrhythmia – a potential model of adult-onset cardiac arrhythmogenesis caused by cardiomyocyte-adhesion failure?

Heart morphology and function was also assessed in *Hand-TARGET>Fit1+2*^{VDRC} adults, with these hearts also exhibiting moderate but significant cardiomyocyte-dissociation with accompanying loss of contractile function, and a significantly higher degree of arrhythmia compared to controls. Both *Fit1* and *Fit2* gene expression also appeared to be depleted in extracted heart tissue – indicating RNAi was being expressed. The increase in arrhythmia, therefore, may potentially be explained by the degeneration of cardiomyocyte-coupling caused by *Fit* depletion. Interestingly, morpholino-knockdown of *Kind2* in zebrafish also led to

a decrease in ventricular fractional shortening, but cardiac rhythmicity was apparently not investigated in this model (DOWLING *et al.* 2008a). It would be predicted that *Kind2*-knockdown hearts would also be significantly arrhythmic compared to controls.

The present result (i.e. loss of junctional integrity in *Fit* RNAi-overexpressing adult cardiomyocytes leading to significant cardiac arrhythmia), potentially indicates a failure of the chemical/electrical/mechanical coupling between adjacent cardiomyocytes in the *Drosophila* heart. Knocking down the *Fits* and disrupting the intercalated disc-like junctions in the adult *Drosophila* heart may also provide a way to model the loss of *Kind2* in human hearts and its hypothesised role in intercalated disc function – illustrated in Figure 6.16.

Further work would include the examination of these lines after 3-weeks at 18°C (i.e. repressive temperature; as well as 29°C), which should have no impact on transgene expression and should not affect heart morphology/function. This is an important control which, in hindsight, would have helped support the conclusion that the significant effects on heart morphology/function exhibited at 29°C were due to the transgene being switched on, rather than a potential background effect. Additionally, the $Fit2^{VDRC}$ RNAi line should also be tested for effects on cardiac morphology/function.

Transmission electron micrographs may be useful in this instance, to visualise any pathological signs indicating loss of junctional integrity – since normal immunohistochemistry did not reveal differences. Similarly, staining for proteins involved in cardiomyocyte-cardiomyocyte signalling (e.g. gap junction proteins) may

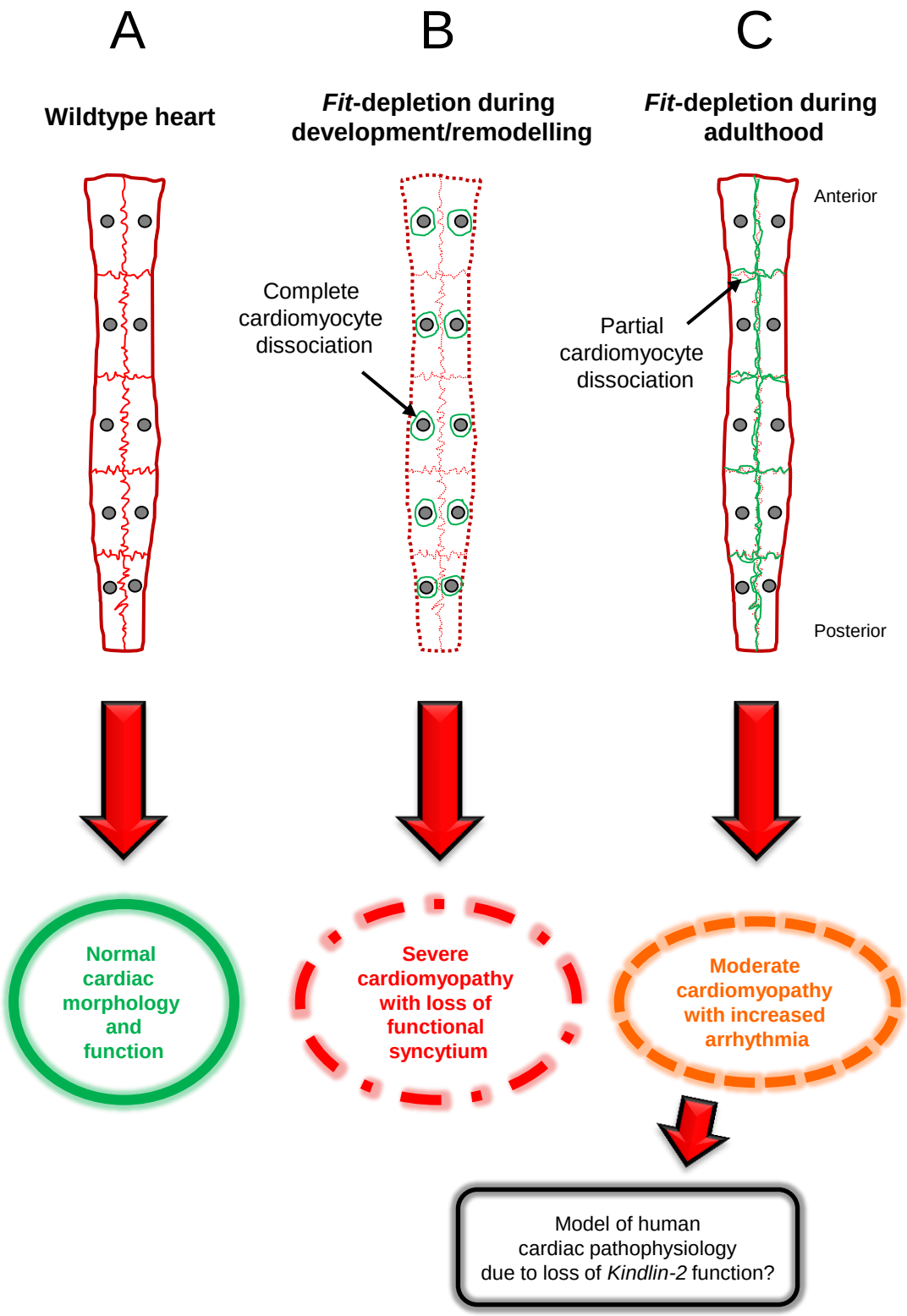

Figure 6.16. Model illustrating effects of *Fermitin* knockdown during development/remodelling and adulthood in the *Drosophila* heart.

A, the wildtype fly heart with fully coupled cardiomyocyte junctions has normal cardiac morphology and function. **B**, loss of *Fit* in the heart during development/remodelling causes severe cardiomyopathy with loss of the functional syncytium. **C**, loss of *Fit1* in the heart during adulthood causes moderate cardiomyopathy with loss of some junctional integrity and an increase in arrhythmia. Loss of *Fit* function in the adult *Drosophila* heart may potentially be used to model loss of *Kindlin* function in the adult human heart.

be informative. From the RT-PCR result, it appeared that *Fit* gene expression was depleted in the hearts of 3-wk old *Hand-TARGET>Fit1+2*^{VDRC} adults. However, since GAL4 also drives transgene expression in the PNs, it is unclear the degree of *Fit* depletion in the cardiomyocytes. Developing a method to measure gene expression levels specifically in the cardiomyocytes (i.e. without associated tissues including PNs) will be essential for the assessment of cardiac-specific gene expression and knockdown.

It would also be important to investigate the effects of adult-only depletion of other cardiomyocyte adhesion proteins – e.g. cadherin. An cardiac-specific inducible deletion of *N-cadherin* in mice led to the dissolution of the intercalated disc in these animals, followed by dilated cardiomyopathy (KOSTETSKII *et al.* 2005). These mice died during the first 2-months after *N-cadherin* deletion, and their deaths were described as "arrhythmic in nature", while β1-integrin was also upregulated in this model, indicating a compensatory mechanism. In same model, loss of *N-cadherin* in the heart resulted in a decreased ventricular conduction velocity, linked to the loss of Connexin-40 and -43 – i.e. electrical decoupling of the cardiomyocytes – which resulted in arrhythmogenesis (LI *et al.* 2005). Intriguingly, loss of *N-cadherin* in the heart using a non-inducible αMHC/Cre transgene led to embryonic lethality (PIVEN *et al.* 2011), while loss of β1-integrin using the same Cre promoter did not (SHAI *et al.* 2002) – giving weight to the "functional hierarchy" hypothesis of different cell adhesion systems, with cadherin-based adhesion highly critical in the heart.

Additionally, chronic integrin activation in the heart - via a truncated version of α5-integrin ($\alpha_{5\text{-}1}$) - also resulted in intercalated disc disintegration, and significant arrhythmias (VALENCIK *et al.* 2006). Importantly, this group found that isolated

cardiomyocytes were functionally normal, and that electrical/mechanical uncoupling of adjacent cardiomyocytes was the reason for the deleterious phenotype.

6.4.5 Summary

In summary, the aim was to generate a system that allowed temporal control of cardiac-specific gene expression – thus paving the way for investigations into adult-only genetic ablation. These TARGET flies were successfully generated and verified – switching ON gene expression at the high permissive temperature, and switching OFF gene expression at non-permissive temperatures. It was subsequently found that *Fit* RNAi overexpression during developmental stages led to severe cardiomyopathies. *Fit* RNAi overexpression during adulthood significantly disrupted intercalated disc-like junctions and appeared to cause significant arrhythmia in these hearts. Therefore, the arrhythmogenesis exhibited in these adults was due to the cardiac disruption of the *Fermitins*. This result highlights the power of this model, and may offer insights into the aetiology of cardiac arrhythmias in humans. Indeed, it would be predicted from this model that disruption of KIND2 function in the myocardium may lead to increased risk of developing arrhythmia, due to problems in cardiomyocyte-cardiomyocyte adhesion.

Chapter 7

Discussion and future perspectives

7.1 Summary of findings

Mechanisms underlying the development of cardiomyopathies are often polygenic in aetiology, making investigations difficult for researchers. The fly heart is an invaluable tool with which to study the genetic and molecular mechanisms underlying heart function and development (CASAD *et al.* 2012; KIM *et al.* 2010; NEELY *et al.* 2010b; WOLF and ROCKMAN 2011). The aim of the research in this thesis was to develop (in our lab) the adult fruit fly as a model of human heart function, in order to screen for conserved genes affecting the development and function of the cardiac syncytium.

Baseline measures of heart function and other factors contributing to variability in heart function (age, and the time of day) were assessed to establish the adult *Drosophila* heart model. An *a priori* RNAi screen was then performed to deplete conserved genes in cardiomyocytes utilising the yeast GAL4/UAS system. By silencing *Fermitin 1* and *Fermitin 2* gene expression in the heart, the *Drosophila* orthologs of the essential cell-adhesion gene, *Kindlin 2* (*Kind2*, predicted to have a role in cardiomyocyte adhesion), caused severe cardiomyopathy characterised by the failure of cardiomyocytes to develop as a functional syncytium and loss of synchrony between cardiomyocytes. A predicted null allele of *Fit1* ($Fit1^{\Delta 161}$) was generated via P-element mobilisation, but this had no impact on heart development or function – though homozygotes exhibited a semi-lethal phenotype. Similarly, silencing *Fit2* failed to significantly affect heart development or function. In contrast, silencing *Fit2* in the cardiomyocytes of *Fit1*-null flies disrupted syncytium development, leading to severe cardiomyopathy. Temperature-sensitive GAL4/$GAL80^{ts}$ lines were generated

to deplete genes in the heart, and utilised to investigate effects of *Fit* knockdown during different stages of development. The strongest effect of *Fit* knockdown on adult cardiac morphology was exhibited during stages of heart development and remodelling, with significant cardiomyocyte decoupling – i.e. gaps between contiguous cardiomyocytes indicating a loss of junctional integrity. Additionally, *Fit* knockdown during adulthood led to moderate but significant cardiomyocyte decoupling with accompanying arrhythmia compared to control animals.

The data presented in this thesis provide clarity about the role of *Kind2* by demonstrating a cell autonomous role for this family in the development of a functional cardiac syncytium in *Drosophila*. The data also demonstrate the *Fermitins* can functionally compensate for each other in order to control syncytium development. This thesis supports the hypothesis that abnormalities in cardiomyocyte KIND2 expression or function may contribute to cardiomyopathies in humans.

7.2 *Drosophila* – an appropriate model organism for the study of human cardiac physiology?

As previously established, there are a variety of animal models which have been exploited for their similarity to the human heart, and on which many hypotheses have been based (ROSS and CHEN 2008). The experiments and conclusions from this thesis help affirm *Drosophila* as powerful genetic model with which to identify genes important for heart development/function, while establishing the fly as a valuable tool to study the development of heart function.

The most powerful aspect of the use of flies for heart research is the ability to easily perform genome-wide deficiency/RNAi screens, with subsequent manipulation of gene expression in a tissue- (and sometimes time-) specific manner. Additionally, manipulation of genes and investigation of phenotypes in higher eukaryotes can be complicated due to potential compensation by paralogs – for instance, in humans there are four versions of *Mef2*, while *Drosophila* harbours only one copy (OLSON 2006). In this thesis, the slightly more unusual instance of genetic and functional redundancy between paralogs in *Drosophila* was investigated.

In terms of gene expression manipulation, there is presently a lack of highly expressed and highly specific cardiomyocyte GAL4 drivers – particularly in the adult fly. The *TinCΔ4* driver is cardiomyocyte-specific but expression is weaker in adult hearts compared to *HandC*, with expression limited to specific subsets of cells (LO and FRASCH 2001). The *HandC* driver, on the other hand, is not cardiomyocyte-specific, with expression in nephrocytes and haematopoietic cells (SELLIN *et al.* 2006). There exists a *Tinman* GAL4 driver line (*GMH5-GAL4*) which contains multiply inserted GAL4/UAS and GFP-containing elements, that does show cardiomyocyte-specific expression in adult hearts (WESSELLS *et al.* 2004). However, this multiply inserted line (5 insertions on 3 chromosomes) is not suited to multiple cross schemes, and also requires selection of strong cardiac-GFP expressers every 2-3 generations as gene expression qualities can be lost over time (Robert Wessells and Karen Ocorr, personal communication). When this GAL4 driver was assessed, it was found that many of the cells in the heart were not GFP-expressing and therefore the line was not utilised in this thesis (data not shown).

7.2.1 The adult *Drosophila* heart and its potential as a tool to identify genes/pathways important for intercalated disc function/pathology in humans

The results presented in this thesis also highlight the intercalated disc-like junctions between adult fly cardiomyocytes as a (previously unexplored) model of the human intercalated disc. With the ability to manipulate gene expression in a stage-specific manner, the adult fruit fly could become a relevant model for screening genes important for intercalated disc function in humans, and cardiac pathogenesis by assessment of heart function either using videomicroscopy or non-invasive (but lower resolution) OCT methods. Thus far, studies concerning cardiomyocyte adhesion in *Drosophila* have primarily employed the embryo to investigate the role of cell adhesion dynamics in heart assembly (MEDIONI *et al.* 2008), whereas little research has been focussed on changes to adult cardiomyocyte-adhesion (ZEITOUNI *et al.* 2007). This exciting, feasible new line of investigation would bolster the practicality of the fruit fly as a model of human cardiac physiology.

Further work should aim to characterise these intercalated disc-like structures in the adult fly heart – also seen by Lehmacher *et al.* (LEHMACHER *et al.* 2012). Investigating the formation of the intercalated disc during embryogenesis would be a crucial first step, and would inform the study of the intercalated disc in the adult fly heart. Similarly, investigating the cardiomyocyte-junctions during remodelling of the non-contractile larval aorta into the robust abdominal fly heart may also elucidate the development of strong mechanical coupling between cardiomyocytes.

7.3 Cell-ECM-Cell adhesion in the adult *Drosophila* cardiac syncytium

Presently, the nature of the adhesion between cardiomyocytes in the adult *Drosophila* cardiac syncytium is unclear. It is likely there is cell-cell adhesion, with cadherin-based structures acting like a "zip" between adjacent cardiomyocytes, ensuring electrical/chemical/mechanical coupling between cells – see Figure 7.1A. Many of the mechanisms underlying cadherin-based cell-adhesion during cardiogenesis have been studied in the *Drosophila* embryo - with Slit/Robo/E-cadherin signalling playing a key role in establishment of the heart and lumen formation (MEDIONI *et al.* 2008; SANTIAGO-MARTINEZ *et al.* 2008) - but studies investigating the function of these processes in the adult are lacking (ZEITOUNI *et al.* 2007).

Alternatively, integrin-based cell-matrix adhesion could also form the basis of the adhesions between cardiomyocytes, with a cell-ECM-cell conformation – see Figure 7.1B. Indeed, it was recently demonstrated that integrins are required for cardioblast polarisation in the developing embryo, with Robo signalling acting in concert with integrins to restrict cadherin localisation (VANDERPLOEG *et al.* 2012). In adult *Drosophila* hearts, thread-like β-integrin staining was observed at the junctions between adjacent cardiomyocytes (particularly between contralateral cardiomyocytes, and importantly in the absence of a ventral longitudinal muscle layer – which could have indicated a cell-ECM link between the cardiomyocytes and this muscle layer), indicating a cell-ECM-cell adhesive role at this site.

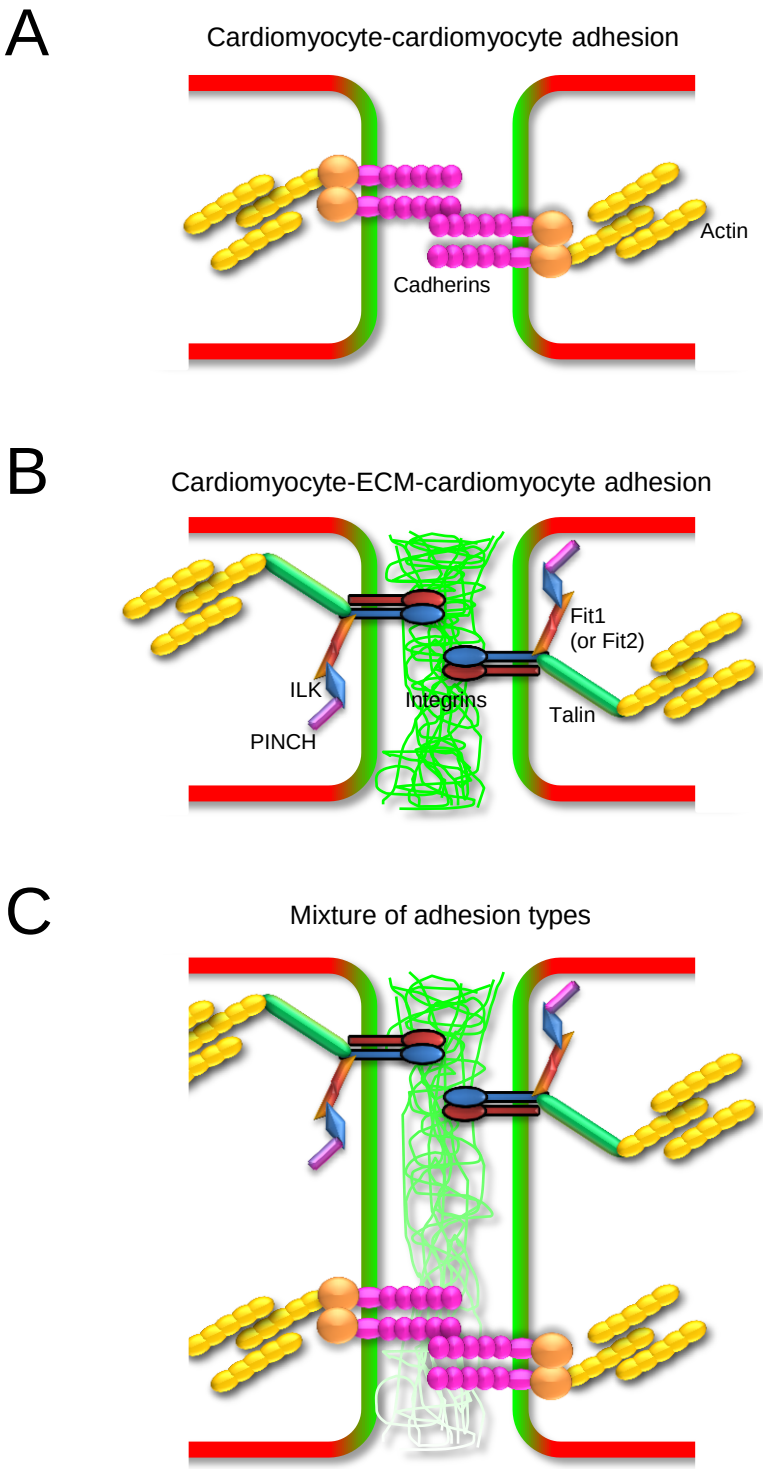

Figure 7.1. Cell adhesion at the intercalated disc-like junctions between cardiomyocytes in the adult *Drosophila* – cell-cell or cell-ECM-cell.
Three potential cell adhesion processes forming the intercalated disc-like structures in the adult *Drosophila* cardiac syncytium. **A**, cadherin-based cell-cell adhesion. **B**, integrin-based cell-ECM-cell adhesion. **C**, a mixture of both cell-cell and cell-ECM-cell adhesion.

It is probably the case that both (direct) cell-cell *and* (indirect) cell-ECM-cell adhesion exist between the cardiomyocytes of the adult cardiac syncytium (see Figure 7.1C) – a phenomenon also seen in the development of the *Drosophila* wing (BROWN 2011; PROKOP *et al.* 1998). The composition of adhesive structures at these cardiomyocyte junctions (or intercalated disc-like junctions (LEHMACHER *et al.* 2012)) is also likely to change over the course of development (BROWN 2011; BULGAKOVA *et al.* 2012) – highlighted in this thesis by the range of phenotypes caused by *Fit*-knockdown at different stages of development.

However, this raises the point of why these adult cardiomyocytes exhibit cell-ECM-cell adhesion at all, as opposed to cell-cell adhesion alone. It might simply be that the ECM provides a rigid architecture that cardiomyocytes can actively associate with (BROWN 2011), while also assisting transmembrane receptor turnover of adhesion sites (HUANG *et al.* 2011). Due to the energetic nature of the cell-thick *Drosophila* cardiac syncytium, it is possible the cell-ECM-cell adhesion forms in response to physical stress, and therefore strengthens the connection between these cells, while keeping them coupled for the propagation of action potentials. In agreement with this, integrins (cell-ECM) have been shown to have a higher failure strength compared to cadherins (cell-cell) (BAUMGARTNER *et al.* 2000; KOKKOLI *et al.* 2004; ZHANG *et al.* 2009), while studies on cardiac micro-tissues indicated "cardiac intercalated discs are exposed to substantially higher forces than cell–cell junctions in other organs" (MCCAIN *et al.* 2012).

7.4 The role of the *Fermitins* in *Drosophila*

In this thesis, the *Drosophila Fermitins* have been demonstrated to be essential for viability, with loss of both paralogs resulting in embryonic lethality, highlighting their importance, and the importance of integrin-based cell-matrix adhesion for development. The *Fermitins* were recently described as core components of the "adhesome" – i.e. the multitude of proteins that contribute to the cell adhesion process – and have been characterised as crucial for the cell adhesion process, with loss of *Fit* function causing phenotypes identical to those seen with *βPS-integrin* or *Talin* loss (BULGAKOVA *et al.* 2012). However, thus far there has been only one publication examining effect of *Fit* loss, and even then these genes were not the sole focus of this paper, which described the results of a screen performed to identify genes involved in muscle assembly (BAI *et al.* 2008). It is likely that the genetic/functional redundancy between the *Fermitins* may have prevented these genes from being identified in past genome-wide screens.

Based on studies performed in other organisms including humans, it is hypothesised the *Fermitins* may act by binding to the cytoplasmic tail of β-integrins via their FERM F3 subdomain, the particular residues of which appear to be conserved (SHI *et al.* 2007). A recent study in nematodes concluded that the *Fermitin* ortholog (UNC-112) could autoinhibit itself (i.e. its N-terminal could bind its C-terminal, preventing integrin binding) via a hinge in the middle of the protein (QADOTA *et al.* 2012) – the 'TEEE' sequence which confers this ability is conserved in *Drosophila* Fermitins and human Kindlin-2 proteins indicating these proteins may also autoinhibit. Interestingly, it was recently identified that *Drosophila* Talin also

possesses the ability to autoinhibit (ELLIS *et al.* 2013). The ability of PAT-4 (ILK) to bind the UNC-112 (but not PAT-3 (β-integrin)) has also been demonstrated (QADOTA *et al.* 2012), leading to a conformational change and 'activating' UNC-112 so it could then bind to PAT-3. In agreement with this, the established view that ILK can activate β-integrin by direct binding (HANNIGAN *et al.* 1996) has been challenged in recent years, with many researchers now convinced that the association is indirect (FUKUDA *et al.* 2011; HANNIGAN *et al.* 2011; WICKSTROM *et al.* 2010). It is now thought that Kindlin-2 is a core mediator of integrin signalling and that it binds directly to the β-integrin cytoplasmic tail, and is connected to the actin-cytoskeleton via the ILK/Pinch/Parvin (IPP) complex (LARJAVA *et al.* 2008; SACHS and SONNENBERG 2013; TU *et al.* 2003). A hypothetical model of Fit/IPP-mediated integrin activation in *Drosophila*, based on the autoinhibitory action of UNC-112, is summarised in Figure 7.2. A similar diagram would be hypothesised for human Kindlin-2.

7.4.1 The evolutionarily conserved role of the Fermitins in the *Drosophila* heart

In the *Drosophila* heart, the Fermitins are essential for the development of a functional cardiac syncytium, a role which appears to be evolutionarily conserved in Kindlin-2. The human Kindlin-1 and -3 proteins are dispensable for cardiac development, whereas Kindlin-2 is essential for implantation and heart development (DOWLING *et al.* 2008a; LAI-CHEONG *et al.* 2010). It is presently unknown which of the Fermitins (Fit1 or Fit2) is expressed in *Drosophila* cardiac syncytium during development (it could be both, and at different time points), thus further work examining *in situ* gene expression would be informative. The Fermitins are required for the development of a functional heart and for the prevention of arrhythmia in

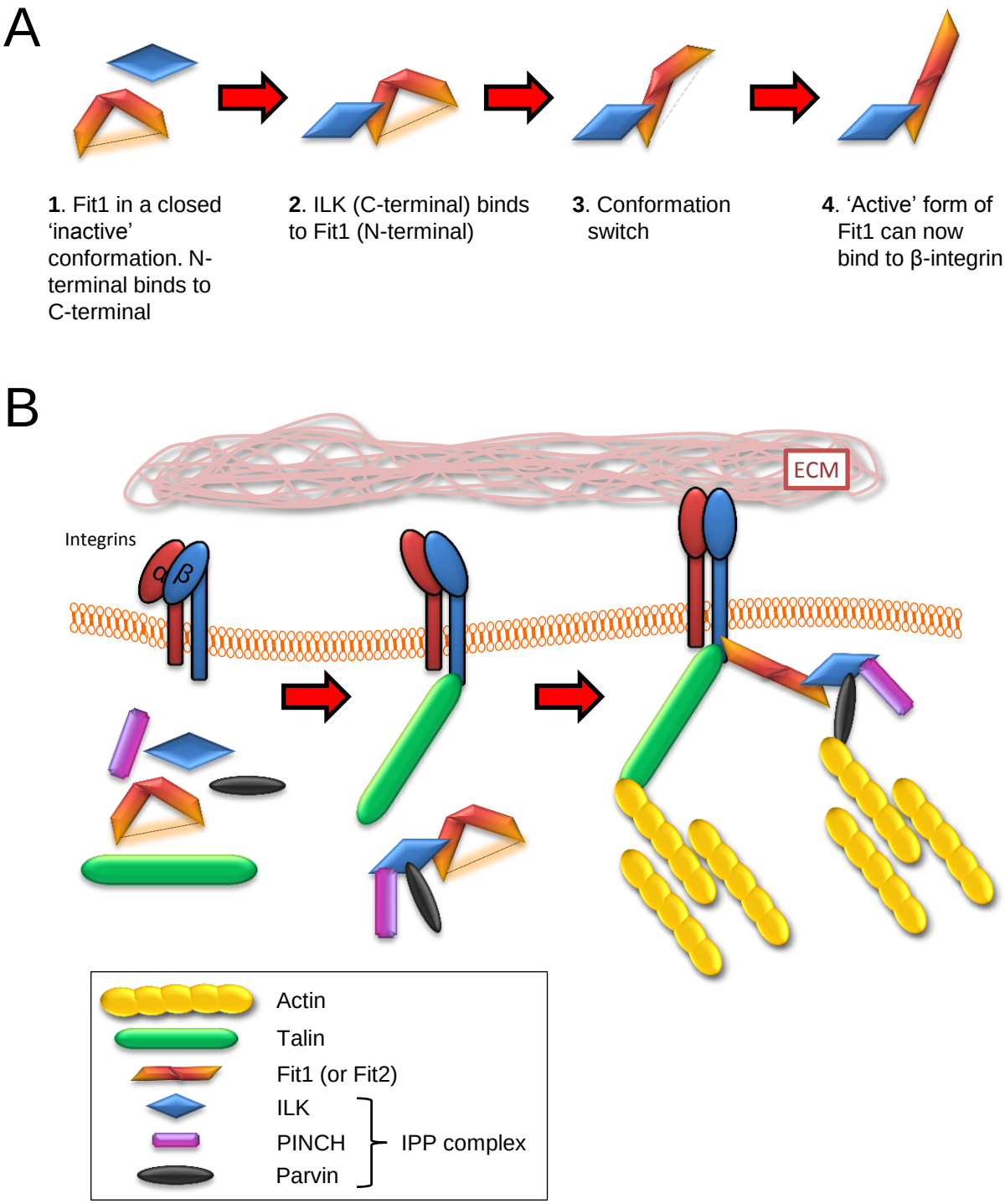

Figure 7.2. The *Drosophila* Fermitin proteins are predicted to bind the cytoplasmic tail of β-integrin, similar to Talin, via a conformational switch. **A**, Fit1 (or Fit2) protein is hypothesised to be activated via ILK, and can then subsequently bind to β-integrin. **B**, hypothetical model of Fermitin activation and subsequent binding to β-integrin. PINCH (*Stck*), Parvin, and ILK can bind to each other (forming the IPP complex). ILK binding to Fit1 (or Fit2) activates the protein which then binds to the cytoplasmic tail of β-integrin in conjunction with Talin. Talin and Parvin can both connect directly to the actin cytoskeleton.

adults. Silencing *Fit* causes mechanical decoupling (with most cardiomyocytes balling up) as well as electrical decoupling (with loss of cardiomyocyte coupling leading to loss of synchrony and likely causing aberrant action potential wave propagation along the heart).

7.5 Implications for the role of *Kindlin-2* in the human myocardium and cardiomyopathy

Given the association between other intercalated disc proteins with different cardiomyopathies (BASSO *et al.* 2006; EHLER *et al.* 2001; KOSTETSKII *et al.* 2005; LI and RADICE 2010; LIANG *et al.* 2009; PERRIARD *et al.* 2003; VALENCIK *et al.* 2006; VASILE *et al.* 2006), it would be predicted that *Kindlin-2* mutations may contribute to human cardiomyopathies (DOWLING *et al.* 2008a). However, human mutations in *Kindlin-2* have not been identified (HATCHER and BASSON 2008). Intriguingly, a missense mutation in the Kindlin-2 binding protein, ILK, was found to be associated with severe dilated cardiomyopathy (KNOLL *et al.* 2007). Since zebrafish and mouse models show similar phenotypes with *Kindlin-2*/*ILK* ablation (POSTEL *et al.* 2008; SOPKO *et al.* 2011; WHITE *et al.* 2006), a similar screen in severe dilated cardiomyopathy patients for mutations in *Kindlin-2* could also hypothetically identify deleterious polymorphisms contributing to this disease.

Although the precise localisation of Fit protein in the *Drosophila* hearts is unknown (from the data presented in this thesis, Fit antibodies would be predicted to display a similar cardiomyocyte-junction staining pattern as the βPS-integrin antibody (BROWER *et al.* 1984)), Kindlin-2 protein, like β1-integrin, has been shown to be localised at the intercalated disc and costameres in murine cardiac tissue (DI

MAURO *et al.* 2009; DOWLING *et al.* 2008a; TERRACIO *et al.* 1991). Genetic ablation of *Kindlin-2* led to early embryonic lethality in mice and precluded further analysis of this gene in heart development, and morpholino-knockdown of *Kindlin-2* in zebrafish resulted in significant cardiomyopathy (DOWLING *et al.* 2008a) – in agreement with many of the results described in this thesis. Additionally, Pluskota and colleagues discovered *Kind2*$^{+/-}$ heterozygote mice displayed abnormal angiogenesis (PLUSKOTA *et al.* 2011). However, there was no mention of the effect of *Kind2* haploinsufficiency on cardiac development or function in this study. The development of inducible cardiomyocyte-specific *Kindlin-2* ablation models (gene knockout and/or dominant-negative protein overexpression) would be ideal, and would help to elucidate the role of Kindlin-2 during cardiogenesis and in the development of cardiac pathology. Since partial ablation of *Kind2* function can lead to significant deleterious effects in angiogenesis (PLUSKOTA *et al.* 2011), it is possible that even partial depletion of *Kind2* in adult murine cardiomyocytes would also lead to cardiomyopathy.

In conclusion, by establishing the adult fruit fly as a model of human heart function, and exploiting this powerful genetic system to screen for conserved genes affecting the development and function of its cardiac syncytium, my thesis provides clarity about the role of *Kind2* in the human heart by demonstrating a cell autonomous role for the *Fermitins* in the development of a functional cardiac syncytium in *Drosophila*. My thesis also demonstrates that the *Fermitins* can functionally compensate for each other in order to control syncytium development. Therefore, my thesis demonstrates the power of the fruit fly as a model of human

cardiac physiology, and supports the concept that abnormalities in cardiomyocyte KIND2 expression or function may contribute to cardiomyopathies in humans.

References

ADAMS, M. D., and J. J. SEKELSKY, 2002 From sequence to phenotype: reverse genetics in Drosophila melanogaster. Nat Rev Genet **3:** 189-198.

AHMAD, S. M., T. R. TANSEY, B. W. BUSSER, M. T. NOLTE, N. JEFFRIES *et al.*, 2012 Two forkhead transcription factors regulate the division of cardiac progenitor cells by a Polo-dependent pathway. Dev Cell **23:** 97-111.

AKAZAWA, H., S. KUDOH, N. MOCHIZUKI, N. TAKEKOSHI, H. TAKANO *et al.*, 2004 A novel LIM protein Cal promotes cardiac differentiation by association with CSX/NKX2-5. J Cell Biol **164:** 395-405.

ALAYARI, N. N., G. VOGLER, O. TAGHLI-LAMALLEM, K. OCORR, R. BODMER *et al.*, 2009 Fluorescent labeling of Drosophila heart structures. J Vis Exp.

ALBRECHT, S., S. S. WANG, A. HOLZ, A. BERGTER and A. PAULULAT, 2006 The ADAM metalloprotease Kuzbanian is crucial for proper heart formation in Drosophila melanogaster. Mechanisms of Development **123:** 372-387.

AN, Z., K. DOBRA, J. G. LOCK, S. STROMBLAD, A. HJERPE *et al.*, 2010 Kindlin-2 is expressed in malignant mesothelioma and is required for tumor cell adhesion and migration. Int J Cancer **127:** 1999-2008.

ANASTASI, G., G. CUTRONEO, R. GAETA, D. DI MAURO, A. ARCO *et al.*, 2009 Dystrophin-glycoprotein complex and vinculin-talin-integrin system in human adult cardiac muscle. Int J Mol Med **23:** 149-159.

ARCHAMBAULT, V., and D. M. GLOVER, 2009 Polo-like kinases: conservation and divergence in their functions and regulation (vol 10, pg 265, 2009). Nature Reviews Molecular Cell Biology **10**.

ASHBURNER, M., K. G. GOLIC and R. S. HAWLEY, 2005 *Drosophila : a laboratory handbook*. Cold Spring Harbor Laboratory Press, Cold Spring Harbor, N.Y.

AZPIAZU, N., and M. FRASCH, 1993 tinman and bagpipe: two homeo box genes that determine cell fates in the dorsal mesoderm of Drosophila. Genes Dev **7:** 1325-1340.

BAI, J., R. BINARI, J. Q. NI, M. VIJAYAKANTHAN, H. S. LI *et al.*, 2008 RNA interference screening in Drosophila primary cells for genes involved in muscle assembly and maintenance. Development **135:** 1439-1449.

BAKER, S. E., J. A. LORENZEN, S. W. MILLER, T. A. BUNCH, A. L. JANNUZI *et al.*, 2002 Genetic interaction between integrins and moleskin, a gene encoding a Drosophila homolog of importin-7. Genetics **162:** 285-296.

BARCZYK, M., S. CARRACEDO and D. GULLBERG, 2010 Integrins. Cell Tissue Res **339:** 269-280.

BASSO, C., E. CZARNOWSKA, M. DELLA BARBERA, B. BAUCE, G. BEFFAGNA *et al.*, 2006 Ultrastructural evidence of intercalated disc remodelling in arrhythmogenic right ventricular cardiomyopathy: an electron microscopy investigation on endomyocardial biopsies. Eur Heart J **27:** 1847-1854.

BAUMGARTNER, W., P. HINTERDORFER, W. NESS, A. RAAB, D. VESTWEBER *et al.*, 2000 Cadherin interaction probed by atomic force microscopy. Proceedings of the National Academy of Sciences of the United States of America **97:** 4005-4010.

BELLEN, H. J., R. W. LEVIS, Y. HE, J. W. CARLSON, M. EVANS-HOLM *et al.*, 2011 The Drosophila gene disruption project: progress using transposons with distinctive site specificities. Genetics **188:** 731-743.

BELLEN, H. J., R. W. LEVIS, G. LIAO, Y. HE, J. W. CARLSON *et al.*, 2004 The BDGP gene disruption project: single transposon insertions associated with 40% of Drosophila genes. Genetics **167:** 761-781.

BELLEN, H. J., C. TONG and H. TSUDA, 2010 100 years of Drosophila research and its impact on vertebrate neuroscience: a history lesson for the future. Nat Rev Neurosci **11:** 514-522.

BERGER, J., T. SUZUKI, K. A. SENTI, J. STUBBS, G. SCHAFFNER *et al.*, 2001 Genetic mapping with SNP markers in Drosophila. Nat Genet **29:** 475-481.

BIALKOWSKA, K., Y. Q. MA, K. BLEDZKA, K. SOSSEY-ALAOUI, L. IZEM *et al.*, 2010 The integrin co-activator Kindlin-3 is expressed and functional in a non-hematopoietic cell, the endothelial cell. J Biol Chem **285:** 18640-18649.

BIER, E., 2005 Drosophila, the golden bug, emerges as a tool for human genetics. Nat Rev Genet **6:** 9-23.

BIER, E., and R. BODMER, 2004 Drosophila, an emerging model for cardiac disease. Gene **342:** 1-11.

BIRN, H., J. C. FYFE, C. JACOBSEN, F. MOUNIER, P. J. VERROUST *et al.*, 2000 Cubilin is an albumin binding protein important for renal tubular albumin reabsorption. Journal of Clinical Investigation **105:** 1353-1361.

BIRSE, R. T., J. CHOI, K. REARDON, J. RODRIGUEZ, S. GRAHAM *et al.*, 2010 High-fat-diet-induced obesity and heart dysfunction are regulated by the TOR pathway in Drosophila. Cell Metab **12:** 533-544.

BLEDZKA, K., J. LIU, Z. XU, H. D. PERERA, S. P. YADAV *et al.*, 2012 Spatial coordination of kindlin-2 with talin head domain in interaction with integrin beta cytoplasmic tails. J Biol Chem **287:** 24585-24594.

BODMER, R., 1993 The Gene Tinman Is Required for Specification of the Heart and Visceral Muscles in Drosophila. Development **118:** 719-729.

BODMER, R., L. Y. JAN and Y. N. JAN, 1990 A New Homeobox-Containing Gene, Msh-2, Is Transiently Expressed Early during Mesoderm Formation of Drosophila. Development **110:** 661-&.

BOKEL, C., and N. H. BROWN, 2002 Integrins in development: Moving on, responding to, and sticking to the extracellular matrix. Developmental Cell **3:** 311-321.

BOTTCHER, R. T., A. LANGE and R. FASSLER, 2009 How ILK and kindlins cooperate to orchestrate integrin signaling. Current Opinion in Cell Biology **21:** 670-675.

BOULTER, E., and E. VAN OBBERGHEN-SCHILLING, 2006 Integrin-linked kinase and its partners: A modular platform regulating cell-matrix adhesion dynamics and cytoskeletal organization. European Journal of Cell Biology **85:** 255-263.

BRAND, A. H., and N. PERRIMON, 1993 Targeted gene expression as a means of altering cell fates and generating dominant phenotypes. Development **118:** 401-415.

BROWER, D. L., 2003 Platelets with wings: the maturation of Drosophila integrin biology. Current Opinion in Cell Biology **15:** 607-613.

BROWER, D. L., T. A. BUNCH, L. MUKAI, T. E. ADAMSON, M. WEHRLI *et al.*, 1995 Nonequivalent requirements for PS1 and PS2 integrin at cell attachments in Drosophila: genetic analysis of the alpha PS1 integrin subunit. Development **121:** 1311-1320.

BROWER, D. L., M. WILCOX, M. PIOVANT, R. J. SMITH and L. A. REGER, 1984 Related cell-surface antigens expressed with positional specificity in Drosophila imaginal discs. Proc Natl Acad Sci U S A **81:** 7485-7489.

BROWN, N. H., 2011 Extracellular matrix in development: insights from mechanisms conserved between invertebrates and vertebrates. Cold Spring Harb Perspect Biol **3**.

BROWN, N. H., S. L. GREGORY, W. L. RICKOLL, L. I. FESSLER, M. PROUT *et al.*, 2002 Talin is essential for integrin function in Drosophila. Dev Cell **3:** 569-579.

BRUMBY, A. M., and H. E. RICHARDSON, 2005 Using Drosophila melanogaster to map human cancer pathways. Nature Reviews Cancer **5:** 626-639.

BULGAKOVA, N. A., B. KLAPHOLZ and N. H. BROWN, 2012 Cell adhesion in Drosophila: versatility of cadherin and integrin complexes during development. Curr Opin Cell Biol **24:** 702-712.

BURKE, J. M., and M. L. ARNOLD, 2001 Genetics and the fitness of hybrids. Annu Rev Genet **35:** 31-52.

BUSHMAN, F. D., N. MALANI, J. FERNANDES, I. D'ORSO, G. CAGNEY *et al.*, 2009 Host cell factors in HIV replication: meta-analysis of genome-wide studies. PLoS Pathog **5:** e1000437.

CAMMARATO, A., C. H. AHRENS, N. N. ALAYARI, E. QELI, J. RUCKER *et al.*, 2011 A mighty small heart: the cardiac proteome of adult Drosophila melanogaster. PLoS One **6:** e18497.

CAMMARATO, A., C. M. DAMBACHER, A. F. KNOWLES, W. A. KRONERT, R. BODMER *et al.*, 2008 Myosin transducer mutations differentially affect motor function, myofibril structure, and the performance of skeletal and cardiac muscles. Molecular Biology of the Cell **19:** 553-562.

CASAD, M. E., L. YU, J. P. DANIELS, M. J. WOLF and H. A. ROCKMAN, 2012 Deletion of Siah-interacting protein gene in Drosophila causes cardiomyopathy. Mol Genet Genomics **287:** 351-360.

CATTERSON, J. H., M. M. HECK and P. S. HARTLEY, 2013 Fermitins, the Orthologs of Mammalian Kindlins, Regulate the Development of a Functional Cardiac Syncytium in. PLoS One **8:** e62958.

CAUCHI, R. J., and M. VAN DEN HEUVEL, 2006 The fly as a model for neurodegenerative diseases: Is it worth the jump? Neurodegenerative Diseases **3:** 338-356.

CERIANI, M. F., J. B. HOGENESCH, M. YANOVSKY, S. PANDA, M. STRAUME *et al.*, 2002 Genome-wide expression analysis in Drosophila reveals genes controlling circadian behavior. J Neurosci **22:** 9305-9319.

CHARTIER, A., S. ZAFFRAN, M. ASTIER, M. SEMERIVA and D. GRATECOS, 2002 Pericardin, a Drosophila type IV collagen-like protein is involved in the morphogenesis and maintenance of the heart epithelium during dorsal ectoderm closure. Development **129:** 3241-3253.

CHATTIPAKORN, N., T. INCHAROEN, N. KANLOP and S. CHATTIPAKORN, 2007 Heart rate variability in myocardial infarction and heart failure. Int J Cardiol **120:** 289-296.

CHINTAPALLI, V. R., J. WANG and J. A. DOW, 2007 Using FlyAtlas to identify better Drosophila melanogaster models of human disease. Nat Genet **39:** 715-720.

CHISWELL, B. P., R. ZHANG, J. W. MURPHY, T. J. BOGGON and D. A. CALDERWOOD, 2008 The structural basis of integrin-linked kinase-PINCH interactions. Proceedings of the National Academy of Sciences of the United States of America **105:** 20677-20682.

CHOMA, M. A., M. J. SUTER, B. J. VAKOC, B. E. BOUMA and G. J. TEARNEY, 2011 Physiological homology between Drosophila melanogaster and vertebrate cardiovascular systems. Disease Models & Mechanisms **4:** 411-420.

CLARK, K. A., M. MCGRAIL and M. C. BECKERLE, 2003 Analysis of PINCH function in Drosophila demonstrates its requirement in integrin-dependent cellular processes. Development **130:** 2611-2621.

COLLINS, B. H., S. DISSEL, E. GATEN, E. ROSATO and C. P. KYRIACOU, 2005 Disruption of Cryptochrome partially restores circadian rhythmicity to the arrhythmic period mutant of Drosophila. Proc Natl Acad Sci U S A **102:** 19021-19026.

COOK, R. K., S. J. CHRISTENSEN, J. A. DEAL, R. A. COBURN, M. E. DEAL *et al.*, 2012 The generation of chromosomal deletions to provide extensive coverage and subdivision of the Drosophila melanogaster genome. Genome Biol **13:** R21.

CROMPTON, D., M. TODMAN, M. WILKIN, S. JI and J. DAVIES, 1995 Essential and neural transcripts from the Drosophila shaking-B locus are differentially expressed in the embryonic mesoderm and pupal nervous system. Dev Biol **170:** 142-158.

CRONIN, S. J., N. T. NEHME, S. LIMMER, S. LIEGEOIS, J. A. POSPISILIK *et al.*, 2009 Genome-wide RNAi screen identifies genes involved in intestinal pathogenic bacterial infection. Science **325:** 340-343.

CURTIS, N. J., J. M. RINGO and H. B. DOWSE, 1999 Morphology of the pupal heart, adult heart, and associated tissues in the fruit fly, Drosophila melanogaster. J Morphol **240:** 225-235.

DAS, D., R. ARADHYA, D. ASHOKA and M. INAMDAR, 2008a Macromolecular uptake in Drosophila pericardial cells requires rudhira function. Exp Cell Res **314:** 1804-1810.

DAS, D., R. ARADHYA, D. ASHOKA and M. INAMDAR, 2008b Post-embryonic pericardial cells of Drosophila are required for overcoming toxic stress but not for cardiac function or adult development. Cell Tissue Res **331:** 565-570.

DASGUPTA, R., M. BOUTROS and N. PERRIMON, 2005 Drosophila Wnt/Fz pathways. Sci STKE **2005:** cm5.

DE ARCANGELIS, A., and E. GEORGES-LABOUESSE, 2000 Integrin and ECM functions: roles in vertebrate development. (vol 16, pg 389, 2000). Trends in Genetics **16:** 536-536.

DELON, I., and N. H. BROWN, 2007 Integrins and the actin cytoskeleton. Current Opinion in Cell Biology **19:** 43-50.

DEN HOED, M., M. EIJGELSHEIM, T. ESKO, B. J. J. M. BRUNDEL, D. S. PEAL *et al.*, 2013 Identification of heart rate-associated loci and their effects on cardiac conduction and rhythm disorders. Nat Genet **advance online publication**.

DENG, C., C. H. CHENG, H. YE, X. HE and L. CHEN, 2010 Evolution of an antifreeze protein by neofunctionalization under escape from adaptive conflict. Proc Natl Acad Sci U S A **107:** 21593-21598.

DEVENPORT, D. N., and N. H. BROWN, 2005 The FERM protein, fermitin, is part of the 'core' integrin adhesion complex that is essential for integrin function

during morphogenesis. Program and Abstracts. 46th Annual Drosophila Research Conference, San Diego, CA, 2005**:** 130.

DI MAURO, D., R. GAETA, A. ARCO, D. MILARDI, S. LENTINI *et al.*, 2009 Distribution of costameric proteins in normal human ventricular and atrial cardiac muscle. Folia Histochem Cytobiol **47:** 605-608.

DIETZL, G., D. CHEN, F. SCHNORRER, K. C. SU, Y. BARINOVA *et al.*, 2007 A genome-wide transgenic RNAi library for conditional gene inactivation in Drosophila. Nature **448:** 151-156.

DOWLING, J. J., E. GIBBS, M. RUSSELL, D. GOLDMAN, J. MINARCIK *et al.*, 2008a Kindlin-2 is an essential component of intercalated discs and is required for vertebrate cardiac structure and function. Circ Res **102:** 423-431.

DOWLING, J. J., A. P. VREEDE, S. KIM, J. GOLDEN and E. L. FELDMAN, 2008b Kindlin-2 is required for myocyte elongation and is essential for myogenesis. Bmc Cell Biology **9**.

DOWSE, H., J. RINGO, J. POWER, E. JOHNSON, K. KINNEY *et al.*, 1995 A congenital heart defect in Drosophila caused by an action-potential mutation. J Neurogenet **10:** 153-168.

DRYSDALE, R., E. RUSHTON and M. BATE, 1993 Genes Required for Embryonic Muscle Development in Drosophila-Melanogaster - a Survey of the X-Chromosome. Rouxs Archives of Developmental Biology **202:** 276-295.

DUFFY, J. B., 2002 GAL4 system in Drosophila: a fly geneticist's Swiss army knife. Genesis **34:** 1-15.

DULCIS, D., and R. B. LEVINE, 2003 Innervation of the heart of the adult fruit fly, Drosophila melanogaster. J Comp Neurol **465:** 560-578.

EHLER, E., R. HOROWITS, C. ZUPPINGER, R. L. PRICE, E. PERRIARD *et al.*, 2001 Alterations at the intercalated disk associated with the absence of muscle LIM protein. J Cell Biol **153:** 763-772.

ELLIS, S. J., J. LONG, M. J. FAIRCHILD, P. LOBO, S. CZERNIECKI *et al.*, 2013 Talin autoinhibition is required for morphogenesis. Program and Abstracts. 54th Annual Drosophila Research Conference, Washington, DC, 2013.

EPSTEIN, J. A., 2000 Developmental cardiology comes of age. Circ Res **87:** 833-834.

ESTRADA, B., S. S. GISSELBRECHT and A. M. MICHELSON, 2007 The transmembrane protein Perdido interacts with Grip and integrins to mediate myotube projection and attachment in the Drosophila embryo. Development **134:** 4469-4478.

FASSLER, R., J. ROHWEDEL, V. MALTSEV, W. BLOCH, S. LENTINI *et al.*, 1996 Differentiation and integrity of cardiac muscle cells are impaired in the absence of beta 1 integrin. J Cell Sci **109 (Pt 13):** 2989-2999.

FERNANDES, C., and Y. RAO, 2011 Genome-wide screen for modifiers of Parkinson's disease genes in Drosophila. Mol Brain **4:** 17.

FIRE, A., S. XU, M. K. MONTGOMERY, S. A. KOSTAS, S. E. DRIVER *et al.*, 1998 Potent and specific genetic interference by double-stranded RNA in Caenorhabditis elegans. Nature **391:** 806-811.

FISCH, S., S. GRAY, S. HEYMANS, S. M. HALDAR, B. Q. WANG *et al.*, 2007 Kruppel-like factor 15 is a regulator of cardiomyocyte hypertrophy. Proceedings of the National Academy of Sciences of the United States of America **104:** 7074-7079.

FOSTER, R. G., and L. KREITZMAN, 2004 *Rhythms of life : the biological clocks that control the daily lives of every living thing*. Profile Books, London.

FOX, K., J. S. BORER, A. J. CAMM, N. DANCHIN, R. FERRARI *et al.*, 2007 Resting heart rate in cardiovascular disease. J Am Coll Cardiol **50:** 823-830.

FRANKE, W. W., C. M. BORRMANN, C. GRUND and S. PIEPERHOFF, 2006 The area composita of adhering junctions connecting heart muscle cells of vertebrates. I. Molecular definition in intercalated disks of cardiomyocytes by immunoelectron microscopy of desmosomal proteins. Eur J Cell Biol **85:** 69-82.

FRASCH, M., 1995 Induction of visceral and cardiac mesoderm by ectodermal Dpp in the early Drosophila embryo. Nature **374:** 464-467.

FUKUDA, K., J. D. KNIGHT, G. PISZCZEK, R. KOTHARY and J. QIN, 2011 Biochemical, proteomic, structural, and thermodynamic characterizations of integrin-linked kinase (ILK): cross-validation of the pseudokinase. J Biol Chem **286:** 21886-21895.

GEIGER, T., and R. ZAIDEL-BAR, 2012 Opening the floodgates: proteomics and the integrin adhesome. Current Opinion in Cell Biology **24:** 562-568.

GHOSH, A., N. MANRIQUE-HOYOS, A. VOIGT, J. B. SCHULZ, M. KREUTZFELDT *et al.*, 2011 Targeted ablation of oligodendrocytes triggers axonal damage. PLoS One **6:** e22735.

GIANCOTTI, F. G., and E. RUOSLAHTI, 1999 Transduction - Integrin signaling. Science **285:** 1028-1032.

GODDEERIS, M. M., E. COOK-WIENS, W. J. HORTON, H. WOLF, J. R. STOLTZFUS *et al.*, 2003 Delayed behavioural aging and altered mortality in Drosophila beta integrin mutants. Aging Cell **2:** 257-264.

GOODMAN, S. L., and M. PICARD, 2012 Integrins as therapeutic targets. Trends in Pharmacological Sciences **33:** 405-412.

GRAVELEY, B. R., A. N. BROOKS, J. W. CARLSON, M. O. DUFF, J. M. LANDOLIN *et al.*, 2011 The developmental transcriptome of Drosophila melanogaster. Nature **471:** 473-479.

GREENSPAN, R. J., 1997 *Fly pushing : the theory and practice of Drosophila genetics*. Cold Spring Harbor Laboratory Press, Plainview, N.Y.

GRIMALDI, D. A., and M. S. ENGEL, 2005 *Evolution of the insects*. Cambridge University Press, Cambridge U.K. ; New York.

GROSSMAN, T. R., A. GAMLIEL, R. J. WESSELLS, O. TAGHLI-LAMALLEM, K. JEPSEN *et al.*, 2011 Over-expression of DSCAM and COL6A2 cooperatively generates congenital heart defects. PLoS Genet **7:** e1002344.

GUTIERREZ, E., D. WIGGINS, B. FIELDING and A. P. GOULD, 2007 Specialized hepatocyte-like cells regulate Drosophila lipid metabolism. Nature **445:** 275-280.

HAAG, T. A., N. P. HAAG, A. C. LEKVEN and V. HARTENSTEIN, 1999 The role of cell adhesion molecules in Drosophila heart morphogenesis: faint sausage, shotgun/DE-cadherin, and laminin A are required for discrete stages in heart development. Dev Biol **208:** 56-69.

HALBLEIB, J. M., and W. J. NELSON, 2006 Cadherins in development: cell adhesion, sorting, and tissue morphogenesis. Genes & Development **20:** 3199-3214.

HAN, Z., and E. N. OLSON, 2005 Hand is a direct target of Tinman and GATA factors during Drosophila cardiogenesis and hematopoiesis. Development **132:** 3525-3536.

HANFT, L. M., F. S. KORTE and K. S. MCDONALD, 2008 Cardiac function and modulation of sarcomeric function by length. Cardiovasc Res **77:** 627-636.

HANNIGAN, G. E., C. LEUNG-HAGESTEIJN, L. FITZ-GIBBON, M. G. COPPOLINO, G. RADEVA *et al.*, 1996 Regulation of cell adhesion and anchorage-dependent growth by a new beta 1-integrin-linked protein kinase. Nature **379:** 91-96.

HANNIGAN, G. E., P. C. MCDONALD, M. P. WALSH and S. DEDHAR, 2011 Integrin-linked kinase: Not so /`pseudo/' after all. Oncogene **30:** 4375-4385.

HANSEN, M., A. L. HSU, A. DILLIN and C. KENYON, 2005 New genes tied to endocrine, metabolic, and dietary regulation of lifespan from a Caenorhabditis elegans genomic RNAi screen. PLoS Genet **1:** 119-128.

HARBURGER, D. S., and D. A. CALDERWOOD, 2009 Integrin signalling at a glance. Journal of Cell Science **122:** 159-163.

HARRIS, T. J., and U. TEPASS, 2010 Adherens junctions: from molecules to morphogenesis. Nat Rev Mol Cell Biol **11:** 502-514.

HARTENSTEIN, V., 1993 *Atlas of Drosophila development*.

HAS, C., C. HERZ, E. ZIMINA, H. Y. QU, Y. H. HE *et al.*, 2009 Kindlin-1 Is Required for RhoGTPase-Mediated Lamellipodia Formation in Keratinocytes. American Journal of Pathology **175:** 1442-1452.

HATCHER, C. J., and C. T. BASSON, 2008 Disrupted intercalated discs. Is kindlin-2 required? Circ Res **102:** 392-394.

HAUSELMANN, S. P., B. I. ROSC-SCHLUTER, V. LORENZ, I. PLAISANCE, M. BRINK *et al.*, 2011 beta(1)-Integrin is up-regulated via Rac1-dependent reactive oxygen species as part of the hypertrophic cardiomyocyte response. Free Radical Biology and Medicine **51:** 609-618.

HAWLEY, R. S., and W. D. GILLILAND, 2006 Sometimes the result is not the answer: The truths and the lies that come from using the complementation test. Genetics **174:** 5-15.

HELENIUS, I. T., and G. J. BEITEL, 2008 The first "Slit" is the deepest: the secret to a hollow heart. J Cell Biol **182:** 221-223.

HELING, A., R. ZIMMERMANN, S. KOSTIN, Y. MAENO, S. HEIN *et al.*, 2000 Increased expression of cytoskeletal, linkage, and extracellular proteins in failing human myocardium. Circ Res **86:** 846-853.

HILL, E., I. D. BROADBENT, C. CHOTHIA and J. PETTITT, 2001 Cadherin superfamily proteins in Caenorhabditis elegans and Drosophila melanogaster. J Mol Biol **305:** 1011-1024.

HOLLEY, S. A., P. D. JACKSON, Y. SASAI, B. LU, E. M. DE ROBERTIS *et al.*, 1995 A conserved system for dorsal-ventral patterning in insects and vertebrates involving sog and chordin. Nature **376:** 249-253.

HUANG, J., L. HUANG, Y. J. CHEN, E. AUSTIN, C. E. DEVOR *et al.*, 2011 Differential regulation of adherens junction dynamics during apical-basal polarization. J Cell Sci **124:** 4001-4013.

HYNES, R. O., 2002 Integrins: bidirectional, allosteric signaling machines. Cell **110:** 673-687.

IKEDA, Y., Y. HIROI, T. HOSODA, T. UTSUNOMIYA, S. MATSUO *et al.*, 2002 Novel point mutation in the cardiac transcription factor CSX/NKX2.5 associated with congenital heart disease. Circ J **66:** 561-563.

IVY, J. R., J. H. CATTERSON and P. S. HARTLEY, 2012 Drosophila Bteb2, a Kruppel-like transcription factor, specifies and maintains adult pericardial nephrocytes. Program and Abstracts. Proceedings of The Physiological Society, Edinburgh, UK, 2012.

JUNION, G., M. SPIVAKOV, C. GIRARDOT, M. BRAUN, E. H. GUSTAFSON *et al.*, 2012 A transcription factor collective defines cardiac cell fate and reflects lineage history. Cell **148:** 473-486.

KARAKOSE, E., H. B. SCHILLER and R. FASSLER, 2010 The kindlins at a glance. J Cell Sci **123:** 2353-2356.

KATO, K., T. SHIOZAWA, J. MITSUSHITA, A. TODA, A. HORIUCHI *et al.*, 2004 Expression of the mitogen-inducible gene-2 (mig-2) is elevated in human uterine leiomyomas but not in leiomyosarcomas. Hum Pathol **35:** 55-60.

KIM, I. M., and M. J. WOLF, 2009 Serial examination of an inducible and reversible dilated cardiomyopathy in individual adult Drosophila. PLoS One **4:** e7132.

KIM, I. M., M. J. WOLF and H. A. ROCKMAN, 2010 Gene deletion screen for cardiomyopathy in adult Drosophila identifies a new notch ligand. Circ Res **106:** 1233-1243.

KIM, Y. O., S. J. PARK, R. S. BALABAN, M. NIRENBERG and Y. KIM, 2004 A functional genomic screen for cardiogenic genes using RNA interference in developing Drosophila embryos. Proc Natl Acad Sci U S A **101:** 159-164.

KIMBRELL, D. A., C. HICE, C. BOLDUC, K. KLEINHESSELINK and K. BECKINGHAM, 2002 The Dorothy enhancer has Tinman binding sites and drives hopscotch-induced tumor formation. Genesis **34:** 23-28.

KISTLER, P. M., P. SANDERS, S. P. FYNN, I. H. STEVENSON, S. J. SPENCE *et al.*, 2004 Electrophysiologic and electroanatomic changes in the human atrium associated with age. J Am Coll Cardiol **44:** 109-116.

KLEBER, A. G., and Y. RUDY, 2004 Basic mechanisms of cardiac impulse propagation and associated arrhythmias. Physiol Rev **84:** 431-488.

KNOLL, R., R. POSTEL, J. WANG, R. KRATZNER, G. HENNECKE *et al.*, 2007 Laminin-alpha4 and integrin-linked kinase mutations cause human cardiomyopathy via simultaneous defects in cardiomyocytes and endothelial cells. Circulation **116:** 515-525.

KNOX, J., K. MOYER, N. YACOUB, C. SOLDAAT, M. KOMOSA *et al.*, 2011 Syndecan contributes to heart cell specification and lumen formation during Drosophila cardiogenesis. Dev Biol **356:** 279-290.

KOHLER, R. E., 1994 *Lords of the fly : Drosophila genetics and the experimental life*. University of Chicago Press, Chicago.

KOKKOLI, E., S. E. OCHSENHIRT and M. TIRRELL, 2004 Collective and single-molecule interactions of alpha(5)beta(1) integrins. Langmuir **20:** 2397-2404.

KOLSCH, V., and A. PAULULAT, 2002 The highly conserved cardiogenic bHLH factor hand is specifically expressed in circular visceral muscle progenitor cells and in all cell types of the dorsal vessel during Drosophila embryogenesis. Development Genes and Evolution **212:** 473-485.

KOSTETSKII, I., J. LI, Y. XIONG, R. ZHOU, V. A. FERRARI *et al.*, 2005 Induced deletion of the N-cadherin gene in the heart leads to dissolution of the intercalated disc structure. Circ Res **96:** 346-354.

KOSTIN, S., M. RIEGER, S. DAMMER, S. HEIN, M. RICHTER *et al.*, 2003 Gap junction remodeling and altered connexin43 expression in the failing human heart. Mol Cell Biochem **242:** 135-144.

KULKARNI, M. M., M. BOOKER, S. J. SILVER, A. FRIEDMAN, P. HONG *et al.*, 2006 Evidence of off-target effects associated with long dsRNAs in Drosophila melanogaster cell-based assays. Nat Methods **3:** 833-838.

LAFAVE, M. C., and J. SEKELSKY, 2011 Transcription Initiation From Within P Elements Generates Hypomorphic Mutations in Drosophila melanogaster. Genetics **188:** 749-752.

LAI-CHEONG, J. E., M. PARSONS and J. A. MCGRATH, 2010 The role of kindlins in cell biology and relevance to human disease. Int J Biochem Cell Biol **42:** 595-603.

LAI-CHEONG, J. E., S. USSAR, K. ARITA, I. R. HART and J. A. MCGRATH, 2008 Colocalization of kindlin-1 kindlin-2, and migfilin at keratinocyte focal adhesion and relevance to the pathophysiology of kindler syndrome. Journal of Investigative Dermatology **128:** 2156-2165.

LAKATTA, E. G., 2003 Arterial and cardiac aging: major shareholders in cardiovascular disease enterprises: Part III: cellular and molecular clues to heart and arterial aging. Circulation **107:** 490-497.

LARJAVA, H., E. F. PLOW and C. WU, 2008 Kindlins: essential regulators of integrin signalling and cell-matrix adhesion. EMBO Rep **9:** 1203-1208.

LAWRENCE, P. A., 1992 *The making of a fly : the genetics of animal design*. Blackwell Science, Oxford England ; Cambridge, Mass., USA.

LAWRENCE, P. A., R. BODMER and J. P. VINCENT, 1995 Segmental patterning of heart precursors in Drosophila. Development **121:** 4303-4308.

LEGATE, K. R., E. MONTANEZ, O. KUDLACEK and R. FASSLER, 2006 ILK, PINCH and parvin: the tIPP of integrin signalling. Nat Rev Mol Cell Biol **7:** 20-31.

LEHMACHER, C., B. ABELN and A. PAULULAT, 2012 The ultrastructure of Drosophila heart cells. Arthropod Struct Dev.

LI, J., V. V. PATEL, I. KOSTETSKII, Y. XIONG, A. F. CHU *et al.*, 2005 Cardiac-specific loss of N-cadherin leads to alteration in connexins with conduction slowing and arrhythmogenesis. Circ Res **97:** 474-481.

LI, J., V. V. PATEL and G. L. RADICE, 2006 Dysregulation of cell adhesion proteins and cardiac arrhythmogenesis. Clin Med Res **4:** 42-52.

LI, J., and G. L. RADICE, 2010 A new perspective on intercalated disc organization: implications for heart disease. Dermatol Res Pract **2010:** 207835.

LIANG, X., Y. SUN, M. YE, M. C. SCIMIA, H. CHENG *et al.*, 2009 Targeted ablation of PINCH1 and PINCH2 from murine myocardium results in dilated cardiomyopathy and early postnatal lethality. Circulation **120:** 568-576.

LIM, H. Y., W. WANG, R. J. WESSELLS, K. OCORR and R. BODMER, 2011 Phospholipid homeostasis regulates lipid metabolism and cardiac function through SREBP signaling in Drosophila. Genes Dev **25:** 189-200.

LIN, N., N. BADIE, L. YU, D. ABRAHAM, H. CHENG *et al.*, 2011 A method to measure myocardial calcium handling in adult Drosophila. Circ Res **108:** 1306-1315.

LIVINGSTONE, M., 1981 Two mutations in Drosophila differentially affect the synthesis of octopamine, dopamine, and serotonin by altering the activities of two different amino acid decarboxylases, pp. 351 in *Soc. Neurosci. Abstr*.

LO, P. C., and M. FRASCH, 2001 A role for the COUP-TF-related gene seven-up in the diversification of cardioblast identities in the dorsal vessel of Drosophila. Mech Dev **104:** 49-60.

LO, P. C., S. ZAFFRAN, S. SENATORE and M. FRASCH, 2007 The Drosophila Hand gene is required for remodeling of the developing adult heart and midgut during metamorphosis. Dev Biol **311:** 287-296.

LOER, B., R. BAUER, R. BORNHEIM, J. GRELL, E. KREMMER *et al.*, 2008 The NHL-domain protein Wech is crucial for the integrin-cytoskeleton link. Nat Cell Biol **10:** 422-U103.

LONG, M., E. BETRAN, K. THORNTON and W. WANG, 2003 The origin of new genes: glimpses from the young and old. Nat Rev Genet **4:** 865-875.

LUONG, N., C. R. DAVIES, R. J. WESSELLS, S. M. GRAHAM, M. T. KING *et al.*, 2006 Activated FOXO-mediated insulin resistance is blocked by reduction of TOR activity. Cell Metab **4:** 133-142.

LYONS, I., L. M. PARSONS, L. HARTLEY, R. LI, J. E. ANDREWS *et al.*, 1995 Myogenic and morphogenetic defects in the heart tubes of murine embryos lacking the homeo box gene Nkx2-5. Genes Dev **9:** 1654-1666.

MA, Y., A. CREANGA, L. LUM and P. A. BEACHY, 2006 Prevalence of off-target effects in Drosophila RNA interference screens. Nature **443:** 359-363.

MACKINNON, A. C., H. QADOTA, K. R. NORMAN, D. G. MOERMAN and B. D. WILLIAMS, 2002 C-elegans PAT-4/ILK functions as an adaptor protein within integrin adhesion complexes. Current Biology **12:** 787-797.

MACMULLIN, A., and J. R. JACOBS, 2006 Slit coordinates cardiac morphogenesis in Drosophila. Dev Biol **293:** 154-164.

MAITRA, S., D. N. DEVENPORT and N. H. BROWN, 2009 Fermitins in integrin-mediated adhesion. Program and Abstracts. 50th Annual Drosophila Research Conference, Chicago, IL, 2009.

MALLIPATTU, S. K., R. J. LIU, F. ZHENG, G. NARLA, A. MA'AYAN *et al.*, 2012 Kruppel-like Factor 15 (KLF15) Is a Key Regulator of Podocyte Differentiation. Journal of Biological Chemistry **287:** 19122-19135.

MARSH, J. L., and L. M. THOMPSON, 2006 Drosophila in the study of neurodegenerative disease. Neuron **52:** 169-178.

MATSUSHITA, T., M. OYAMADA, K. FUJIMOTO, Y. YASUDA, S. MASUDA *et al.*, 1999 Remodeling of cell-cell and cell-extracellular matrix interactions at the border zone of rat myocardial infarcts. Circ Res **85:** 1046-1055.

MCCAIN, M. L., H. LEE, Y. ARATYN-SCHAUS, A. G. KLEBER and K. K. PARKER, 2012 Cooperative coupling of cell-matrix and cell-cell adhesions in cardiac muscle. Proc Natl Acad Sci U S A **109:** 9881-9886.

MCGUIRE, S. E., P. T. LE, A. J. OSBORN, K. MATSUMOTO and R. L. DAVIS, 2003 Spatiotemporal rescue of memory dysfunction in Drosophila. Science **302:** 1765-1768.

MCGUIRE, S. E., Z. MAO and R. L. DAVIS, 2004 Spatiotemporal gene expression targeting with the TARGET and gene-switch systems in Drosophila. Sci STKE **2004:** pl6.

MEDER, B., I. G. HUTTNER, F. SEDAGHAT-HAMEDANI, S. JUST, T. DAHME *et al.*, 2011 PINCH proteins regulate cardiac contractility by modulating integrin-linked kinase-protein kinase B signaling. Mol Cell Biol **31:** 3424-3435.

MEDIONI, C., M. ASTIER, M. ZMOJDZIAN, K. JAGLA and M. SEMERIVA, 2008 Genetic control of cell morphogenesis during Drosophila melanogaster cardiac tube formation. J Cell Biol **182:** 249-261.

MEDIONI, C., S. SENATORE, P. A. SALMAND, N. LALEVEE, L. PERRIN *et al.*, 2009 The fabulous destiny of the Drosophila heart. Curr Opin Genet Dev **19:** 518-525.

MELKANI, G. C., R. BODMER, K. OCORR and S. I. BERNSTEIN, 2011 The UNC-45 chaperone is critical for establishing myosin-based myofibrillar organization and cardiac contractility in the Drosophila heart model. PLoS One **6:** e22579.

MERY, A., O. TAGHLI-LAMALLEM, K. A. CLARK, M. C. BECKERLE, X. WU *et al.*, 2008 The Drosophila muscle LIM protein, Mlp84B, is essential for cardiac function. J Exp Biol **211:** 15-23.

MILLER, A., 1950 The internal anatomy and histology of the imago of Drosophila melanogaster. Biology of Drosophila.**:** 420-534.

MILLS, R. P., and R. C. KING, 1965 The pericardial cells of Drosophila melanogaster. Q J Microsc Sci **106:** 261-268.

MIRANTI, C. K., and J. S. BRUGGE, 2002 Sensing the environment: a historical perspective on integrin signal transduction. Nat Cell Biol **4:** E83-E90.

MOHR, S. E., and N. PERRIMON, 2012 RNAi screening: new approaches, understandings, and organisms. Wiley Interdiscip Rev RNA **3:** 145-158.

MOLINA, M. R., and R. M. CRIPPS, 2001 Ostia, the inflow tracts of the Drosophila heart, develop from a genetically distinct subset of cardial cells. Mechanisms of Development **109:** 51-59.

MOLLOVA, M., K. BERSELL, S. WALSH, J. SAVLA, L. T. DAS *et al.*, 2013 Cardiomyocyte proliferation contributes to heart growth in young humans. Proc Natl Acad Sci U S A **110:** 1446-1451.

MONIER, B., M. ASTIER, M. SEMERIVA and L. PERRIN, 2005 Steroid-dependent modification of Hox function drives myocyte reprogramming in the Drosophila heart. Development **132:** 5283-5293.

MONTANEZ, E., S. USSAR, M. SCHIFFERER, M. BOSL, R. ZENT *et al.*, 2008 Kindlin-2 controls bidirectional signaling of integrins. Genes Dev **22:** 1325-1330.

MORGAN, T. H., 1910 Sex Limited Inheritance in Drosophila. Science **32:** 120-122.

MORRIS, C. J., J. N. YANG and F. A. SCHEER, 2012 The impact of the circadian timing system on cardiovascular and metabolic function. Prog Brain Res **199:** 337-358.

MOSER, M., K. R. LEGATE, R. ZENT and R. FASSLER, 2009 The tail of integrins, talin, and kindlins. Science **324:** 895-899.

MUKHERJEE, T., J. C. HOMBRIA and M. P. ZEIDLER, 2005 Opposing roles for Drosophila JAK/STAT signalling during cellular proliferation. Oncogene **24:** 2503-2511.

MULLER, H. J., 1927 Artificial Transmutation of the Gene. Science **66:** 84-87.

MULLER, P., M. BOUTROS and M. P. ZEIDLER, 2008 Identification of JAK/STAT pathway regulators--insights from RNAi screens. Semin Cell Dev Biol **19:** 360-369.

MUMMERY-WIDMER, J. L., M. YAMAZAKI, T. STOEGER, M. NOVATCHKOVA, S. BHALERAO *et al.*, 2009 Genome-wide analysis of Notch signalling in Drosophila by transgenic RNAi. Nature **458:** 987-992.

NA, J., L. P. MUSSELMAN, J. PENDSE, T. J. BARANSKI, R. BODMER *et al.*, 2013 A Drosophila model of high sugar diet-induced cardiomyopathy. PLoS Genet **9:** e1003175.

NAGAFUCHI, A., 2001 Molecular architecture of adherens junctions. Curr Opin Cell Biol **13:** 600-603.

NAYAL, A., D. J. WEBB and A. F. HORWITZ, 2004 Talin: an emerging focal point of adhesion dynamics. Current Opinion in Cell Biology **16:** 94-98.

NEELY, G. G., A. HESS, M. COSTIGAN, A. C. KEENE, S. GOULAS *et al.*, 2010a A genome-wide Drosophila screen for heat nociception identifies alpha2delta3 as an evolutionarily conserved pain gene. Cell **143:** 628-638.

NEELY, G. G., K. KUBA, A. CAMMARATO, K. ISOBE, S. AMANN *et al.*, 2010b A global in vivo Drosophila RNAi screen identifies NOT3 as a conserved regulator of heart function. Cell **141:** 142-153.

NELSON, W. J., 2008 Regulation of cell-cell adhesion by the cadherin-catenin complex. Biochem Soc Trans **36:** 149-155.

NENE, V., J. R. WORTMAN, D. LAWSON, B. HAAS, C. KODIRA *et al.*, 2007 Genome sequence of Aedes aegypti, a major arbovirus vector. Science **316:** 1718-1723.

NEUMULLER, R. A., C. RICHTER, A. FISCHER, M. NOVATCHKOVA, K. G. NEUMULLER *et al.*, 2011 Genome-wide analysis of self-renewal in Drosophila neural stem cells by transgenic RNAi. Cell Stem Cell **8:** 580-593.

NI, J. Q., M. MARKSTEIN, R. BINARI, B. PFEIFFER, L. P. LIU *et al.*, 2008 Vector and parameters for targeted transgenic RNA interference in Drosophila melanogaster. Nat Methods **5:** 49-51.

NISHIMURA, T., and M. TAKEICHI, 2009 Remodeling of the Adherens Junctions during Morphogenesis. Tissue Remodeling and Epithelial Morphogenesis **89:** 33-54.

NOORMAN, M., M. A. VAN DER HEYDEN, T. A. VAN VEEN, M. G. COX, R. N. HAUER *et al.*, 2009 Cardiac cell-cell junctions in health and disease: Electrical versus mechanical coupling. J Mol Cell Cardiol **47:** 23-31.

NUSSLEIN-VOLHARD, C., H. G. FROHNHOFER and R. LEHMANN, 1987 Determination of anteroposterior polarity in Drosophila. Science **238:** 1675-1681.

NUSSLEIN-VOLHARD, C., and E. WIESCHAUS, 1980 Mutations affecting segment number and polarity in Drosophila. Nature **287:** 795-801.

NUSSLEIN-VOLHARD, C., E. WIESCHAUS and H. KLUDING, 1984 Mutations Affecting the Pattern of the Larval Cuticle in Drosophila-Melanogaster .1. Zygotic Loci on the 2nd Chromosome. Wilhelm Rouxs Archives of Developmental Biology **193:** 267-282.

OCORR, K., T. AKASAKA and R. BODMER, 2007a Age-related cardiac disease model of Drosophila. Mech Ageing Dev **128:** 112-116.

OCORR, K., M. FINK, A. CAMMARATO, S. BERNSTEIN and R. BODMER, 2009 Semi-automated Optical Heartbeat Analysis of small hearts. J Vis Exp.

OCORR, K., L. PERRIN, H. Y. LIM, L. QIAN, X. WU *et al.*, 2007b Genetic control of heart function and aging in Drosophila. Trends Cardiovasc Med **17:** 177-182.

OCORR, K., N. L. REEVES, R. J. WESSELLS, M. FINK, H. S. CHEN *et al.*, 2007c KCNQ potassium channel mutations cause cardiac arrhythmias in Drosophila that mimic the effects of aging. Proc Natl Acad Sci U S A **104:** 3943-3948.

ODA, H., and M. TAKEICHI, 2011 Evolution Structural and functional diversity of cadherin at the adherens junction. Journal of Cell Biology **193:** 1137-1146.

OHNO, S., 1970 *Evolution by gene duplication*. Springer-Verlag, Berlin, New York,.

OLSON, E. N., 2006 Gene regulatory networks in the evolution and development of the heart. Science **313:** 1922-1927.

PEDERSEN, G. A., S. CHAKRABORTY, A. L. STEINHAUSER, L. M. TRAUB and M. MADSEN, 2010 AMN directs endocytosis of the intrinsic factor-vitamin B(12) receptor cubam by engaging ARH or Dab2. Traffic **11:** 706-720.

PERRIARD, J. C., A. HIRSCHY and E. EHLER, 2003 Dilated cardiomyopathy: a disease of the intercalated disc? Trends Cardiovasc Med **13:** 30-38.

PERRIMON, N., J. Q. NI and L. PERKINS, 2010 In vivo RNAi: today and tomorrow. Cold Spring Harb Perspect Biol **2:** a003640.

PERRIN, L., B. MONIER, R. PONZIELLI, M. ASTIER and M. SEMERIVA, 2004 Drosophila cardiac tube organogenesis requires multiple phases of Hox activity. Dev Biol **272:** 419-431.

PIAZZA, N., and R. J. WESSELLS, 2011 Drosophila models of cardiac disease. Prog Mol Biol Transl Sci **100:** 155-210.

PIVEN, O. O., I. E. KOSTETSKII, L. L. MACEWICZ, Y. M. KOLOMIETS, G. L. RADICE *et al.*, 2011 Requirement for N-cadherin-catenin complex in heart development. Exp Biol Med (Maywood) **236:** 816-822.

PLUSKOTA, E., J. J. DOWLING, N. GORDON, J. A. GOLDEN, D. SZPAK *et al.*, 2011 The integrin coactivator kindlin-2 plays a critical role in angiogenesis in mice and zebrafish. Blood **117:** 4978-4987.

PONZIELLI, R., M. ASTIER, A. CHARTIER, A. GALLET, P. THEROND *et al.*, 2002 Heart tube patterning in Drosophila requires integration of axial and segmental information provided by the Bithorax Complex genes and hedgehog signaling. Development **129:** 4509-4521.

POSPISILIK, J. A., D. SCHRAMEK, H. SCHNIDAR, S. J. F. CRONIN, N. T. NEHME *et al.*, 2010 Drosophila Genome-wide Obesity Screen Reveals Hedgehog as a Determinant of Brown versus White Adipose Cell Fate. Cell **140:** 148-160.

POSTEL, R., C. MARGADANT, B. FISCHER, M. KREFT, H. JANSSEN *et al.*, 2013 Kindlin-1 mutant zebrafish as an in vivo model sytem to study adhesion mechanisms in the epidermis. J Invest Dermatol.

POSTEL, R., P. VAKEEL, J. TOPCZEWSKI, R. KNOLL and J. BAKKERS, 2008 Zebrafish integrin-linked kinase is required in skeletal muscles for strengthening the integrin-ECM adhesion complex. Developmental Biology **318:** 92-101.

PROKOP, A., M. D. MARTIN-BERMUDO, M. BATE and N. H. BROWN, 1998 Absence of PS integrins or laminin A affects extracellular adhesion, but not intracellular assembly, of hemiadherens and neuromuscular junctions in Drosophila embryos. Dev Biol **196:** 58-76.

PRONOVOST, S. M., M. C. BECKERLE and J. L. KADRMAS, 2013 Elevated Expression of the Integrin-Associated Protein PINCH Suppresses the Defects of Drosophila melanogaster Muscle Hypercontraction Mutants. PLoS Genet **9:** e1003406.

PROUT, M., Z. DAMANIA, J. SOONG, D. FRISTROM and J. W. FRISTROM, 1997 Autosomal mutations affecting adhesion between wing surfaces in Drosophila melanogaster. Genetics **146:** 275-285.

PUNZO, C., S. PLAZA, M. SEIMIYA, P. SCHNUPF, S. KURATA *et al.*, 2004 Functional divergence between eyeless and twin of eyeless in Drosophila melanogaster. Development **131:** 3943-3953.

QADOTA, H., D. G. MOERMAN and G. M. BENIAN, 2012 A Molecular Mechanism for the Requirement of PAT-4 (Integrin-linked Kinase (ILK)) for the Localization of UNC-112 (Kindlin) to Integrin Adhesion Sites. Journal of Biological Chemistry **287:** 28537-28551.

QIAN, L., and R. BODMER, 2009 Partial loss of GATA factor Pannier impairs adult heart function in Drosophila. Hum Mol Genet **18:** 3153-3163.

QIAN, L., B. MOHAPATRA, T. AKASAKA, J. LIU, K. OCORR *et al.*, 2008 Transcription factor neuromancer/TBX20 is required for cardiac function in Drosophila with implications for human heart disease. Proc Natl Acad Sci U S A **105:** 19833-19838.

QIAN, L., J. D. WYTHE, J. LIU, J. CARTRY, G. VOGLER *et al.*, 2011 Tinman/Nkx2-5 acts via miR-1 and upstream of Cdc42 to regulate heart function across species. J Cell Biol **193:** 1181-1196.

REITER, L. T., L. POTOCKI, S. CHIEN, M. GRIBSKOV and E. BIER, 2001 A systematic analysis of human disease-associated gene sequences in Drosophila melanogaster. Genome Research **11:** 1114-1125.

ROGALSKI, T. M., G. P. MULLEN, M. M. GILBERT, B. D. WILLIAMS and D. G. MOERMAN, 2000 The UNC-112 gene in Caenorhabditis elegans encodes a novel component of cell-matrix adhesion structures required for integrin localization in the muscle cell membrane. J Cell Biol **150:** 253-264.

RONG, Y. S., and K. G. GOLIC, 2000 Gene targeting by homologous recombination in Drosophila. Science **288:** 2013-2018.

RORTH, P., 1996 A modular misexpression screen in Drosophila detecting tissue-specific phenotypes. Proc Natl Acad Sci U S A **93:** 12418-12422.

RORTH, P., K. SZABO, A. BAILEY, T. LAVERTY, J. REHM *et al.*, 1998 Systematic gain-of-function genetics in Drosophila. Development **125:** 1049-1057.

ROSS, R. S., and J. CHEN, 2008 Models that Buzz, Squeak, Ribbit and Oink: Using a Variety of Species to Study Cardiovascular Disease. Drug Discov Today Dis Models **5:** 113-115.

RUBIN, G. M., and A. C. SPRADLING, 1982 Genetic transformation of Drosophila with transposable element vectors. Science **218:** 348-353.

RUGENDORFF, A., A. YOUNOSSIHARTENSTEIN and V. HARTENSTEIN, 1994 Embryonic Origin and Differentiation of the Drosophila Heart. Rouxs Archives of Developmental Biology **203:** 266-280.

RYDER, E., F. BLOWS, M. ASHBURNER, R. BAUTISTA-LLACER, D. COULSON *et al.*, 2004 The DrosDel collection: a set of P-element insertions for generating custom chromosomal aberrations in Drosophila melanogaster. Genetics **167:** 797-813.

SACHS, N., and A. SONNENBERG, 2013 Cell-matrix adhesion of podocytes in physiology and disease. Nat Rev Nephrol **9:** 200-210.

SANTIAGO-MARTINEZ, E., N. H. SOPLOP, R. PATEL and S. G. KRAMER, 2008 Repulsion by Slit and Roundabout prevents Shotgun/E-cadherin-mediated

cell adhesion during Drosophila heart tube lumen formation. Journal of Cell Biology **182:** 241-248.

SCHOTT, J. J., D. W. BENSON, C. T. BASSON, W. PEASE, G. M. SILBERBACH *et al.*, 1998 Congenital heart disease caused by mutations in the transcription factor NKX2-5. Science **281:** 108-111.

SCHUPBACH, T., and E. WIESCHAUS, 1986 Maternal-Effect Mutations Altering the Anterior-Posterior Pattern of the Drosophila Embryo. Rouxs Archives of Developmental Biology **195:** 302-317.

SELLIN, J., S. ALBRECHT, V. KOLSCH and A. PAULULAT, 2006 Dynamics of heart differentiation, visualized utilizing heart enhancer elements of the Drosophila melanogaster bHLH transcription factor Hand. Gene Expr Patterns **6:** 360-375.

SERLUCA, F. C., and M. C. FISHMAN, 2006 Big, bad hearts: from flies to man. Proc Natl Acad Sci U S A **103:** 3947-3948.

SHAH, A. P., U. NONGTHOMBA, K. K. KELLY TANAKA, M. L. DENTON, S. M. MEADOWS *et al.*, 2011 Cardiac remodeling in Drosophila arises from changes in actin gene expression and from a contribution of lymph gland-like cells to the heart musculature. Mech Dev **128:** 222-233.

SHAI, S. Y., A. E. HARPF, C. J. BABBITT, M. C. JORDAN, M. C. FISHBEIN *et al.*, 2002 Cardiac myocyte-specific excision of the beta1 integrin gene results in myocardial fibrosis and cardiac failure. Circ Res **90:** 458-464.

SHAIK, K. S., F. MEYER, A. V. VAZQUEZ, M. FLOTENMEYER, M. E. CERDAN *et al.*, 2012 delta-Aminolevulinate synthase is required for apical transcellular barrier formation in the skin of the Drosophila larva. European Journal of Cell Biology **91:** 204-215.

SHEN, Z., Y. YE, L. DONG, S. VAINIONPAA, H. MUSTONEN *et al.*, 2012 Kindlin-2: a novel adhesion protein related to tumor invasion, lymph node metastasis, and patient outcome in gastric cancer. Am J Surg **203:** 222-229.

SHI, X., Y. Q. MA, Y. TU, K. CHEN, S. WU *et al.*, 2007 The MIG-2/integrin interaction strengthens cell-matrix adhesion and modulates cell motility. J Biol Chem **282:** 20455-20466.

SIN, S., F. BONIN, V. PETIT, D. MESEURE, F. LALLEMAND *et al.*, 2011 Role of the focal adhesion protein kindlin-1 in breast cancer growth and lung metastasis. J Natl Cancer Inst **103:** 1323-1337.

SINGLETON, K., and R. I. WOODRUFF, 1994 The osmolarity of adult Drosophila hemolymph and its effect on oocyte-nurse cell electrical polarity. Dev Biol **161:** 154-167.

SMITH, J. H., C. R. GREEN, N. S. PETERS, S. ROTHERY and N. J. SEVERS, 1991 Altered patterns of gap junction distribution in ischemic heart disease. An immunohistochemical study of human myocardium using laser scanning confocal microscopy. Am J Pathol **139:** 801-821.

SOPKO, N., Y. QIN, A. FINAN, A. DADABAYEV, S. CHIGURUPATI *et al.*, 2011 Significance of thymosin beta4 and implication of PINCH-1-ILK-alpha-parvin (PIP) complex in human dilated cardiomyopathy. PLoS One **6:** e20184.

SPRADLING, A. C., D. STERN, A. BEATON, E. J. RHEM, T. LAVERTY *et al.*, 1999 The Berkeley Drosophila Genome Project gene disruption project: Single P-element insertions mutating 25% of vital Drosophila genes. Genetics **153:** 135-177.

SPRADLING, A. C., D. M. STERN, I. KISS, J. ROOTE, T. LAVERTY *et al.*, 1995 Gene Disruptions Using P-Transposable Elements - an Integral Component of the Drosophila Genome Project. Proceedings of the National Academy of Sciences of the United States of America **92:** 10824-10830.

SPRAGG, D. D., and D. A. KASS, 2005 Controlling the gap: myocytes, matrix, and mechanics. Circ Res **96:** 485-487.

ST JOHNSTON, D., 2002 The art and design of genetic screens: Drosophila melanogaster. Nat Rev Genet **3:** 176-188.

STARK, K. A., G. H. YEE, C. E. ROOTE, E. L. WILLIAMS, S. ZUSMAN *et al.*, 1997 A novel alpha integrin subunit associates with beta PS and functions in tissue morphogenesis and movement during Drosophila development. Development **124:** 4583-4594.

STEBBINGS, L. A., M. G. TODMAN, R. PHILLIPS, C. E. GREER, J. TAM *et al.*, 2002 Gap junctions in Drosophila: developmental expression of the entire innexin gene family. Mech Dev **113:** 197-205.

STORZ, J. F., F. G. HOFFMANN, J. C. OPAZO and H. MORIYAMA, 2008 Adaptive functional divergence among triplicated alpha-globin genes in rodents. Genetics **178:** 1623-1638.

SUH, J. M., D. ZEVE, R. MCKAY, J. SEO, Z. SALO *et al.*, 2007 Adipose is a conserved dosage-sensitive antiobesity gene. Cell Metabolism **6:** 195-207.

TADOKORO, S., S. J. SHATTIL, K. ETO, V. TAI, R. C. LIDDINGTON *et al.*, 2003 Talin binding to integrin beta tails: a final common step in integrin activation. Science **302:** 103-106.

TAGHLI-LAMALLEM, O., T. AKASAKA, G. HOGG, U. NUDEL, D. YAFFE *et al.*, 2008 Dystrophin deficiency in Drosophila reduces lifespan and causes a dilated cardiomyopathy phenotype. Aging Cell **7:** 237-249.

TANAKA, M., Z. CHEN, S. BARTUNKOVA, N. YAMASAKI and S. IZUMO, 1999 The cardiac homeobox gene Csx/Nkx2.5 lies genetically upstream of multiple genes essential for heart development. Development **126:** 1269-1280.

TANENTZAPF, G., and N. H. BROWN, 2006 An interaction between integrin and the talin FERM domain mediates integrin activation but not linkage to the cytoskeleton. Nat Cell Biol **8:** 601-606.

TERRACIO, L., K. RUBIN, D. GULLBERG, E. BALOG, W. CARVER *et al.*, 1991 Expression of collagen binding integrins during cardiac development and hypertrophy. Circ Res **68:** 734-744.

THUM, A. S., S. KNAPEK, J. RISTER, E. DIERICHS-SCHMITT, M. HEISENBERG *et al.*, 2006 Differential potencies of effector genes in adult Drosophila. J Comp Neurol **498:** 194-203.

THUMMEL, C. S., 1996 Flies on steroids--Drosophila metamorphosis and the mechanisms of steroid hormone action. Trends Genet **12:** 306-310.

TOGEL, M., G. PASS and A. PAULULAT, 2008 The Drosophila wing hearts originate from pericardial cells and are essential for wing maturation. Dev Biol **318:** 29-37.

TSUJI, H., M. G. LARSON, F. J. VENDITTI, JR., E. S. MANDERS, J. C. EVANS *et al.*, 1996 Impact of reduced heart rate variability on risk for cardiac events. The Framingham Heart Study. Circulation **94:** 2850-2855.

TSUJI, H., F. J. VENDITTI, JR., E. S. MANDERS, J. C. EVANS, M. G. LARSON *et al.*, 1994 Reduced heart rate variability and mortality risk in an elderly cohort. The Framingham Heart Study. Circulation **90:** 878-883.

TU, Y., S. WU, X. SHI, K. CHEN and C. WU, 2003 Migfilin and Mig-2 link focal adhesions to filamin and the actin cytoskeleton and function in cell shape modulation. Cell **113:** 37-47.

TU, Y. Z., Y. HUANG, Y. J. ZHANG, Y. HUA and C. Y. WU, 2001 A new focal adhesion protein that interacts with integrin-linked kinase and regulates cell adhesion and spreading. Journal of Cell Biology **153:** 585-598.

USSAR, S., M. MOSER, M. WIDMAIER, E. ROGNONI, C. HARRER *et al.*, 2008 Loss of Kindlin-1 causes skin atrophy and lethal neonatal intestinal epithelial dysfunction. PLoS Genet **4:** e1000289.

USSAR, S., H. V. WANG, S. LINDER, R. FASSLER and M. MOSER, 2006 The Kindlins: subcellular localization and expression during murine development. Exp Cell Res **312:** 3142-3151.

VAKALOGLOU, K. M., M. CHOUNTALA and C. G. ZERVAS, 2012 Functional analysis of parvin and different modes of IPP-complex assembly at integrin sites during Drosophila development. J Cell Sci **125:** 3221-3232.

VALENCIK, M. L., D. ZHANG, B. PUNSKE, P. HU, J. A. MCDONALD *et al.*, 2006 Integrin activation in the heart: a link between electrical and contractile dysfunction? Circ Res **99:** 1403-1410.

VANDERPLOEG, J., L. L. VAZQUEZ PAZ, A. MACMULLIN and J. R. JACOBS, 2012 Integrins are required for cardioblast polarisation in Drosophila. BMC Dev Biol **12:** 8.

VASILE, V. C., S. R. OMMEN, W. D. EDWARDS and M. J. ACKERMAN, 2006 A missense mutation in a ubiquitously expressed protein, vinculin, confers susceptibility to hypertrophic cardiomyopathy. Biochem Biophys Res Commun **345:** 998-1003.

VENKEN, K. J., and H. J. BELLEN, 2005 Emerging technologies for gene manipulation in Drosophila melanogaster. Nat Rev Genet **6:** 167-178.

VOELKER, R. A., A. L. GREENLEAF, H. GYURKOVICS, G. B. WISELY, S. M. HUANG *et al.*, 1984 Frequent Imprecise Excision among Reversions of a P-Element-Caused Lethal Mutation in Drosophila. Genetics **107:** 279-294.

VOGLER, G., and K. OCORR, 2009 Visualizing the beating heart in Drosophila. J Vis Exp.

WALSH, E. P., and N. H. BROWN, 1998 A screen to identify drosophila genes required for integrin-mediated adhesion. Genetics **150:** 791-805.

WANG, J., Y. TAO, I. REIM, K. GAJEWSKI, M. FRASCH *et al.*, 2005 Expression, regulation, and requirement of the toll transmembrane protein during dorsal vessel formation in Drosophila melanogaster. Mol Cell Biol **25:** 4200-4210.

WANG, J. W., A. M. WONG, J. FLORES, L. B. VOSSHALL and R. AXEL, 2003 Two-photon calcium imaging reveals an odor-evoked map of activity in the fly brain. Cell **112:** 271-282.

WARD, E. J., and J. B. SKEATH, 2000 Characterization of a novel subset of cardiac cells and their progenitors in the Drosophila embryo. Development **127:** 4959-4969.

WATERHOUSE, R. M., F. TEGENFELDT, J. LI, E. M. ZDOBNOV and E. V. KRIVENTSEVA, 2013 OrthoDB: a hierarchical catalog of animal, fungal and bacterial orthologs. Nucleic Acids Res **41:** D358-365.

WEAVERS, H., S. PRIETO-SANCHEZ, F. GRAWE, A. GARCIA-LOPEZ, R. ARTERO *et al.*, 2009 The insect nephrocyte is a podocyte-like cell with a filtration slit diaphragm. Nature **457:** 322-U325.

WESSELLS, R., E. FITZGERALD, N. PIAZZA, K. OCORR, S. MORLEY *et al.*, 2009 d4eBP acts downstream of both dTOR and dFoxo to modulate cardiac functional aging in Drosophila. Aging Cell **8:** 542-552.

WESSELLS, R. J., E. FITZGERALD, J. R. CYPSER, M. TATAR and R. BODMER, 2004 Insulin regulation of heart function in aging fruit flies. Nat Genet **36:** 1275-1281.

WHITE, D. E., P. COUTU, Y. F. SHI, J. C. TARDIF, S. NATTEL *et al.*, 2006 Targeted ablation of ILK from the murine heart results in dilated cardiomyopathy and spontaneous heart failure. Genes Dev **20:** 2355-2360.

WHITE, S. J., and W. H. MCLEAN, 2005 Kindler surprise: mutations in a novel actin-associated protein cause Kindler syndrome. J Dermatol Sci **38:** 169-175.

WICKSTROM, S. A., A. LANGE, E. MONTANEZ and R. FASSLER, 2010 The ILK/PINCH/parvin complex: the kinase is dead, long live the pseudokinase! EMBO J **29:** 281-291.

WILLIAMS, B. D., and R. H. WATERSTON, 1994 Genes critical for muscle development and function in Caenorhabditis elegans identified through lethal mutations. J Cell Biol **124:** 475-490.

WING, J., L. ZHOU, L. SCHWARTZ and J. NAMBU, 1999 Distinct cell killing properties of the Drosophila reaper, head involution defective, and grim genes. Cell Death Differ **6:** 212-213.

WOLF, M. J., H. AMREIN, J. A. IZATT, M. A. CHOMA, M. C. REEDY *et al.*, 2006 Drosophila as a model for the identification of genes causing adult human heart disease. Proc Natl Acad Sci U S A **103:** 1394-1399.

WOLF, M. J., and H. A. ROCKMAN, 2011 Drosophila, genetic screens, and cardiac function. Circ Res **109:** 794-806.

WOLFSON, M., A. BUDOVSKY, R. TACUTU and V. FRAIFELD, 2009 The signaling hubs at the crossroad of longevity and age-related disease networks. International Journal of Biochemistry & Cell Biology **41:** 516-520.

WU, C., 2005 Migfilin and its binding partners: from cell biology to human diseases. J Cell Sci **118:** 659-664.

XIE, H. B., and K. G. GOLIC, 2004 Gene deletions by ends-in targeting in Drosophila melanogaster. Genetics **168:** 1477-1489.

YANG, W. Y., S. Y. WEN, Y. D. HUANG, M. Q. YE, X. J. DENG *et al.*, 2006 Functional divergence of six isoforms of antifungal peptide Drosomycin in Drosophila melanogaster. Gene **379:** 26-32.

YARNITZKY, T., and T. VOLK, 1995 Laminin Is Required for Heart, Somatic Muscles, and Gut Development in the Drosophila Embryo. Developmental Biology **169:** 609-618.

YI, P., A. N. JOHNSON, Z. HAN, J. WU and E. N. OLSON, 2008 Heterotrimeric G proteins regulate a noncanonical function of septate junction proteins to maintain cardiac integrity in Drosophila. Dev Cell **15:** 704-713.

YIN, L., N. WU, J. C. CURTIN, M. QATANANI, N. R. SZWERGOLD *et al.*, 2007 Rev-erb alpha, a heme sensor that coordinates metabolic and circadian pathways. Science **318:** 1786-1789.

YIN, Z., X. L. XU and M. FRASCH, 1997 Regulation of the twist target gene tinman by modular cis-regulatory elements during early mesoderm development. Development **124:** 4971-4982.

YOUNG, M. E., P. RAZEGHI, A. M. CEDARS, P. H. GUTHRIE and H. TAEGTMEYER, 2001 Intrinsic diurnal variations in cardiac metabolism and contractile function. Circ Res **89:** 1199-1208.

YU, L., J. DANIELS, A. E. GLASER and M. J. WOLF, 2013 Raf-mediated cardiac hypertrophy in adult Drosophila. Disease Models & Mechanisms.

YU, L., T. LEE, N. LIN and M. J. WOLF, 2010 Affecting Rhomboid-3 function causes a dilated heart in adult Drosophila. PLoS Genet **6:** e1000969.

YU, Y., J. WU, Y. WANG, T. ZHAO, B. MA *et al.*, 2012 Kindlin 2 forms a transcriptional complex with beta-catenin and TCF4 to enhance Wnt signalling. EMBO Rep.

ZAFFRAN, S., I. REIM, L. QIAN, P. C. LO, R. BODMER *et al.*, 2006 Cardioblast-intrinsic Tinman activity controls proper diversification and differentiation of myocardial cells in Drosophila. Development **133:** 4073-4083.

ZAIDEL-BAR, R., S. ITZKOVITZ, A. MA'AYAN, R. IYENGAR and B. GEIGER, 2007 Functional atlas of the integrin adhesome. Nat Cell Biol **9:** 858-868.

ZEITOUNI, B., S. SENATORE, D. SEVERAC, C. AKNIN, M. SEMERIVA *et al.*, 2007 Signalling pathways involved in adult heart formation revealed by gene expression profiling in Drosophila. PLoS Genet **3:** 1907-1921.

ZERVAS, C. G., and N. H. BROWN, 2002 Integrin adhesion: When is a kinase a kinase? Current Biology **12:** R350-R351.

ZERVAS, C. G., S. L. GREGORY and N. H. BROWN, 2001 Drosophila integrin-linked kinase is required at sites of integrin adhesion to link the cytoskeleton to the plasma membrane. J Cell Biol **152:** 1007-1018.

ZERVAS, C. G., E. PSARRA, V. WILLIAMS, E. SOLOMON, K. M. VAKALOGLOU *et al.*, 2011 A central multifunctional role of integrin-linked kinase at muscle attachment sites. J Cell Sci **124:** 1316-1327.

ZHAN, Z., Y. DING, R. ZHAO, Y. ZHANG, H. YU *et al.*, 2012 Rapid functional divergence of a newly evolved polyubiquitin gene in Drosophila and its role in the trade-off between male fecundity and lifespan. Mol Biol Evol **29:** 1407-1416.

ZHANG, F., Y. ZHAO, Y. CHAO, K. MUIR and Z. HAN, 2013 Cubilin and amnionless mediate protein reabsorption in Drosophila nephrocytes. J Am Soc Nephrol **24:** 209-216.

ZHANG, Y., Y. TU, V. GKRETSI and C. WU, 2006 Migfilin interacts with vasodilator-stimulated phosphoprotein (VASP) and regulates VASP localization to cell-matrix adhesions and migration. J Biol Chem **281:** 12397-12407.

ZHANG, Y. X., S. SIVASANKAR, W. J. NELSON and S. CHU, 2009 Resolving cadherin interactions and binding cooperativity at the single-molecule level. Proceedings of the National Academy of Sciences of the United States of America **106:** 109-114.

ZHU, X., S. M. AHMAD, A. ABOUKHALIL, B. W. BUSSER, Y. KIM *et al.*, 2012 Differential regulation of mesodermal gene expression by Drosophila cell type-specific Forkhead transcription factors. Development **139:** 1457-1466.

Appendix

HUMAN TO FLY : Genes expressed >3 fold in human heart with homologs expressed >3 fold in fly heart.

	HUMAN						DROSOPHILA							
Sequence identity (%)	**Ensembl Gene ID**	**Associated Gene Name**	**Ensembl Description**	**OMIM**	**Known role in heart or muscle?**	**REFS**	**Ensembl Gene ID**	**Associated Gene Name**	**Full name**	**Role in fly heart?**	**VDRC**	**Obtained?**	**P-element?**	**Linkouts**
49	ENSG00000023330	ALAS1	aminolevulinate, delta-, synthase 1 [Source:HGNC Symbol;Acc:396]	http://www.omim.org/entry/125290?search=ALAS1&highlight=alas1	No		FBgn0020764	Alas	Aminolevulinate synthase [Source:FlyBase gene name;Acc:FBgn0020764]		48774, 105958	yes, yes	http://flybase.org/reports/FBti0110323.html, Bloomington stock = 15225 caused by insertion of P{SUPor-P}AlasKG10015 in 5' region of gene, allele is balanced over CyO kyoto stock = 206608 caused by insertion of y1 w67c23; P{GSV6}GS16372/SM1 near the pSUPor insertion.	
31	ENSG00000053254	FOXN3	forkhead box N3 [Source:HGNC Symbol;Acc:1928]	http://www.omim.org/entry/602628?search=FOXN3&highlight=foxn3	Interacts with SKIP a homolog of Fly Bx42 - which is expressedi n the heart		FBgn0029504	CHES-1-like	Checkpoint suppressor homologue [Source:FlyBase gene name;Acc:FBgn0029504]	Care - lots of human orthologs. Does this interact with Bx42 too?	15742, 105641	yes, yes	http://flybase.org/cgi-bin/uniq.html?FBgn0029504%3Efbst	Links out to homology with FOXP4 not FOXN3, FOXP4 mice have two hearts
42	ENSG00000095587	TLL2	tolloid-like 2 [Source:HGNC Symbol;Acc:11844]	http://www.omim.org/entry/606743?search=TLL2&highlight=tll2	NO but TLL1 is at least involved in heart development	http://www.ncbi.nlm.nih.gov/pubmed/19366374	FBgn0003719	tld	tolloid [Source:FlyBase gene name;Acc:FBgn0003719]		1215, 1216	yes, yes	http://flybase.org/cgi-bin/uniq.html?FBgn0003719%3Efbst	might interact with Timp in heart?
41	ENSG00000101400	SNTA1	syntrophin, alpha 1 (dystrophin-associated protein A1, 59kDa, acidic component) [Source:HGNC Symbol;Acc:11167]	http://www.omim.org/entry/601017?search=SNTA1&highlight=snta1	Yes - but limited data, 1 allelic variant is associated with long QT	Ueda, K., Valdivia, C., Medeiros-Domingo, A., Tester, D. J., Vatta, M., Farrugia, G., Ackerman, M. J., Makielski, J. C. Syntrophin mutation associated with long QT syndrome through activation of the nNOS-SCN5A macromolecular complex. Proc. Nat. Acad. Sci. 105: 9355-9360, 2008. [PubMed: 18591664, related citations]	FBgn0037130	Syn1	Syntrophin-like 1 [Source:FlyBase gene name;Acc:FBgn0037130]		27893, 104992	yes, yes		
32	ENSG00000131669	NINJ1	ninjurin 1 [Source:HGNC Symbol;Acc:7824]				FBgn0036101	NijA	Ninjurin A [Source:FlyBase gene name;Acc:FBgn0036101]		5208, 103439	yes, no	NijA isoform A coding sequences are cloned into the "pRmHa-3" plasmid which contains a MtnA promoter and a T:Ivir\HA1 tag.	
30	ENSG00000131670	NINJ2	ninjurin 1 [Source:HGNC Symbol;Acc:7824]				FBgn0036822	CG11637	Ninjurin B		48786 , 48787	yes, yes		
21	ENSG00000157150	TIMP4	TIMP metallopeptidase inhibitor 4 [Source:HGNC Symbol;Acc:11823]				FBgn0025879	Timp	Tissue inhibitor of metalloproteases [Source:FlyBase gene name;Acc:FBgn0025879]		15372, 15373	yes, yes	http://flybase.org/reports/FBal0218943.html	
58	ENSG00000072163	LIMS2	LIM and senescent cell antigen-like domains 2 [Source:HGNC Symbol;Acc:16084]	http://www.omim.org/entry/607908?search=lims2&highlight=lims2	YES - Cardiomyopathy in ablation models	http://www.ncbi.nlm.nih.gov/pubmed?term=LIMS2%20AND%20heart	FBgn0020249	stck	steamer duck [Source:FlyBase gene name;Acc:FBgn0020249]		52537, 52538	yes, yes	http://flybase.org/cgi-bin/uniq.html?FBgn0020249%3Efbst	Links out to LIMS1
48	ENSG00000073712	KIND2	fermitin family member 2 [Source:HGNC Symbol;Acc:15767]	http://omim.org/entry/607746	YES - Cardiomyopathy in ablation models	http://www.ncbi.nlm.nih.gov/pubmed/?term=Kindlin+2+AND+heart	FBgn0035498	Fit1	Fermitin 1 [Source:FlyBase gene name;Acc:FBgn0035498]		46494, 46495	yes, yes	http://flybase.org/reports/FBgn0035498.html	
18	ENSG00000163884	KLF15	Kruppel-like factor 15 [Source:HGNC Symbol;Acc:14536]	http://omim.org/entry/606465	YES - Cardiomyopathy in ablation models	http://www.ncbi.nlm.nih.gov/pubmed/?term=klf15+heart	FBgn0025679	Bteb2	Bteb2 [Source:FlyBase gene name;Acc:FBgn0025679]		110761	yes, yes	http://flybase.org/reports/FBgn0025679.html	

Second-site non-complementation screen

1 *mys1/FM4* X *w1118/Y*

	mys1	*FM4*
w1118	*33*	*95*
Y	*0*	*33*

Total flies	Trans-Het/Total progeny*100	Expected Trans-Het progeny (%)	"WT" progeny	Expected "WT" progeny	Observed/Expected Trans-Het*100
161	20.50	25	79.50	75	81.99

2 *mys1/FM4* X *yw/Y; ; Fit1KG05576*

	mys1; ; Fit1KG05576	*FM4; ; Fit1KG05576*
yw; ; +	*96*	*133*
Y; ; +	*0*	*85*

Total flies	Trans-Het/Total progeny*100	Expected Trans-Het progeny (%)	"WT" progeny	Expected "WT" progeny	Observed/Expected Trans-Het*100
314	30.57	25	69.43	75	122.29

3 *mys1/FM4* X *yw/Y; ; Fit2EY08530*

	mys1; ; Fit2EY08530	*FM4; ; Fit2EY08530*
yw; ; +	*108*	*120*
Y; ; +	*0*	*77*

Total flies	Trans-Het/Total progeny*100	Expected Trans-Het progeny (%)	"WT" progeny	Expected "WT" progeny	Observed/Expected Trans-Het*100
305	35.41	25	64.59	75	141.64

4 *mys1/FM4* X *w*/Y; ; Fit1 Δ 81*

	mys1; ; Fit1Δ81	*FM4; ; Fit1Δ81*
w; ; +*	*92*	*117*
Y; ; +	*0*	*80*

Total flies	Trans-Het/Total progeny*100	Expected Trans-Het progeny (%)	"WT" progeny	Expected "WT" progeny	Observed/Expected Trans-Het*100
289	31.83	25	68.17	75	127.34

5 *mys1/FM4* X *w*/Y; ; Fit1 Δ 161*

	mys1; ; Fit1Δ161	*FM4; ; Fit1Δ161*
w; ; +*	*94*	*143*
Y; ; +	*0*	*42*

Total flies	Trans-Het/Total progeny*100	Expected Trans-Het progeny (%)	"WT" progeny	Expected "WT" progeny	Observed/Expected Trans-Het*100
279	33.69	25	66.31	75	134.77

6 *mys1/FM4* X *w*/Y; ; Fit1 Δ193/TM3, GFP, Ser1*

	mys1; ; Fit1Δ193	*FM4; ; Fit1Δ193*	*mys1; ; TM3, GFP, Ser1*	*FM4; ; TM3, GFP, Ser1*
w; ; +*	*53*	*63*	31	60
Y; ; +	*0*	*30*	*0*	11

Total flies	Trans-Het/Total progeny*100	Expected Trans-Het progeny (%)	"WT" progeny	Expected "WT" progeny	Observed/Expected Trans-Het*100
248	21.37	12.5	78.63	87.5	170.97

7 *mys1/FM4* X *w*/Y; ; Fit1 Δ161 Fit2EY08530/TM3, GFP, Ser1*

	mys1; ; Fit1Δ161 Fit2EY08530	*FM4; ; Fit1Δ161 Fit2EY08530*	*mys1; ; TM3, GFP, Ser1*	*FM4; ; TM3, GFP, Ser1*
w; ; +*	*48*	*61*	47	60
Y; ; +	*0*	*36*	*0*	9

Total flies	Trans-Het/Total progeny*100	Expected Trans-Het progeny (%)	"WT" progeny	Expected "WT" progeny	Observed/Expected Trans-Het*100
261	18.39	12.5	81.61	87.5	147.13

Second-site non-complementation screen

1 *mewM6/FM7c* **X** *w1118/Y*

	mewM6	*FM7c*
w1118	*168*	*145*
Y	*0*	*111*

Total flies	Trans-Het/Total progeny*100	Expected Trans-Het progeny (%)	"WT" progeny	Expected "WT" progeny	Observed/Expected Trans-Het*100
424	39.62	25	60.38	75	158.49

2 *mewM6/FM7c* **X** *yw/Y; ; Fit1KG05576*

	mewM6; ; Fit1KG05576	*FM7c; ; Fit1KG05576*
yw; ; +	*158*	*163*
Y; ; +	*0*	*96*

Total flies	Trans-Het/Total progeny*100	Expected Trans-Het progeny (%)	"WT" progeny	Expected "WT" progeny	Observed/Expected Trans-Het*100
417	37.89	25	62.11	75	151.56

3 *mewM6/FM7c* **X** *yw/Y; ; Fit2EY08530*

	mewM6; ; Fit2EY08530	*FM7c; ; Fit2EY08530*
yw; ; +	*189*	*166*
Y; ; +	*0*	*113*

Total flies	Trans-Het/Total progeny*100	Expected Trans-Het progeny (%)	"WT" progeny	Expected "WT" progeny	Observed/Expected Trans-Het*100
468	40.38	25	59.62	75	161.54

4 *mewM6/FM7c* **X** *w*/Y; ; Fit1 Δ 81*

	mewM6; ; Fit1Δ81	*FM7c; ; Fit1Δ81*
w; ; +*	*148*	*140*
Y; ; +	*0*	*90*

Total flies	Trans-Het/Total progeny*100	Expected Trans-Het progeny (%)	"WT" progeny	Expected "WT" progeny	Observed/Expected Trans-Het*100
378	39.15	25	60.85	75	156.61

5 *mewM6/FM7c* **X** *w*/Y; ; Fit1 Δ 161*

	mewM6; ; Fit1Δ161	*FM7c; ; Fit1Δ161*
w; ; +*	*200*	*162*
Y; ; +	*0*	*138*

Total flies	Trans-Het/Total progeny*100	Expected Trans-Het progeny (%)	"WT" progeny	Expected "WT" progeny	Observed/Expected Trans-Het*100
500	40.00	25	60.00	75	160.00

6 *mewM6/FM7c* **X** *w*/Y; ; Fit1 Δ193/TM3, GFP, Ser1*

	mewM6; ; Fit1Δ193	*FM7c; ; Fit1Δ193*	*mewM6; ; TM3, GFP, Ser1*	*FM7c; ; TM3, GFP, Ser1*
w; ; +*	*130*	*75*	53	73
Y; ; +	*0*	*37*	*0*	24

Total flies	Trans-Het/Total progeny*100	Expected Trans-Het progeny (%)	"WT" progeny	Expected "WT" progeny	Observed/Expected Trans-Het*100
392	33.16	12.5	66.84	87.5	265.31

7 *mewM6/FM7c* **X** *w*/Y; ; Fit1 Δ161 Fit2EY08530/TM3, GFP, Ser1*

	mewM6; ; Fit1Δ161 Fit2EY08530	*FM7c; ; Fit1Δ161 Fit2EY08530*	*mewM6; ; TM3, GFP, Ser1*	*FM7c; ; TM3, GFP, Ser1*
w; ; +*	*128*	*85*	46	70
Y; ; +	*0*	*52*	*0*	39

Total flies	Trans-Het/Total progeny*100	Expected Trans-Het progeny (%)	"WT" progeny	Expected "WT" progeny	Observed/Expected Trans-Het*100
420	30.48	12.5	69.52	87.5	243.81

Second-site non-complementation screen

1 *ifB2/FM7c* **X** *w1118/Y*

	ifB2	FM7c
w1118	93	90
Y	0	79

Total flies	Trans-Het/Total progeny*100	Expected Trans-Het progeny (%)	"WT" progeny	Expected "WT" progeny	Observed/Expected Trans-Het*100
262	35.50	25	64.50	75	141.98

2 *ifB2/FM7c* **X** *yw/Y; ; Fit1KG05576*

	ifB2; ; Fit1KG05576	FM7c; ; Fit1KG05576
yw; ; +	99	116
Y; ; +	0	56

Total flies	Trans-Het/Total progeny*100	Expected Trans-Het progeny (%)	"WT" progeny	Expected "WT" progeny	Observed/Expected Trans-Het*100
271	36.53	25	63.47	75	146.13

3 *ifB2/FM7c* **X** *yw/Y; ; Fit2EY08530*

	ifB2; ; Fit2EY08530	FM7c; ; Fit2EY08530
yw; ; +	92	83
Y; ; +	0	69

Total flies	Trans-Het/Total progeny*100	Expected Trans-Het progeny (%)	"WT" progeny	Expected "WT" progeny	Observed/Expected Trans-Het*100
244	37.70	25	62.30	75	150.82

4 *ifB2/FM7c* **X** *w*/Y; ; Fit1 Δ 81*

	ifB2; ; Fit1Δ81	FM7c; ; Fit1Δ81
w*; ; +	127	81
Y; ; +	0	52

Total flies	Trans-Het/Total progeny*100	Expected Trans-Het progeny (%)	"WT" progeny	Expected "WT" progeny	Observed/Expected Trans-Het*100
260	48.85	25	51.15	75	195.38

5 *ifB2/FM7c* **X** *w*/Y; ; Fit1 Δ 161*

	ifB2; ; Fit1Δ161	FM7c; ; Fit1Δ161
w*; ; +	134	102
Y; ; +	0	62

Total flies	Trans-Het/Total progeny*100	Expected Trans-Het progeny (%)	"WT" progeny	Expected "WT" progeny	Observed/Expected Trans-Het*100
298	44.97	25	55.03	75	179.87

6 *ifB2/FM7c* **X** *w*/Y; ; Fit1 Δ193/TM3, GFP, Ser1*

	ifB2; ; Fit1Δ193	FM7c; ; Fit1Δ193	ifB2; ; TM3, GFP, Ser1	FM7c; ; TM3, GFP, Ser1
w*; ; +	67	58	52	52
Y; ; +	0	40	0	16

Total flies	Trans-Het/Total progeny*100	Expected Trans-Het progeny (%)	"WT" progeny	Expected "WT" progeny	Observed/Expected Trans-Het*100
285	23.51	12.5	76.49	87.5	188.07

7 *ifB2/FM7c* **X** *w*/Y; ; Fit1 Δ161 Fit2EY08530/TM3, GFP, Ser1*

	ifB2; ; Fit1Δ161 Fit2EY08530	FM7c; ; Fit1Δ161 Fit2EY08530	ifB2; ; TM3, GFP, Ser1	FM7c; ; TM3, GFP, Ser1
w*; ; +	71	76	54	50
Y; ; +	0	64	0	38

Total flies	Trans-Het/Total progeny*100	Expected Trans-Het progeny (%)	"WT" progeny	Expected "WT" progeny	Observed/Expected Trans-Het*100
353	20.11	12.5	79.89	87.5	160.91

Second-site non-complementation screen

1 ***yw/yw; ; rhea1/TM6B, Tb1*** **X** ***w1118/Y***

	yw; ; rhea1	yw; ; TM6B, Tb1
w1118; ; +	95	96
Y; ; +	114	69

Total flies	Trans-Het/Total progeny*100	Expected Trans-Het progeny (%)	"WT" progeny	Expected "WT" progeny	Observed/Expected Trans-Het*100
374	55.88	50	44.12	50	111.76

2 ***yw/yw; ; rhea1/TM6B, Tb1*** **X** ***yw/Y; ; Fit1KG05576***

	yw; ; rhea1	yw; ; TM6B, Tb1
yw; ; Fit1KG05576	99	98
Y; ; Fit1KG05576	82	94

Total flies	Trans-Het/Total progeny*100	Expected Trans-Het progeny (%)	"WT" progeny	Expected "WT" progeny	Observed/Expected Trans-Het*100
373	48.53	50	51.47	50	97.05

3 ***yw/yw; ; rhea1/TM6B, Tb1*** **X** ***yw/Y; ; Fit2EY08530***

	yw; ; rhea1	yw; ; TM6B, Tb1
yw; ; Fit2EY08530	144	59
Y; ; Fit2EY08530	130	70

Total flies	Trans-Het/Total progeny*100	Expected Trans-Het progeny (%)	"WT" progeny	Expected "WT" progeny	Observed/Expected Trans-Het*100
403	67.99	50	32.01	50	135.98

4 ***yw/yw; ; rhea1/TM6B, Tb1*** **X** ***w*/Y; ; Fit1 Δ 81***

	yw; ; rhea1	yw; ; TM6B, Tb1
w*; ; Fit1Δ81	66	48
Y; ; Fit1Δ81	65	49

Total flies	Trans-Het/Total progeny*100	Expected Trans-Het progeny (%)	"WT" progeny	Expected "WT" progeny	Observed/Expected Trans-Het*100
228	57.46	50	42.54	50	114.91

5 ***yw/yw; ; rhea1/TM6B, Tb1*** **X** ***w*/Y; ; Fit1 Δ 161***

	yw; ; rhea1	yw; ; TM6B, Tb1
w*; ; Fit1Δ161	106	56
Y; ; Fit1Δ161	94	72

Total flies	Trans-Het/Total progeny*100	Expected Trans-Het progeny (%)	"WT" progeny	Expected "WT" progeny	Observed/Expected Trans-Het*100
328	60.98	50	39.02	50	121.95

6 ***yw/yw; ; rhea1/TM6B, Tb1*** **X** ***w*/Y; ; Fit1 Δ193/TM3, GFP, Ser1***

	yw; ; rhea1	yw; ; TM6B, Tb1
w*; ; Fit1Δ193	53	35
Y; ; Fit1Δ193	59	47
w*; ; TM3, GFP, Ser1	50	24
Y; ; TM3, GFP, Ser1	43	22

Total flies	Trans-Het/Total progeny*100	Expected Trans-Het progeny (%)	"WT" progeny	Expected "WT" progeny	Observed/Expected Trans-Het*100
333	33.63	25	66.37	75	134.53

7 ***yw/yw; ; rhea1/TM6B, Tb7*** **X** ***w*/Y; ; Fit1 Δ161 Fit2EY08530/TM3, GFP, Ser1***

	yw; ; rhea1	yw; ; TM6B, Tb1
w*; ; Fit1Δ161 Fit2EY08530	66	42
Y; ; Fit1Δ161 Fit2EY08530	45	50
w*; ; TM3, GFP, Ser1	55	37
Y; ; TM3, GFP, Ser1	63	38

Total flies	Trans-Het/Total progeny*100	Expected Trans-Het progeny (%)	"WT" progeny	Expected "WT" progeny	Observed/Expected Trans-Het*100
396	28.03	25	71.97	75	112.12

Second-site non-complementation screen

1 *+/+; ; Ilk1/TM3, Sb1* **X** *w1118/Y*

	+; ; Ilk1	+; ; TM3, Sb1
w1118; ; +	181	133
Y; ; +	149	150

Total flies	Trans-Het/Total progeny*100	Expected Trans-Het progeny (%)	"WT" progeny	Expected "WT" progeny	Observed/Expected Trans-Het*100
613	53.83	50	46.17	50	107.67

2 *+/+; ; Ilk1/TM3, Sb1* **X** *yw/Y; ; Fit1KG05576*

	+; ; Ilk1	+; ; TM3, Sb1
yw; ; Fit1KG05576	156	127
Y; ; Fit1KG05576	150	92

Total flies	Trans-Het/Total progeny*100	Expected Trans-Het progeny (%)	"WT" progeny	Expected "WT" progeny	Observed/Expected Trans-Het*100
525	58.29	50	41.71	50	116.57

3 *+/+; ; Ilk1/TM3, Sb1* **X** *yw/Y; ; Fit2EY08530*

	+; ; Ilk1	+; ; TM3, Sb1
yw; ; Fit2EY08530	170	151
Y; ; Fit2EY08530	159	128

Total flies	Trans-Het/Total progeny*100	Expected Trans-Het progeny (%)	"WT" progeny	Expected "WT" progeny	Observed/Expected Trans-Het*100
608	54.11	50	45.89	50	108.22

4 *+/+; ; Ilk1/TM3, Sb1* **X** *w*/Y; ; Fit1 Δ 81*

	+; ; Ilk1	+; ; TM3, Sb1
w*; ; Fit1Δ81	153	113
Y; ; Fit1Δ81	128	107

Total flies	Trans-Het/Total progeny*100	Expected Trans-Het progeny (%)	"WT" progeny	Expected "WT" progeny	Observed/Expected Trans-Het*100
501	56.09	50	43.91	50	112.18

5 *+/+; ; Ilk1/TM3, Sb1* **X** *w*/Y; ; Fit1 Δ 161*

	+; ; Ilk1	+; ; TM3, Sb1
w*; ; Fit1Δ161	160	136
Y; ; Fit1Δ161	151	109

Total flies	Trans-Het/Total progeny*100	Expected Trans-Het progeny (%)	"WT" progeny	Expected "WT" progeny	Observed/Expected Trans-Het*100
556	55.94	50	44.06	50	111.87

6 *+/+; ; Ilk1/TM3, Sb1* **X** *w*/Y; ; Fit1 Δ193/TM3, GFP, Ser1*

	+; ; Ilk1	+; ; TM3, Sb1
w*; ; Fit1Δ193	112	74
Y; ; Fit1Δ193	105	58
w*; ; TM3, GFP, Ser1	91	0
Y; ; TM3, GFP, Ser1	73	0

Total flies	Trans-Het/Total progeny*100	Expected Trans-Het progeny (%)	"WT" progeny	Expected "WT" progeny	Observed/Expected Trans-Het*100
513	42.30	25	57.70	75	169.20

7 *+/+; ; Ilk1/TM3, Sb1* **X** *w*/Y; ; Fit1 Δ161 Fit2EY08530/TM3, GFP, Ser1*

	+; ; Ilk1	+; ; TM3, Sb1
w*; ; Fit1Δ161 Fit2EY08530	96	92
Y; ; Fit1Δ161 Fit2EY08530	88	81
w*; ; TM3, GFP, Ser1	103	0
Y; ; TM3, GFP, Ser1	94	0

Total flies	Trans-Het/Total progeny*100	Expected Trans-Het progeny (%)	"WT" progeny	Expected "WT" progeny	Observed/Expected Trans-Het*100
554	33.21	25	66.79	75	132.85

Second-site non-complementation screen

1 *yw/yw; ; stck3R-17/TM6B, Tb1* **X** *w1118/Y*

	yw; ; stck3R-17	yw; ; TM6B, Tb1
w1118; ; +	147	75
Y; ; +	154	61

Total flies	Trans-Het/Total progeny*100	Expected Trans-Het progeny (%)	"WT" progeny	Expected "WT" progeny	Observed/Expected Trans-Het*100
437	68.88	50	31.12	50	137.76

2 *yw/yw; ; stck3R-17/TM6B, Tb1* **X** *yw/Y; ; Fit1KG05576*

	yw; ; stck3R-17	yw; ; TM6B, Tb1
yw; ; Fit1KG05576	121	79
Y; ; Fit1KG05576	89	85

Total flies	Trans-Het/Total progeny*100	Expected Trans-Het progeny (%)	"WT" progeny	Expected "WT" progeny	Observed/Expected Trans-Het*100
374	56.15	50	43.85	50	112.30

3 *yw/yw; ; stck3R-17/TM6B, Tb1* **X** *yw/Y; ; Fit2EY08530*

	yw; ; stck3R-17	yw; ; TM6B, Tb1
yw; ; Fit2EY08530	122	82
Y; ; Fit2EY08530	113	68

Total flies	Trans-Het/Total progeny*100	Expected Trans-Het progeny (%)	"WT" progeny	Expected "WT" progeny	Observed/Expected Trans-Het*100
385	61.04	50	38.96	50	122.08

4 *yw/yw; ; stck3R-17/TM6B, Tb1* **X** *w*/Y; ; Fit1 Δ 81*

	yw; ; stck3R-17	yw; ; TM6B, Tb1
w*; ; Fit1Δ81	114	88
Y; ; Fit1Δ81	114	63

Total flies	Trans-Het/Total progeny*100	Expected Trans-Het progeny (%)	"WT" progeny	Expected "WT" progeny	Observed/Expected Trans-Het*100
379	60.16	50	39.84	50	120.32

5 *yw/yw; ; stck3R-17/TM6B, Tb1* **X** *w*/Y; ; Fit1 Δ 161*

	yw; ; stck3R-17	yw; ; TM6B, Tb1
w*; ; Fit1Δ161	136	88
Y; ; Fit1Δ161	111	80

Total flies	Trans-Het/Total progeny*100	Expected Trans-Het progeny (%)	"WT" progeny	Expected "WT" progeny	Observed/Expected Trans-Het*100
415	59.52	50	40.48	50	119.04

6 *yw/yw; ; stck3R-17/TM6B, Tb1* **X** *w*/Y; ; Fit1 Δ193/TM3, GFP, Ser1*

	yw; ; stck3R-17	yw; ; TM6B, Tb1
w*; ; Fit1Δ193	87	60
Y; ; Fit1Δ193	70	44
w*; ; TM3, GFP, Ser1	59	34
Y; ; TM3, GFP, Ser1	57	15

Total flies	Trans-Het/Total progeny*100	Expected Trans-Het progeny (%)	"WT" progeny	Expected "WT" progeny	Observed/Expected Trans-Het*100
426	36.85	25	63.15	75	147.42

7 *yw/yw; ; stck3R-17/TM6B, Tb1* **X** *w*/Y; ; Fit1 Δ161 Fit2EY08530/TM3, GFP, Ser1*

	yw; ; stck3R-17	yw; ; TM6B, Tb1
w*; ; Fit1Δ161 Fit2EY08530	82	52
Y; ; Fit1Δ161 Fit2EY08530	88	52
w*; ; TM3, GFP, Ser1	75	47
Y; ; TM3, GFP, Ser1	87	34

Total flies	Trans-Het/Total progeny*100	Expected Trans-Het progeny (%)	"WT" progeny	Expected "WT" progeny	Observed/Expected Trans-Het*100
517	32.88	25	67.12	75	131.53

Second-site non-complementation screen

1 *arm4/FM7c* **X** *w1118/Y*

	arm4	*FM7c*
w1118	*86*	*96*
Y	*0*	*45*

Total flies	Trans-Het/Total progeny*100	Expected Trans-Het progeny (%)	"WT" progeny	Expected "WT" progeny	Observed/Expected Trans-Het*100
227	37.89	25	62.11	75	151.54

2 *arm4/FM7c* **X** *yw/Y; ; Fit1KG05576*

	arm4; ; Fit1KG05576	*FM7c; ; Fit1KG05576*
yw; ; +	*57*	*54*
Y; ; +	*0*	*44*

Total flies	Trans-Het/Total progeny*100	Expected Trans-Het progeny (%)	"WT" progeny	Expected "WT" progeny	Observed/Expected Trans-Het*100
155	36.77	25	63.23	75	147.10

3 *arm4/FM7c* **X** *yw/Y; ; Fit2EY08530*

	arm4; ; Fit2EY08530	*FM7c; ; Fit2EY08530*
yw; ; +	*120*	*91*
Y; ; +	*0*	*83*

Total flies	Trans-Het/Total progeny*100	Expected Trans-Het progeny (%)	"WT" progeny	Expected "WT" progeny	Observed/Expected Trans-Het*100
294	40.82	25	59.18	75	163.27

4 *arm4/FM7c* **X** *w*/Y; ; Fit1 Δ 81*

	arm4; ; Fit1Δ81	*FM7c; ; Fit1Δ81*
w; ; +*	*134*	*118*
Y; ; +	*0*	*53*

Total flies	Trans-Het/Total progeny*100	Expected Trans-Het progeny (%)	"WT" progeny	Expected "WT" progeny	Observed/Expected Trans-Het*100
305	43.93	25	56.07	75	175.74

5 *arm4/FM7c* **X** *w*/Y; ; Fit1 Δ 161*

	arm4; ; Fit1Δ161	*FM7c; ; Fit1Δ161*
w; ; +*	*119*	*108*
Y; ; +	*0*	*94*

Total flies	Trans-Het/Total progeny*100	Expected Trans-Het progeny (%)	"WT" progeny	Expected "WT" progeny	Observed/Expected Trans-Het*100
321	37.07	25	62.93	75	148.29

6 *arm4/FM7c* **X** *w*/Y; ; Fit1 Δ193/TM3, GFP, Ser1*

	arm4; ; Fit1Δ193	*FM7c; ; Fit1Δ193*	*arm4; ; TM3, GFP, Ser1*	*FM7c; ; TM3, GFP, Ser1*
w; ; +*	*61*	*48*	62	61
Y; ; +	*0*	*53*	*0*	41

Total flies	Trans-Het/Total progeny*100	Expected Trans-Het progeny (%)	"WT" progeny	Expected "WT" progeny	Observed/Expected Trans-Het*100
326	18.71	12.5	81.29	87.5	149.69

7 *arm4/FM7c* **X** *w*/Y; ; Fit1 Δ161 Fit2EY08530/TM3, GFP, Ser1*

	arm4; ; Fit1Δ161 Fit2EY08530	*FM7c; ; Fit1Δ161 Fit2EY08530*	*arm4; ; TM3, GFP, Ser1*	*FM7c; ; TM3, GFP, Ser1*
w; ; +*	*72*	*74*	49	45
Y; ; +	*0*	*41*	*0*	47

Total flies	Trans-Het/Total progeny*100	Expected Trans-Het progeny (%)	"WT" progeny	Expected "WT" progeny	Observed/Expected Trans-Het*100
328	21.95	12.5	78.05	87.5	175.61

21380

Second-site non-complementation screen

1 *+/+; ; ; pan2/GFP[unc-13GJ]* X *w1118/Y*

	+; ; ; pan2	+; ; ; GFP[unc-13GJ]
w1118; ; +	150	102
Y; ; +	129	112

Total flies	Trans-Het/Total progeny*100	Expected Trans-Het progeny (%)	"WT" progeny	Expected "WT" progeny	Observed/Expected Trans-Het*100
493	56.59	50	43.41	50	113.18

2 *+/+; ; ; pan2/GFP[unc-13GJ]* X *yw/Y; ; Fit1KG05576*

	+; ; ; pan2	+; ; ; GFP[unc-13GJ]
yw; ; Fit1KG05576	105	92
Y; ; Fit1KG05576	106	114

Total flies	Trans-Het/Total progeny*100	Expected Trans-Het progeny (%)	"WT" progeny	Expected "WT" progeny	Observed/Expected Trans-Het*100
417	50.60	50	49.40	50	101.20

3 *+/+; ; ; pan2/GFP[unc-13GJ]* X *yw/Y; ; Fit2EY08530*

	+; ; ; pan2	+; ; ; GFP[unc-13GJ]
yw; ; Fit2EY08530	140	120
Y; ; Fit2EY08530	120	132

Total flies	Trans-Het/Total progeny*100	Expected Trans-Het progeny (%)	"WT" progeny	Expected "WT" progeny	Observed/Expected Trans-Het*100
512	50.78	50	49.22	50	101.56

4 *+/+; ; ; pan2/GFP[unc-13GJ]* X *w*/Y; ; Fit1 Δ 81*

	+; ; ; pan2	+; ; ; GFP[unc-13GJ]
w*; ; Fit1Δ81	95	100
Y; ; Fit1Δ81	93	85

Total flies	Trans-Het/Total progeny*100	Expected Trans-Het progeny (%)	"WT" progeny	Expected "WT" progeny	Observed/Expected Trans-Het*100
373	50.40	50	49.60	50	100.80

5 *+/+; ; ; pan2/GFP[unc-13GJ]* X *w*/Y; ; Fit1 Δ 161*

	+; ; ; pan2	+; ; ; GFP[unc-13GJ]
w*; ; Fit1Δ161	138	137
Y; ; Fit1Δ161	145	123

Total flies	Trans-Het/Total progeny*100	Expected Trans-Het progeny (%)	"WT" progeny	Expected "WT" progeny	Observed/Expected Trans-Het*100
543	52.12	50	47.88	50	104.24

6 *+/+; ; ; pan2/GFP[unc-13GJ]* X *w*/Y; ; Fit1 Δ193/TM3, GFP, Ser1*

	+; ; ; pan2	+; ; ; GFP[unc-13GJ]
w*; ; Fit1Δ193	68	65
Y; ; Fit1Δ193	58	73
w*; ; TM3, GFP, Ser1	56	57
Y; ; TM3, GFP, Ser1	55	50

Total flies	Trans-Het/Total progeny*100	Expected Trans-Het progeny (%)	"WT" progeny	Expected "WT" progeny	Observed/Expected Trans-Het*100
482	26.14	25	73.86	75	104.56

7 *+/+; ; ; pan2/GFP[unc-13GJ]* X *w*/Y; ; Fit1 Δ161 Fit2EY08530/TM3, GFP, Ser1*

	+; ; ; pan2	+; ; ; GFP[unc-13GJ]
w*; ; Fit1Δ161 Fit2EY08530	69	67
Y; ; Fit1Δ161 Fit2EY08530	67	62
w*; ; TM3, GFP, Ser1	71	69
Y; ; TM3, GFP, Ser1	75	57

Total flies	Trans-Het/Total progeny*100	Expected Trans-Het progeny (%)	"WT" progeny	Expected "WT" progeny	Observed/Expected Trans-Het*100
537	25.33	25	74.67	75	101.30

Life is what happens to you while you're busy making other plans.

- John Winston Ono Lennon